

Tensor Network Methods for Quantum Phases

Jacob C. Bridgeman

A thesis submitted to fulfil requirements for the degree of Doctor of Philosophy

School of Physics
The University of Sydney

November 2017

Contents

Abstract	vi
Statement of Student Contribution	vii
Statement of Originality	viii
Acknowledgements	ix
1 Introduction	1
1.1 Many-body spin models	1
1.1.1 Quantum phases	2
1.1.2 Symmetries in many-body models	3
1.1.3 Phases with no broken symmetry: Topological order	4
1.1.4 Many-body models and computation	7
1.2 Thesis overview	8
2 Hand-waving and Interpretive Dance: An Introductory Course on Tensor Networks	9
JACOB C. BRIDGEMAN AND CHRISTOPHER T. CHUBB	
<i>Journal of Physics A: Mathematical and Theoretical</i> 50 , 223001 (2017), arXiv:1603.03039	
2.0 Introduction	11
2.1 Introduction to Tensor Network Notation	12
2.1.1 Tensors	12
2.1.2 Tensor operations	12
2.1.3 Tensor networks	15
2.1.4 Bubbling	16
2.1.5 Computational Complexity	17
2.1.6 Problems	18
Bibliography	19
2.2 Quantum information examples	21
2.2.1 Bell state and the Bell basis	21
2.2.2 Quantum Teleportation	21
2.2.3 Purification	23
2.2.4 Stinespring's Dilation Theorem	23
2.2.5 Problems	24
Bibliography	25
2.3 Matrix Product States	26
2.3.1 1D Projected Entangled Pair States	27
2.3.2 Some MPS states	28

2.3.3	MPS Properties	30
2.3.4	Renormalising Matrix Product States	32
2.3.5	Mixed States and Many Body Operators	32
2.3.6	Problems	34
	Bibliography	35
2.4	Classifying Gapped Phases in 1D	37
2.4.1	Quantum Phases	37
2.4.2	Injective MPS	38
2.4.3	No Topological Order	38
2.4.4	Symmetry Respecting Phases	39
2.4.5	Problems	45
	Bibliography	45
2.5	Tensor network algorithms	47
2.5.1	DMRG (The Computer Scientist’s approach)	47
2.5.2	TEBD (The Physicist’s approach)	50
2.5.3	Implementation	51
2.5.4	Problems	51
	Bibliography	52
2.6	Projected Entangled Pair States	55
2.6.1	One Dimensional Systems: MPS	55
2.6.2	Extending to Higher Dimensions	56
2.6.3	Some PEPS examples	57
2.6.4	2D Cluster State and the complexity of PEPS	61
2.6.5	Properties of PEPS	61
2.6.6	Problems	64
	Bibliography	65
2.7	Multiscale Entanglement Renormalisation Ansatz	67
2.7.1	Properties of MERA	67
2.7.2	Renormalisation Group Transformation	70
2.7.3	AdS/CFT	70
2.7.4	Some Simple MERA States	71
2.7.5	Problems	73
	Bibliography	73

Appendices

2.A	PEPOs for local Hamiltonians: The ‘particle decay’ construction	76
2.A.1	1D	76
2.A.2	2D and higher	77
2.A.3	Other examples	79
	Bibliography	79
2.B	Solutions: Introduction to Tensor Networks	80
2.C	Solutions: Quantum information examples	84
2.D	Solutions: Matrix Product States	85
2.E	Solutions: Classifying Gapped Phases in 1D	89
2.F	Solutions: Tensor network algorithms	91
2.G	Solutions: Projected Entangled Pair States	92
2.H	Solutions: Multiscale Entanglement Renormalisation Ansatz	95

3 Detecting Topological Order with Ribbon Operators 100

JACOB C. BRIDGEMAN, STEVEN T. FLAMMIA, AND DAVID POULIN
 Physical Review B 94, 205123 (2016), arXiv:1603.02275

3.0.1 Prior Approaches 101

3.1 Properties of Anyons 103

3.2 Definition of Ribbon Operators 105

3.2.1 The Method of Ribbon Operators 105

3.2.2 Our Cost Function 106

3.3 Heuristic Justification for the Norm 108

3.4 Finding Ribbon Operators 109

3.4.1 Optimizing 109

3.5 Numerical Results 110

3.5.1 \mathbb{Z}_d Quantum Double-Ising model 110

3.5.2 The Quantum Compass Model 114

3.5.3 Kitaev’s Honeycomb Model 115

3.6 Ribbons As Logical Operators 117

3.7 Summary and Outlook 118

Bibliography 120

Appendices

3.A \mathbb{Z}_2 Quantum Double 124

4 Anomalies and entanglement renormalization 126

JACOB C. BRIDGEMAN AND DOMINIC J. WILLIAMSON
 Physical Review B 96, 125104 (2017), arXiv:1703.07782

4.1 Symmetries and anomalies in MERA 128

4.1.1 Symmetries on the lattice 128

4.1.2 MERA and symmetry 129

4.1.3 On-site symmetry 130

4.1.4 Anomalous MPO symmetries 131

4.1.5 Physical data from MERA 132

4.2 Symmetry twists and topological sectors 132

4.2.1 Symmetry twist and topological correction to conformal spin 133

4.2.2 Projective representations and topological sectors 134

4.3 A class of MPO symmetric MERA 136

4.3.1 Disentangling an MPO 136

4.3.2 A class of anomalous \mathbb{Z}_N^3 MPO symmetries 137

4.3.3 Symmetric MERA tensors 138

4.4 Example: A \mathbb{Z}_2^3 symmetric model 139

4.4.1 Family of Hamiltonians 139

4.4.2 Scaling dimensions and topological sectors 140

4.4.3 Duality and domain walls 142

4.4.4 An anomaly protected gapless phase 142

4.5 Conclusions 143

Bibliography 145

Appendices

4.A	Conformal data in all topological sectors	154
4.B	MPO group representations and third cohomology	160
4.C	Ansatz for MERA tensors with type-III \mathbb{Z}_N^3 symmetry	163
4.C.1	4:2 MERA	163
4.C.2	Ternary MERA	164
4.D	Generalized \mathbb{Z}_N CZX model and its gapless boundary theory	165
4.D.1	Definitions	165
4.D.2	Hamiltonian and ground state	165
4.D.3	Symmetry	166
4.D.4	Boundary theory	166
4.D.5	General $(1 + 1)$ D \mathcal{G} SPT duality at the edge of a $(2 + 1)$ D $\mathcal{G} \times \mathcal{H}^2(\mathcal{G}, \text{U}(1))$ SPT	168
5	Tensor Networks with a Twist: Anyon-permuting domain walls and defects in PEPS	170
	JACOB C. BRIDGEMAN, STEPHEN D. BARTLETT AND ANDREW C. DOHERTY arXiv:1708.08930	
5.1	Review: Topological order and PEPS	171
5.1.1	Topological order and anyon-permuting symmetries	171
5.1.2	Projected entangled pair states	173
5.2	Anyon-permuting symmetries of the toric code	175
5.2.1	Topological PEPS	175
5.2.2	Anyon-permuting symmetry	176
5.2.3	Symmetry defects and twists	180
5.3	Color Code	182
5.3.1	Excitations, anyon-permuting symmetries and domain wall operators	184
5.3.2	Anyon-permuting symmetry twists for the color code	185
5.3.3	Symmetry protected nature of the domain wall	186
5.4	Conclusions	187
	Bibliography	188
	Appendices	
5.A	Hamiltonians for twists	192
5.B	Abelian quantum double models	194
5.B.1	Lattice Hamiltonian and PEPS	194
5.B.2	Domain wall operators	195
5.B.3	Prime dimension codes	196
6	Conclusion	197
	Bibliography	199

Abstract

The physics that emerges when large numbers of particles interact can be complex and exotic. The collective behaviour may not reflect the underlying constituents, for example fermionic quasi-particles can emerge from models of interacting bosons. Due to this emergent complexity, many-body phenomena can be very challenging to study, but also very useful. A theoretical understanding of such systems is important for robust quantum information storage and processing.

The emergent, macroscopic physics can be classified using the idea of a quantum phase. All models within a given phase exhibit similar low-energy emergent physics, which is distinct from that displayed by models in different phases. In this thesis, we utilise tensor networks to study many-body systems in a range of quantum phases. These include topologically ordered phases, gapless symmetry-protected phases, and symmetry-enriched topological phases.

Statement of Student Contribution

This thesis primarily consists of a review paper and three research papers. On all four, I am the primary author. On two of the papers, both authors are students. On the remaining works, I am the sole student author.

Formatting changes have been made to each paper to adapt to the single column format. We have chosen to retain separate bibliographies for each paper. Therefore, in Chapters 3-5, citations will take the form ‘chapter number’.‘citation number’ and the appropriate bibliography can be found at the end of the chapter. Since Chapter 2 is structured as a series of lectures, the citations there take the form ‘chapter number’.‘lecture number’.‘citation number’ and a bibliography can be found at the end of each lecture. For the introduction and conclusion (Chapters 1 and 6), the bibliography can be found at the end of the thesis.

Due to differing journal requirements, Chapters 3-5 are written in American English, whilst the remainder of the thesis is written in British/Australian English.

Chapter 2: Hand-waving and Interpretive Dance: An Introductory Course on Tensor Networks

This chapter contains the published paper: *Journal of Physics A: Mathematical and Theoretical* **50**, 223001 (2017), arXiv:1603.03039.

This work is a review article. Sections 2.3, 2.4, 2.6 and 2.7 were written primarily by me, Section 2.0 was written jointly and the remainder was primarily written by Christopher Chubb. All sections were edited jointly.

Chapter 3: Detecting Topological Order with Ribbon Operators

This chapter contains the published paper: *Physical Review B* **94**, 205123 (2016), arXiv:1603.02275.

The research represented in this paper was undertaken by me, with supervision from Steven Flammia. The work was based on ideas previously discussed by Steven and David Poulin. In particular, they had developed the idea leading to Eqn. 3.10. All ideas and implementations leading to the numerical results in the paper are my own work. The paper was written jointly with Steven Flammia with edits from all authors.

Chapter 4: Anomalies and entanglement renormalization

This chapter contains the published article: *Physical Review B* **96**, 125104 (2017), arXiv:1703.07782.

Sections 4.2 and 4.D primarily represent the work of Dominic Williamson, whilst Sections 4.4.2, 4.4.4 and 4.A, including all numerical work represents primarily my work. Both authors contributed equally to the remainder. The paper was written and edited jointly.

This document also appears in Dominic Williamson's PhD thesis.

Chapter 5: Tensor Networks with a Twist: Anyon-permuting domain walls and defects in PEPS

This chapter contains the preprint: arXiv:1708.08930. This work is currently under review. The research represented in this paper was undertaken by me, with supervision from Stephen Bartlett and Andrew Doherty. The paper was written by me with edits from all authors.

Statement of Originality

This is to certify that to the best of my knowledge, the content of this thesis is my own work. This thesis has not been submitted for any degree or other purposes.

I certify that the intellectual content of this thesis is the product of my own work and that all the assistance received in preparing this thesis and sources have been acknowledged.



Jacob C. Bridgeman

Acknowledgements

This thesis would not have been possible without the support of a large number of people. Firstly, I would like to thank my supervisor Stephen Bartlett. He has provided constant assistance, support and patience. I would also like to thank my associate supervisors Andrew Doherty and Steve Flammia. Both have also provided a great deal of support, guidance, and time.

I would like to thank all my coauthors for patience, enthusiasm and interesting discussions. In addition to my supervisors, these are David Poulin, Christopher Chubb and Dominic Williamson.

Working in the Sydney Quantum Information Theory group has been constantly interesting and inspiring. Many thanks are due to the group members. Specifically, thanks go to Rafael Alexander, Harrison Ball, Andrew Darmawan, Sam Elman, Natasha Gabay, Christopher Granade, Robin Harper, Angela Karanjai, Kamil Korzekwa, Sam Roberts, Thomas Smith, and Paul Webster.

I am also grateful to my friends and family for all their support. Special thanks to my parents Cate and Adam for constant patience.

Finally, thanks to Chanel Leong. Without you, I would not have made it this far.

Chapter 1

Introduction

From the standard model of particle physics to condensed matter and quantum chemistry to quantum information, the study of large numbers of interacting quantum particles is at the centre of modern science. From simple constituent particles and local interactions, complex phenomena such as magnetism, superconductivity and topological order can emerge. Understanding these emergent, low energy properties of a given many-body Hamiltonian can be incredibly challenging.

In the limit where the constituent particles are weakly interacting, perturbation theory has proven very successful. Away from this limit, the perturbative approach breaks down and other techniques must be employed. One of the most widely utilised methods is (quantum) Monte Carlo sampling. Although this class of methods is very powerful, Monte Carlo techniques are also limited in their applicability. In particular, the *sign problem* occurs when the partition function obtained from a quantum-to-classical mapping does not correspond to a sum of positive weights [1]. When this occurs, the sampling time is exponential in the system size and so precludes accurate approximation of physical quantities. Many physically interesting models exhibit a sign problem, including systems of interacting fermions such as the standard model, and frustrated quantum magnets. At low temperatures, these frustrated magnets can exhibit *topological order*, a kind of long-range ordering without symmetry breaking, which can be utilised for quantum computing applications [2–5].

In this thesis, we use a new family of methods, collectively known as *tensor networks methods*, to study a range of physical systems in one and two dimensions. These techniques aim to provide a framework for efficiently computing physical quantities without requiring weak interactions or the lack of a sign problem.

1.1 Many-body spin models

Many-body spin models are toy models for physical systems, which attempt to realise the physical phenomena of interest without taking into account the full complexity of the real system. For example, vibrational degrees of freedom may be neglected if they are expected to decouple from the spin degrees of freedom. The most basic example of such a toy model is the Ising ferromagnet

$$H_{\text{Ising}} = -J \sum_{\langle i,j \rangle} Z_i Z_j - \lambda \sum_i X_i, \quad (1.1)$$

where Z_i is the Pauli Z operator at lattice site i and X_i is the Pauli X operator. This Hamiltonian models a quantum (anti-)ferromagnet for ($J < 0$) $J > 0$ in a transverse field with interaction strength J and field strength λ . In one (spatial) dimension, this model exhibits a quantum phase transition at $J = \lambda$. At this point, the gap between the lowest energy state and the excited states

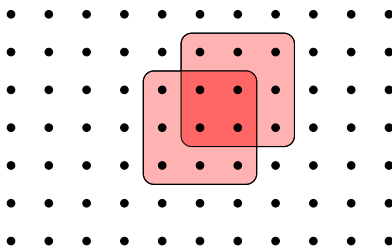


Figure 1.1: A many-body spin model is defined by a local Hamiltonian on some lattice of finite dimensional spins. The interaction terms (indicated) are usually taken to be geometrically local, as defined by the underlying lattice.

closes. This gap-closing allows the physics in the low energy space to change dramatically, in this case the ground state degeneracy changes. Despite the apparent simplicity of this model, the location of the quantum phase transition in two-dimensions is not known analytically. One way to study this model is by considering the low energy excitations out of the ground state. When $\lambda \gg J$, the ground state is the state $|\Omega\rangle = |+\rangle^{\otimes N}$, and a local excitation at site j can be created by applying Z_j . When $\lambda \ll J$, excitations correspond to loops created by applying X to all sites within some region. As discussed in Sec. 1.1.4, the excitation is located at the perimeter of the region.

In this thesis, we will discuss models with more exotic behaviour than the Ising model. A key property of these models will be their locality structure. More generally, a spin model is described by a finite dimensional Hilbert space \mathbb{C}^d at each ‘site’ defined using some lattice (or more generally graph) which we will refer to as Λ . The energy of each state is specified using a local Hamiltonian

$$H = \sum_{j \in \Lambda} h_j, \quad (1.2)$$

where h_j is some hermitian operator acting on a small number (constant in the lattice size) of spins. The locality structure of the underlying lattice is usually used to impose locality on the Hamiltonian terms as shown in Fig. 1.1, meaning that the spins only interact with their neighbours.

Despite the apparent simplicity of such models, they can realise a wide range of physical phenomena. These include magnetic behaviours [6], gauge theories [7–9], emergent fermions [2] and even more exotic emergent quasi-particles [10], and resource states for quantum computing requiring only measurement [11].

Due to the complexity inherent in studying many-particle systems, it is convenient to find ways to extract relevant properties of a system of interest without fully solving the model. In classical statistical mechanics, much of the essential physics can be understood by analysing the structure of (thermal) phases and phase transitions. This can be generalised to quantum systems using the concept of a *quantum phase*.

1.1.1 Quantum phases

At the macroscopic scale we are often not concerned with the microscopic details of a system, rather we are interested in the emergent, macroscopic, low energy physics. This leads us to the concept of a quantum phase. These phases are equivalence classes of states or Hamiltonians which have similar coarse-grained, long-wavelength, or low-energy, physics. To remove any thermal effects which might wash out the quantum fluctuations, a quantum phase is defined in the zero temperature limit [6].

In this limit, the free energy density becomes the ground state energy

$$\lim_{\beta \rightarrow \infty} -\frac{1}{\beta} \log \text{Tr} \exp(-\beta H) = E_0. \quad (1.3)$$

In the thermal case, a (continuous) phase transition occurs when the free energy becomes nonanalytic. For quantum systems, this corresponds to the ground state energy becoming a nonanalytic function of the Hamiltonian parameters. Two Hamiltonians are therefore said to be in the same quantum phase if they can be continuously deformed into each other without closing the gap between the (possibly degenerate) ground space and the excited space. States are in the same phase if they are the ground states of such Hamiltonians.

Whilst the gap remains open, the physics of the low energy space cannot change drastically. In particular, the entanglement structure is essentially unchanged and the ground space degeneracy is unchanged (in the thermodynamic limit). Quasi-particle excitations become locally dressed when the Hamiltonian is deformed, but their general properties, such as exchange statistics, are unchanged. At the phase transition, when the gap closes, the macroscopic physics can change drastically.

The simplest example of a quantum phase transition occurs in the Ising model of Eqn. 1.1, where we assume spins on a one-dimensional chain. When $\lambda \gg J$, there is a unique ground state $(|+\rangle)^{\otimes N}$ which is symmetric under the Hamiltonian symmetry $\prod X_j$. In the other limit ($\lambda \ll J$), the ground space is doubly degenerate, spanned by $|0\rangle^{\otimes N}$ and $|1\rangle^{\otimes N}$. The degenerate phase spontaneously breaks the symmetry, and corresponds to the ordered phase.

Most classical (thermal) phase transitions are understood through symmetry breaking in this way¹. Other mechanisms can be used to distinguish quantum phases, in particular the structure of entanglement in the ground space [13]. Intrinsic topological phases have long range entangled ground spaces, which cannot be related to unentangled product states without closing the gap. Such phases are distinct without any symmetry being imposed. Other quantum phases are known as symmetry-protected and symmetry-enriched topological phases. These have an entanglement pattern in the ground space which is protected by the symmetry; the entanglement cannot be removed without either closing the gap or breaking the symmetry.

Given two Hamiltonians H_0 and H_1 , we say that they are in the same phase if H_0 can be continuously deformed into H_1 without ever closing the gap. We say two states $|\psi_0\rangle$ and $|\psi_1\rangle$ are in the same phase if they are ground states of Hamiltonians which are in the same phase. In the absence of any symmetry considerations, this defines the *intrinsic topological* phase. When symmetries are imposed, symmetry-breaking and symmetry-protected phases emerge as shown in Fig. 1.2.

In this thesis, we will study symmetry-breaking, symmetry-protected, and intrinsic topological phases, in addition to the transitions between them.

1.1.2 Symmetries in many-body models

As discussed above, symmetries can greatly constrain the behaviour of physical systems. In the context of phases, imposing symmetries leads to a far richer and more detailed classification. Here, we briefly introduce group-like symmetries.

We say a quantum system defined by a Hamiltonian H is *symmetric* under a group \mathcal{G} if

$$U_g H = H U_g, \quad (1.4)$$

¹Although other mechanisms exist, such as the Kosterlitz-Thouless transition in the two-dimensional XY model [12].

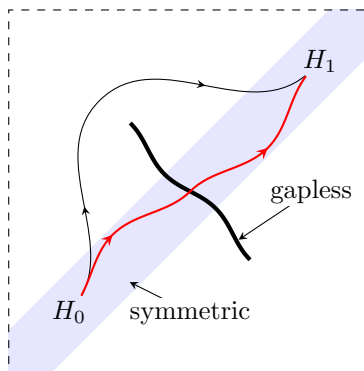


Figure 1.2: Hamiltonians are in the same phase if they can be continuously deformed into one another without closing the gap. When only considering Hamiltonians which respect a symmetry (blue band), the classification of phases becomes more refined. Imposing that the Hamiltonians remain symmetric along the interpolating path may cause them to become gapless.

where U_g forms a representation of \mathcal{G} . Due to the locality structure of the model, we usually assume that U_g is *transversal* or *on-site*. This means that it acts independently on each spin

$$U_g = \bigotimes_{j \in \Lambda} u_g^{(j)}, \quad (1.5)$$

where $u_g^{(j)}$ itself forms a representation of \mathcal{G} .

Although we can frequently think about blocking sites together until any symmetry becomes on-site, some symmetries cannot be made to act in this way. These include anomalous symmetries (the topic of Chapter 4), and spatial symmetries such as translation. More generally, one may assume the symmetry action is merely *locality preserving* (as studied in Chapter 5). This class includes group actions realised as constant (in the system size) depth quantum circuits, and spatial symmetries such as translations and rotations, and any other action which does not increase the support of any local operator by more than a constant amount.

1.1.3 Phases with no broken symmetry: Topological order

As in the traditional case, the phase transition in the quantum Ising model described above is associated with the breaking of a symmetry. Quantum models permit richer classes of phases, referred to as intrinsic topological phases, which are not associated with any broken symmetry. The simplest model realising such a phase is the two-dimensional toric code [2]. This model can be defined on a square lattice with qubits (spin-1/2s) placed on the edges. The Hamiltonian for the model is

$$H = - \sum_{v \in \text{vertices}} -Z \begin{array}{c} | \\ Z \\ | \end{array} Z - \sum_{p \in \text{plaquettes}} \begin{array}{c} \lceil X \rceil \\ X \quad X \\ \lfloor X \rfloor \end{array}. \quad (1.6)$$

Since all the terms in this Hamiltonian commute, have eigenvalues ± 1 , and the model is unfrustrated, the excitations are relatively simple to obtain. The ground state is the mutual +1 eigenstate of every Hamiltonian term, while local excitations correspond to -1 eigenstates of a given term. These excitations are created using string-like operators as shown in Fig. 1.3a. Along their length, these strings commute with all Hamiltonian terms, and so do not contribute to the

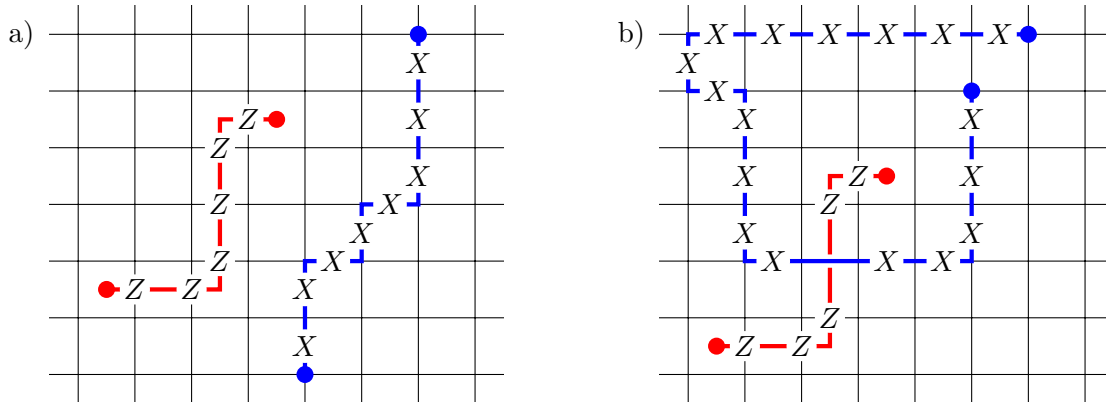


Figure 1.3: Excitations of the toric code.

a) The excitations of the toric code are created using string operators. Away from their end points, these strings commute with the Hamiltonian and therefore do not carry energy. The end points anti-commute with H , so correspond to localised quasi-particles. We refer to the particle living on vertices (created by a string of X s) as an e or electric particle. Particles living on plaquettes (created by Z strings) are called m or magnetic particles. There is no way to remove the strings without creating or removing excitations.

b) The process of braiding an e around an m allows us to understand the exchange statistics of the particles. Due to the crossing of the strings, this process differs from the ‘trivial’ braid (not enclosing the m) by a factor of -1 .

energy of the state. At the end points, the operator anti-commutes with a term, leading to an energy of 2 units above the ground space. The end points of the strings therefore correspond to localised quasi-particles.

The excitations of the toric code have several interesting properties. Firstly, the paths of the strings can be deformed by multiplying by Hamiltonian terms. Since these terms act as $+1$ on the state, this does not transform the state in any way. Although the existence of the string cannot be avoided, the path can be deformed arbitrarily. Only the end points, where the particles are located, are fixed in place. Since a string must have two ends, excitations of the toric code always occur in pairs, and are their own anti-particles. There are three kinds of particles in the toric code, electric or e excitations living on the plaquettes, magnetic or m particles on the vertices, and a particle em obtained by fusing an e with an m .

The existence of the string operators leads to interesting exchange statistics. If we consider the process of braiding an e around an m , as depicted in Fig. 1.3b, we can understand the mutual statistics of these particles. When this process occurs, the strings must cross. The red (Z) string is applied to the ground state first, followed by the blue (X) string. Since $XZ = -ZX$, this process contributes a phase of -1 to the wavefunction compared to moving the e around first, then moving the m to the centre of the loop. The particles are therefore mutual fermions. The composite particle em acts as a self-fermion. This is different to the Ising model (Eqn. 1.1), where the excitations are local spin flips and are therefore bosonic. Since the particles statistics are an invariant of the phase [14], this demonstrates that the toric code is in a distinct phase from those in the 2D Ising model.

The e and m particles are the simplest examples of *anyons* [2]. These quasi-particles can have exchange statistics far more exotic than those of bosons and fermions. Braiding can introduce general phases into the wavefunction, or even be used to enact unitary transformations on the ground space [15, 16]. In Chapter 3, we introduce a numerical scheme for finding the exchange phases of the excitations for general two-dimensional Hamiltonians. Since the particular path chosen in Fig. 1.3b is not important, only whether it encircles the other particle, these *topological phases*

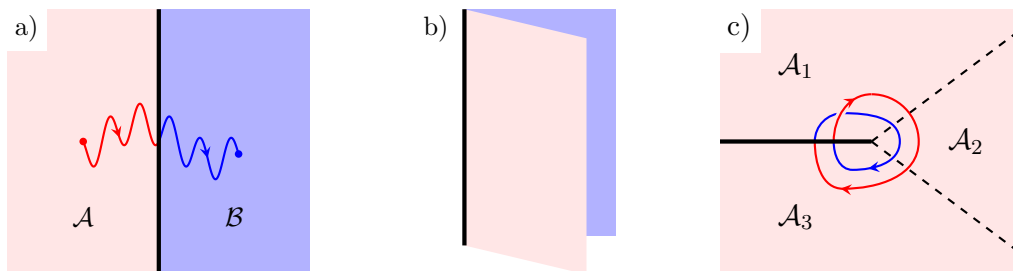


Figure 1.4: Gapped domain walls between topological phases.

a) When two topological phases \mathcal{A} and \mathcal{B} are placed next to each other, a domain wall occurs between them. Some excitations (particles) can move across the wall, a process which may transform both the particles and the wall.

b) Domain walls can be understood as boundaries of folded systems. Particles ‘condense’ into the vacuum when moving across the boundary. Only particles with bosonic self- and mutual- statistics can undergo condensation.

c) Defect or twists can be created when multiple copies of the same phase are placed next to each other. The dashed line indicates the ‘trivial’ boundary, whilst the solid black line is some boundary which exchanges particles. At the end of the boundary, generalised excitations occur. Braiding around this defect exchanges particle types.

are a promising platform for quantum computational tasks. The topological nature of the phases provides a natural protection against local, environmental noise.

Boundaries in topological models

So far we have discussed topological models without considering boundary conditions. We will now discuss how domain walls between topological phases can be introduced. This is particularly important from a quantum computational perspective, since the inclusion of domain walls leads to the incorporation of point-like defects or *twists*. These twists can be used to increase the computational power of a topological phase, and the storage capacity of the phase when used as a quantum memory [17].

Consider placing a topological material in phase \mathcal{A} next to another phase \mathcal{B} as shown in Fig. 1.4a. The regions \mathcal{A} and \mathcal{B} can be thought of as distinct domains of order, in analogy to the magnetic domains that form in ferromagnetic materials, or the crystalline domains in solid materials. At the interface, a domain wall occurs. The physics of these domain walls alters the topological properties of the material, in particular the domain wall can alter the behaviour of the quasi-particle excitations. Since the excitations in phases \mathcal{A} and \mathcal{B} may be distinct, if an excitation is moved across the wall from phase \mathcal{A} to phase \mathcal{B} , it may be transformed. In general, such a process may also transform the wall itself [18]. For such a process to be possible, the braiding relations of the particles crossing the wall should be unchanged. The simplest case is when phase \mathcal{B} is the vacuum. In this case, any particles crossing the boundary ‘condense’. Since the vacuum is a bosonic state, the self- and mutual- statistics of any set of quasi-particles should also be bosonic. In the case of the toric code discussed above, this means that a boundary can condense e or m , since they are both self bosons, but cannot condense em or $\{e, m\}$, since em is a self fermion, and $\{e, m\}$ are mutual semions (phase of -1 under a full braid). There are therefore two kinds of condensing boundary for this phase. All domain walls can be thought of as boundaries by considering the bilayer phase $\bar{\mathcal{A}} \times \mathcal{B}$ obtained by folding along the wall [18] as shown in Fig. 1.4b.

Perhaps the most interesting properties of domain walls occur when more than two phases are placed next to each other. Consider the situation depicted in Fig. 1.4c, where three copies of phase

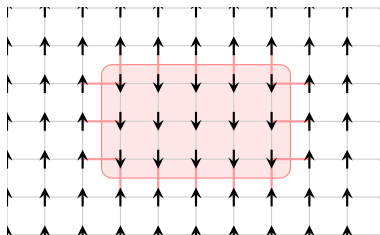


Figure 1.5: The energy cost required to flip a domain of spins is proportional to the perimeter of the region. The cost to flip all of the spins scales as the linear system size, so classical information can be protected by making the system size bigger. At low temperatures, the creation on domains of flipped spins is suppressed, so the encoded information is protected.

\mathcal{A} are brought together. Between $\mathcal{A}_1|\mathcal{A}_2$ and $\mathcal{A}_2|\mathcal{A}_3$ we use the ‘trivial’ domain wall. This interface is invisible and performs no transformation on the excitations. Between $\mathcal{A}_1|\mathcal{A}_3$, place an interface that exchanges two particles $a \leftrightarrow b$. In the toric code there is such a wall, which implements $e \leftrightarrow m$. At the meeting point of the three phases there is a point-like defect, which we refer to as a twist. This point acts similarly to the anyons in the phase, however the braiding statistics can be far more exotic. When we braid a particle of type a around the twist, its is changed to a type b particle when crossing the wall $\mathcal{A}_1|\mathcal{A}_3$. The particle therefore must be braided twice before it can be fused with its antiparticle back to the vacuum. The study of such domain walls and twists is the topic of Chapter 5.

1.1.4 Many-body models and computation

One of the primary motivations to study the exotic materials considered in this thesis is their potential use as platforms for quantum computation. There is a long history of using the physics of many-body systems for information storage and processing. The simplest case occurs in classical computation, where the 2D Ising model of Eqn. 1.1 with $\lambda = 0$ (i.e. a ferromagnet) can be used as a robust memory. By aligning all of the spins in a particular direction, a single logical bit can be redundantly encoded into many physical spins. The logical state can be read out by measuring the average magnetisation. The energy cost to flip a domain of spins (Fig. 1.5) is proportional to the number of anti-aligned neighbours, and so the perimeter of the region. To corrupt the encoded information, more than half the spins must be flipped, which carries an energy cost proportional to the (linear) system size. At low temperature, the entropy gained by adding flipped domains is not sufficient to offset the energy gain and the system orders. In this phase, the system is a *self-correcting* classical memory. At higher temperatures, the system undergoes a Curie transition from ferro- to para-magnetism, and ceases to be magnetised and therefore ceases to self-correct.

This example demonstrates the intricate connection between the physics of phases and phase transitions, and the usefulness of materials for information storage, and more generally information processing tasks. One of the most important questions in quantum information theory is finding a self-correcting quantum memory, analogous to the Ising model in the classical case. The 4-dimensional generalisation of the toric code is known to have this property [19], and there has been a large effort to realise this in fewer dimensions [20–25]. Many of these proposals are inspired by the statistical mechanics of the models, for example Ref. 23 attempted to use an entropic barrier to prevent excitations spreading to the point where the encoded information is corrupted. Unfortunately, such approaches have been shown to be impossible, with a growing energy barrier (just like the classical Ising model) being essential [26]. There are a range of no-go results to realising

self-correcting memories, however many are linked to the special case of stabiliser codes [4]. Due to their special structure, stabiliser codes are relatively simple (compared to general Hamiltonians) to analyse. It is therefore important to develop techniques that allow analysis beyond this restricted class. One such technique for detecting topological order is introduced in Chapter 3.

1.2 Thesis overview

In this thesis, we explore the properties of various many-body models using a variety of tensor network methods. Some of these models have topological orders, others have exotic symmetries, and others combine both topological order and symmetry. We primarily study models which are well understood, thereby learning about the strengths and weaknesses of the tensor network methods themselves.

In Chapter 2, we review the conventional notation for tensor networks. With this notation established, we then review a range of common tensor networks and some of the key results of the field. Written as a series of lectures, this chapter aims to bring the non-expert to the point where research papers are accessible.

In Chapter 3, we propose and implement a variational technique to identify (abelian) topological order in two-dimensional spin models. By using matrix product operators (MPOs), this technique aims to numerically optimise operators which move anyons around the lattice. By avoiding ground state optimisation, this technique bypasses the prohibitive computational complexity of finding ground states [27, 28]. Additionally, this method is naturally one-dimensional, which leads to a far more efficient algorithm in practice. By using this technique, we are able to find ribbon operators in the Kitaev honeycomb model [3]. To the best of our knowledge, nobody has found these operators previously.

In Chapter 4, we design a variational subclass of the multiscale entanglement renormalisation ansatz (MERA) states which realise an exotic symmetry action. These states are designed to simulate the ground states of gapless, one-dimensional Hamiltonians. The symmetries supported by our subclass are represented using MPOs with an obstruction to reducing the bond dimension. This class of symmetries arises naturally when studying two-dimensional SPT state, and self-dual critical points in one-dimension. Both of these classes of models are expected to be gapless, and it is therefore important that they can be simulated in a fully symmetric manner using a technique tailored to gapless models. For a particular model, we optimise over the variational class and extract the full topological data of the model, in addition to the conformal data.

In Chapter 5, we combine topological order and symmetry. Using projected entangled pair states (PEPS) and MPOs, we investigate anyon permuting domain walls and symmetry defects. By working on the virtual level of a topologically ordered PEPS, we are able to construct operators realising the topological symmetries of the associated anyon model without reference to a Hamiltonian. Further, we are able to construct states with symmetry defects and construct Hamiltonians with such defect states as their ground states.

Finally, in Chapter 6, we provide an overview of the thesis, discuss possible extensions of this line of research, and provide concluding remarks.

Each chapter (2-5) is self contained, and begins with a review of the relevant literature.

Chapter 2

Hand-waving and Interpretive Dance: An Introductory Course on Tensor Networks

JACOB C. BRIDGEMAN^{1,2} AND CHRISTOPHER T. CHUBB^{1,2}

¹CENTRE FOR ENGINEERED QUANTUM SYSTEMS, SCHOOL OF PHYSICS, THE UNIVERSITY OF SYDNEY, SYDNEY, AUSTRALIA

²AUSTRALIAN INSTITUTE OF NANOSCALE SCIENCE AND TECHNOLOGY, SYDNEY NANOSCIENCE HUB, THE UNIVERSITY OF SYDNEY, SYDNEY, AUSTRALIA

Journal of Physics A: Mathematical and Theoretical **50**, 223001 (2017), [arXiv:1603.03039](https://arxiv.org/abs/1603.03039)

Abstract

The curse of dimensionality associated with the Hilbert space of spin systems provides a significant obstruction to the study of condensed matter systems. Tensor networks have proven an important tool in attempting to overcome this difficulty in both the numerical and analytic regimes.

These notes form the basis for a seven lecture course, introducing the basics of a range of common tensor networks and algorithms. In particular, we cover: introductory tensor network notation, applications to quantum information, basic properties of matrix product states, a classification of quantum phases using tensor networks, algorithms for finding matrix product states, basic properties of projected entangled pair states, and multiscale entanglement renormalisation ansatz states.

The lectures are intended to be generally accessible, although the relevance of many of the examples may be lost on students without a background in many-body physics/quantum information. For each lecture, several problems are given, with worked solutions in an ancillary file.

Acknowledgments

We thank everyone who stayed awake for the presentation of these lectures in January of 2016 at the Australian Institute of Nanoscience. We thank Stephen Bartlett, Andrew Doherty, Christopher Granade, Robin Harper, Marco Tomamichel, Dominic Williamson, and especially Doriane Drolet and David Tuckett, for their input. For suggesting that we give these lectures and editorial assistance, we give special thanks for the best-selling childrens' author^a Chris Ferrie. We acknowledge support from the Australian Research Council via the Centre of Excellence in Engineered Quantum Systems (EQuS), project number CE110001013.

Much of the material was reproduced from memory after one of the authors attended the [Tensor Network Summer School at Universiteit Gent in 2015](#).

^aSource 1, Source 2.

2.0 Introduction

One of the biggest obstacles to the theoretical and numerical study of quantum many-body systems is the *curse of dimensionality*, the exponential growth of the Hilbert space of quantum states. In general this curse prevents efficient description of states, providing a significant complexity barrier to their study. Despite this, physically relevant states often possess additional structure not found in arbitrary states, and as such *do not* exhibit this pathological complexity, allowing them to be efficiently described and studied.

Tensor networks have proven to be an incredibly important technique in studying condensed matter systems, with much of the modern theory and numerics used to study these systems involving tensor networks.

In the numerical regime, tensor networks provide variational classes of states which can be efficiently described. By, for example, minimising the energy over one of these classes, one can learn a great deal about the low-energy behaviour some physical system of interest. The key variational classes are: matrix product states (MPS), projected entangled pair states (PEPS), and multiscale entanglement renormalisation ansatz (MERA). Due to their importance, and prevalence in the literature, we devote a chapter to each of these.

By studying the structure and properties of classes tensor networks, for example MPS, one can learn a great deal about the types of states which they can describe. Tensor network states therefore provide an important analytic framework for understanding the universal properties of classes of states which possess particular properties, such as those which only support certain entanglement or correlation structures.

In addition to their application to many-body physics, tensor networks can also be used to understand many of the foundational results in quantum information. The understanding of concepts such as quantum teleportation, purification, and the church of the larger Hilbert space, can be understood relatively simply when the tensor network framework is utilised. Some examples of this are presented in Section 2.2. These lectures aim to introduce, and make familiar, the notation conventionally used for tensor network calculations. As a warm up, we present some key quantum information results in this notation.

After introducing the class of MPS, we present some of the key properties, as well as several analytic matrix product states examples, which can serve as useful toy models. To demonstrate the analytic power of MPS we will then consider a key result in condensed matter theory: the classification of one-dimensional phases. This serves as an example of a result which, within the tensor network formalism, can be much more succinctly and clearly explained than it can in more standard linear algebraic notation.

When utilising tensor networks numerically, algorithms must be designed which, for example, minimise the energy of some Hamiltonian over the variational class. We introduce two such algorithms, namely DMRG and TEBD, which are particularly prevalent. These have become standard tools in numerical many-body physics.

We then introduce the class of PEPS, a class designed for two-dimensional many-body systems. We discuss some of the properties, and some of the challenges to simulating using this class of networks.

Finally, we introduce another class, MERA, which can be utilised for the study of gapless one-dimensional (and higher!) systems. This class has many interesting properties, including an interpretation as a renormalisation group. This has sparked interest in a wide range of field, from quantum information to string theory.

2.1 Introduction to Tensor Network Notation

One of the primary reasons that tensor networks are so useful is the straightforward and transparent notation usually used to describe them. Using a graphical language, the structure is manifest. Many general properties of the objects under study, particularly quantum states, can be identified directly from the structure of the network needed to describe them.

Tensor network notation (TNN) can be considered a generalisation of Einstein summation notation. In this lecture we will define tensor networks, starting with an introduction to tensors and the operations we can perform upon them.

2.1.1 Tensors

Tensors are a generalisation of vectors and matrices. A d -dimensional vector can be considered an element of \mathbb{C}^d , and a $n \times m$ -dimensional matrix an element of $\mathbb{C}^{n \times m}$. Correspondingly a rank- r tensor of dimensions $d_1 \times \dots \times d_r$ is an element of $\mathbb{C}^{d_1 \times \dots \times d_r}$. We can clearly see that scalars, vectors and matrices are all therefore rank 0, 1 and 2 tensors respectively.

In tensor network notation a single tensor is simply represented by a geometric shape with legs sticking out of it, each corresponding to an index, analogous to the indices of Einstein notation. For example a rank-four tensor R would be represented as

$$R^\rho_{\sigma\mu\nu} \implies \textcircled{R} . \quad (2.1.1)$$

In some contexts the shape used and direction of the legs can imply certain properties of the tensor or index — for a general network however, neither carry any special significance. When representing quantum states, it is often convenient to use the direction of legs to denote whether the corresponding vectors live in the Hilbert space (‘kets’) or its dual (‘bras’). By adhering to this convention, certain prohibited contractions can be easily disallowed, such as contraction between two kets. This is notationally analogous to the convention of upper and lower denoting co- and contra-variant indices in Einstein or Penrose notation (a specialised form of TNN) employed in the study of general relativity or quantum field theory.

Because quantum mechanics, in contrast to general relativity, is complex, care has to be taken with complex conjugation. This is usually indicated either by explicitly labelling the tensor or adopting some index convention, such as flipping a network (upward and downward legs being exchanged) carrying an implicit conjugation.

2.1.2 Tensor operations

The main advantage in TNN comes in representing tensors that are themselves composed of several other tensors. The two main operations we will consider are those of the tensor product and trace, typically used in the joint operation of contraction. As well as these two operations, the rank of a tensor can be altered by grouping/splitting indices.

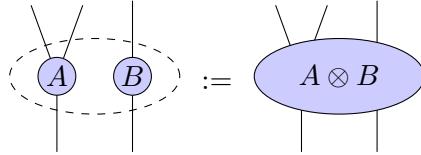
Tensor product

The first operation we will consider is the tensor product, a generalisation of the outer product of vectors. The value of the tensor product on a given set of indices is the element-wise product of the values of each constituent tensor. Explicitly written out in index notation, the binary tensor

product has the form:

$$[A \otimes B]_{i_1, \dots, i_r, j_1, \dots, j_s} := A_{i_1, \dots, i_r} \cdot B_{j_1, \dots, j_s}. \quad (2.1.2)$$

Diagrammatically the tensor product is simply represented by two tensors being placed next to each other. As such the value of a network containing disjoint tensors is simply the product of the constituent values.



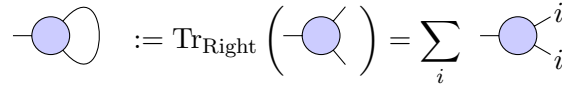
$$:= \quad (2.1.3)$$

Trace

The next operation is that of the (partial) trace. Given a tensor A , for which the x th and y th indices have identical dimensions ($d_x = d_y$), the partial trace over these two dimensions is simply a joint summation over that index:

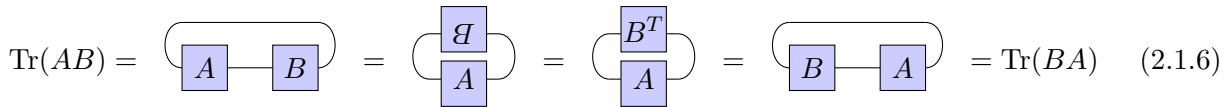
$$[\text{Tr}_{x,y} A]_{i_1, \dots, i_{x-1}, i_{x+1}, \dots, i_{y-1}, i_{y+1}, \dots, i_r} = \sum_{\alpha=1}^{d_x} A_{i_1, \dots, i_{x-1}, \alpha, i_{x+1}, \dots, i_{y-1}, \alpha, i_{y+1}, \dots, i_r} \quad (2.1.4)$$

Similar to Einstein notation, this summation is implicit in TNN, indicated by the corresponding legs being joined. An advantage over Einstein notation is that these summed-over indices need not be named, making the notation less clunky for large networks. For example, consider tracing over the two indices of a rank-3 tensor:



$$:= \text{Tr}_{\text{Right}} \left(\begin{array}{c} \text{---} \circ \text{---} \\ \text{---} \end{array} \right) = \sum_i \begin{array}{c} \text{---} \circ \text{---} \\ \text{---}^i \\ \text{---}_i \end{array} \quad (2.1.5)$$

One property of the trace we can trivially see from this notation is that of its cyclic property. By simply sliding one of the matrices around – which only changes the placement of the tensors in the network, and therefore not the value – we can cycle the matrices around (being careful of transpositions), proving $\text{Tr}(AB) = \text{Tr}(BA)$.



$$\text{Tr}(AB) = \quad (2.1.6)$$

Whilst this serves as a trivial example, the higher rank equivalents of this statement are not always so obvious, and the fact that these properties hold ‘more obviously’ in TNN is often useful.

Contraction

The most common tensor operation used is *contraction*, corresponding to a tensor product followed by a trace between indices of the two tensors. An example would be the contraction between two pairs of indices of two rank-3 tensors, which is drawn as:

$$\text{---} \circ \text{---} := \sum_{i,j} \text{---} \overset{i}{\circ} \text{---} \underset{j}{\circ} \text{---} \quad (2.1.7)$$

Familiar examples of contraction are vector inner products, matrix-vector multiplication, matrix-matrix multiplication, and the trace of a matrix:

Conventional	Einstein	TNN
$\langle \vec{x}, \vec{y} \rangle$	$x_\alpha y^\alpha$	
$M\vec{v}$	$M^\alpha_\beta v^\beta$	
AB	$A^\alpha_\beta B^\beta_\gamma$	
$\text{Tr}(X)$	X^α_α	

Grouping and splitting

Rank is a rather fluid concept in the study of tensor networks. The space of tensors $\mathbb{C}^{a_1 \times \dots \times a_n}$ and $\mathbb{C}^{b_1 \times \dots \times b_m}$ are isomorphic as vector spaces whenever the overall dimensions match ($\prod_i a_i = \prod_i b_i$). Using this we can extend concepts and techniques only previously defined for vectors and matrices to all tensors. To do this, we can *group* or *split* indices to lower or raise the rank of a given tensor respectively.

Consider the case of contracting two arbitrary tensors. If we group together the indices which are and are not involved in this contraction, this procedure simply reduces to matrix multiplication:

$$\text{---} \circ \text{---} = \text{---} \circ \text{---} = \text{---} \text{---} \quad (2.1.8)$$

It should be noted that not only is this reduction to matrix multiplication pedagogically handy, but this is precisely the manner in which numerical tensor packages perform contraction, allowing them to leverage highly optimised matrix multiplication code.

Owing to the freedom in choice of basis, the precise details of grouping and splitting are not unique. One specific choice of convention is the *tensor product basis*, defining a basis on the product space simply given by the product of the respective bases. The canonical use of tensor product bases in quantum information allows for the grouping and splitting described above to be dealt with implicitly. Statements such as $|0\rangle \otimes |1\rangle \equiv |01\rangle$ omit precisely this grouping: notice that the tensor product on the left is a 2×2 dimensional matrix, whilst the right hand-side is a 4-dimensional vector. The ‘tensor product’ used in quantum information is often in fact a *Kronecker product*, given by a true tensor product followed by just such a grouping.

More concretely, suppose we use an index convention that can be considered a higher-dimensional generalisation of column-major ordering. If we take a rank $n+m$ tensor, and group its first n indices and last m indices together to form a matrix

$$T_{I,J} := T_{i_1, \dots, i_n; j_1, \dots, j_m} \quad (2.1.9)$$

where we have defined our grouped indices as

$$I := i_1 + d_1^{(i)} \cdot i_2 + d_1^{(i)} d_2^{(i)} \cdot i_3 + \dots + d_1^{(i)} \dots d_{n-1}^{(i)} \cdot i_n, \quad (2.1.10)$$

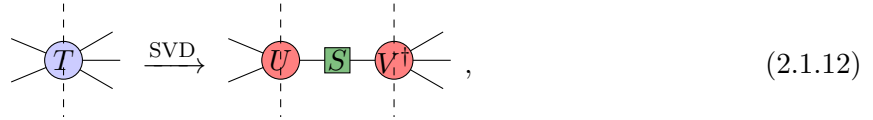
$$J := j_1 + d_1^{(j)} \cdot j_2 + d_1^{(j)} d_2^{(j)} \cdot j_3 + \dots + d_1^{(j)} \dots d_{m-1}^{(j)} \cdot j_m, \quad (2.1.11)$$

where $d_x^{(i)}$ ($d_x^{(j)}$) is the dimension of the x th index of type i (j). When such a grouping is given, we can now treat this tensor as a matrix, performing standard matrix operations.

An important example is the singular value decomposition (SVD), given by $T_{I,J} = \sum_{\alpha} U_{I,\alpha} S_{\alpha,\alpha} \bar{V}_{J,\alpha}$. By performing the above grouping, followed by the SVD, and then splitting the indices back out, we get a higher dimensional version of the SVD

$$T_{i_1, \dots, i_n; j_1, \dots, j_m} = \sum_{\alpha} U_{i_1, \dots, i_n, \alpha} S_{\alpha, \alpha} \bar{V}_{j_1, \dots, j_m, \alpha}.$$

So long as we choose them to be consistent, the precise method by which we group and split is immaterial in this overall operation. As a result we will keep this grouping purely implicit, as in the first equality Equation (2.1.8). This will be especially useful for employing notions defined for matrices and vectors to higher rank objects, implicitly grouping then splitting. Graphically the above SVD will simply be denoted



where U and V are isometric ($U^\dagger U = V^\dagger V = \mathbb{1}$) across the indicated partitioning, and where the conjugation in V^\dagger is included for consistency with conventional notation and also taken with respect to this partitioning. We will refer to such a partitioning of the indices in to two disjoint sets as a *bisection* of the tensor.

Aside 1: Why do we care so much about the singular value decomposition?

One of the main uses of tensor networks in quantum information is representing states which belong to small but physically relevant corners of an otherwise prohibitively large Hilbert space, such as low-entanglement states. The central backbone of this idea is that of low matrix-rank approximations. Suppose we have some matrix, and we want the ideal low matrix-rank approximation thereof. Eckart and Young [2.1.1] showed that if we measure error in the Frobenius norm, then trimming the singular value decomposition is an ideal approximation. Specifically take $X = USV^\dagger$ to be the SVD of X , then the trimmed version of X is given by

$$X^{(k)} = US^{(k)}V^\dagger$$

where $S^{(k)}$ has had all but the largest k singular values set to zero (i.e. has matrix-rank k), then Eckart-Young theorem says that $\|X - X^{(k)}\|_F \leq \|X - Y\|_F$ for all Y of matrix-rank k . Mirsky further generalised this result in Ref. [2.1.2] to show optimality in all unitarily invariant norms. Whenever we use the term *trim*, we are referring to this very method of low-rank approximation.

2.1.3 Tensor networks

Combining the above tensor operations, we can now give a single definition of a tensor network. A tensor network is a diagram which tells us how to combine several tensors into a single composite tensor. The rank of this overall tensor is given by the number of unmatched legs in the diagram. The value for a given configuration of external indices, is given by the product of the values of the

constituent tensors, summed over all internal index labellings consistent with the contractions. A generic example of this is given below:

$$\begin{array}{c} \diagup \quad \diagdown \\ \circ \quad \circ \\ \diagdown \quad \diagup \\ \circ \quad \circ \\ \diagup \quad \diagdown \\ \circ \quad \circ \\ \diagdown \quad \diagup \\ \circ \quad \circ \end{array} = \begin{array}{c} \diagup \quad \diagdown \\ \circ \\ \diagdown \quad \diagup \end{array} \quad \text{where} \quad \begin{array}{c} i \quad j \\ \circ \\ \diagdown \quad \diagup \end{array} := \sum_{\substack{\alpha, \beta, \gamma, \delta \\ \epsilon, \zeta, \eta}} \prod \left\{ \begin{array}{c} i \quad j \\ \circ \quad \circ \\ \alpha \quad \beta \quad \gamma \quad \epsilon \\ \beta \quad \epsilon \quad \zeta \quad \eta \\ \alpha \quad \delta \quad \delta \quad \zeta \quad \eta \\ \circ \quad \circ \end{array} \right\} \quad (2.1.13)$$

2.1.4 Bubbling

Whilst tensor networks are defined in such a way that their values are independent of the order in which the constituent tensors are contracted, such considerations do influence the complexity and practicality of such computations. Tensor networks can be contracted by beginning with a single tensor and repeatedly contracting it against tensors one-at-a-time. The order in which tensors are introduced and contracted is known as a *bubbling*. As the bubbling is performed the network is swallowed into the stored tensor, until only the result remains.

Many networks admit both efficient and inefficient bubbings, highlighting the need for prudence when planning out contractions. Take for example a ladder-shaped network (we'll see a few of these in the following lectures). One bubbling we may consider is to contract along the top of the ladder, then back along the bottom. Showing both this bubbling, as well as the partially contracted tensor that is kept in memory (in red), we see this bubbling looks like:

$$\begin{array}{c} \circ \quad \circ \quad \circ \\ \diagdown \quad \diagup \\ \circ \quad \circ \quad \circ \\ \diagdown \quad \diagup \\ \circ \quad \circ \quad \circ \\ \diagdown \quad \diagup \\ \circ \quad \circ \quad \circ \end{array} \rightarrow \begin{array}{c} \circ \quad \circ \quad \circ \\ \diagdown \quad \diagup \\ \circ \quad \circ \quad \circ \\ \diagdown \quad \diagup \\ \circ \quad \circ \quad \circ \\ \diagdown \quad \diagup \\ \circ \quad \circ \quad \circ \end{array} \rightarrow \begin{array}{c} \circ \quad \circ \quad \circ \\ \diagdown \quad \diagup \\ \circ \quad \circ \quad \circ \\ \diagdown \quad \diagup \\ \circ \quad \circ \quad \circ \\ \diagdown \quad \diagup \\ \circ \quad \circ \quad \circ \end{array} \rightarrow \begin{array}{c} \circ \quad \circ \quad \circ \\ \diagdown \quad \diagup \\ \circ \quad \circ \quad \circ \\ \diagdown \quad \diagup \\ \circ \quad \circ \quad \circ \\ \diagdown \quad \diagup \\ \circ \quad \circ \quad \circ \end{array} \rightarrow \begin{array}{c} \circ \quad \circ \quad \circ \\ \diagdown \quad \diagup \\ \circ \quad \circ \quad \circ \\ \diagdown \quad \diagup \\ \circ \quad \circ \quad \circ \\ \diagdown \quad \diagup \\ \circ \quad \circ \quad \circ \end{array} \rightarrow \begin{array}{c} \circ \quad \circ \quad \circ \\ \diagdown \quad \diagup \\ \circ \quad \circ \quad \circ \\ \diagdown \quad \diagup \\ \circ \quad \circ \quad \circ \\ \diagdown \quad \diagup \\ \circ \quad \circ \quad \circ \end{array} \quad (2.1.14)$$

$$\begin{array}{c} \circ \quad \circ \quad \circ \\ \diagdown \quad \diagup \\ \circ \quad \circ \quad \circ \\ \diagdown \quad \diagup \\ \circ \quad \circ \quad \circ \\ \diagdown \quad \diagup \\ \circ \quad \circ \quad \circ \end{array} \rightarrow \begin{array}{c} \circ \quad \circ \quad \circ \\ \diagdown \quad \diagup \\ \circ \quad \circ \quad \circ \\ \diagdown \quad \diagup \\ \circ \quad \circ \quad \circ \\ \diagdown \quad \diagup \\ \circ \quad \circ \quad \circ \end{array} \rightarrow \begin{array}{c} \circ \quad \circ \quad \circ \\ \diagdown \quad \diagup \\ \circ \quad \circ \quad \circ \\ \diagdown \quad \diagup \\ \circ \quad \circ \quad \circ \\ \diagdown \quad \diagup \\ \circ \quad \circ \quad \circ \end{array} \rightarrow \begin{array}{c} \circ \quad \circ \quad \circ \\ \diagdown \quad \diagup \\ \circ \quad \circ \quad \circ \\ \diagdown \quad \diagup \\ \circ \quad \circ \quad \circ \\ \diagdown \quad \diagup \\ \circ \quad \circ \quad \circ \end{array} \rightarrow \begin{array}{c} \circ \quad \circ \quad \circ \\ \diagdown \quad \diagup \\ \circ \quad \circ \quad \circ \\ \diagdown \quad \diagup \\ \circ \quad \circ \quad \circ \\ \diagdown \quad \diagup \\ \circ \quad \circ \quad \circ \end{array} \rightarrow \begin{array}{c} \circ \quad \circ \quad \circ \\ \diagdown \quad \diagup \\ \circ \quad \circ \quad \circ \\ \diagdown \quad \diagup \\ \circ \quad \circ \quad \circ \\ \diagdown \quad \diagup \\ \circ \quad \circ \quad \circ \end{array} \rightarrow \begin{array}{c} \circ \quad \circ \quad \circ \\ \diagdown \quad \diagup \\ \circ \quad \circ \quad \circ \\ \diagdown \quad \diagup \\ \circ \quad \circ \quad \circ \\ \diagdown \quad \diagup \\ \circ \quad \circ \quad \circ \end{array} \quad (2.1.15)$$

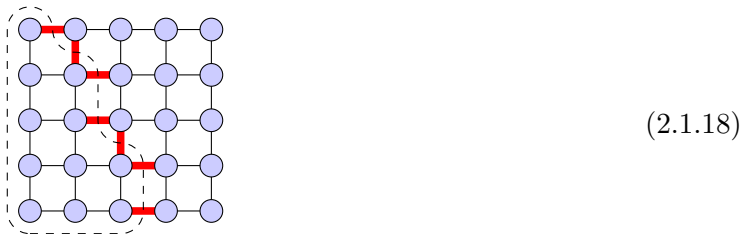
The scaling of this procedure is however quite unfavourable; consider a ladder of length n . At the midpoint of this contraction, when the top has been contracted, the tensor being tracked has rank n , and thus the number of entries is scaling exponentially with n . As such the memory and time footprints of this contraction are also exponential, rendering it infeasible for large n . If however we contract each rung in turn, the tracked tensor has a rank never more than 3, giving constant memory and linear time costs.

$$\begin{array}{c} \circ \quad \circ \quad \circ \\ \diagdown \quad \diagup \\ \circ \quad \circ \quad \circ \\ \diagdown \quad \diagup \\ \circ \quad \circ \quad \circ \\ \diagdown \quad \diagup \\ \circ \quad \circ \quad \circ \end{array} \rightarrow \begin{array}{c} \circ \quad \circ \quad \circ \\ \diagdown \quad \diagup \\ \circ \quad \circ \quad \circ \\ \diagdown \quad \diagup \\ \circ \quad \circ \quad \circ \\ \diagdown \quad \diagup \\ \circ \quad \circ \quad \circ \end{array} \rightarrow \begin{array}{c} \circ \quad \circ \quad \circ \\ \diagdown \quad \diagup \\ \circ \quad \circ \quad \circ \\ \diagdown \quad \diagup \\ \circ \quad \circ \quad \circ \\ \diagdown \quad \diagup \\ \circ \quad \circ \quad \circ \end{array} \rightarrow \begin{array}{c} \circ \quad \circ \quad \circ \\ \diagdown \quad \diagup \\ \circ \quad \circ \quad \circ \\ \diagdown \quad \diagup \\ \circ \quad \circ \quad \circ \\ \diagdown \quad \diagup \\ \circ \quad \circ \quad \circ \end{array} \rightarrow \begin{array}{c} \circ \quad \circ \quad \circ \\ \diagdown \quad \diagup \\ \circ \quad \circ \quad \circ \\ \diagdown \quad \diagup \\ \circ \quad \circ \quad \circ \\ \diagdown \quad \diagup \\ \circ \quad \circ \quad \circ \end{array} \rightarrow \begin{array}{c} \circ \quad \circ \quad \circ \\ \diagdown \quad \diagup \\ \circ \quad \circ \quad \circ \\ \diagdown \quad \diagup \\ \circ \quad \circ \quad \circ \\ \diagdown \quad \diagup \\ \circ \quad \circ \quad \circ \end{array} \quad (2.1.16)$$

$$\begin{array}{c} \circ \quad \circ \quad \circ \\ \diagdown \quad \diagup \\ \circ \quad \circ \quad \circ \\ \diagdown \quad \diagup \\ \circ \quad \circ \quad \circ \\ \diagdown \quad \diagup \\ \circ \quad \circ \quad \circ \end{array} \rightarrow \begin{array}{c} \circ \quad \circ \quad \circ \\ \diagdown \quad \diagup \\ \circ \quad \circ \quad \circ \\ \diagdown \quad \diagup \\ \circ \quad \circ \quad \circ \\ \diagdown \quad \diagup \\ \circ \quad \circ \quad \circ \end{array} \rightarrow \begin{array}{c} \circ \quad \circ \quad \circ \\ \diagdown \quad \diagup \\ \circ \quad \circ \quad \circ \\ \diagdown \quad \diagup \\ \circ \quad \circ \quad \circ \\ \diagdown \quad \diagup \\ \circ \quad \circ \quad \circ \end{array} \rightarrow \begin{array}{c} \circ \quad \circ \quad \circ \\ \diagdown \quad \diagup \\ \circ \quad \circ \quad \circ \\ \diagdown \quad \diagup \\ \circ \quad \circ \quad \circ \\ \diagdown \quad \diagup \\ \circ \quad \circ \quad \circ \end{array} \rightarrow \begin{array}{c} \circ \quad \circ \quad \circ \\ \diagdown \quad \diagup \\ \circ \quad \circ \quad \circ \\ \diagdown \quad \diagup \\ \circ \quad \circ \quad \circ \\ \diagdown \quad \diagup \\ \circ \quad \circ \quad \circ \end{array} \rightarrow \begin{array}{c} \circ \quad \circ \quad \circ \\ \diagdown \quad \diagup \\ \circ \quad \circ \quad \circ \\ \diagdown \quad \diagup \\ \circ \quad \circ \quad \circ \\ \diagdown \quad \diagup \\ \circ \quad \circ \quad \circ \end{array} \rightarrow \begin{array}{c} \circ \quad \circ \quad \circ \\ \diagdown \quad \diagup \\ \circ \quad \circ \quad \circ \\ \diagdown \quad \diagup \\ \circ \quad \circ \quad \circ \\ \diagdown \quad \diagup \\ \circ \quad \circ \quad \circ \end{array} \quad (2.1.17)$$

The memory footprint at any step during the contraction corresponds to the product of the dimensions of each leg passing through the boundary of the contracted region (see the red legs in Eqn. (2.1.18)). Whilst the above ladder arrangement possesses both good and bad bubbings, some networks possess an underlying graph structure that does not admit *any* efficient contraction ordering. A good example of this is the 2D grid; due to the 2D structure of this lattice, it is clear that the contracted region must, somewhere near the middle of the contracting procedure, have a perimeter on the order of \sqrt{n} where n is the number of tensors. As a result such contractions

generically take exponential time/memory to perform. An example of a high cost step during such a bubbling is shown below, with the prohibitively large perimeter indicated by the red legs.



Although the bubblings we have depicted here involve picking a single tensor and contracting others into it one-by-one, this will frequently not be the most efficient order; often a multibubbling approach is faster. Ref. [2.1.3] provides code which allows for finding optimal bubbling order for networks of up to 30-40 tensors. This code interfaces with that provided in Ref. [2.1.4] and Ref. [2.1.5], providing a complete tensor network package.

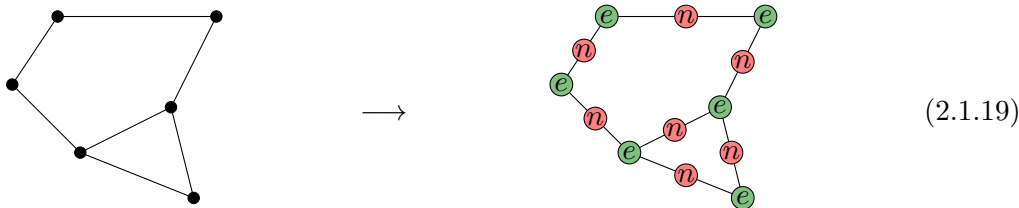
2.1.5 Computational Complexity

Above we've described that there exist networks which stymie the specific contraction procedures we've outlined. In this section we'll see that there also exist networks for which there are complexity theoretic obstructions which do not allow for *any* contraction procedure to be efficient.

We will now consider the computational complexity associated with tensor network contractions. Whilst all of the tensor networks we will consider in later lectures constitute memory-efficient representations of objects such as quantum states, not all permit efficient manipulation. This demonstrates that how one wishes to manipulate a tensor network is an important part of considering them as ansätze.

Whilst algorithms which can speed up tensor network contractions by optimising the bubbling used [2.1.3–2.1.5], as discussed above, the underlying computational problem is NP-complete [2.1.6, 2.1.7]

Even ignoring the specific bubbling used, the complexity of the overall contraction procedure can also be shown to be prohibitive in general. Consider a network made from the binary tensors e and n . The value of e is 1 if and only if all indices are identical, and zero otherwise, whilst n has value 1 if and only if all legs differ and 0 otherwise. Take an arbitrary graph, and construct a tensor network with an e tensor at each vertex and n tensor in the middle of each edge, with the connectedness inherited from the graph.



By construction, the non-zero contributions to the above tensor network correspond to an assignment of index values to each vertex (enforced by e) of the original graph, such that no two neighbouring vertices share the same value (enforced by n). If each index is q -dimensional this is a vertex q -colouring of the graph, and the value of the tensor network corresponds to the number of

such q -colourings. As determining the existence of a q -colouring is an NP-complete problem [2.1.8], contracting this graph is therefore #P-complete [2.1.9]. Indeed similar constructions exist for tensor networks corresponding to #SAT and other #P-complete problems [2.1.10]. As we will see later in Section 2.6, there also exists a quantum hardness result which shows approximate contraction to be Post-BQP-hard, putting it inside a class of problems not believed to be efficiently solvable on even a quantum computer.

Problems 1

Solutions in Appendix 2.B

1. Consider the following tensors, in which all indices are three-dimensional, indexed from 0:

$$\begin{matrix} \textcircled{A} \\ | \\ j \\ - \\ i \end{matrix} = i^2 - 2j, \qquad \begin{matrix} i \\ / \\ \textcircled{B} \\ - \\ k \\ \backslash \\ j \end{matrix} = -3^i j + k, \qquad (2.1.20)$$

$$\begin{matrix} j \\ | \\ \textcircled{C} \\ - \\ i \end{matrix} = j, \qquad \begin{matrix} i \\ - \\ \textcircled{D} \\ / \\ j \\ \backslash \\ k \end{matrix} = ijk. \qquad (2.1.21)$$

Calculate the value of the following tensor network:

$$(2.1.22)$$

2. In this question we are going to consider expanding out a contraction sequence, in a manner which would be needed when coding up contractions. Given a network, and an associated bubbling, we wish to write out a table keeping track of the indices of the current object, the tensor currently being contracted in, the indices involved in that contraction, and new indices left uncontracted. For example for the network

$$(2.1.23)$$

where the bubbling is performed in alphabetical order, then the table in question looks like

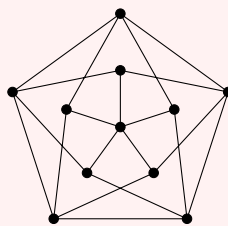
Current	Tensor	Contract	New
-	A	-	α, β
α, β	B	α	γ
β, γ	C	β, γ	δ

For the tensor network

$$(2.1.24)$$

construct a corresponding table, where contraction is once again done in alphabetical order.

3. (a) Calculate the contraction of the tensor network in Equation (2.1.19) for bond dimension 3, i.e. calculate the number of three-colourings of the corresponding graph.
- (b) Using the e and n tensors from Section 2.1.5, come up with a construction for a tensor network which gives the number of *edge* colourings. For a planar graphs, construct an analogous network to count *face* colourings.
- (c) Using tensor networks, determine the minimum number of colours required to vertex and edge colour the below graph (known as the chromatic number and index respectively).



$$(2.1.25)$$

4. Much like the singular value decomposition, given a bisection of the indices we can consider norms of tensors.
 - (a) Does the operator norm depend on the bisection, i.e. are the operator norms across any two bisections of the same tensor necessarily equal?
 - (b) What about the Frobenius norm? If they can differ, give an example, if not draw a tensor network diagram that shows it to be manifestly independent of bisection.
5. Write out the Einstein notation corresponding to the network in Equation (2.7.1).

Bibliography

- 2.1.1 C. Eckart and G. Young, The approximation of one matrix by another of lower rank, [Psychometrika](#) **1**, (1936).
- 2.1.2 L. Mirsky, Symmetric gauge functions and unitarily invariant norms, [The Quarterly Journal of Mathematics](#) **11**, 1, 50–59, (1960).
- 2.1.3 R. N. C. Pfeifer, J. Haegeman, and F. Verstraete, Faster identification of optimal contraction sequences for tensor networks, [Physical Review E](#) **90** 033315, [arXiv:1304.6112](#), (2014).
- 2.1.4 R. N. C. Pfeifer, G. Evenbly, S. Singh, and G. Vidal, NCON: A tensor network contractor for MATLAB, [arXiv:1402.0939](#), (2014).

- 2.1.5 G. Evenbly and R. N. C. Pfeifer, Improving the efficiency of variational tensor network algorithms, [Physical Review B](#) **89** 245118, [arXiv:1402.0939](#), (2014).
- 2.1.6 I. Arad and Z. Landau, Quantum computation and the evaluation of tensor networks, [SIAM Journal on Computing](#) **39** 3089, [arXiv:0805.0040](#), (2010).
- 2.1.7 L. Chi-Chung, P. Sadayappan, and R. Wenger, On Optimizing a Class of Multi-Dimensional Loops with Reduction for Parallel Execution, [Parallel Processing Letters](#) **07** 157–168, (1997).
- 2.1.8 M. R. Garey, D. S. Johnson, and L. Stockmeyer, Some simplified NP-complete problems, in [Proceedings of the sixth annual ACM symposium on Theory of computing - STOC '74](#), 47–63, ACM Press, (1974).
- 2.1.9 M. Dyer, L. A. Goldberg, C. Greenhill, and M. Jerrum, The Relative Complexity of Approximate Counting Problems, [Algorithmica](#) **38** 471–500, (2004).
- 2.1.10 J. D. Biamonte, J. Morton, and J. Turner, Tensor Network Contractions for #SAT, [Journal of Statistical Physics](#) **160** 1389–1404, [arXiv:1405.7375](#), (2015).

2.2 Quantum information examples

In this lecture we will cover a few examples of concepts in quantum information which can be better understood in tensor network notation. This lecture won't serve as much as an introduction to these concepts, but instead as a Rosetta stone for those familiar with quantum information and not with TNN. For a more thorough introduction to quantum information see the textbooks of Refs. [2.2.1–2.2.3] or lecture notes of Refs. [2.2.4,2.2.5]. We note that for the study of open quantum systems, a more specialised form of TNN was developed in Ref. [2.2.6].

2.2.1 Bell state and the Bell basis

The Bell basis forms a convenient orthonormal set of two qubit states that exhibit maximal entanglement. The standard notation for this basis is

$$|\Phi^\pm\rangle := (|0\rangle \otimes |0\rangle \pm |1\rangle \otimes |1\rangle)/\sqrt{2} \quad \text{and} \quad |\Psi^\pm\rangle := (|0\rangle \otimes |1\rangle \pm |1\rangle \otimes |0\rangle)/\sqrt{2}.$$

The first of this basis, $|\Phi^+\rangle$, we shall denote $|\Omega\rangle$ and simply refer to as *the* Bell state. Thought of as a matrix, Ω is proportional to the one qubit identity,

$$|\Omega\rangle = \frac{1}{\sqrt{2}} \begin{pmatrix} 1 \\ 0 \\ 0 \\ 1 \end{pmatrix} \xrightleftharpoons[\text{Matricise}]{\text{Vectorise}} \frac{1}{\sqrt{2}} \begin{pmatrix} 1 & 0 \\ 0 & 1 \end{pmatrix} = I/\sqrt{2}. \quad (2.2.1)$$

In tensor network notation, this is represented simply as a line connecting its two legs.

$$\boxed{\Omega} = \frac{1}{\sqrt{2}} \text{---} \cup \text{---} \quad (2.2.2)$$

Next we will define $\Omega(O)$ to be the vectorisation of an operator O , such that $|\Omega(O)\rangle = (O \otimes I)|\Omega\rangle$.

$$\boxed{\Omega(O)} = \frac{1}{\sqrt{2}} \text{---} \boxed{O} \text{---} \cup \text{---} \quad (2.2.3)$$

Given this definition, we can see that the Bell basis simply corresponds to a vectorisation of the Pauli operators

$$|\Phi^+\rangle = |\Omega(I)\rangle, \quad |\Phi^-\rangle = |\Omega(Z)\rangle, \quad |\Psi^+\rangle = |\Omega(X)\rangle, \quad |\Psi^-\rangle \propto |\Omega(Y)\rangle.$$

Thus we see that the Bell basis is intimately linked to the Pauli operators, with the Euclidean inner product on Bell basis states corresponding to the Hilbert-Schmidt inner product on Paulis.

2.2.2 Quantum Teleportation

Given this notation for the Bell basis, we can now understand Quantum Teleportation in TNN. The idea here is for two parties (Alice and Bob, say) to share a Bell state. Given this shared resource of entanglement, we then allow Alice to perform local operations on her half of the pair, and an arbitrary fiducial qubit. After transmitting only two classical bits, Bob can then correct his half of the pair such that he recovers the state of the original fiducial qubit, successfully teleporting the data within.

The procedure for teleportation goes as follows. First Alice performs a projective measurement in the Bell basis on both the fiducial qubit and her Bell qubit, receiving outcome $|\Omega(p)\rangle$. The result of this measurement is then (classically) transmitted to Bob, requiring two communication bits. Bob then performs the corresponding Pauli p on his Bell qubit, correcting the influence of the measurement. Taking the fiducial state to be $|\psi\rangle$, and supposing the measurement outcome corresponds to $|\Omega(p)\rangle$, then this procedure gives Bob a final state of $|\phi\rangle = |\psi\rangle/2$:

$$|\phi\rangle = \overbrace{\left(p_B\right)}^{\text{Correction}} \overbrace{\left(\langle\Omega_{A_1A_2}(p)|\right)}^{\text{Teleportation}} \overbrace{\left(|\psi_{A_1}\rangle \otimes |\Omega_{A_2B}\rangle\right)}^{\text{Setup}} = |\psi\rangle/2 \quad (2.2.4)$$

where A_1 and A_2 correspond to the single qubit registers of Alice, and B to Bob's qubit. In tensor network notation this can be clearly seen:

$$|\phi\rangle = \begin{array}{c} \begin{array}{c} \frac{1}{\sqrt{2}} \begin{array}{c} \boxed{p^\dagger} \text{---} \boxed{\psi} \\ \text{Alice} \end{array} \\ \text{---} \end{array} \\ \text{---} \end{array} \begin{array}{c} \frac{1}{\sqrt{2}} \\ \text{Bob} \end{array} \quad (2.2.5)$$

$$= \frac{1}{2} \text{---} \boxed{p} \text{---} \boxed{p^\dagger} \text{---} \boxed{\psi} \quad (2.2.6)$$

$$= |\psi\rangle/2 \quad (2.2.7)$$

where the dashed line indicates the physical separation of the two parties.

As such we can see that $|\psi\rangle$ is correctly transmitted for any measurement outcome p , each of which is seen with probability $1/4$. Thus we see that in spite of the non-deterministic intermediary states, the overall procedure is deterministic. Analogous procedures can work for p being elements of any set of operators which are orthonormal with respect to the Hilbert-Schmidt inner product, e.g. higher dimensional Paulis.

Gate Teleportation

The idea behind gate teleportation is similar to regular teleportation, but utilises a general maximally entangled state instead of the Bell state specifically. Suppose we prepare a maximally entangled state $|\Omega(U^T)\rangle$ corresponding to a unitary U , and post select on a Bell basis measurement of $|\Omega(p)\rangle$, followed by a correcting unitary C_p , then Bob ends up with the state:

$$|\phi\rangle = \overbrace{\left(C_p\right)}^{\text{Correction}} \overbrace{\left(\langle\Omega_{A_1A_2}(p)|\right)}^{\text{Teleportation}} \overbrace{\left(|\psi_{A_1}\rangle \otimes |\Omega_{A_2B}(U^T)\rangle\right)}^{\text{Setup}} \quad (2.2.8)$$

$$= \begin{array}{c} \begin{array}{c} \frac{1}{\sqrt{2}} \begin{array}{c} \boxed{p^\dagger} \text{---} \boxed{\psi} \\ \text{Alice} \end{array} \\ \text{---} \end{array} \\ \text{---} \end{array} \begin{array}{c} \frac{1}{\sqrt{2}} \\ \text{Bob} \end{array} \quad (2.2.9)$$

$$= \frac{1}{2} \text{---} \boxed{C_p} \text{---} \boxed{U} \text{---} \boxed{p^\dagger} \text{---} \boxed{\psi} \quad (2.2.10)$$

$$= C_p U p^\dagger |\psi\rangle/2 \quad (2.2.11)$$

If we take $C_p := UpU^\dagger$ then Bob receives $U|\psi\rangle$ for all measurement outcomes, i.e. $|\phi\rangle \propto U|\psi\rangle$. If U is a Clifford operator¹, this correction is also a Pauli, making the procedure no more resource intensive in terms of the gates used than standard teleportation.

An example of where this is useful is in the case where Paulis can be reliably performed, but Cliffords can only be applied non-deterministically. Gate teleportation allows us to prepare the $|U^T\rangle$ first, simply retrying the non-deterministic procedure until it succeeds. Once this has succeeded, we can use gate teleportation to apply this unitary on the data state using only Pauli operations. As such we can avoid needing to apply non-deterministic gates directly on our target state, endangering the data stored within.

2.2.3 Purification

For a given mixed state ρ , a purification is a pure state $|\psi\rangle$ which is extended into a larger system (the added subsystem is known as the *purification system*), such that the reduced density on the original system is ρ . One such purification is given by $|\psi\rangle \propto (\sqrt{\rho} \otimes I)|\Omega\rangle = |\Omega(\sqrt{\rho})\rangle$, which can be simply seen by considering the corresponding tensor networks. The definition of the state is

$$\psi = \sqrt{\rho} \quad (2.2.12)$$

which gives a reduced density of

$$\text{Tr}_2(|\psi\rangle\langle\psi|) = \psi \psi = \sqrt{\rho} \sqrt{\rho} = \rho \quad (2.2.13)$$

By dimension counting, it can be shown that the above purification is unique up to an isometric freedom on the purification system, i.e. all purifications are of the form $(\sqrt{\rho} \otimes U)|\Omega\rangle$ where $U^\dagger U = \mathbb{1}$. Equivalently all purifications can be considered to be proportional to $(\sqrt{\rho} \otimes I)|\Omega\rangle$, where $|\Omega\rangle$ is some maximally entangled state other than the Bell state.

2.2.4 Stinespring’s Dilation Theorem

Stinespring’s Theorem says that any quantum channel \mathcal{E} – a completely positive trace preserving (CPTP) map – can be expressed as a unitary map V acting on a larger system followed by a partial trace, i.e.

$$\mathcal{E}(\rho) = \text{Tr}_1 \left[V^\dagger (\rho \otimes |0\rangle\langle 0|) V \right]. \quad (2.2.14)$$

Physically this means that dynamics of an open system is equivalent to those of a subsystem of a larger, closed system — the founding tennet of the Church of the Larger Hilbert Space. Any CPTP map can be represented by a set of Kraus operators K_i such that

$$\mathcal{E}(\rho) = \sum_i K_i^\dagger \rho K_i \quad \text{where} \quad \sum_i K_i K_i^\dagger = I. \quad (2.2.15)$$

¹The Cliffords are the group of unitaries which map Paulis to Paulis under conjugation.

In TNN this looks like

$$\text{---} \left[\begin{array}{c} \text{---} \\ \text{---} \end{array} \right] \rho \text{---} = \text{---} \left[\begin{array}{c} \text{---} \\ \text{---} \end{array} \right] K^\dagger \rho \left[\begin{array}{c} \text{---} \\ \text{---} \end{array} \right] K \text{---} \quad \text{where} \quad \text{---} \left[\begin{array}{c} \text{---} \\ \text{---} \end{array} \right] K \left[\begin{array}{c} \text{---} \\ \text{---} \end{array} \right] K^\dagger \text{---} = \text{---} \quad (2.2.16)$$

where the transposition in the Hermitian conjugate is done with respect to the horizontal legs, and the upper leg corresponds to the virtual index i .

Next we define the tensor U as

$$\left[\begin{array}{c} \text{---} \\ \text{---} \end{array} \right] U \text{---} := \text{---} \left[\begin{array}{c} \text{---} \\ \text{---} \end{array} \right] K^\dagger \text{---} \quad (2.2.17)$$

where we can see that U is an isometry ($U^\dagger U = I$), which we can think of as a unitary V with an omitted ancilla

$$\left[\begin{array}{c} \text{---} \\ \text{---} \end{array} \right] U \text{---} = \text{---} \left[\begin{array}{c} \text{---} \\ \text{---} \end{array} \right] V |0\rangle \text{---} . \quad (2.2.18)$$

Using this, and partial tracing over the upper index, we get the Stinespring Dilation Theorem as desired:

$$\mathcal{E}(\rho) = \sum_i K_i^\dagger \rho K_i = \text{---} \left[\begin{array}{c} \text{---} \\ \text{---} \end{array} \right] K^\dagger \rho \left[\begin{array}{c} \text{---} \\ \text{---} \end{array} \right] K \text{---} \quad (2.2.19)$$

$$= \text{---} \left[\begin{array}{c} \text{---} \\ \text{---} \end{array} \right] K^\dagger \rho \left[\begin{array}{c} \text{---} \\ \text{---} \end{array} \right] K \text{---} \quad (2.2.20)$$

$$= \text{---} \left[\begin{array}{c} \text{---} \\ \text{---} \end{array} \right] U \rho \left[\begin{array}{c} \text{---} \\ \text{---} \end{array} \right] U^\dagger \text{---} \quad (2.2.21)$$

$$= \text{---} \left[\begin{array}{c} \text{---} \\ \text{---} \end{array} \right] V |0\rangle \langle 0| \left[\begin{array}{c} \text{---} \\ \text{---} \end{array} \right] V^\dagger \text{---} \quad (2.2.22)$$

$$= \text{Tr}_1 \left[V^\dagger (\rho \otimes |0\rangle \langle 0|) V \right] \quad (2.2.23)$$

Problems 2

Solutions in Appendix 2.C

1. Consider the inverse of teleportation. Alice wishes to send classical bits to Bob, and possesses a quantum channel through which she can send Bob qubits. How many bits of information can be communicated in a single qubit? For simplicity consider the case where Bob can only perform projective measurements.
2. Suppose Alice and Bob initially shared a Bell pair. Does this pre-shared entanglement

resource boost the amount of classical information that can be successfully communicated, and if so by how much? *Hint: Notice that the four possible Bell states differ by a Pauli acting on a single qubit.*

Bibliography

- 2.2.1 M. A. Nielsen and I. L. Chuang, Quantum Computation and Quantum Information 10th Anniversary Edition, [Cambridge University Press](#), (2011).
- 2.2.2 N. D. Mermin, Quantum Computer Science: An Introduction, [Cambridge University Press](#), (2007), <http://www.lassp.cornell.edu/mermin/qcomp/CS483.html>.
- 2.2.3 M. M. Wilde, Quantum Information Theory, [Cambridge University Press](#), [arXiv:1106.1445](#) (2013).
- 2.2.4 J. Preskill, Quantum Computation, <http://www.theory.caltech.edu/people/preskill/ph229/>.
- 2.2.5 J. Watrous, Theory of Quantum Information and Introduction to Quantum Computing, <https://cs.uwaterloo.ca/watrous/LectureNotes.html>.
- 2.2.6 C. J. Wood, J. D. Biamonte, and D. G. Cory, Tensor networks and graphical calculus for open quantum systems, [Quantum Information and Computation](#) **15**, 0759, [arXiv:1111.6950](#), (2015).

2.3 Matrix Product States

Now that we have established the notation, the remaining lectures will examine some key tensor networks and algorithms for strongly interacting quantum many body systems. We begin with one dimensional models.

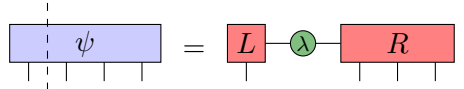
Matrix product states (MPS) are a natural choice for efficient representation of 1D quantum low energy states of physically realistic systems [2.3.1–2.3.6]. This lecture will begin by motivating and defining MPS in two slightly different ways. We will then give some analytic examples of MPS, demonstrating some of the complexity which can be captured with this simple network. Some simple properties of MPS will then be explained, followed by a generalisation of the network to operators rather than pure states.

Let $|\psi\rangle = \sum_{j_1, j_2, \dots, j_N=0}^{d-1} C_{j_1 j_2 \dots j_N} |j_1\rangle \otimes |j_2\rangle \otimes \dots \otimes |j_N\rangle$ be the (completely general) state of N qudits (d dimensional quantum system). The state is completely specified by knowledge of the rank- N tensor C .

By splitting the first index out from the rest, and performing an SVD, we get the Schmidt decomposition

$$|\psi\rangle = \sum_i \lambda_i |L_i\rangle \otimes |R_i\rangle, \quad (2.3.1)$$

where λ_i are the Schmidt weights and $\{|L_i\rangle\}$ and $\{|R_i\rangle\}$ are orthonormal sets of vectors. Graphically this looks like



$$\psi = L \lambda R, \quad (2.3.2)$$

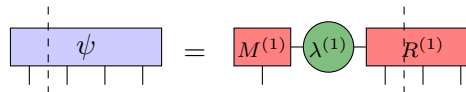
where λ is a diagonal matrix containing the Schmidt weights.

The α -Rényi entropy is given by

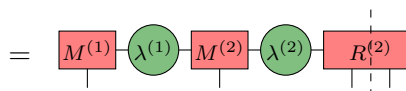
$$S_\alpha(\rho) = \frac{1}{1-\alpha} \log \text{Tr} \rho^\alpha, \quad (2.3.3)$$

where ρ is some density matrix. Note that the *entanglement rank* S_0 is simply the (log of the) number of nonzero Schmidt weights and the von Neumann entropy is recovered for $\alpha \rightarrow 1$. We also note that the Schmidt weights now correspond precisely to the singular values of the decomposition Equation (2.3.2), and so these values capture the entanglement structure along this cut.

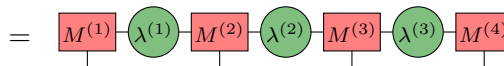
We can now perform successive singular value decompositions along each cut in turn, splitting out the tensor into local tensors M , and diagonal matrices of singular values λ quantifying the entanglement across that cut.



$$\psi = M^{(1)} \lambda^{(1)} R^{(1)} \quad (2.3.4)$$



$$= M^{(1)} \lambda^{(1)} M^{(2)} \lambda^{(2)} R^{(2)} \quad (2.3.5)$$



$$= M^{(1)} \lambda^{(1)} M^{(2)} \lambda^{(2)} M^{(3)} \lambda^{(3)} M^{(4)} \quad (2.3.6)$$

By now contracting² the singular values tensors $\lambda^{(i)}$ into the local tensors $M^{(i)}$ we get the more generic form

$$|\psi\rangle = \begin{array}{c} \boxed{A^{(1)}} \text{---} \boxed{A^{(2)}} \text{---} \boxed{A^{(3)}} \text{---} \boxed{A^{(4)}} \\ | \quad | \quad | \quad | \\ \cdot \end{array} \quad (2.3.7)$$

This is the *matrix product state*. It is not yet clear that we have done anything useful. The above construction is both general and exact, so we have the same number of coefficients in an arguably much more complicated form.

Suppose however we consider states for which the entanglement rank across any bisection of the chain is bounded. In particular, suppose that only D of the Schmidt weights were non-zero. Then we can use the MPS form to take advantage of this by truncating the λ matrix to make use of this property. In particular, any state with a so-called *strong area law* such that $S_0 \leq \log c$ for some constant c along any bipartition can be expressed (exactly) using an MPS with only $\mathcal{O}(dNc^2)$ coefficients. As discussed in Section 2.5, there are many relevant states for which an area law for the von Neumann entropy ($S_1 = \mathcal{O}(1)$) is sufficient to guarantee arbitrarily good approximation with an MPS of only $\text{poly}(N)$ bond dimension [2.3.1–2.3.3].

In TNN, the name matrix product state is a misnomer, as most tensors involved are in fact rank-3. The uncontracted index is referred to as the *physical* index, whilst the other two are *virtual*, *bond* or *matrix* indices. For reasons of convenience, as well as to capture periodic states most efficiently, the MPS ansatz is usually modified from Eqn. (2.3.7) to

$$\left| \psi \left[A^{(1)}, A^{(2)}, \dots, A^{(N)} \right] \right\rangle = \sum_{i_1 i_2 \dots i_N} \text{Tr} \left[A_{i_1}^{(1)} A_{i_2}^{(2)} \dots A_{i_N}^{(N)} \right] |i_1 i_2 \dots i_N\rangle, \quad (2.3.8)$$

or in the translationally invariant case

$$|\psi[A]\rangle = \sum_{i_1 i_2 \dots i_N} \text{Tr} [A_{i_1} A_{i_2} \dots A_{i_N}] |i_1 i_2 \dots i_N\rangle. \quad (2.3.9)$$

Note that in this form the matrix indices are suppressed and matrix multiplication is implied. The graphical form of this MPS is

$$|\psi[A]\rangle = \begin{array}{c} \boxed{} \text{---} \boxed{} \text{---} \boxed{} \text{---} \boxed{} \text{---} \boxed{} \text{---} \boxed{} \text{---} \boxed{} \text{---} \boxed{} \text{---} \boxed{} \\ | \quad | \quad | \quad | \quad | \quad | \quad | \quad | \quad | \\ \cdot \end{array} \quad (2.3.10)$$

2.3.1 1D Projected Entangled Pair States

In addition to the above construction, MPS can (equivalently) be viewed as a special case of the *projected entangled pair states* (PEPS) construction [2.3.2, 2.3.7, 2.3.8]. This proceeds by laying out entangled pair states $|\phi\rangle$ on some lattice and applying some linear map \mathcal{P} between pairs

$$|\psi\rangle = \begin{array}{c} \text{---} \text{---} \text{---} \text{---} \text{---} \text{---} \text{---} \text{---} \text{---} \text{---} \\ \circ \text{---} \circ \text{---} \circ \text{---} \circ \text{---} \circ \text{---} \circ \text{---} \circ \text{---} \circ \text{---} \circ \\ \mathcal{P} \quad \mathcal{P} \quad \mathcal{P} \quad \mathcal{P} \quad \mathcal{P} \quad \mathcal{P} \quad \mathcal{P} \quad \mathcal{P} \quad \mathcal{P} \\ \bullet \quad \bullet \quad \bullet \quad \bullet \quad \bullet \quad \bullet \quad \bullet \quad \bullet \quad \bullet \end{array}, \quad (2.3.11)$$

where

$$|\phi\rangle = \bullet \text{---} \bullet \quad (2.3.12)$$

²Into precisely which tensor the singular values are contracted can be important, and relates to gauge fixing the MPS, see Section 2.3.3.

is the chosen entangled pair. In Lecture 2.6, we will generalise this construction to arbitrary dimensions and arbitrary lattices.

It is clear that this construction is equivalent to the tensor network construction by letting $|\phi\rangle = \sum_{j=0}^{d-1} |dd\rangle$. We can write the linear map \mathcal{P} as

$$\mathcal{P} = \sum_{i,\alpha,\beta} A_{i;\alpha,\beta} |i\rangle \langle \alpha\beta|. \quad (2.3.13)$$

The tensor A is exactly the MPS tensor introduced above, and the choice of entangled pair ensures that the A tensor corresponding to a pair of PEPS ‘projectors’ applied to the Bell state above is exactly the contraction of the corresponding A tensors:

$$\mathcal{P}^{(1)} \otimes \mathcal{P}^{(2)} |\phi\rangle_{2,3} = \sum_{i_1, i_2; \alpha_1, \beta_1, \alpha_2, \beta_2, j} A_{i_1; \alpha_1, \beta_1}^{(1)} A_{i_2; \alpha_2, \beta_2}^{(2)} |i_1 i_2\rangle \langle \alpha_1 \beta_1 \alpha_2 \beta_2 | (\mathbb{1} \otimes |jj\rangle \otimes \mathbb{1}) \quad (2.3.14)$$

$$= \sum_{i_1, i_2; \alpha_1, \beta_1, \beta_2} A_{i_1; \alpha_1, \beta_1}^{(1)} A_{i_2; \beta_1, \beta_2}^{(2)} |i_1 i_2\rangle \langle \alpha_1 \beta_2|. \quad (2.3.15)$$

Thus, we see that the two descriptions are equivalent, and interchanged through the applications of local unitaries to the virtual indices of A or equivalently changing the maximally entangled pair in the PEPS.

We note that this should not generally be seen as a practical preparation procedure. Generically the PEPS tensors will map states down into a non-trivial subspace, with the physical implementation of this requiring post-selected measurements. If one of these fails, we need to go back and begin the construction from the start, meaning this procedure is not generally scalable.

2.3.2 Some MPS states

Product State

Let

$$A_0 = (1), \quad A_1 = (0). \quad (2.3.16)$$

This gives the state $|00\dots 0\rangle$, as does

$$A_0 = \begin{pmatrix} 1 & 0 \\ 0 & 0 \end{pmatrix}, \quad A_1 = \begin{pmatrix} 0 & 0 \\ 0 & 0 \end{pmatrix}. \quad (2.3.17)$$

W State

What state do we get when we set

$$A_0 = \begin{pmatrix} 1 & 0 \\ 0 & 1 \end{pmatrix}, \quad A_1 = \begin{pmatrix} 0 & 1 \\ 0 & 0 \end{pmatrix}, \quad (2.3.18)$$

and we choose the boundary conditions of the MPS to be

$$|\psi[A]\rangle = \left[\begin{array}{cccccccc} \square & \square & \square & \square & \square & \square & \square & \square & X \end{array} \right] ? \quad (2.3.19)$$

We have $A_0 A_0 = A_0$, $A_0 A_1 = A_1$, $A_1^2 = 0$ and $\text{Tr}[A_1 X] = 1$, so we get

$$|W\rangle = \sum_{j=1}^N |000\dots 01_j 000\dots 0\rangle, \quad (2.3.20)$$

the W-state [2.3.2].

GHZ State

If we choose $|\phi\rangle = |00\rangle + |11\rangle$ and $\mathcal{P} = |0\rangle\langle 00| + |1\rangle\langle 11|$, or the equivalent MPS tensor

$$A_0 = \begin{pmatrix} 1 & 0 \\ 0 & 0 \end{pmatrix}, \quad A_1 = \begin{pmatrix} 0 & 0 \\ 0 & 1 \end{pmatrix}, \quad (2.3.21)$$

then we get the Greenberger-Horne-Zeilinger (GHZ) state [2.3.2]

$$|GHZ\rangle = |00\dots 0\rangle + |11\dots 1\rangle. \quad (2.3.22)$$

AKLT State

Suppose we wish to construct an $SO(3)$ symmetric spin-1 state [2.3.5, 2.3.6, 2.3.9]. Let $|\phi\rangle = |01\rangle - |10\rangle$ be the $SO(3)$ invariant singlet state. Let $\mathcal{P} : \mathbb{C}^{2 \times 2} \rightarrow \mathbb{C}^3$ be the projector onto the spin-1 subspace

$$\mathcal{P} = |\tilde{1}\rangle\langle 00| + |\tilde{0}\rangle\frac{\langle 01| + \langle 10|}{\sqrt{2}} + |-\tilde{1}\rangle\langle 11|. \quad (2.3.23)$$

The advantage is that the spin operators on the corresponding systems pull through \mathcal{P} , meaning it commutes with rotations. Let (S_x, S_y, S_z) be the spin vector on the spin-1 particle, and $(X_i, Y_i, Z_i)/2$ the spin vector on the i th qubit, then this means:

$$S_Z \mathcal{P} = (|\tilde{1}\rangle\langle \tilde{1}| - |-\tilde{1}\rangle\langle -\tilde{1}|) \left(|\tilde{1}\rangle\langle 00| + |\tilde{0}\rangle\frac{\langle 01| + \langle 10|}{\sqrt{2}} + |-\tilde{1}\rangle\langle 11| \right) \quad (2.3.24)$$

$$= |\tilde{1}\rangle\langle 00| - |-\tilde{1}\rangle\langle 11| \quad (2.3.25)$$

$$= \mathcal{P} \frac{Z_1 + Z_2}{2} \quad (2.3.26)$$

$$S_X \mathcal{P} = \frac{|\tilde{0}\rangle(\langle \tilde{1}| + \langle -\tilde{1}|) + (|\tilde{1}\rangle + |-\tilde{1}\rangle)\langle \tilde{0}|}{\sqrt{2}} \left(|\tilde{1}\rangle\langle 00| + |\tilde{0}\rangle\frac{\langle 01| + \langle 10|}{\sqrt{2}} + |-\tilde{1}\rangle\langle 11| \right) \quad (2.3.27)$$

$$= \left(\frac{|\tilde{0}\rangle(\langle 00| + \langle 11|)}{\sqrt{2}} + \frac{(|\tilde{1}\rangle + |-\tilde{1}\rangle)(\langle 01| + \langle 10|)}{2} \right) \quad (2.3.28)$$

$$= \mathcal{P} \frac{X_1 + X_2}{2}, \quad (2.3.29)$$

with the same holding for S_Y . Thus the state obtained after this projection is fully $SO(3)$ symmetric, but has a nontrivial entanglement structure (which would not be obtained if the state was simply a singlet at each site for example).

This state has many interesting properties. We can write a 2-local Hamiltonian for which this is the ground state. Let Π_2 be the projector onto the spin-2 subspace of a pair of spin-1 particles. This operator has eigenvalues $\{0, 1\}$. Π_2 annihilates an adjacent pair of spin-1 particles, since they are built from two spin-1/2s and a spin-0, so have no overlap with the spin-2 subspace. It is simple to check that on periodic boundary conditions the ground state of $H = \sum \Pi_2$ is unique (and gapped).

If we examine the action of rotations about the three axes of the spin-1, we see that

$$R_{\hat{n}}(\theta) \mathcal{P} = \mathcal{P} R_{\hat{n}}(\theta) \otimes R_{\hat{n}}(\theta). \quad (2.3.30)$$

In particular, $R_{\hat{x}}(\pi) \mapsto -XX$, $R_{\hat{y}}(\pi) \mapsto -YY$, $R_{\hat{z}}(\pi) \mapsto -ZZ$. In Sec. 2.4 we will see that this tells us the AKLT state is in a nontrivial symmetry protected topological (SPT) phase.

Cluster State

It is convenient to write a bond dimension 2 MPS for this state where a physical site contains a pair of spins. Let

$$A_{00} = \begin{pmatrix} 1 & 0 \\ 1 & 0 \end{pmatrix} \quad A_{01} = \begin{pmatrix} 0 & 1 \\ 0 & 1 \end{pmatrix} \quad A_{10} = \begin{pmatrix} 1 & 0 \\ -1 & 0 \end{pmatrix} \quad A_{11} = \begin{pmatrix} 0 & -1 \\ 0 & 1 \end{pmatrix}, \quad (2.3.31)$$

or equivalently the map from virtual to physical spin-1/2 particles

$$\mathcal{P} = \begin{pmatrix} 1 & 0 & 1 & 0 \\ 0 & 1 & 0 & 1 \\ 1 & 0 & -1 & 0 \\ 0 & -1 & 0 & 1 \end{pmatrix}, \quad (2.3.32)$$

where the entangled pairs are in the Bell state $|\phi\rangle = |00\rangle + |11\rangle$. The map \mathcal{P} corresponds to the circuit



$$(2.3.33)$$

Notice in this case our PEPS tensor \mathcal{P} simply corresponds to unitary circuit. As such this is one of the exceptional cases in which the PEPS description *can* be considered a scalable preparation procedure.

Given an explicit MPS description of this state, we can now back out a Hamiltonian for which it is a ground state, allowing us to infer certain properties.

The initial state is constructed from entangled pairs $\prod |\phi\rangle_{2j,2j+1}$, and is the unique ground state of the Hamiltonian

$$H = - \sum_j (X_{2j}X_{2j+1} + Z_{2j}Z_{2j+1}). \quad (2.3.34)$$

Applying the circuit (between Bell pairs with first qubit odd and second even), we see that this transforms to

$$H' = - \sum_j (Z_{2j-1}X_{2j}Z_{2j+1} + Z_{2j}X_{2j+1}Z_{2j+2}) \quad (2.3.35)$$

$$= - \sum_k Z_{k-1}X_kZ_{k+1}. \quad (2.3.36)$$

This is precisely the cluster state Hamiltonian. The physical symmetry of this model is $\mathbb{Z}_2 \times \mathbb{Z}_2$, where $S_1 = \prod_j X_{2j-1}$ and $S_2 = \prod_j X_{2j}$. Pushing this backwards through the circuit, we see that it is equivalent to act on the virtual spins with $S_1 = \prod_j Z_{2j}Z_{2j+1}$ and $S_2 = \prod_j X_{2j}X_{2j+1}$.

This action tells us that, just like the AKLT state, the cluster state possesses SPT order.

2.3.3 MPS Properties

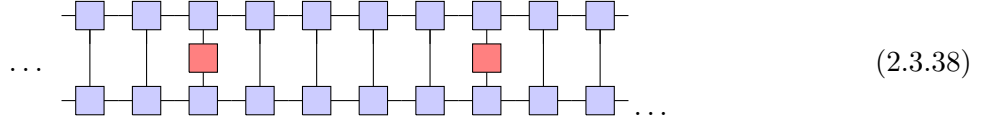
MPS form a vanishingly small corner of the full Hilbert space, and thus we cannot hope to use them to approximate arbitrary states. If physically relevant states correspond to those which *can* be well approximated by MPS, and MPS manifest the same non-generic properties as these physical states, then they represent an extremely useful tool to study these systems.

Decay of Correlations

We have already seen that MPS have bounded levels of entanglement, manifesting as strict area laws. We will now investigate the type of correlations which can be represented. Let \mathcal{O} be some operator for which we wish to compute the two point correlator

$$\langle \psi[A] | \mathcal{O}_0 \mathcal{O}_{j+1} | \psi[A] \rangle, \tag{2.3.37}$$

where the subscript denotes the site at which the operator \mathcal{O} is applied. Graphically this expectation value is written as:



We refer to the object

$$\mathbb{E}_{\mathcal{O}} = \sum_{i,j=0}^{d-1} \mathcal{O}_{i,j} A_i \otimes \bar{A}_j = \tag{2.3.39}$$

as the \mathcal{O} -transfer matrix. Note that we usually just refer to $\mathbb{E}_{\mathbb{1}}$ as the transfer matrix and simply denote it \mathbb{E} .

The correlator (in the thermodynamic limit) can then be written as

$$\langle \psi[A] | \mathcal{O}_0 \mathcal{O}_{j+1} | \psi[A] \rangle = \text{Tr} (\mathbb{E}^{\infty} \mathbb{E}_{\mathcal{O}_0} \mathbb{E}^j \mathbb{E}_{\mathcal{O}_{j+1}} \mathbb{E}^{\infty}) \tag{2.3.40}$$

$$\propto V_L^{\dagger} \mathbb{E}^j V_R. \tag{2.3.41}$$

where V_L and V_R are the dominant left and right eigenvectors of \mathbb{E} respectively. The only change required when calculating longer range correlators is inserting higher powers of \mathbb{E} in Eqn. (2.3.41). The decay of correlators is therefore controlled by the eigenvalues of \mathbb{E} . We can normalise A so that the dominant eigenvalue of \mathbb{E} is 1, with the rest lying inside the unit disk. Thus any correlator can either decay exponentially with distance or be constant. Thus we see that MPS can only capture states with exponentially decaying correlations [2.3.6].

Gauge Freedom

Not all MPS represent different physical states [2.3.2]. The set of transformations of the description (i.e. the MPS) which leaves the physical state invariant are known as *gauge transformations*. In the case of MPS, these correspond to basis transformations on the virtual level:

$$|\psi[A]\rangle = \tag{2.3.42}$$

$$= \tag{2.3.43}$$

$$= |\psi[B]\rangle, \tag{2.3.44}$$

where $B_j = MA_jM^{-1}$. Note that M is only required to have a left inverse, so can be rectangular and enlarge the bond dimension.

Another freedom is blocking. We can combine several MPS tensors $A_{i_1}, A_{i_2}, \dots, A_{i_j}$ into a single effective tensor B_k , on a larger physical region

A number of canonical forms exist which partially gauge fix the MPS description. One of the most common is the left-isometric or left-canonical form (with right-isometric or right-canonical defined analogously). Here the MPS tensors obey

$$\sum_{j=0}^{d-1} A_j^\dagger A_j = \mathbb{1}_{D \times D}, \tag{2.3.45}$$



$$\tag{2.3.46}$$

This is most useful on open boundary systems where a simple algorithm exists to put any MPS into this form. It is frequently used in numerical applications, in particular when using variational minimisation to optimise an MPS description of a ground state (DMRG), a mixed left/right isometric form is used.

Putting an MPS into this form is a *partial* gauge fixing. The remaining freedom is that of a unitary³ on the virtual level, rather than general invertible matrix. This technique is heavily used in tensor network algorithms as a method of increasing numerical stability.

2.3.4 Renormalising Matrix Product States

When we renormalise a system, we usually think about attempting to write down an effective model at a longer length scale which captures the low energy portion of the original model. This can be achieved by blocking sites together, then discarding degrees of freedom to ensure the description remains useful. In the MPS, blocking can be achieved by simply contracting tensors together. How to discard only high energy degrees of freedom is a challenging question. MPS allows us to avoid having to answer this question all together [2.3.10].

Since we care only about expectation values of operators, we can work entirely in the transfer matrix picture. Blocking sites together simply consists of taking products of transfer matrices

$$\tilde{\mathbb{E}} = \mathbb{E}\mathbb{E}\mathbb{E}\mathbb{E}\mathbb{E}\dots\mathbb{E}, \tag{2.3.47}$$

with sandwiched operators \mathbb{E}_O being renormalised similarly. Note that the dimension of $\tilde{\mathbb{E}}$ remains D^4 at all times, so we never need to worry about discarding degrees of freedom. We can also use transfer matrices formed from different MPS to get off-diagonal terms of the form $\langle \psi|O|\phi \rangle$.

2.3.5 Mixed States and Many Body Operators

As described above, an MPS can be used to represent a pure state. How is a mixed state represented in this language?

³If you include the ability to expand the bond dimension then this grows to an isometric freedom.

Let $|\psi[A]\rangle$ be some (pure) MPS state. We can write the density matrix corresponding to $|\psi[A]\rangle$ as

$$\rho[A] = |\psi[A]\rangle\langle\psi[A]| \quad (2.3.48)$$

$$= \cdots \begin{array}{cccccccc} \square & \square & \square & \square & \square & \square & \square & \square \\ | & | & | & | & | & | & | & | \\ \square & \square & \square & \square & \square & \square & \square & \square \\ | & | & | & | & | & | & | & | \end{array} \cdots \quad (2.3.49)$$

The reduced density matrix on some subset of spins R will therefore be represented as

$$\rho[A]_R = |\psi[A]\rangle\langle\psi[A]| \quad (2.3.50)$$

$$= \left[\begin{array}{cccc} \square & \square & \square & \square \\ | & | & | & | \\ \square & \square & \square & \square \\ | & | & | & | \end{array} \right], \quad (2.3.51)$$

where we have used the left and right normal forms to bring in the boundary terms.

The above network is an example of what is referred to as *matrix product operators* (MPOs) [2.3.5, 2.3.11, 2.3.12]. The general form of MPOs we will be considering is

$$\begin{array}{cccccccc} \circ & \square & \square & \square & \square & \square & \square & \circ \\ | & | & | & | & | & | & | & | \\ \square & \square & \square & \square & \square & \square & \square & \square \\ | & | & | & | & | & | & | & | \end{array} \cdot \quad (2.3.52)$$

In addition to being used to represent density matrices, MPOs can be used to represent a large class of many body operators, including small depth quantum circuits and local Hamiltonians. For example, the transverse field Ising Hamiltonian

$$H = -J \sum X_j X_{j+1} - h \sum Z_j \quad (2.3.53)$$

can be represented on a line with the (operator valued) matrix

$$M = \begin{pmatrix} \mathbb{1} & 0 & 0 \\ X & 0 & 0 \\ -hZ & -JX & \mathbb{1} \end{pmatrix} \quad (2.3.54)$$

and end vectors

$$v_L = (0 \ 0 \ 1) \quad \text{and} \quad v_R = \begin{pmatrix} 1 \\ 0 \\ 0 \end{pmatrix}. \quad (2.3.55)$$

The Hamiltonian on N sites is then obtained as

$$H = v_L M^N v_R. \quad (2.3.56)$$

The Heisenberg model

$$H = -J_X \sum X_j X_{j+1} - J_Y \sum Y_j Y_{j+1} - J_Z \sum Z_j Z_{j+1} - h \sum Z_j \quad (2.3.57)$$

can be obtained in the same fashion with

$$v_L = (0 \ 0 \ 0 \ 0 \ 1), \quad M = \begin{pmatrix} \mathbb{1} & 0 & 0 & 0 & 0 \\ X & 0 & 0 & 0 & 0 \\ Y & 0 & 0 & 0 & 0 \\ Z & 0 & 0 & 0 & 0 \\ -hZ & -J_X X & -J_Y Y & -J_Z Z & \mathbb{1} \end{pmatrix}, \quad v_R = \begin{pmatrix} 1 \\ 0 \\ 0 \\ 0 \\ 0 \end{pmatrix}. \quad (2.3.58)$$

More generally, an MPO can be used to represent any operator which does not increase the Schmidt rank of any state too much. An existing explicit analytic construction of MPOs for 1D local Hamiltonians, as well as a new generalisation for higher dimensional Hamiltonians, is covered in more detail in Section 2.A.

Problems 3

Solutions in Appendix 2.D

1. Describe the state given by an MPS with tensor

$$A = \begin{matrix} & 0 & 1 \\ 00 & \begin{pmatrix} 1 & 0 \\ 0 & 1 \end{pmatrix} \\ 10 & \\ 01 & \begin{pmatrix} 1/2 & -1/2 \\ 1/2 & -1/2 \end{pmatrix} \\ 11 & \end{matrix} \quad \begin{matrix} 1 - \boxed{A} - 3 \\ | \\ 2 \end{matrix}, \quad (2.3.59)$$

where index ordering is as shown and indices 1 and 2 are combined. Boundary conditions require inserting a Pauli Z before closing periodic BCs, similar to Equation (2.3.19).

2. Describe the state given by the MPS whose only nonzero components are

$$0 - \boxed{A} - 0 = 1 - \boxed{A} - 1 = 0 - \boxed{A} - 1 = 1 - \boxed{A} - 0 = 1, \quad (2.3.60)$$

where the left and right boundary conditions are $|0\rangle$.

Hint: Writing out the matrices corresponding to fixing the physical index might help!

3. Describe the qudit state given by the MPS

$$i - \boxed{A} - i \oplus j = 1 \quad (2.3.61)$$

where $i, j \in \mathbb{Z}_d$, \oplus denotes addition mod d , the left boundary condition is $|0\rangle$, and the right boundary is $|q\rangle$ for some $q \in \mathbb{Z}_d$.

4. Let \mathcal{G} be some group. Describe the operator given by the MPO with

$$\begin{array}{c}
 h \\
 | \\
 g - \boxed{M} - g \cdot h \\
 | \\
 h
 \end{array} = 1 \tag{2.3.62}$$

where the left boundary condition is $|1\rangle$, the right boundary is $|q\rangle$ for some $q \in \mathcal{G}$, and $g \cdot h$ denotes group multiplication.

5. Suppose the local basis is labelled by particle number. What is the action of the following operator (bond dimension linearly increasing left to right)?

$$\begin{array}{c}
 m \\
 | \\
 n - \boxed{M} - n + m \\
 | \\
 m
 \end{array} = 1 \tag{2.3.63}$$

with left vector $L = |0\rangle$ and right vector $R = \sum_{i=0}^N i|i\rangle$.

6. Write an MPO for the transverse-field-cluster Hamiltonian

$$H = -J \sum_j Z_{j-1} X_j Z_{j+1} - h \sum_j X_j. \tag{2.3.64}$$

Hint: This can be done with bond dimension 4.

7. Use the ideas of MPSs and MPOs to prove that log depth quantum circuits can be simulated efficiently on a classical computer.

Bibliography

- 2.3.1 F. Verstraete and J. Cirac, Matrix product states represent ground states faithfully, [Physical Review B](#) **73**, 94423, [arXiv:cond-mat/0505140v6](#), (2006).
- 2.3.2 D. Perez-Garcia, F. Verstraete, M. M. Wolf, and J. I. Cirac, Matrix Product State Representations, [Quantum Information & Computation](#) **7**, 401–430, [arXiv:quant-ph/0608197](#), (2007).
- 2.3.3 M. B. Hastings, An area law for one-dimensional quantum systems, [Journal of Statistical Mechanics](#) **2007**, P08024, [arXiv:0705.2024](#), (2007).
- 2.3.4 X. Chen, Z. C. Gu, and X. G. Wen, Local unitary transformation, long-range quantum entanglement, wave function renormalization, and topological order, [Physical Review B](#) **82**, 155138, [arXiv:1004.3835](#), (2010).
- 2.3.5 U. Schollwöck, The density-matrix renormalization group in the age of matrix product states, [Annals of Physics](#) **326**, 96–192, [arXiv:1008.3477](#), (2011).
- 2.3.6 R. Orús, A practical introduction to tensor networks: Matrix product states and projected entangled pair states, [Annals of Physics](#) **349**, 117–158, [arXiv:1306.2164](#), (2014).

- 2.3.7 F. Verstraete, V. Murg, and J. Cirac, Matrix product states, projected entangled pair states, and variational renormalization group methods for quantum spin systems, [Advances in Physics](#) **57**, 143–224, [arXiv:0907.2796](#), (2008).
- 2.3.8 N. Schuch, D. Pérez-García, and I. Cirac, Classifying quantum phases using matrix product states and projected entangled pair states, [Physical Review B](#) **84**, 165139, [arXiv:1010.3732](#), (2011).
- 2.3.9 I. Affleck, T. Kennedy, E. H. Lieb, and H. Tasaki, Rigorous results on valence-bond ground states in antiferromagnets, [Physical Review Letters](#) **59**, 799, (1987).
- 2.3.10 F. Verstraete, J. Cirac, J. Latorre, E. Rico, and M. Wolf, Renormalization-Group Transformations on Quantum States, [Physical Review Letters](#) **94**, 140601, [arXiv:quant-ph/0410227](#), (2005).
- 2.3.11 B. Pirvu, V. Murg, J. I. Cirac, and F. Verstraete, Matrix product operator representations, [New Journal of Physics](#) **12**, 025012, [arXiv:0804.3976](#), (2010).
- 2.3.12 I. P. McCulloch, From density-matrix renormalization group to matrix product states, [Journal of Statistical Mechanics: Theory and Experiment](#) **2007**, P10014, [arXiv:cond-mat/0701428](#), (2007).

2.4 Classifying Gapped Phases in 1D

Matrix product states are extremely useful in both analytic and numerical applications. One of the most powerful results in the field of tensor network analytics is a complete classification of gapped phases in 1D.

To begin this lecture, we will introduce quantum phases. We will then argue that in the absence of symmetry constraints, all MPS are in the same phase. Finally, we will show how symmetries change this classification. Whilst interesting in its own right, this material also serves to demonstrate the analytic power of TNN.

2.4.1 Quantum Phases

The classical definition of a phase, or more particularly a phase transition, is usually associated to some nonanalytic behaviour of the free energy density

$$f(\beta, \mathbf{v}) = -\frac{\log \text{tr} e^{-\beta H(\mathbf{v})}}{\beta}, \quad (2.4.1)$$

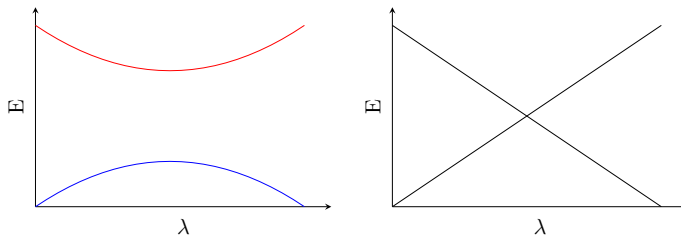
where \mathbf{v} is some vector of parameters of the model (pressures, masses, coupling strengths, etc.) and H the Hamiltonian of our system. Clearly when we take the quantum limit ($\beta \rightarrow \infty$), the free energy is simply the ground state energy. A *quantum phase transition* is thus associated with the ground state [2.4.1].

At a classical phase transition, correlations become long ranged

$$\langle \mathcal{O}_0 \mathcal{O}_x \rangle - \langle \mathcal{O}_0 \rangle \langle \mathcal{O}_x \rangle \sim |x|^{-\nu}, \quad (2.4.2)$$

where the averages are taken with respect to some thermal distribution. We therefore say that a thermal (classical) phase transition is driven by thermal fluctuations, where the variance measures the increasingly long range of these fluctuations. A quantum phase transition also has divergent correlation length, however there is no thermal average — the statistics are purely quantum in origin [2.4.1].

A classical phase corresponds to a range of deformations of H and β which can be made without causing nonanalyticities in the free energy f . Likewise, a quantum phase transition occurs where the ground state energy becomes nonanalytic (in the thermodynamic limit) as a function of some Hamiltonian parameters (not temperature this time!). Suppose we have a continuous family of quantum Hamiltonians $H(\lambda)$. The lowest energy levels generically act in one of the following ways [2.4.1]:



On the left, there is no phase transition, whilst on the right a transition occurs when the roles of the ground and first excited states cross.

For our purposes, a phase transition will be associated with a gapless point in the spectrum. Therefore, we will say that two states $|\psi_0\rangle$ and $|\psi_1\rangle$ are in the same phase if there is a continuous

family of Hamiltonians $H(\lambda)$ such that $|\psi_0\rangle$ is the ground state of $H(0)$, $|\psi_1\rangle$ is the ground state of $H(1)$, and the gap remains open for all $\lambda \in [0, 1]$.

An equivalent notion is finite time evolution under a local Hamiltonian [2.4.2]. Two states are in the same phase if they can be interconverted by time evolution for a finite period. This is linked to the possibility of one state naturally evolving into the other.

It is simpler, and essentially equivalent, to ask which states can be interconverted by a local quantum circuit of depth constant in the system size [2.4.3, 2.4.4]. We will work within this framework. One may also ask the more complicated question of how phases change if we impose a symmetry; if we insist that all of the Hamiltonians $H(\lambda)$ commute with some symmetry group $U_g(\lambda)$. In the circuit picture, this corresponds to restricting the gate set to only gates which commute with this symmetry [2.4.4–2.4.6].

2.4.2 Injective MPS

In this lecture, we will restrict ourselves to the case of *injective* MPS [2.4.7, 2.4.8]. If we assume the MPS is in left canonical form

$$\sum_{j=0}^{d-1} A_j^\dagger A_j = \mathbb{1}_{D \times D} \quad \text{or} \quad \begin{array}{c} \square \\ | \\ \square \end{array} = \square, \quad (2.4.3)$$

then injective MPS are those for which the identity is the *unique* eigenvalue 1 left eigenvector of the transfer matrix. Moreover this means that there exists a unique full-rank⁴ density matrix ρ which is a 1 right eigenvector, i.e.

$$\sum_{j=0}^{d-1} A_j \rho A_j^\dagger =: \mathcal{E}(\rho) = \rho \quad (2.4.4)$$

$$\begin{array}{c} \square \\ | \\ \square \end{array} \begin{array}{c} \square \\ | \\ \square \end{array} = \begin{array}{c} \square \\ | \\ \square \end{array} \rho. \quad (2.4.5)$$

These MPS correspond to unique gapped ground states of local Hamiltonians [2.4.9]. The arguments we will present here generalise to non-injective MPS, however they become very technical.

2.4.3 No Topological Order

We will refer to states which cannot be connected by any constant depth local circuit as being in distinct *topological phases*, or having distinct *topological order*. This is to distinguish them from the symmetric phases we will discuss later in this lecture. In fact, we will see that there are no nontrivial topological phases in 1D [2.4.3].

Let A_j define some injective MPS, and construct the transfer matrix \mathbb{E} ⁵

$$\mathbb{E} = \begin{array}{c} \square \\ | \\ \square \end{array}. \quad (2.4.6)$$

As discussed in the previous lecture, this can be used to renormalise the MPS. Taking products of this transfer matrix corresponds to blocking sites of the original MPS. Since the MPS is injective,

⁴Were ρ not full rank we could reduce the bond dimension such that it were without changing any observables in the thermodynamic limit.

⁵Note that \mathbb{E} is the ‘Liouville superoperator’ form of the channel \mathcal{E} (Eqn. 2.4.4)

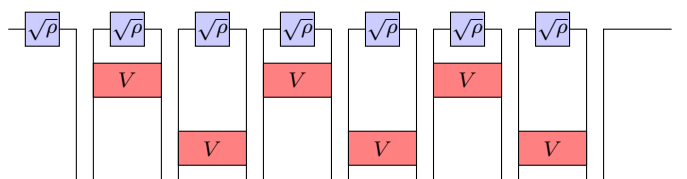
the leading eigenvalue of \mathbb{E} is 1 and all other eigenvalues are strictly smaller. Therefore, by taking the k th power of the transfer matrix, we obtain a new transfer matrix which is

$$\mathbb{E}^k = \left[\begin{array}{c} \rho \\ \hline \rho \end{array} \right] + \tilde{\mathcal{O}}(|\lambda_2|^k), \quad (2.4.7)$$

where $|\lambda_2| < 1$ is the second eigenvalue of the transfer matrix and ρ is the fixed point of the channel. This transfer matrix can be decomposed to give a new effective MPS tensor describing the long wavelength physics

$$\tilde{A} = \left[\begin{array}{c} \sqrt{\rho} \\ \hline \sqrt{\rho} \end{array} \right]. \quad (2.4.8)$$

On the regions we blocked together, we could have first applied a unitary to the state without changing the blocked transfer matrix. Since we only required a constant number of sites to be blocked to achieve this MPS tensor, this unitary freedom is restricted to a constant depth unitary circuit – precisely the equivalence we wish to allow. Now, let V be some unitary which acts as $\sum_{j,k} \sqrt{\rho_{j,k}} |j, k\rangle \rightarrow |0, 0\rangle$ on the state given by $\sqrt{\rho}$ and arbitrarily on the rest of the space. We can now use this to apply two circuit layers to the MPS



$$(2.4.9)$$

which completely disentangles the MPS, giving the state $|00 \cdots 0\rangle$.

Notice that this was all achieved by simply blocking a constant number of sites together, so we have only used a constant depth quantum circuit. Therefore, all injective MPS are in the same (topological) phase as the product state, and therefore each other.

2.4.4 Symmetry Respecting Phases

The proofs in this section are translated into TNN from Ref. [2.4.8].

Since there are no nontrivial topological phases, we will now examine what happens when a symmetry restriction is imposed on the allowed gates. Let \mathcal{G} be some symmetry group for a state which acts on-site as $U_g := u_g^{\otimes n}$ for each $g \in \mathcal{G}$, where u_g is a unitary representation of \mathcal{G} acting on a single site. Recall that for u_g to be a representation, we must have

$$u_g u_h = u_{gh} \quad (2.4.10)$$

for all $g, h \in \mathcal{G}$.

Let A be an MPS tensor such that $|\psi[A]\rangle$ is symmetric, meaning that $U_g |\psi[A]\rangle = e^{i\phi_g} |\psi[A]\rangle$ for all $g \in \mathcal{G}$. We will now examine how this symmetry is realised on the MPS tensor itself.

We require an understanding of the action of unitaries on the physical level of an MPS, and when they can be ‘pushed through’ to act on the virtual level. There, they won’t be touched by the action of constant depth symmetric circuits on the physical legs, so any properties associated with the virtual action of the symmetry will be an invariant of the phase.

We require two lemmas.

Lemma 1. *Let u be some unitary and A an injective MPS tensor. Then the largest eigenvalue λ of the u -transfer matrix*

$$\mathbb{E}_u = \begin{array}{c} \square \\ u \\ \square \end{array} \quad (2.4.11)$$

is contained within the unit disk.

Proof. Let v^\dagger (note that we are not assuming that this is unitary) be a left eigenvector of \mathbb{E}_u

$$\begin{array}{c} \circ v^\dagger \\ \square \\ u \\ \square \end{array} = \lambda \begin{array}{c} \circ v^\dagger \\ \square \end{array} \quad (2.4.12)$$

We therefore get for some density matrix ρ

$$\lambda \begin{array}{c} \circ v^\dagger \\ \circ v \\ \square \rho \end{array} = \begin{array}{c} \circ v^\dagger \\ \square \\ u \\ \square \\ \circ v \\ \square \rho \end{array} \quad (2.4.13)$$

Once again let ρ be the (unique) right eigenvector of \mathbb{E} with eigenvalue 1. We can view the above expression as an inner product between two vectors

$$\lambda \begin{array}{c} \circ v \\ \circ v^\dagger \\ \square \rho \end{array} = \begin{array}{c} \square \\ \sqrt{u} \\ \sqrt{u} \\ \square \\ \circ v^\dagger \end{array} \begin{array}{c} \circ v \\ \sqrt{\rho} \\ \sqrt{\rho} \\ \square \end{array} \quad (2.4.14)$$

We can now apply the Cauchy-Schwarz inequality across the dotted line, giving

$$\left| \begin{array}{c} \square \\ \sqrt{u} \\ \sqrt{u} \\ \square \\ \circ v^\dagger \end{array} \begin{array}{c} \circ v \\ \sqrt{\rho} \\ \sqrt{\rho} \\ \square \end{array} \right|^2 \leq \begin{array}{c} \square \\ \sqrt{u} \\ \sqrt{u} \\ \square \\ \circ v^\dagger \end{array} \begin{array}{c} \circ v \\ \sqrt{\rho} \\ \sqrt{\rho} \\ \square \end{array} \times \begin{array}{c} \circ v \\ \sqrt{u^\dagger} \\ \sqrt{u} \\ \square \\ \circ v^\dagger \end{array} \begin{array}{c} \sqrt{\rho} \\ \sqrt{\rho} \\ \square \end{array} \quad (2.4.15)$$

$$= \begin{array}{c} \square \\ \square \\ \square \end{array} \begin{array}{c} \circ v \\ \circ v^\dagger \\ \rho \end{array} \times \begin{array}{c} \circ v \\ \circ v^\dagger \\ \square \\ \square \end{array} \begin{array}{c} \rho \\ \rho \end{array} \quad (2.4.16)$$

$$= \begin{array}{c} \circ v \\ \rho \\ \circ v^\dagger \end{array} \times \begin{array}{c} \circ v \\ \rho \\ \circ v^\dagger \end{array} \quad (2.4.17)$$

where the vertical lines indicate absolute value. Thus we have

$$|\lambda| \begin{array}{c} \circ v \\ | \\ \rho \\ | \\ \circ v^\dagger \end{array} \leq \begin{array}{c} \circ v \\ | \\ \rho \\ | \\ \circ v^\dagger \end{array}, \quad (2.4.18)$$

and so $|\lambda| \leq 1$. \square

Lemma 2. *Equality is achieved in Lemma 1 if and only if there exists a unitary v and an angle θ such that*

$$\begin{array}{c} \square \\ | \\ \square u \end{array} = e^{i\theta} \begin{array}{c} \circ v \\ | \\ \square \\ | \\ \circ v^\dagger \end{array}. \quad (2.4.19)$$

Proof. First we prove the ‘if’ direction. Assume that Eqn. 2.4.19 holds. Then

$$\begin{array}{c} \circ v^\dagger \\ | \\ \square \\ | \\ \square u \end{array} = e^{i\theta} \begin{array}{c} \square \\ | \\ \circ v^\dagger \end{array} \quad (2.4.20)$$

$$\Rightarrow \begin{array}{c} \circ v^\dagger \\ | \\ \square \\ | \\ \square u \\ | \\ \square \end{array} = e^{i\theta} \begin{array}{c} \square \\ | \\ \square \\ | \\ \square \\ | \\ \circ v^\dagger \end{array} \quad (2.4.21)$$

$$\Rightarrow \begin{array}{c} \circ v^\dagger \\ | \\ \square \\ | \\ \square u \\ | \\ \square \end{array} = e^{i\theta} \begin{array}{c} \circ v^\dagger \\ | \\ \square \end{array}, \quad (2.4.22)$$

and so we have found a left eigenvector v^\dagger of \mathbb{E}_u with a modulus 1 eigenvalue of $\lambda = e^{i\theta}$.

Now we prove the ‘only if’ direction. Assume there exists a left eigenvector v^\dagger with eigenvalue of modulus 1, then the Cauchy-Schwarz inequality Eqn. 2.4.15 must become an equality. Therefore, there is some scalar α such that

$$\begin{array}{c} \square \\ | \\ \square v \\ | \\ \square \sqrt{\rho} \end{array} = \alpha \begin{array}{c} \circ v \\ | \\ \square \\ | \\ \square \sqrt{\rho} \end{array}. \quad (2.4.23)$$

Taking the norm of each side as vectors, we have

$$\begin{array}{c} \square \\ | \\ \square v \\ | \\ \square \sqrt{\rho} \\ | \\ \square \sqrt{\rho} \\ | \\ \square v^\dagger \end{array} = |\alpha|^2 \begin{array}{c} \circ v \\ | \\ \square \\ | \\ \square \sqrt{\rho} \\ | \\ \square \sqrt{\rho} \\ | \\ \circ v^\dagger \end{array} \quad (2.4.24)$$

$$\Rightarrow \begin{array}{c} \square \\ | \\ \square v \\ | \\ \square \rho \\ | \\ \square v^\dagger \end{array} = |\alpha|^2 \begin{array}{c} \circ v \\ | \\ \square \\ | \\ \square \rho \\ | \\ \circ v^\dagger \end{array} \quad (2.4.25)$$

$$\Rightarrow \begin{array}{c} \circlearrowleft v \\ \square \rho \\ \circlearrowright v^\dagger \end{array} = |\alpha|^2 \begin{array}{c} \circlearrowleft v \\ \square \rho \\ \circlearrowright v^\dagger \end{array} . \quad (2.4.26)$$

Therefore, $|\alpha| = 1$, so $\alpha = e^{i\theta}$.

Since ρ is full rank, it is invertible, so

$$\begin{array}{c} \square \\ \square \sqrt{u} \end{array} \circlearrowleft v = e^{i\theta} \circlearrowleft v \begin{array}{c} \square \\ \square \sqrt{u^\dagger} \end{array} . \quad (2.4.27)$$

Now, rearranging this and left multiplying by v^\dagger , we have

$$\circlearrowright v^\dagger \begin{array}{c} \square \\ \square u \end{array} \circlearrowleft v = e^{i\theta} \circlearrowright v^\dagger \circlearrowleft v \begin{array}{c} \square \\ \square \end{array} . \quad (2.4.28)$$

$$\Rightarrow \begin{array}{c} \circlearrowright v^\dagger \circlearrowleft v \\ \square u \\ \square \end{array} = e^{i\theta} \begin{array}{c} \circlearrowright v^\dagger \circlearrowleft v \\ \square \\ \square \end{array} . \quad (2.4.29)$$

$$\Rightarrow \lambda \begin{array}{c} \circlearrowright v^\dagger \circlearrowleft v \\ \square \end{array} = e^{i\theta} \begin{array}{c} \circlearrowright v^\dagger \circlearrowleft v \\ \square \\ \square \end{array} . \quad (2.4.30)$$

We therefore see that $v^\dagger v$ is a left eigenvector of the transfer matrix \mathbb{E} with norm-1 eigenvalue. By assuming injectivity however we require that the only norm-1 eigenvalue is the non-degenerate $+1$ eigenvalue, whose left eigenvector is the identity. Thus we conclude v is, after rescaling, unitary, and that Eqn. 2.4.19 therefore holds. \square

So far, we have established that a unitary u can be ‘pushed through’ the MPS tensor if and only if the u -transfer matrix has an eigenvalue of unit magnitude. We will now show that u is a local symmetry if and only if it can be pushed through. This will complete our understanding of the action of local symmetries on MPS tensors.

Theorem 1 (Symmetries push through). *Let \mathcal{G} be a group. A unitary representation u_g is a local symmetry if and only if*

$$\begin{array}{c} \square \\ \square u_g \end{array} = e^{i\theta_g} \begin{array}{c} \circlearrowleft v_g \\ \square \\ \circlearrowright v_g^\dagger \end{array} . \quad (2.4.31)$$

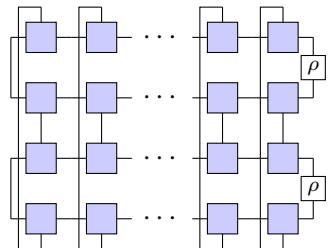
for v_g unitary and $\theta_g \in [0, 2\pi)$.

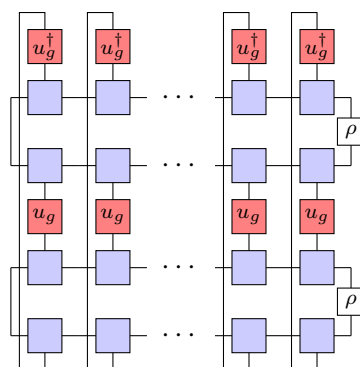
Proof. If Eqn. 2.4.31 holds, it is clear that u_g is a symmetry since v_g is simply a gauge transformation on the MPS.

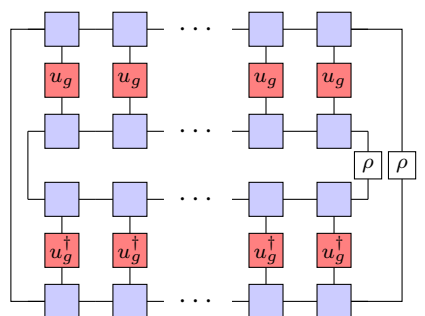
Let

$$\sigma_k = \begin{array}{c} \square \square \dots \square \square \\ \square \square \dots \square \square \\ \square \square \dots \square \square \end{array} \rho \quad (2.4.32)$$

be the reduced density matrix on k sites, where ρ is the right fixed point of \mathbb{E} . By construction, $\text{tr}(\sigma_k) = 1$, but σ_k will generically be mixed, so $\text{tr}(\sigma_k^2) \leq 1$. Recall that the purity of a density matrix is lower bounded by the inverse of the matrix-rank, i.e. $\text{tr}(\sigma_k^2) \geq 1/\text{rank}(\sigma_k)$. Since our reduced density matrix is obtained from a bond dimension D MPS, it has rank at most D^2 . Therefore

$$\frac{1}{D^2} \leq \text{tr}(\sigma_k^2) =$$

(2.4.33)

$$=$$

(2.4.34)

$$=$$

(2.4.35)

where the second equality holds because u_g is a local symmetry.

Here, the left and right boundary vectors ($\mathbb{1}$ and ρ) are independent of the number of sites upon which σ_k is supported, so this inequality holds for all k . This can only be the case if \mathbb{E}_{u_g} has an eigenvalue of magnitude 1, as it would otherwise have to possess exponential decay. From [Lemma 2](#), this implies that there exists some unitary v_g and an angle θ_g such that

$$\begin{array}{c} \square \\ | \\ \square \\ | \\ \square \end{array} = e^{i\theta_g} \begin{array}{c} \circ \\ | \\ \square \\ | \\ \circ \end{array}$$
(2.4.36)

which completes the proof. \square

We now investigate the properties of the virtual action of the symmetry. As discussed above, if we apply a constant depth circuit with symmetric gates to the MPS (i.e. mapping us to any other state in the phase), we can push the symmetry action first through the circuit and then onto the virtual level. Therefore, any properties it has will be an invariant of the phase.

Aside 2: Projective representations

Let \mathcal{G} be some group. A (linear) representation u_g obeys

$$u_g u_h = u_{gh} \quad \forall g, h \in \mathcal{G}. \quad (2.4.37)$$

This is not the most general way of acting with a group however. We could also ask for

$$v_g v_h = \omega[g, h] v_{gh} \quad \forall g, h \in \mathcal{G}, \quad (2.4.38)$$

where $\omega[g, h] = e^{i\phi[g, h]}$ is a scalar which depends on both g and h independently. This is known as a projective representation. One might ask whether this is simply a more complicated way of writing a linear representation. Maybe we can rephase v_g to obtain Eqn. 2.4.37. Let $\beta[g]$ be some phase depending only on g then after a rephasing $v_g \mapsto \beta[g]v_g$, we have

$$v_g v_h = \omega[g, h] \frac{\beta[gh]}{\beta[g]\beta[h]} v_{gh} = \omega'[g, h] v_{gh}. \quad (2.4.39)$$

We say that ω and ω' are equivalent if they are related in this way, so

$$\omega \sim \omega' \iff \exists \beta : \omega'[g, h] = \frac{\beta[gh]}{\beta[g]\beta[h]} \omega[g, h]. \quad (2.4.40)$$

A projective representation is therefore equivalent to a linear representation if the phases can be completely removed, i.e. there exists a β such that

$$\omega[g, h] = \frac{\beta[g]\beta[h]}{\beta[gh]}. \quad (2.4.41)$$

As you will show in Problems 4, there are projective representations which are *not* equivalent to any linear representation.

Suppose we act with u_g followed by u_h on the MPS tensor, then

$$= e^{i\theta_g} \dots = e^{i\theta_g} e^{i\theta_h} \dots \quad (2.4.42)$$

We could also have combined $u_g u_h = u_{gh}$ before pushing through, which tells us

$$= e^{i\theta_{gh}} \dots \quad (2.4.43)$$

Therefore

$$(v_g \otimes v_g^\dagger)(v_h \otimes v_h^\dagger) = \frac{e^{i\theta_{gh}}}{e^{i\theta_g} e^{i\theta_h}} v_{gh} \otimes v_{gh}^\dagger, \quad (2.4.44)$$

so $(v_g \otimes v_g^\dagger)$ is equivalent to a linear representation. We can split this across the tensor product, telling us that in general

$$v_g v_h = \omega[g, h] v_{gh}, \tag{2.4.45}$$

where ω is some phase. We cannot say anything about the phase in this case, since *anything* would be cancelled by tensoring with the conjugate.

The only freedom we have to change v_g within a phase is local rephasing, therefore the equivalence classes of ω label the different phases of injective MPS with a symmetry restriction. These equivalence classes are indexed by the so-called second group cohomology class of the group \mathcal{G} , an object usually written as $\mathcal{H}^2(\mathcal{G}, U(1))$ [2.4.2, 2.4.10].

Problems 4

Solutions in Appendix 2.E

1. The group $\mathbb{Z}_2 \times \mathbb{Z}_2$ has the presentation $\mathbb{Z}_2 \times \mathbb{Z}_2 = \langle x, z | x^2 = z^2 = e, xz = zx \rangle$. Show that the Pauli matrices form a projective representation of $\mathbb{Z}_2 \times \mathbb{Z}_2$.

Hint: let $v_x = X$, $v_z = Z$, $v_{xz=zx} = Y$ and show that $v_g v_h = \omega[g, h] v_{gh}$, where ω is some phase.

2. Determine the *factor system* $\omega[g, h]$ for the Pauli matrices.
3. Show that the Pauli projective representation is not equivalent to a linear representation.

Hint: $xz = zx$, can we rephase v_x and v_z to make $v_x v_z - v_z v_x = 0$?

4. Recall from Sec. 2.3.2 that the symmetry of the cluster state is $\mathbb{Z}_2 \times \mathbb{Z}_2$, with the action on the MPS tensor being

$$\begin{array}{c} \square \\ \text{X} \end{array} = \begin{array}{c} \circ \text{Z} \square \circ \text{Z} \end{array}, \quad \begin{array}{c} \square \\ \text{X} \end{array} = \begin{array}{c} \circ \text{X} \square \circ \text{X} \end{array}. \tag{2.4.46}$$

What can we conclude about the cluster state?

Bibliography

- 2.4.1 S. Sachdev, Quantum phase transitions 2nd edition, Cambridge University Press, (2011).
- 2.4.2 X. Chen, Z. C. Gu, and X. G. Wen, Classification of Gapped Symmetric Phases in 1D Spin Systems, *Physical Review B* **83**, 035107, [arXiv:1008.3745](https://arxiv.org/abs/1008.3745), (2011).
- 2.4.3 X. Chen, Z. C. Gu, and X. G. Wen, Local unitary transformation, long-range quantum entanglement, wave function renormalization, and topological order, *Physical Review B* **82**, 155138, [arXiv:1004.3835](https://arxiv.org/abs/1004.3835), (2010).

- 2.4.4 Y. Huang, and X. Chen, Quantum circuit complexity of one-dimensional topological phases, *Physical Review B* **91**, 195143, [arXiv:1401.3820](https://arxiv.org/abs/1401.3820), (2015).
- 2.4.5 X. Chen, Z. C. Gu, Z. X. Liu, and X. G. Wen, Symmetry protected topological orders and the group cohomology of their symmetry group, *Physical Review B* **87**, 155114, [arXiv:1106.4772](https://arxiv.org/abs/1106.4772), (2011).
- 2.4.6 “Can a symmetry-preserving unitary transformation that goes from a trivial SPT to a non-trivial SPT be local?”, Stack Exchange - <http://physics.stackexchange.com/questions/184570/can-a-symmetry-preserving-unitary-transformation-that-goes-from-a-trivial-spt-to>, (2015).
- 2.4.7 D. Perez-Garcia, F. Verstraete, M. M. Wolf, and J. I. Cirac, Matrix Product State Representations, *Quantum Information & Computation* **7**, 401–430, [arXiv:quant-ph/0608197](https://arxiv.org/abs/quant-ph/0608197), (2007).
- 2.4.8 D. Pérez-García, M. M. Wolf, M. Sanz, F. Verstraete, and J. Cirac, String Order and Symmetries in Quantum Spin Lattices, *Physical Review Letters* **100**, 167202, [arXiv:0802.0447v1](https://arxiv.org/abs/0802.0447v1), (2008).
- 2.4.9 N. Schuch, I. Cirac, and D. Pérez-García, PEPS as ground states: Degeneracy and topology, *Annals of Physics* **325**, 2153–2192, [arXiv:1001.3807](https://arxiv.org/abs/1001.3807), (2010).
- 2.4.10 N. Schuch, D. Pérez-García, and I. Cirac, Classifying quantum phases using matrix product states and projected entangled pair states, *Physical Review B* **84**, 165139, [arXiv:1010.3732](https://arxiv.org/abs/1010.3732), (2011).

2.5 Tensor network algorithms

One area in which tensor networks have had exceptional practical success is in low-temperature simulation of condensed matter systems. A relatively well-understood toy model is finding ground states of one-dimensional spin systems. Even under the assumption of a local Hamiltonian, this seemingly narrow problem retains QMA-completeness [2.5.1] (a quantum analogue of NP), dashing any hope of general simulation, even on a quantum computer. Whilst this may at first seem like a significant problem, many ‘physically realistic’ systems don’t exhibit this prohibitive complexity. Tensor networks can be used to exploit, and to a certain extent understand, this structure.

As discussed previously, states of low entanglement are well represented in the form of MPS. If we consider the case of local and *gapped* Hamiltonians, it has been shown that the relevant ground states cannot be highly entangled [2.5.2–2.5.5, 2.5.12] (see Ref. [2.5.6] for a review). This restricted entanglement means that such states admit efficient MPS approximations [2.5.7], and moreover that they may be efficiently approximated [2.5.8–2.5.12], showing that the presence of the gap causes the complexity to plummet from QMA-complete all the way down to P, removing the complexity barrier to simulation. We note that despite the challenges, both complexity theoretic and physical, in applying MPS to gapless models, they have been successfully utilised for this purpose [2.5.13–2.5.15].

More concretely, the way in which we plan to approximate the ground state is by minimising the Rayleigh quotient of the Hamiltonian H (the energy) over some restricted domain \mathcal{D} to yield an approximate ground state $|\Gamma\rangle$ given as

$$|\Gamma\rangle := \arg \min_{|\psi\rangle \in \mathcal{D}} \frac{\langle \psi | H | \psi \rangle}{\langle \psi | \psi \rangle}. \quad (2.5.1)$$

As we know that the exact solution is well-approximated by MPS, we will restrict ourselves to the domain \mathcal{D} of MPS of a bounded bond dimension. The idea behind DMRG and TEBD is to start in some MPS state⁶ then variationally move along this domain, minimising the energy as we go. The difference between both methods is the manner in which this variation step is performed, with DMRG and TEBD taking more computational and physical approaches respectively.

Although the algorithms we discuss here are designed for finding MPS ground states, they can be adapted to simulate time evolution [2.5.16, 2.5.17], find Gibbs states [2.5.18], or optimise other operators acting on a statespace of interest [2.5.19].

2.5.1 DMRG (The Computer Scientist’s approach)

By far the most studied and successful of the algorithms in the field is DMRG. For clarity we will be restricting ourselves to finite DMRG, though there do exist thermodynamic variants. DMRG is an umbrella term which encompasses several similar algorithms, the algorithm we will discuss here is a simplified but nonetheless effective example. As the introduction of this algorithm in Ref. [2.5.20] pre-dates TNN, its description has historically been presented in a far more physically motivated and technically complicated manner. Due to the corresponding shift in interpretation, the original acronym now holds little relevance to the modern tensor network interpretation of DMRG, and so for clarity we intentionally omit defining precisely the expansion of DMRG as an acronym⁷. For a full review in pre-TNN notation see Ref. [2.5.21], and see Ref. [2.5.22] for a TNN treatment.

⁶Typically a random MPS is sufficient in practice, though one could use an educated guess if available.

⁷Though a curious reader is free to [Google it](#), at their own peril.

Representing the Hamiltonian by an MPO, optimising the Rayleigh quotient over MPS looks like the following:

$$\text{arg min} \left[\text{MPS-MPO contraction} \right] \quad / \quad \text{Optimized MPS chain} \quad (2.5.2)$$

The difficulty is that as we need the contraction of these MPS tensors; the overall objective function is highly non-linear, but it does however only depend quadratically on each individual tensor. The key heuristic behind DMRG is to exploit the simplicity of these local problems, approximating the multivariate (multi-tensor) optimisation by iterated univariate (single tensor) optimisations.

Note that while the DMRG algorithm we are going to outline only calculates ground states, related generalisations exist which can be used to simulate excited states, dynamics etc.

One-site

The simplest interpretation of the above sketch of DMRG is known as DMRG1 (or one-site DMRG). For a fixed site i , the sub-step involves fixing all but a single MPS tensor, which is in turn optimised over, i.e.

$$A_i \leftarrow \text{arg min}_{A_i} \frac{\langle \psi(A_i) | H | \psi(A_i) \rangle}{\langle \psi(A_i) | \psi(A_i) \rangle}. \quad (2.5.3)$$

In TNN these step look like:

$$\text{arg min} \left[\text{MPS-MPO contraction} \right] \quad / \quad \text{Contracted MPS-MPO} \quad (2.5.4)$$

Next we define the *environment tensors*

$$\mathcal{H}_i := \text{Closed MPS-MPO contraction}, \quad (2.5.5)$$

$$\mathcal{I}_i := \text{Closed MPS-MPO contraction}, \quad (2.5.6)$$

which correspond to taking closed tensor networks — the expectation values of H and the I respectively — and removing the objective tensor. Given these environments, the sub-step in Equa-

tion (2.5.4) becomes

$$\begin{array}{c} \boxed{i} \\ \vdots \end{array} \longleftarrow \arg \min_{\begin{array}{c} \boxed{i} \\ \vdots \end{array}} \left(\begin{array}{c} \boxed{i} \\ \vdots \\ \mathcal{H}_i \\ \vdots \\ \boxed{i} \end{array} \right) / \left(\begin{array}{c} \boxed{i} \\ \vdots \\ \mathcal{I}_i \\ \vdots \\ \boxed{i} \end{array} \right). \quad (2.5.7)$$

Vectorising this equation yields

$$A_i \longleftarrow \arg \min_{A_i} \frac{\langle A_i | \mathcal{H}_i | A_i \rangle}{\langle A_i | \mathcal{I}_i | A_i \rangle}. \quad (2.5.8)$$

Finally we can simplify the denominator of this objective function by appropriately gauge-fixing our MPS to be in canonical form. By putting the parts of the MPS left of our site in left-canonical form, and those to the right in right-canonical form, then we get that \mathcal{I}_i simply reduces to the identity:

$$\begin{array}{c} \boxed{\mathcal{I}_i} \\ \vdots \end{array} = \begin{array}{c} \square \square \square \\ \square \square \square \end{array} \left| \begin{array}{c} \square \square \square \\ \square \square \square \end{array} \right. = \begin{array}{c} \square \square \square \\ \square \square \square \end{array} \left| \begin{array}{c} \square \square \square \\ \square \square \square \end{array} \right. = \dots = \begin{array}{c} | \\ | \\ | \end{array} \quad (2.5.9)$$

Given this canonicalisation, the problem thus reduces to

$$A_i \longleftarrow \arg \min_{A_i} \frac{\langle A_i | \mathcal{H}_i | A_i \rangle}{\langle A_i | A_i \rangle}. \quad (2.5.10)$$

As \mathcal{H}_i is Hermitian, this optimisation has a closed form solution given by the minimum eigenvector⁸ of \mathcal{H}_i . By sweeping back and forth along the chain, solving this localised eigenvector problem, and then shifting along the canonicalisation as necessary, we complete our description of the algorithm.

The main advantage of DMRG1 is that the state stays within the MPS manifold without the bond dimension growing, meaning that the algorithm is greedy⁹. This strict restriction on the bond dimension can however be a double-edged sword; this means that there is no particularly convenient method of gently growing the bond dimension as the algorithm runs¹⁰, and no information is gained regarding the appropriateness of the choice of bond dimension. Both of these problems are addressed in turn by the improved, albeit slightly more complicated, DMRG2 algorithm.

Two-site

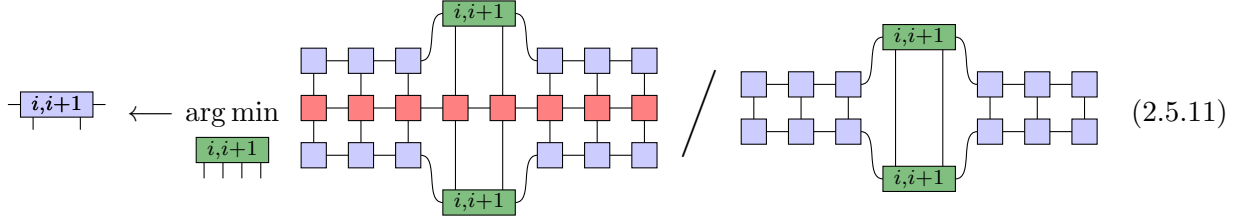
The idea with DMRG2 is to block two sites together, perform an optimisation in the vein DMRG1, then split the sites back out. This splitting process gives DMRG2 its power, allowing for dynamic control of the bond dimension, as well as providing information about the amount of error caused by trimming, which helps to inform the choice of bond-dimension.

⁸If we had not canonicalised the MPS then a closed form solution still exists in the form of the *generalised* eigenvector of \mathcal{H}_i and \mathcal{I}_i , but in general the cost of canonicalisation is well-justified by the increased stability it yields.

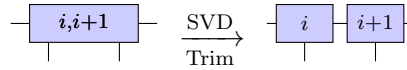
⁹A greedy algorithm is one which solves local problems, such that the cost function (energy in this case) monotonically decreases.

¹⁰There are however somewhat involved methods that allow for auxiliary data to be injected in a non-local fashion such as Refs. [2.5.23, 2.5.24] (see Ref. [2.5.25] for a review), achieving a similar goal.

First an optimisation is performed:



which can once again be solved by taking the minimum eigenvector of an environment tensor with respect to two sites, $\mathcal{H}_{i,i+1}$, once again in mixed canonical form. After this the two-site tensor is split apart by performing an SVD¹¹ and a bond trimming:



This trimmed SVD has two key features. Firstly the bond dimension to which we trim could be higher than that we originally started with, allowing us to gently expand out into the space of higher bond dimension MPS. Secondly we can use the truncated singular values to quantify the error associated with this projection back down into the lower bond dimension space, better informing our choice of bond dimension.

2.5.2 TEBD (The Physicist's approach)

Time-evolving block decimation (TEBD) [2.5.27, 2.5.28] is a tensor network algorithm that allows the dynamics of 1D spin systems to be simulated. By simulating *imaginary*-time-evolution low-temperature features such as the ground state may be calculated as well.

To simulate imaginary-time-evolution, we need to approximate the imaginary-time-evolution operator $U(\tau) = \exp(-\tau H)$. The problem here is that whilst we may have an efficient representation of H , any exponential of it will not necessarily have a succinct representation. Take the example of a two-body Hamiltonian with corresponding imaginary-time-evolution operator

$$U(\tau) = e^{-\tau \sum_i h_i} \quad \text{where} \quad H = \sum_i h_i$$

and h_i is an interaction term acting on spins i and $i + 1$. Whilst H has a constant Schmidt rank, admitting an efficient representation as an MPO, $U(\tau)$ generically has exponential bond dimension for almost all τ .

Let $H_o(H_e)$ denote the sum of terms h_i for odd(even) i . As all the terms within $H_o(H_e)$ are commuting, $e^{-\tau H_o}(e^{-\tau H_e})$ can be efficiently computed and represented. The problem of approximating $U(\tau)$ can therefore be reduced to the problem of approximating $e^{-t(A+B)}$ when only terms of the form $e^{-\tau A}$ and $e^{-\tau B}$ can be computed.

The central mathematical tool to TEBD are the *exponential product approximations*. The first order of these approximation is the Suzuki-Trotter formula, which approximates the total evolution by simply evolving each subsystem:

$$e^{-\tau(A+B)} = e^{-\tau A} e^{-\tau B} + \mathcal{O}(\tau^2).$$

¹¹Whilst other factorisations such as QR and LU can also be used, SVD is preferred over other rank-revealing decompositions due to the optimality of singular value truncation as a low-rank approximation (see Aside 1).

It turns out there exist entire families of such approximations [2.5.29], though for our purposes we will just illustrate the procedure for Suzuki-Trotter.

The TEBD algorithm works by approximating the imaginary-time-evolution operator by the above exponential product formulae, applying it to a given MPS, and trimming the bond dimension to project back down into the space of MPS.

Our approximation to the imaginary-time-evolution operator is given by a product of layers containing only nearest-neighbour two-site operators, meaning we need only be able to contract these operators into our MPS. Suppose we want to apply an operator U to the spins at sites i and $i + 1$. The idea is to apply the operator, contract everything into a single tensor, then once again use an SVD trimming to truncate the bond dimension back down.

$$\begin{array}{c} \text{---} \end{array} \begin{array}{|c|} \hline i \\ \hline \end{array} \begin{array}{|c|} \hline i+1 \\ \hline \end{array} \begin{array}{c} \text{---} \\ \hline U \\ \hline \end{array} \begin{array}{c} \text{---} \\ \hline \text{Cont.} \\ \hline \end{array} \begin{array}{|c|} \hline i, i+1 \\ \hline \end{array} \begin{array}{c} \text{---} \\ \hline \text{SVD} \\ \hline \text{Trim} \\ \hline \end{array} \begin{array}{|c|} \hline i \\ \hline \end{array} \begin{array}{|c|} \hline i+1 \\ \hline \end{array} \begin{array}{c} \text{---} \\ \hline \end{array} \quad (2.5.12)$$

The benefits this trimming procedure gave to DMRG2 — namely control over bond dimension growth and quantification of trimming errors — are also seen in TEBD. As the above procedure is entirely localised, TEBD also admits a large amount of parallelisation, not typically available to DMRG.

2.5.3 Implementation

From-scratch implementation of these simple algorithms can be achieved with relative ease, however several high performance libraries exist for research level simulations. We direct the interested reader to investigate ITensor [2.5.30] (C++), evoMPS [2.5.31] (Python), Matrix Product Toolkit [2.5.32] (C++), uni10 (C++) [2.5.33], Tensor Operations [2.5.34] (Julia) among others. A simple tensor class can also be easily written in MATLAB.

Problems 5

Solutions in Appendix 2.F

1. Consider the critical transverse Ising model

$$H = - \sum_{i=1}^{n-1} X_i X_{i+1} - \sum_{i=1}^n Z_i. \quad (2.5.13)$$

For open boundary conditions, it is known that the ground state energy as a function of n has the form [2.5.35]

$$E(n) = 1 - \csc \left(\frac{\pi}{\alpha n + \beta} \right) \quad (2.5.14)$$

for some integers α and β . Using either DMRG or TEBD, estimate the ground state energy for several chain lengths and calculate α and β .

2. It is known that the LOCAL HAMILTONIAN problem is in P for 1D gapped Hamiltonians [2.5.8–2.5.12]. DMRG and TEBD are the most common techniques for numerically finding the ground states of such systems. For a gapped and 1D local Hamiltonian, prove that DMRG or TEBD converge.

Bibliography

- 2.5.1 A. Y. Kitaev, A. H. Shen, and M. N. Vyalyi, [Classical and Quantum Computation](#), Graduate Studies in Mathematics, AMS, (2002).
- 2.5.2 M. B. Hastings, An area law for one-dimensional quantum systems, [Journal of Statistical Mechanics](#) **2007**, P08024, [arXiv:0705.2024](#), (2007).
- 2.5.3 I. Arad, Z. Landau, and U. Vazirani, Improved one-dimensional area law for frustration-free systems, [Physical Review B](#) **85**, 195145, [arXiv:1111.2970](#), (2012).
- 2.5.4 I. Arad, A. Kitaev, Z. Landau, and U. Vazirani, An area law and sub-exponential algorithm for 1D systems, [arXiv:1301.1162](#), (2013).
- 2.5.5 Y. Huang, Area law in one dimension: Renyi entropy and degenerate ground states, [arXiv:1403.0327](#), (2014).
- 2.5.6 J. Eisert, M. Cramer, and M. B. Plenio, Colloquium: Area laws for the entanglement entropy, [Reviews of Modern Physics](#) **82**, 277–306, [arXiv:0808.3773](#), (2010).
- 2.5.7 F. Verstraete and J. Cirac, Matrix product states represent ground states faithfully, [Physical Review B](#) **73**, 094423, [arXiv:cond-mat/0505140](#), (2006).
- 2.5.8 Z. Landau, U. Vazirani, and T. Vidick, A polynomial-time algorithm for the ground state of 1D gapped local Hamiltonians, [Proceedings of the 5th Conference on Innovations in Theoretical Computer Science](#) and [Nature Physics](#) **11**, 566–569, [arXiv:1307.5143](#), (2013).
- 2.5.9 C. T. Chubb and S. T. Flammia, Computing the Degenerate Ground Space of Gapped Spin Chains in Polynomial Time, [Chicago Journal of Theoretical Computer Science](#) **2016**, 9, [arXiv:1502.06967](#), (2016).
- 2.5.10 Y. Huang, A polynomial-time algorithm for approximating the ground state of 1D gapped Hamiltonians, [arXiv:1406.6355](#), (2014).
- 2.5.11 Y. Huang, Computing energy density in one dimension, [arXiv:1505.00772](#), (2015).
- 2.5.12 I. Arad, Z. Landau, U. Vazirani, and T. Vidick, Rigorous RG algorithms and area laws for low energy eigenstates in 1D, [Communications in Mathematical Physics](#), [arXiv:1602.08828](#), (2017).
- 2.5.13 L. Tagliacozzo, T. R. de Oliveira, S. Iblisdir, and J. I. Latorre, Scaling of entanglement support for Matrix Product States, [Physical Review B](#) **78**, 024410, [arXiv:0712.1976](#), (2008).
- 2.5.14 F. Pollmann, S. Mukerjee, A. Turner, and J. E. Moore, Theory of finite-entanglement scaling at one-dimensional quantum critical points, [Physical Review Letters](#) **102**, 255701, [arXiv:0812.2903](#), (2008).

- 2.5.15 V. Stojevic, J. Haegeman, I. P. McCulloch, L. Tagliacozzo, and F. Verstraete, Conformal Data from Finite Entanglement Scaling, *Physical Review B* **91**, 035120, [arXiv:1401.7654](#), (2015).
- 2.5.16 A. J. Daley, C. Kollath, U. Schollwoeck, and G. Vidal, Time-dependent density-matrix renormalization-group using adaptive effective Hilbert spaces, *Journal of Statistical Mechanics: Theory and Experiment* **2004**, P04005, [arXiv:cond-mat/0403313](#), (2004).
- 2.5.17 S. R. White, and A. E. Feiguin, Real-Time Evolution Using the Density Matrix Renormalization Group, *Physical Review Letters* **93**, 076401, [arXiv:cond-mat/0403310](#), (2004).
- 2.5.18 F. Verstraete, J. J. García-Ripoll, and J. I. Cirac, Matrix Product Density Operators: Simulation of finite-T and dissipative systems, *Physical Review Letters* **93**, 207204, [arXiv:cond-mat/0406426](#), (2004).
- 2.5.19 J. C. Bridgeman, S. T. Flammia, and D. Poulin, Detecting Topological Order with Ribbon Operators, *Physical Review B* **93**, 207204, [arXiv:1603.02275](#), (2016).
- 2.5.20 S. R. White, Density matrix formulation for quantum renormalization groups, *Physical Review Letters* **69**, 2863–2866, (1992).
- 2.5.21 U. Schollwöck, The density-matrix renormalization group, *Reviews of Modern Physics* **77**, 259–315, [arXiv:cond-mat/0409292](#), (2005).
- 2.5.22 U. Schollwöck, The density-matrix renormalization group in the age of matrix product states, *Annals of Physics* **326**, 96–192, [arXiv:1008.3477](#), (2011).
- 2.5.23 S. R. White, Density matrix renormalization group algorithms with a single center site, *Physical Review B* **72**, 180403, [arXiv:cond-mat/0508709](#), (2005).
- 2.5.24 S. V. Dolgov and D. V. Savostyanov, Alternating Minimal Energy Methods for Linear Systems in Higher Dimensions, *SIAM Journal on Scientific Computing* **36**, A2248–A2271, [arXiv:1301.6068](#), (2014).
- 2.5.25 S. V. Dolgov and D. V. Savostyanov, One-site density matrix renormalization group and alternating minimum energy algorithm, *Numerical Mathematics and Advanced Applications*, [arXiv:1312.6542](#), (2013).
- 2.5.26 C. Eckart and G. Young, The approximation of one matrix by another of lower rank, *Psychometrika* **1**, (1936).
- 2.5.27 G. Vidal, Efficient Classical Simulation of Slightly Entangled Quantum Computations, *Physical Review Letters* **91**, 147902, [arXiv:quant-ph/0301063](#), (2003).
- 2.5.28 G. Vidal, Efficient Simulation of One-Dimensional Quantum Many-Body Systems, *Physical Review Letters* **93**, 40502, [arXiv:quant-ph/0310089](#), (2004).
- 2.5.29 N. Hatano and M. Suzuki, Finding Exponential Product Formulas of Higher Orders, *Quantum Annealing and Other Optimization Methods*, [arXiv:math-ph/0506007](#), (2005).
- 2.5.30 ITensor <http://itensor.org/>
- 2.5.31 evoMPS <http://amilsted.github.io/evoMPS/>

2.5.32 Matrix Product Toolkit <http://physics.uq.edu.au/people/ianmcc/mptoolkit/index.php>

2.5.33 uni10 <http://uni10.org/>

2.5.34 Tensor Operations <https://github.com/Jutho/TensorOperations.jl>

2.5.35 N. S. Izmailian and C.-K. Hu, phBoundary conditions and amplitude ratios for finite-size corrections of a one-dimensional quantum spin model, *Nuclear Physics B* **808**, 613, [arXiv:1005.1710](https://arxiv.org/abs/1005.1710), (2009).

2.6 Projected Entangled Pair States

Many of the ideas behind MPS generalise to higher dimensions via *projected entangled pair states* or *PEPS* [2.6.1, 2.6.2]. We will see how this is a misnomer in two ways, there is not necessarily a projector and there is not necessarily an entangled pair.

We begin by recalling the PEPS description of matrix product states, then generalise this to two dimensional models. After giving several examples, we will examine the properties of PEPS, identifying both the similarities and differences to MPS.

2.6.1 One Dimensional Systems: MPS

We have already seen the PEPS construction in 1D. Let $|\phi\rangle \in \mathbb{C}^D \otimes \mathbb{C}^D$ be some (usually) entangled pair and $\mathcal{P} : \mathbb{C}^D \otimes \mathbb{C}^D \rightarrow \mathbb{C}^d$ some linear map. Then

$$|\psi\rangle = \text{---} \quad (2.6.1)$$

where

$$|\phi\rangle = \text{---} \text{---} \quad (2.6.2)$$

is the chosen entangled pair. As we saw, we have a large choice in the exact description we use. We can transform the local basis of each spin in the entangled pair by any (left) invertible matrix

$$|\phi\rangle \rightarrow (A \otimes B)|\phi\rangle, \quad (2.6.3)$$

since we can modify \mathcal{P} to compensate

$$\mathcal{P} \rightarrow \mathcal{P}(B^{-1} \otimes A^{-1}). \quad (2.6.4)$$

One thing to note is that $|\phi\rangle$ does not necessarily need to be a valid quantum state. We usually leave it unnormalised for convenience.

In addition to this gauge freedom, we have additional choices in the description. We could use entangled triplets for example. Let $|\psi\rangle = |000\rangle + |111\rangle$, then we could choose our PEPS to be

$$|\psi\rangle = \text{---} \quad (2.6.5)$$

Clearly this doesn't offer any more descriptive power than using entangled pairs. Suppose we have some PEPS projector \mathcal{Q} acting on pairs, then we can extend this to a \mathcal{P} acting on triplets by

$$\mathcal{P} = \mathcal{Q}(\mathbb{1} \otimes (|0\rangle\langle 00| + |1\rangle\langle 11|)). \quad (2.6.6)$$

In the other direction, we can build a product of triplets using a minor modification of the GHZ MPS presented above and then use \mathcal{Q} to build our state of interest.

2.6.2 Extending to Higher Dimensions

The extension from one to higher dimensional systems proceeds straightforwardly. We will discuss the simple case of a hypercubic lattice, but the framework can be carried out on any graph. In particular, we will restrict to 2D.

As before, we allow $|\phi\rangle$ to be some entangled pair. The PEPS is built as the natural generalisation to 2D

where

$$\mathcal{P} : (\mathbb{C}^D)^{\otimes 4} \rightarrow \mathbb{C}^d \tag{2.6.8}$$

is some linear operator from the virtual to the physical space.

Clearly there is a large amount of gauge freedom in this description as there was in the 1D case. Any invertible transformation of each virtual spin can be compensated in the definition of the PEPS ‘projector’ \mathcal{P} , analogous to Equation (2.6.4).

As in the MPS, one may ask whether using different entanglement structures leads to greater descriptive power. It is easy to see that this is not the case in general. Suppose we choose to lay down plaquettes in a GHZ state and then act with PEPS projectors between plaquettes.

We can use a standard PEPS to prepare this resource state, so any state which can be prepared from this ‘projected entangled plaquette’ construction can be prepared from a PEPS at small additional cost.

2.6.3 Some PEPS examples

We will now look at several example PEPs.

Product State

We have already seen this example in 1D. Exactly the same thing works in 2D, for example take

$$\mathcal{P} = |0\rangle \left\langle \begin{array}{cc} 0 & 0 \\ 0 & 0 \end{array} \right|. \tag{2.6.10}$$

GHZ State

Directly generalising the 1D case, we can use

$$\mathcal{P} = |0\rangle \left\langle \begin{array}{cc} 0 & 0 \\ 0 & 0 \end{array} \right| + |1\rangle \left\langle \begin{array}{cc} 1 & 1 \\ 1 & 1 \end{array} \right| \tag{2.6.11}$$

to build the GHZ state.

RVB State

Let $D = 3$ be the bond dimension and let



$$= 1 \tag{2.6.12}$$

for $\alpha \in \{1, 2\}$, as well as all rotations on the virtual level, be the only nonzero elements of the PEPS tensor. Suppose we tile these tensors and project the dangling indices onto the $|2\rangle$ state. What is the resulting physical state?

This state is known as the resonating valence bond state [2.6.2–2.6.4] and consists of a superposition of all complete tilings of the lattice with maximally entangled pairs

$$\left| \begin{array}{cccc} | & | & | & | \\ | & | & | & | \\ | & | & | & | \\ | & | & | & | \end{array} \right\rangle + \left| \begin{array}{cccc} | & | & | & | \\ | & | & | & | \\ \text{---} & \text{---} & \text{---} & \text{---} \\ | & | & | & | \end{array} \right\rangle + \left| \begin{array}{cccc} | & \text{---} & | & | \\ | & \text{---} & | & | \\ | & \text{---} & | & | \\ | & \text{---} & | & | \end{array} \right\rangle + \left| \begin{array}{cccc} \text{---} & \text{---} & \text{---} & \text{---} \\ | & | & | & | \\ | & | & | & | \\ | & | & | & | \end{array} \right\rangle + \dots,$$

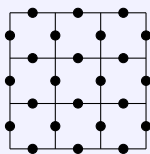
where

$$\text{---} = |00\rangle + |11\rangle.$$

Aside 3: Kitaev’s Toric code

Kitaev’s Toric code [2.6.5] is a canonical example of a topologically ordered model Here we will construct a Hamiltonian with the code space as the ground space of the model. The ground state of this Hamiltonian is the superposition of all closed loops of flipped spins.

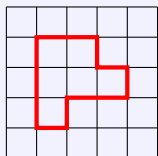
We place qubits on the edges of a square lattice.



We wish to create a Hamiltonian with closed loop states (of flipped spins) as the ground state. Suppose all spins are initially in the $|0\rangle$ state. Then around every vertex v place an interaction

$$A_v = - \begin{array}{c} | \\ Z \\ -Z \\ Z \\ | \end{array} -Z- . \quad (2.6.13)$$

To be in the ground state of this term, the number of edges flipped to $|1\rangle$ neighbouring a given vertex must be even. Drawing edges carrying flipped spins in red, we can trace the effect of this on the lattice

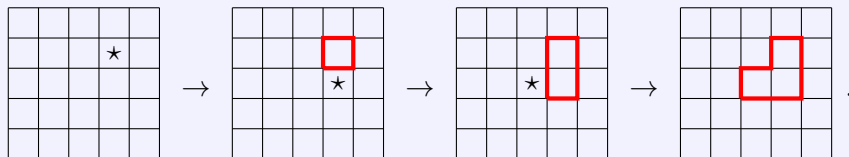


We can see that on a square graph, requiring an even number of edges incident on each vertex enforces that all of our loops are closed.

At this point, our ground space contains all states with only closed loops. We want an equal superposition of all closed loop states. This is achieved by placing an interaction around plaquettes or squares on the lattice, which convert between loop states. To be an eigenstate, all loop states reachable from the vacuum state must be in the superposition. At each plaquette p , place an interaction

$$B_p = - \begin{array}{c} \boxed{X} \\ X \quad X \\ \boxed{X} \end{array} . \quad (2.6.14)$$

This has the desired effect. Placing the interaction at the indicated plaquette performs the following transformation of loops



It's not hard to convince yourself that all loop states can be reached from the empty state, so all closed loop patterns must be in the superposition. The final Hamiltonian is

$$H_{\text{TC}} = - \sum_{v \in \text{vertices}} \begin{array}{c} | \\ Z \\ -Z-Z- \\ | \\ Z \end{array} - \sum_{p \in \text{plaquettes}} \begin{array}{c} X \\ \diagup \quad \diagdown \\ X \quad X \\ \diagdown \quad \diagup \\ X \end{array} \quad (2.6.15)$$

and the ground state is an equal superposition over all closed loop states:

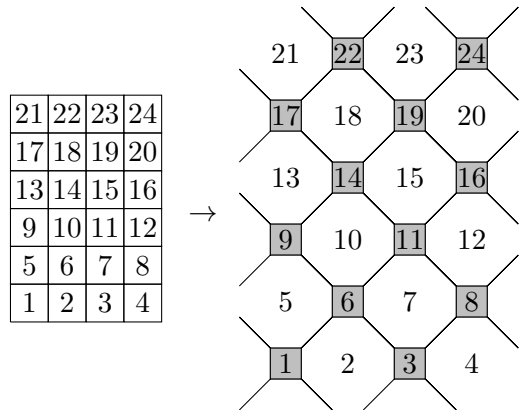
$$| \quad \rangle + | \text{flower} \rangle + | \text{two loops} \rangle + | \text{two loops} \rangle + | \text{complex loop} \rangle + \dots \quad (2.6.16)$$

Note that the Toric code Hamiltonian is usually presented in the $|+\rangle/|-\rangle$ basis rather than the $|0\rangle/|1\rangle$ basis.

Toric code ground state

The simplest way to construct a PEPS for the toric code uses the structure of the ground state. The PEPS tensor is constructed to ensure the superposition of closed loop patterns is achieved upon contraction. The most natural way to achieve this it to write a single tensor for every second plaquette rather than each site.

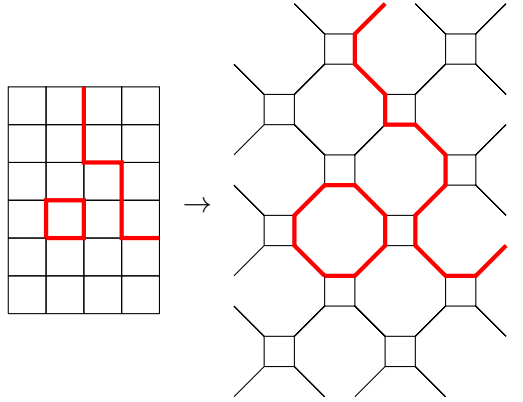
We begin by adding new edges to the lattice. These edges will become the bonds in the tensor network.



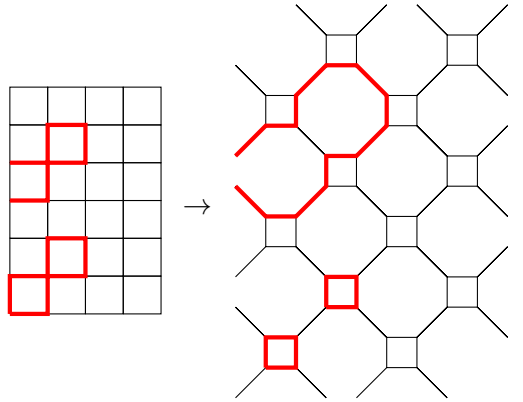
where the plaquettes are numbered for clarity.

Recall that the ground state is built using loops of $|1\rangle$ in a background of $|0\rangle$. We choose the

state of the added edges such that the loop pattern is preserved



where $\color{red}{\rule{0.5em}{0.4pt}}$ indicates a spin in the $|1\rangle$ state on that edge. We choose the following convention when it is ambiguous

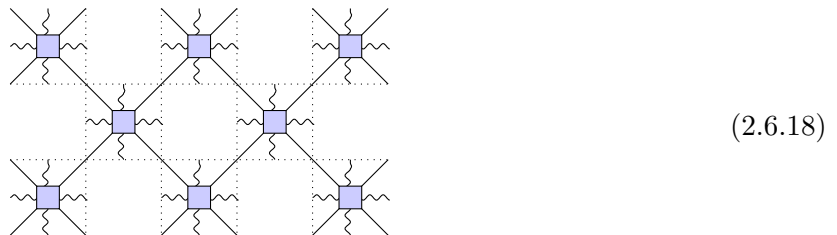


which makes everything consistent.

Interpreting these added edges as bonds in a tensor network, we obtain a PEPS tensor for every second plaquette in the original lattice with four physical indices. The nonzero components are

$$\begin{array}{c}
 \begin{array}{c}
 l \\
 \color{red}{\rule{0.5em}{0.4pt}} \\
 l+i \quad k+l \\
 \color{red}{\rule{0.5em}{0.4pt}} \quad \color{red}{\rule{0.5em}{0.4pt}} \\
 i \color{red}{\rule{0.5em}{0.4pt}} \quad k \\
 \color{red}{\rule{0.5em}{0.4pt}} \quad \color{red}{\rule{0.5em}{0.4pt}} \\
 i+j \quad j+k \\
 \color{red}{\rule{0.5em}{0.4pt}} \\
 j
 \end{array}
 = 1,
 \end{array}
 \tag{2.6.17}$$

where $i, j, k, l \in \mathbb{Z}_2$. In this tensor the straight legs indicate virtual indices, and the wavy legs physical indices, specifically the four qubits on the given plaquette. The network looks as below, with the dotted lines representing the original lattice:



This tensor simply ensures that if adjacent physical indices are in the $|1\rangle$ state, i.e. carrying a loop, then the virtual index between them does not carry a loop which would leave the plaquette. Conversely, if only one is in the $|1\rangle$ state, the loop must leave the plaquette.

Since an even number of the virtual bonds must be in the $|1\rangle$ state for the tensor entry to be nonzero, the PEPS tensor has a property called \mathcal{G} -injectivity [2.6.6]. This means that there is a symmetry on the virtual level

$$(2.6.19)$$

This turns out to be closely related to the topological order present in this model.

2.6.4 2D Cluster State and the complexity of PEPS

Let $D = 2$ be the bond dimension and let

$$(2.6.20)$$

be the only nonzero elements of the PEPS tensor. The physical state generated is the 2D cluster state, a universal resource for measurement based quantum computing [2.6.7, 2.6.8].

If we could efficiently take the inner product between PEPS (i.e. contract a square grid network), then we can clearly classically simulate single qubit post selected measurements by simply contracting rank 1 projectors onto the physical indices of these PEPS tensors. This shows us that we cannot contract even simple PEPS states efficiently, unless post-selected quantum computing can be classically simulated (Post-BQP=BPP) [2.6.9].

Numerical PEPS

Although we will not discuss the details of numerical implementation of PEPS algorithms, we note that the status is not as dire as the previous section would imply. In many practical situations, approximate contraction of PEPS networks can be achieved in both the finite [2.6.10] and infinite [2.6.11, 2.6.12] system size limits.

2.6.5 Properties of PEPS

Above, we saw a number of properties of 1D PEPS or MPS. We will now see which properties hold in two dimensions. One might naïvely expect MPS and more general PEPS to share similar properties. As we will see below, these two tensor network states share qualitatively different properties, both in terms of the physics the corresponding states exhibit, and in the computational power of the tensor networks.

Aside 4: Tensor network for classical partition function

Let $H[s] = \sum_{\langle i,j \rangle} h[s_i, s_j]$ be some classical Hamiltonian. We frequently want to calculate the partition function $\mathcal{Z} = \sum_{\{s\}} e^{-\beta H[s]}$ for such a system at a temperature β . We can use a simple tensor network to help.

Define the two tensors

$$\begin{array}{c} k \\ | \\ i - \boxed{D} - l \\ | \\ j \end{array} = \delta_{i,j,k,l}, \quad i - \boxed{M} - j = e^{-\beta h[s_i, s_j]}. \quad (2.6.21)$$

Placing a D tensor at every classical spin and an M tensor corresponding to each interaction, the following network evaluates to the partition function.

$$\mathcal{Z} = \begin{array}{cccc} \begin{array}{c} \color{red}\square \\ | \\ \color{blue}\square \\ | \\ \color{red}\square \\ | \\ \color{blue}\square \\ | \\ \color{red}\square \end{array} & \begin{array}{c} \color{red}\square \\ | \\ \color{blue}\square \\ | \\ \color{red}\square \\ | \\ \color{blue}\square \\ | \\ \color{red}\square \end{array} & \begin{array}{c} \color{red}\square \\ | \\ \color{blue}\square \\ | \\ \color{red}\square \\ | \\ \color{blue}\square \\ | \\ \color{red}\square \end{array} & \begin{array}{c} \color{red}\square \\ | \\ \color{blue}\square \\ | \\ \color{red}\square \\ | \\ \color{blue}\square \\ | \\ \color{red}\square \end{array} \\ \color{red}\square & \color{red}\square & \color{red}\square & \color{red}\square \\ \color{red}\square & \color{red}\square & \color{red}\square & \color{red}\square \\ \color{red}\square & \color{red}\square & \color{red}\square & \color{red}\square \\ \color{red}\square & \color{red}\square & \color{red}\square & \color{red}\square \end{array} \quad (2.6.22)$$

Thermal expectation values can be calculated by inserting local tensors into this network. For example

$$\mathcal{Z} \times \langle s_n \rangle = \sum_{\{s\}} s_n e^{-\beta H[s]} = \begin{array}{cccc} \begin{array}{c} \color{red}\square \\ | \\ \color{blue}\square \\ | \\ \color{red}\square \\ | \\ \color{blue}\square \\ | \\ \color{red}\square \end{array} & \begin{array}{c} \color{red}\square \\ | \\ \color{blue}\square \\ | \\ \color{red}\square \\ | \\ \color{blue}\square \\ | \\ \color{red}\square \end{array} & \begin{array}{c} \color{red}\square \\ | \\ \color{blue}\square \\ | \\ \color{red}\square \\ | \\ \color{blue}\square \\ | \\ \color{red}\square \end{array} & \begin{array}{c} \color{red}\square \\ | \\ \color{blue}\square \\ | \\ \color{red}\square \\ | \\ \color{blue}\square \\ | \\ \color{red}\square \end{array} \\ \color{red}\square & \color{red}\square & \color{red}\square & \color{red}\square \\ \color{red}\square & \color{red}\square & \color{red}\square & \color{red}\square \\ \color{red}\square & \color{red}\square & \color{red}\square & \color{red}\square \\ \color{red}\square & \color{red}\square & \color{red}\square & \color{red}\square \end{array}, \quad (2.6.23)$$

where

$$\color{orange}\bullet = \sigma^Z, \quad (2.6.24)$$

has been inserted at site n .

Notice that by combining D and M tensors, the partition function can be described with

a single tensor

$$\begin{array}{c} k \\ | \\ i - \boxed{Q} - l \\ | \\ j \end{array} = \sum_{s_a} e^{-\frac{\beta}{2}(h[s_i, s_a] + h[s_j, s_a] + h[s_k, s_a] + h[s_l, s_a])}. \quad (2.6.25)$$

Let

$$H = -J \sum_{\langle i, j \rangle} s_i s_j, \quad (2.6.26)$$

where $s \in \{\pm 1\}$, the classical Ising model. The tensor Q then simplifies to

$$\begin{array}{c} k \\ | \\ i - \boxed{Q} - l \\ | \\ j \end{array} = 2 \cosh \left(\frac{\beta J}{2} (s_i + s_j + s_k + s_l) \right). \quad (2.6.27)$$

Algebraic decay of correlations

As we saw above, MPS can only capture states with exponential decay of correlations (or constant correlations of course). We will now see if this holds in the case of PEPS. We can build a PEPS state corresponding to a classical partition function by modifying the above construction [2.6.3].

Let

$$\begin{array}{c} k \\ | \\ i - \boxed{D} - l \\ / \quad \backslash \\ x \quad j \end{array} = \delta_{i,j,k,l,x}, \quad i - \boxed{M} - j = e^{-\frac{\beta}{2}h[s_i, s_j]}, \quad (2.6.28)$$

or equivalently combine these into

$$\begin{array}{c} k \\ | \\ i - \boxed{Q} - l \\ / \quad \backslash \\ x \quad j \end{array} = e^{-\frac{\beta}{4}(h[s_i, s_x] + h[s_j, s_x] + h[s_k, s_x] + h[s_l, s_x])}. \quad (2.6.29)$$

This defines a PEPS state

(2.6.30)

Note this is a pure state, and *not* a thermal state. It is however not normalised, with $\langle \psi | \psi \rangle = Z$. Correlation functions computed using this state are equal to those computed using classical statistical physics. Suppose we were to consider a classical model with a thermal phase transition (such as the Ising model above). Such a model will exhibit algebraic decay of correlations at the critical temperature, implying that the corresponding PEPS does as well. Thus we can see that unlike MPS, the states described by PEPS *can* exhibit algebraic decay of correlations.

Gauge freedom

The gauge freedom of a PEPS tensor is a simple generalisation of the MPS freedom. As before, we can block tensors together without changing the global state. In addition, we can perform the following transformation (on a translationally invariant PEPS):

(2.6.31)

where N and M are invertible matrices.

Recall that in the MPS case, we could use this freedom to bring the tensors into a canonical form. This cannot be done exactly in the case of PEPS, though there do exist numerical methods to bring PEPS into *approximate* canonical forms [2.6.13].

Problems 6

Solutions in Appendix 2.G

1. What is the PEPS tensor required to build the GHZ state on the honeycomb lattice where spins reside on vertices?

2. Which 2 qubit gate is obtained by contracting the following tensors along the horizontal index?

$$\begin{array}{c} j \\ | \\ \boxed{u} - k \\ | \\ i \end{array} = \delta_{i,j} (\delta_{k,0} + (-1)^i \delta_{k,1}), \quad \begin{array}{c} y \\ | \\ \boxed{v} \\ | \\ x \end{array} = \delta_{x,y,z}. \quad (2.6.32)$$

3. The cluster state can be prepared from the all $|+\rangle$ state by applying CZ between all adjacent spins. Show that Equation (2.6.20) indeed gives the cluster state.

Hint: Consider the decomposition of a gate given in the above problem.

4. Investigate how logical operators on the physical spins of the Toric code can be pulled onto the virtual level of the PEPS. Can you see why \mathcal{G} -injectivity is so important for topologically ordered PEPS?
5. Convince yourself that evaluating expectation values on the PEPS constructed from a classical partition function indeed reproduces the thermal expectation values.

Bibliography

- 2.6.1 F. Verstraete, J. I. Cirac, and V. Murg, Matrix Product States, Projected Entangled Pair States, and variational renormalization group methods for quantum spin systems, [Advances in Physics](#) **57**, 143–224, [arXiv:0907.2796](#), (2009).
- 2.6.2 R. Orús, A practical introduction to tensor networks: Matrix product states and projected entangled pair states, [Annals of Physics](#) **349**, 117–158, [arXiv:1306.2164](#), (2014).
- 2.6.3 F. Verstraete, M. M. Wolf, D. Perez-Garcia, and J. I. Cirac, Criticality, the area law, and the computational power of projected entangled pair states., [Physical Review Letters](#) **96**, 220601, [arXiv:quant-ph/0601075](#), (2006).
- 2.6.4 N. Schuch, D. Poilblanc, J. I. Cirac, and D. Pérez-García, Resonating valence bond states in the PEPS formalism, [Physical Review B](#) **86**, 115108, [arXiv:1203.4816](#), (2012).
- 2.6.5 A. Y. Kitaev, Fault-tolerant quantum computation by anyons, [Annals of Physics](#) **303**, 2–30, [arXiv:quant-ph/9707021](#), (2003).
- 2.6.6 N. Schuch, I. Cirac, and D. Pérez-García, PEPS as ground states: Degeneracy and topology, [Annals of Physics](#) **325**, 2153–2192, [arXiv:1001.3807](#), (2010).
- 2.6.7 F. Verstraete and J. I. Cirac, Valence-bond states for quantum computation, [Physical Review A](#) **70**, 060302, [arXiv:quant-ph/0311130](#), (2004).
- 2.6.8 N. Schuch, M. Wolf, F. Verstraete, and J. Cirac, Entropy Scaling and Simulability by Matrix Product States, [Physical Review Letters](#) **100**, 30504, [arXiv:0705.0292](#), (2008).
- 2.6.9 N. Schuch, M. Wolf, F. Verstraete, and J. Cirac, The computational complexity of PEPS, [Physical Review Letters](#) **98**, 140506, [arXiv:quant-ph/0611050](#), (2008).

- 2.6.10 M. Lubasch, J. Cirac, and M.-C. Bañuls, Algorithms for finite projected entangled pair states, [Physical Review B](#) **90**, 064425, [arXiv:1405.3259](#), (2014).
- 2.6.11 J. Jordan, R. Orus, G. Vidal, F. Verstraete, and J. Cirac, Classical simulation of infinite-size quantum lattice systems in two spatial dimensions, [Physical Review Letters](#) **101**, 250602, [arXiv:cond-mat/0703788](#), (2008).
- 2.6.12 H. N. Phien, J. A. Bengua, H. D. Tuan, P. Corboz, and R. Orus, The iPEPS algorithm, improved: fast full update and gauge fixing, [Physical Review B](#) **92**, 035142, [arXiv:1503.05345](#), (2015).
- 2.6.13 D. Pérez-García, M. Sanz, C. E. González-Guillén, M. M. Wolf, and J. I. Cirac, Characterizing symmetries in a projected entangled pair state, [New Journal of Physics](#) **12**, 025010, [arXiv:0908.1674](#), (2010).

2.7 Multiscale Entanglement Renormalisation Ansatz

MPS are extremely useful for understanding low energy states of 1D quantum models. Despite this, they cannot capture the essential features of some important classes of states. In particular, they cannot reproduce the correlations seen in gapless ground states. Recall that MPS always have exponentially decaying correlations, whereas gapless ground states generically support correlations with power law decay. Similarly MPS also have a strict area law for entanglement entropy, where gapless states admit a logarithmic divergence. The multiscale entanglement renormalisation ansatz is a tensor network designed to overcome these problems.

As mentioned in lecture 2.5, although MPS do not naturally support the kind of correlations expected in critical models, they have been successfully applied for the study of such systems nonetheless. Using MPS for this purpose requires a family of MPS of increasing bond dimension to examine how the correlations behave. The MERA state functions differently. As we will discuss, a single MERA state can naturally capture the physics of a gapless ground state.

Here, we will present the tensor network as an ansatz and argue that it is well suited to representing ground states of gapless Hamiltonians in 1D. Suppose the state can be written as

$$|\psi\rangle = \text{[Diagram of a MERA tensor network with blue and green tensors]} , \quad (2.7.1)$$

where

$$\begin{array}{|c|} \hline u \\ \hline \\ \hline u^\dagger \\ \hline \end{array} = \begin{array}{|c|} \hline \\ \hline \\ \hline \end{array} , \quad \begin{array}{|c|} \hline w \\ \hline \\ \hline w^\dagger \\ \hline \end{array} = \begin{array}{|c|} \hline \\ \hline \\ \hline \end{array} . \quad (2.7.2)$$

As we will see, these constraints on the tensors have both a physical and computational impact. Note that the u and w tensors do not have to be identical, although we frequently restrict to this case if we expect translationally and scale invariant states. The class of states which are expressed as Eqn. 2.7.1 are known as Multiscale Entanglement Renormalisation Ansatz (MERA) states [2.7.1–2.7.5].

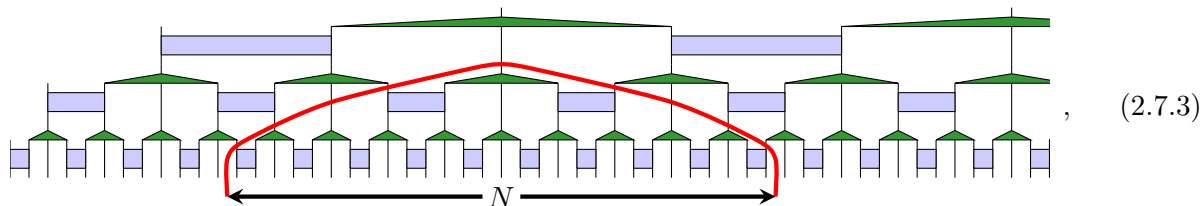
Although we will not discuss it here, the MERA can be straightforwardly generalised to higher dimensional systems [2.7.6–2.7.9]. Unlike PEPS, the network can be efficiently optimised in higher dimensions, although the scaling makes the numerics very challenging!

2.7.1 Properties of MERA

Logarithmic violation of the area law

One of the key properties realised in the MERA which cannot be realised in MPS is a scaling of entanglement entropy. This is easily seen by bond counting. Recall that if n bonds must be broken to separate a region from the rest of the network, the maximum entanglement entropy that can be supported is $n \log D$, where D is the bond dimension. Recall that in the case of MPS any reduced state on a contiguous region can be removed by cutting $n = 2$ bonds.

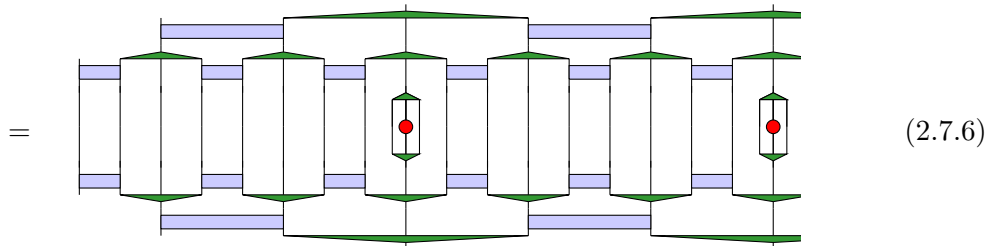
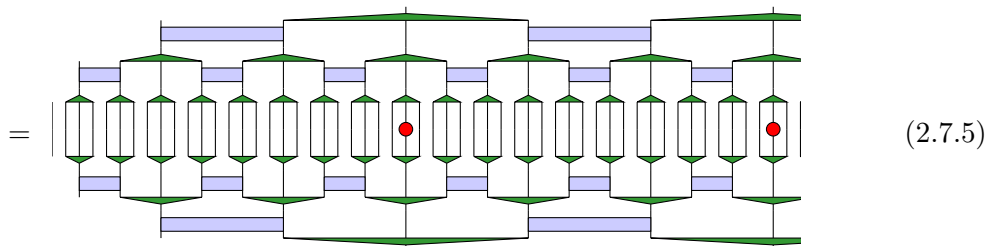
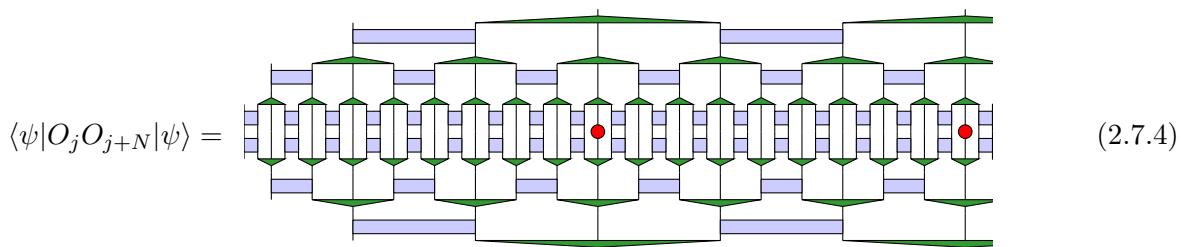
By inspecting the diagram



it is straightforward to see that to remove a block of N physical indices from the rest of the network, $\mathcal{O}(\log N)$ bonds must be cut. This shows that the maximum entropy scales as $\log N \log D$ [2.7.1, 2.7.2].

Power law decay of correlations

Using the constraints on the tensors (Eqn. 2.7.2), we can simplify the evaluation of a two point correlator on a MERA state [2.7.3].



$$= \begin{array}{c} \text{Diagram 1: A large green trapezoid containing a smaller green trapezoid, which contains a red dot. The entire structure is enclosed in a black rectangular frame with a red dot in the center.} \\ \text{Diagram 2: A large green trapezoid containing a smaller green trapezoid, which contains a red dot. The entire structure is enclosed in a black rectangular frame with a red dot in the center.} \end{array} \quad (2.7.7)$$

Note that the length scale behaviour of the correlator is completely determined by the application of a superoperator

$$\mathcal{S}(\phi) = \begin{array}{c} \text{Diagram: A green trapezoid with a red circle containing the symbol } \phi \text{ inside.} \end{array}, \quad (2.7.8)$$

where the w tensor can be viewed as a set of Kraus operators

$$M_k = \begin{array}{c} \text{Diagram: A green trapezoid with a vertical line passing through it, labeled } k \text{ at the bottom.} \end{array} \quad (2.7.9)$$

obtained by grouping the indices indicated.

Thus, \mathcal{S} is a completely positive, unital map and all eigenvalues λ of \mathcal{S} are $|\lambda| \leq 1$. We can bring operators separated by N sites together by applying $\mathcal{S} \sim \log N$ times. Considering eigenoperators of the \mathcal{S} superoperator, the correlator acts as

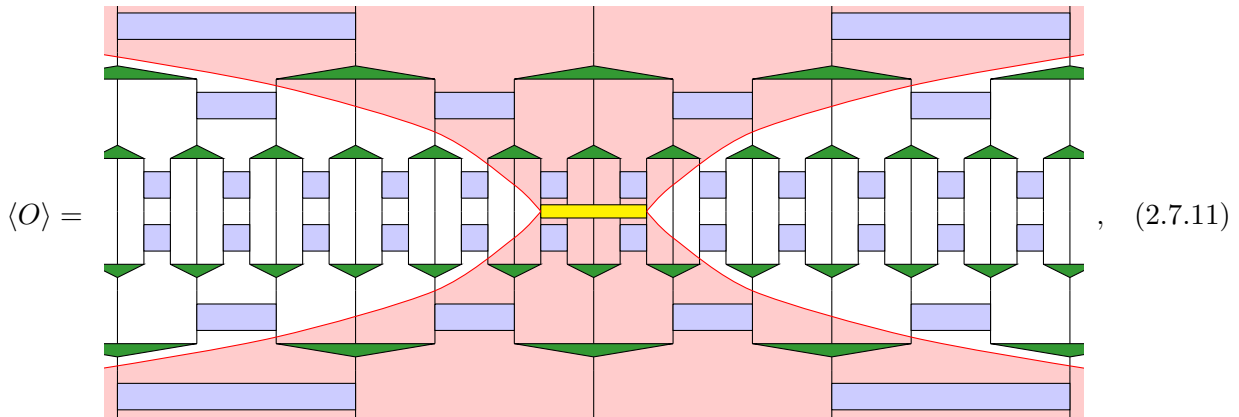
$$\langle A_j B_k \rangle \sim \frac{\langle A_0 B_1 \rangle}{|j - k|^{\Delta_A + \Delta_B}}, \quad (2.7.10)$$

where $\Delta_\phi = -\log_3 \lambda_\phi$, $\Delta_\phi \geq 0$ are known as scaling dimensions, where λ_ϕ is the corresponding eigenvalue of \mathcal{S} . Therefore, a MERA state can support algebraic decay of correlations. Although this discussion required the operators to be placed at special sites, it can be easily generalised.

Efficient Manipulation

As described in Section 2.1.5, a good tensor network ansatz should fulfil two properties. First, it should be efficiently storable. All of the networks we have discussed thus far have this property, as only a small number of coefficients are required to represent these states. The second property is more subtle; one should be able to extract physical data efficiently. Although this works for the 1D MPS network, it fails for 2D PEPS states; the contractions required to calculate expectation values of local operators is incredibly hard.

It turns out the MERA has both of these properties. One can efficiently store the state data, and, thanks to the constraints in Eqn. 2.7.2, one can efficiently compute local expectation values and correlators. We have already seen how this works. The isometric constraints ensure that local operators on the physical level of the network are mapped to local operators on the higher levels [2.7.10]. Therefore, computing expectation values only requires manipulation of a small number of tensors in the *causal cone* of the operator



$$\langle O \rangle = \text{[Diagram of MERA tensor network for } \langle O \rangle \text{]}, \quad (2.7.11)$$

where the shaded region indicates the causal cone of the five site operator on the physical level indicated in yellow. Notice that the number of tensors on each subsequent level does not grow. Indeed, after a single layer of tensors, the operator becomes a three site operator, and the range never grows. Thus, we see that the layers of the MERA act to map local operators to local operators.

2.7.2 Renormalisation Group Transformation

Much of the discussion above concerned interpretation of the layers of the MERA as Kraus operators, defining a unital CP map on local operators. Evaluating expectation values can be seen as application of many superoperators followed by the inner product with some state on a smaller number of sites

$$\langle \psi_0 | O | \psi_0 \rangle = \langle \psi_{k+1} | \mathcal{A}_k \circ \dots \circ \mathcal{A}_1 \circ \mathcal{A}_0(O) | \psi_{k+1} \rangle, \quad (2.7.12)$$

where \mathcal{A}_j is a map from 3^{N-j} spins to $3^{N-j}/3$ spins. This can be seen as a renormalisation group or scale transformation. The state $|\psi_j\rangle$ is supported on 3^{N-j} spins, and contains only the physical data necessary to understand the physics on that length scale. As we saw, if O is a local operator, $\mathcal{A}(O)$ is easy to evaluate. This allows us to understand the effective operator as a function of length scale [2.7.1, 2.7.3, 2.7.4].

The thermodynamic or macroscopic observables can be seen as the operators obtained by applying a formally infinite number of MERA layers to the high energy or microscopic observables. Thus, the macroscopic physics, or phase structure, is determined by fixed points of the maps \mathcal{A} . Some particularly interesting states are the scale invariant states. If the MERA tensors are all the same after some layer, the state is scale invariant. For these states, we do not expect the physics to change as a function of length or energy scale. The fixed point observables of these states are particularly simple to understand, and distinct scale invariant states characterise the different phases.

Since there is no characteristic length scale set by either the spectral gap or correlation length, gapless ground states are expected to be scale invariant. The MERA therefore allows us to understand the long range physics of these states incredibly efficiently [2.7.3, 2.7.10]. Another way to achieve a scale invariant state is to have zero correlation length — these states characterise gapped phases.

2.7.3 AdS/CFT

In the appropriate limit, the low energy physics of the gapless spin chains considered here is described by a *conformal field theory* (CFT) [2.7.12, 2.7.13]. The physics of CFTs is thought to be related to gravitational theories in one additional dimension [2.7.14–2.7.16].

This duality can be observed in the MERA network [2.7.17–2.7.19]. Imposing the graph metric on the MERA, we find a discretised anti-de Sitter (AdS) metric [2.7.17], whilst the edge theory is a ‘discretised’ CFT. In addition to being a concrete realisation of the holographic principle, the MERA/CFT duality provides avenues towards designing quantum error correcting codes [2.7.20].

We note that the AdS/MERA connection remains an open research question. Limits on the ability of MERA states to replicate physics on scales less than the AdS radius have been shown [2.7.19]. Additionally, whether the geometry is best understood as anti-de Sitter [2.7.17] or de Sitter [2.7.18] is currently unclear. Whatever the status, the connection is intriguing. We encourage the interested reader to explore the rapidly expanding literature on the topic [2.7.19–2.7.28].

2.7.4 Some Simple MERA States

Product State

Let

$$w = \begin{matrix} & & 0 & 1 \\ & 000 & \left(\begin{array}{cc} 1/2 & 0 \\ 1/2 & 0 \\ 0 & 1/2 \\ 0 & 1/2 \\ 1/2 & 0 \\ 1/2 & 0 \\ 0 & 1/2 \\ 0 & 1/2 \end{array} \right) \\ & 100 & \\ & 010 & \\ & 110 & \\ & 001 & \\ & 101 & \\ & 011 & \\ & 111 & \end{matrix} \quad (2.7.13)$$

and $u = \mathbb{1}$.

If we build $\log_3 N$ layers using these tensors, we end up with a state on N sites. The network still has a free index at the top, so we need to define a one-index ‘top tensor’ T to obtain the final state. Let $T = |+\rangle$. The state obtained is $|+\rangle^{\otimes N}$.

GHZ State

Let

$$\begin{matrix} & l \\ & \diagup \quad \diagdown \\ & \text{---} \\ & \diagdown \quad \diagup \\ i & j & k \end{matrix} = \delta_{i,j,k,l}, \quad (2.7.14)$$

and $u = \mathbb{1}$. Let the top tensor be $T = |+\rangle$. The state obtained is $\frac{|0\rangle^{\otimes N} + |1\rangle^{\otimes N}}{\sqrt{2}}$.

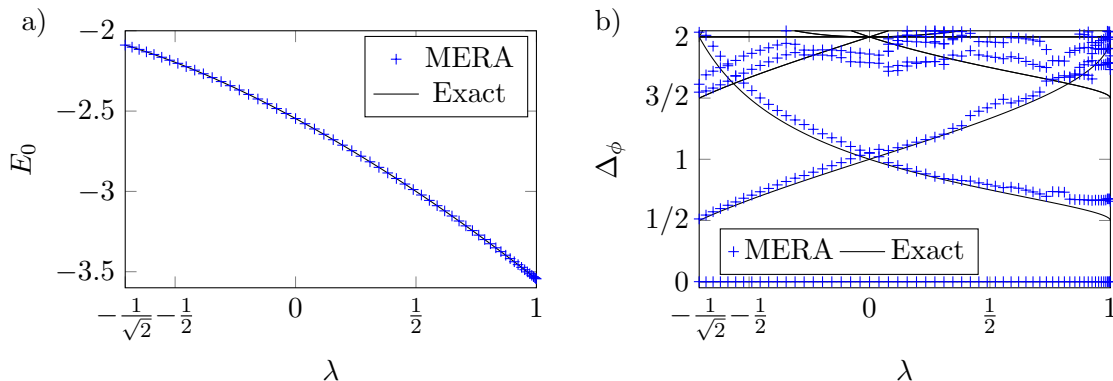


Figure 2.7.1: a) Ground state energy density extracted from a ternary MERA after optimising the tensors to locally minimise the energy. b) Correlation decay exponents for the transverse field cluster model obtained from a ternary MERA. Figures reproduced from Ref. [2.7.29].

Cluster State

It is more convenient to define the cluster state on a binary MERA than a ternary. Place two spins at each site and let

$$(2.7.15)$$

where $\bullet\text{---}\bullet$ is a controlled-Z gate and H is the Hadamard. If we pick a top tensor $T = |++\rangle$, we obtain the cluster state on periodic boundary conditions.

Gapless states

Recently, a family of analytic MERA for the critical point of the transverse field Ising model was proposed [2.7.11]. One can also use numerical techniques to obtain a MERA approximation to the ground state of a local Hamiltonian however. Here, we will present some physical data obtained for a model known as the transverse field cluster model [2.7.29]. In particular, we will present the ground state energy and the decay exponents (Δ_ϕ in Eqn. 2.7.10).

This model is most straightforwardly defined with a pair of spin half particles at each site. The Hamiltonian for this model is

$$\begin{aligned}
 H = & - \sum_j \left(X_j^{(1)} + X_j^{(2)} + Z_{j-1}^{(2)} X_j^{(1)} Z_j^{(2)} + Z_j^{(1)} X_j^{(2)} Z_{j+1}^{(1)} \right) \\
 & - \lambda \sum_j \left(X_j^{(1)} X_j^{(2)} + Z_j^{(1)} Y_j^{(2)} Y_{j+1}^{(1)} Z_{j+1}^{(2)} \right).
 \end{aligned}
 \tag{2.7.16}$$

This is the cluster state Hamiltonian with transverse fields and an additional interaction with variable strength. The Hamiltonian remains gapless for a range of values of λ , over which the ground state energy varies continuously as seen in Fig. 2.7.1a). The decay exponents also vary over this range, meaning that the thermodynamic physics or RG fixed point is dependent on λ . These

exponents can easily be extracted from an optimised MERA by finding the eigenvalues of the \mathcal{S} superoperator in Eqn. 2.7.8. The MERA results are shown in Fig. 2.7.1b).

Problems 7

Solutions in Appendix 2.H

1. Can you find a MERA for the W state?
2. What state is given by the MERA with



$$\text{Diagram} = \text{Diagram}, \tag{2.7.17}$$

$u = \mathbb{1}$ and top tensor $T = \frac{1}{\sqrt{2}}(|00\rangle + |11\rangle)$?

3. The above state is the ground state of the Hamiltonian

$$H = - \sum_{j=1}^{N/2} (X_{2j} X_{2j+1} + Z_{2j} Z_{2j+1}) \tag{2.7.18}$$

on periodic boundary conditions. Is that clear? Can you find a unitary $U_{2j-1,2j}$ which transforms this Hamiltonian into

$$H = - \sum_{j=1}^{N/2} (Z_{2j-1} X_{2j} Z_{2j+1} + Z_{2j} X_{2j+1} Z_{2j+2})? \tag{2.7.19}$$

4. Act with the above transformation U on the MERA tensor to obtain another MERA tensor. What is this state?
5. What is the maximum range of thermodynamic observables in a ternary MERA scheme?
6. What does the reduced density matrix on a few sites of the MERA look like? Notice that it corresponds to the top tensor being passed through a CPTP map several times, this is usually called the *descending superoperator*.
7. Do tree tensor networks (i.e. MERA for $u = \mathbb{1}$) have any area law violation on contiguous regions?

Bibliography

2.7.1 G. Vidal, Entanglement renormalization, [Physical Review Letters](#) **99**, 220405, [arXiv:cond-mat/0512165](#), (2007).

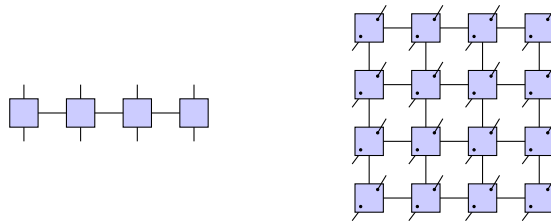
- 2.7.2 G. Vidal, Class of Quantum Many-Body States That Can Be Efficiently Simulated, [Physical Review Letters](#) **101**, 110501, [arXiv:quant-ph/0610099](#), (2008).
- 2.7.3 R. N. C. Pfeifer, G. Evenbly, and G. Vidal, Entanglement renormalization, scale invariance, and quantum criticality, [Physical Review A](#) **79**, 040301, [arXiv:0810.0580](#), (2009).
- 2.7.4 G. Evenbly and G. Vidal, Algorithms for entanglement renormalization, [Physical Review B](#) **79**, 149903, [arXiv:1201.1144](#), (2009).
- 2.7.5 G. Vidal, Entanglement Renormalization: An Introduction, in Understanding quantum phase transitions (L. Carr, ed.), ch. 5, p. 115–138, [CRC Press](#), [arXiv:0912.1651](#), (2011).
- 2.7.6 G. Evenbly and G. Vidal, Entanglement renormalization in fermionic systems, [Physical Review B](#) **81**, 235102, [arXiv:0710.0692](#), (2010).
- 2.7.7 L. Cincio, J. Dziarmaga and M. M. Rams, Multi-scale Entanglement Renormalization Ansatz in Two Dimensions: Quantum Ising Model, [Physical Review Letters](#) **100**, 240603, [arXiv:0710.3829](#), (2008).
- 2.7.8 M. Aguado and G. Vidal, Entanglement renormalization and topological order, [Physical Review Letters](#) **100**, 070404, [arXiv:0712.0348](#), (2008).
- 2.7.9 G. Evenbly and G. Vidal, Entanglement renormalization in two spatial dimensions, [Physical Review Letters](#) **102**, 180406, [arXiv:0811.0879](#), (2009).
- 2.7.10 G. Evenbly and G. Vidal, Quantum Criticality with the Multi-scale Entanglement Renormalization Ansatz, in Strongly Correlated Systems. Numerical Methods (A. Avella and F. Mancini, ed.), ch. 4, [Springer](#), [arXiv:1109.5334](#), (2013).
- 2.7.11 G. Evenbly and S. R. White, Entanglement renormalization and wavelets, [Physical Review Letters](#) **116**, 140403, [arXiv:1602.01166](#), (2016).
- 2.7.12 P. Di Francesco, P. Mathieu and D. Sénéchal, Conformal Field Theory. [Springer](#), (1997).
- 2.7.13 P. Christe and M. Henkel, Introduction to Conformal Invariance and Its Applications to Critical Phenomena. [Springer-Verlag](#), (1993).
- 2.7.14 J. M. Maldacena, The Large N Limit of Superconformal Field Theories and Supergravity, [International Journal of Theoretical Physics](#) **38**, 1113, [arXiv:hep-th/9711200](#), (1998).
- 2.7.15 E. Witten, Anti De Sitter Space And Holography, [Advances in Theoretical and Mathematical Physics](#) **2**, 253, [arXiv:hep-th/9802150](#), (1998).
- 2.7.16 S. S. Gusber, I. R. Klebanov and A. M. Polyakov Gauge theory correlators from non-critical string theory, [Physics Letters B](#) **428**, 105, [arXiv:hep-th/9802109](#), (1998).
- 2.7.17 B. Swingle, Entanglement Renormalization and Holography, [Physical Review D](#) **86**, 065007, [arXiv:0905.1317](#), (2012).
- 2.7.18 C. Bény, Causal structure of the entanglement renormalization ansatz, [New Journal of Physics](#) **15**, 023020, [arXiv:1110.4872](#), (2013).
- 2.7.19 N. Bao, C. Cao, S. M. Carroll and A. Chatwin-Davies, Consistency Conditions for an AdS/MERA Correspondence, [Physical Review D](#) **91**, 125036, [arXiv:1504.06632](#), (2015).

- 2.7.20 F. Pastawski, B. Yoshida, D. Harlow and J. Preskill, Holographic quantum error-correcting codes: Toy models for the bulk/boundary correspondence, [Journal of High Energy Physics](#) **6**, 149, [arXiv:1503.06237](#), (2015).
- 2.7.21 G. Evenbly and G. Vidal, Tensor network states and geometry, [Journal of Statistical Physics](#) **145**, 891, [arXiv:1106.1082](#), (2011).
- 2.7.22 M. Nozaki, S. Ryu, and T. Takayanagi, Holographic Geometry of Entanglement Renormalization in Quantum Field Theories, [Journal of High Energy Physics](#) **2012**, 193, [arXiv:1208.3469](#), (2012).
- 2.7.23 B. Swingle, Constructing holographic spacetimes using entanglement renormalization, [arXiv:1209.3304](#), (2012).
- 2.7.24 T. Hartman and J. Maldacena, Time Evolution of Entanglement Entropy from Black Hole Interiors, [Journal of High Energy Physics](#) **2013**, 014, [arXiv:1303.1080](#), (2013).
- 2.7.25 M. Miyaji, S. Ryu, T. Takayanagi, and X. Wen, Boundary States as Holographic Duals of Trivial Spacetimes, [Journal of High Energy Physics](#) **2015**, 152, [arXiv:1412.6226](#), (2015).
- 2.7.26 M. Miyaji and T. Takayanagi, Surface/State Correspondence as a Generalized Holography, [Progress of Theoretical and Experimental Physics](#) **2015**, 073B03, [arXiv:1503.03542](#), (2015).
- 2.7.27 M. Miyaji, T. Numasawa, N. Shiba, T. Takayanagi, and K. Watanabe, cMERA as Surface/State Correspondence in AdS/CFT, [Physical Review Letters](#) **115**, 171602, [arXiv:1506.01353](#), (2015).
- 2.7.28 W. -C. Gan, F. -W. Shu, and M. -H. Wu, Thermal geometry from CFT at finite temperature, [Physics Letters B](#) **750**, 796, [arXiv:1506.01353](#), (2015).
- 2.7.29 J. C. Bridgeman, A. O'Brien, S. D. Bartlett, and A. C. Doherty, Multiscale entanglement renormalization ansatz for spin chains with continuously varying criticality, [Physical Review B](#) **91**, 165129, [arXiv:1501.02817](#), (2015).

Appendices

2.A PEPOs for local Hamiltonians: The ‘particle decay’ construction

In numerical algorithms such as DMRG, operators such as Hamiltonians are often represented in the form of Matrix Product Operators (MPO) in 1D, and Projected Entangled Pair Operators (PEPO) in 2D and higher, as seen below. For highly structured Hamiltonians, such as those which are local and translation invariant, an analytic MPO construction of such operators is known in 1D [2.1.1]. In this section we review this, and outline a generalisation which allows for local Hamiltonians (and even slightly less structured operators) to be optimally expressed as a PEPOs in arbitrary spatial dimensions.



Much like in Equations (2.3.54) and (2.3.58) we are going to omit the physical indices, as such we will consider MPO tensors to be (operator-valued) matrices, and PEPO tensors to be (operator-valued) rank- $2D$ tensors in D spatial dimensions.

In this section we will need to specify individual tensor values, as well as the values of a tensor network for a specific index designation. For brevity, we will therefore omit the legs in our diagrams, indicating specific entries in a tensor by a \square surrounded by the index values. For example the identity is given by $i \square i = 1$ for all i . To make the constructions more clear we will also allow for non-numeric index values, and denote the index set by I .

2.A.1 1D

In this notation, if we label our indices $I = \{ \cdot, 1, \rightarrow \}$, then the transverse Ising model Hamiltonian given in Equation (2.3.54) is given by

$$\cdot \square \cdot = \rightarrow \square \rightarrow = 1 \tag{2.A.1}$$

$$\rightarrow \square \cdot = -hZ \quad \rightarrow \square 1 = X \quad 1 \square \cdot = -JX \tag{2.A.2}$$

where the boundary terms fix the far left and right indices to $|\rightarrow\rangle$ and $|\cdot\rangle$ respectively.

One common interpretation of this construction is in terms of finite-state automata, with the index values corresponding to the automaton states, and the non-zero index values to the transition

rules. The automaton moves from left to right¹², with the boundary vectors setting the initial state to $|\rightarrow\rangle$ and final state to $|\cdot\rangle$. With only these restrictions, the automaton can transition from $|\rightarrow\rangle$ to $|\cdot\rangle$ either directly (giving the field term $-hZ$), or via 1 (giving the Ising term $-JXX$) at any location.

To make the higher dimensional generalisation clear we will slightly modify this finite-state automata language, to that of particles and their decay. We can think of \rightarrow as a right-moving particle, and \cdot as the vacuum. The first two transition rules (2.A.1) correspond to both the vacuum and particle being stable states, with the remaining transitions (2.A.2) to valid decay routes of the particle. Thus we can interpret the value of the overall MPO as being a superposition over all decays, with each corresponding to a term in the Hamiltonian.

Heisenberg Model

Suppose we wish to construct a Hamiltonian containing multiple two-body terms, such as the Heisenberg anti-ferromagnet, which contains the terms $-J_X XX$, $-J_Y YY$, $-J_Z ZZ$, as well as a field $-hZ$. An MPO of this model is given in standard notation in Equation (2.3.58).

Added Hamiltonian terms can be accommodated in this construction by extra decay chains. Take our index set to be $I = \{\cdot, x, y, z, \rightarrow\}$ and our MPO to have terms:

$$\cdot \square \cdot = \mathbb{1} \qquad \rightarrow \square \rightarrow = \mathbb{1} \qquad (2.A.3)$$

$$\rightarrow \square x = X \qquad x \square \cdot = -J_X X \qquad (2.A.4)$$

$$\rightarrow \square y = Y \qquad y \square \cdot = -J_Y Y \qquad (2.A.5)$$

$$\rightarrow \square z = Z \qquad z \square \cdot = -J_Z Z \qquad (2.A.6)$$

$$\rightarrow \square \cdot = -hZ \qquad (2.A.7)$$

Again Equations 2.A.3 correspond to stable vacuum and particles, and each of the transition rules Equations (2.A.4) to (2.A.7) to each term in the Hamiltonian.

Cluster Model

The Cluster Hamiltonian contains three body terms of the form ZXZ . Larger terms such as this can be accommodated by longer decay chains. Take an index set $I = \{\cdot, 1, 2, \rightarrow\}$ and include the standard stable vacuum/particle terms as well as

$$\rightarrow \square 2 = Z \qquad 2 \square 1 = X \qquad 1 \square \cdot = Z. \qquad (2.A.8)$$

By combining the above two techniques, we can construct arbitrary local Hamiltonians.

2.A.2 2D and higher

In higher dimensions we can use a similar construction. Suppose we want to construct a 2D field Hamiltonian, consisting of a Z at every site. Take our index set to be $I = \{\rightarrow, \cdot\}$. Our typical stable vacuum/particle terms that we will always include now become

$$\begin{array}{c} \cdot \\ \cdot \square \cdot = \rightarrow \square \rightarrow = \mathbb{1}. \\ \cdot \end{array} \qquad (2.A.9)$$

¹²Though a right-to-left convention is more commonly used in this 1D construction, a left-to-right convention will prove useful for consistency with the higher dimensional construction.

For the field Hamiltonian we need only allow for a simple particle decay of

$$\begin{array}{c} \cdot \\ \rightarrow \square \cdot = Z \\ \cdot \end{array} \quad (2.A.10)$$

As for the boundary conditions, along the top, right and bottom boundaries we will once again fix the only non-zero indices to be the vacuum $|\cdot\rangle$. Along the left edge, the boundary condition is a virtual W-state (c.f. Equation (2.3.18)) on indices $\{\rightarrow, \cdot\}$, i.e. the equal superposition of all single-particle states. As such we can see that all the non-zero contributions to the Hamiltonian are of the form:

$$\begin{array}{cccccc} \cdot & \cdot & \cdot & \cdot & \cdot & \cdot \\ \cdot & \square & \cdot & \square & \cdot & \square & \cdot \\ \cdot & \cdot & \cdot & \cdot & \cdot & \cdot & \cdot \\ \rightarrow & \square & \rightarrow & \square & \rightarrow & \square & \cdot \\ \cdot & \cdot & \cdot & \cdot & \cdot & \cdot & \cdot \\ \cdot & \square & \cdot & \square & \cdot & \square & \cdot \\ \cdot & \cdot & \cdot & \cdot & \cdot & \cdot & \cdot \end{array} = \begin{array}{cccccc} \mathbb{1} & \mathbb{1} & \mathbb{1} & \mathbb{1} & \mathbb{1} & \\ \mathbb{1} & \mathbb{1} & \mathbb{1} & Z & \mathbb{1} & \\ \mathbb{1} & \mathbb{1} & \mathbb{1} & \mathbb{1} & \mathbb{1} & \mathbb{1} \end{array}$$

As with 1D, by introducing intermediary states and different decay rules, arbitrary local Hamiltonians in any dimension can be similarly constructed. For example suppose we wanted a 9-body plaquette term of the form:

$$\begin{array}{ccc} J & K & L \\ M & N & O \\ P & Q & R \end{array}$$

Take $I = \{\cdot, 1, 2, \rightarrow\}$ and our non-trivial decay modes to be

$$\begin{array}{ccc} \cdot & \cdot & \cdot \\ \rightarrow & \square & 2 = J, & 2 & \square & 1 = K, & 1 & \square & \cdot = L, \\ & 2 & & 2 & & 2 & & 2 & \\ & 2 & & 2 & & 2 & & 2 & \\ \cdot & \square & 1 = M, & 2 & \square & 1 = N, & 1 & \square & \cdot = O, \\ & 1 & & 1 & & 1 & & 1 & \\ & 1 & & 1 & & 1 & & 1 & \\ \cdot & \square & 2 = P, & 2 & \square & 1 = Q, & 1 & \square & \cdot = R. \\ \cdot & \cdot & \cdot & \cdot & \cdot & \cdot & \cdot & \cdot & \cdot \end{array}$$

then we can see that the non-zero contributions to the Hamiltonian are of the form

$$\begin{array}{cccccccc} \cdot & \cdot & \cdot & \cdot & \cdot & \cdot & \cdot & \cdot \\ \cdot & \square & \cdot & \square & \cdot & \square & \cdot & \square & \cdot \\ \cdot & \cdot & \cdot & \cdot & \cdot & \cdot & \cdot & \cdot & \cdot \\ \rightarrow & \square & \rightarrow & \square & \rightarrow & \square & 2 & \square & 1 & \square & \cdot & \square & \cdot \\ \cdot & \cdot & \cdot & \cdot & \cdot & \cdot & \cdot & \cdot & \cdot & \cdot & \cdot & \cdot & \cdot \\ \cdot & \square & \cdot & \square & \cdot & \square & 2 & \square & 1 & \square & \cdot & \square & \cdot \\ \cdot & \cdot & \cdot & \cdot & \cdot & \cdot & \cdot & \cdot & \cdot & \cdot & \cdot & \cdot & \cdot \\ \cdot & \square & \cdot & \square & \cdot & \square & 2 & \square & 1 & \square & \cdot & \square & \cdot \\ \cdot & \cdot & \cdot & \cdot & \cdot & \cdot & \cdot & \cdot & \cdot & \cdot & \cdot & \cdot & \cdot \\ \cdot & \square & \cdot & \square & \cdot & \square & \cdot & \square & \cdot & \square & \cdot & \square & \cdot \\ \cdot & \cdot & \cdot & \cdot & \cdot & \cdot & \cdot & \cdot & \cdot & \cdot & \cdot & \cdot & \cdot \end{array} = \begin{array}{cccccccc} \mathbb{1} & \mathbb{1} & \mathbb{1} & \mathbb{1} & \mathbb{1} & \mathbb{1} & \mathbb{1} & \mathbb{1} \\ \mathbb{1} & \mathbb{1} & J & K & L & \mathbb{1} & \mathbb{1} & \mathbb{1} \\ \mathbb{1} & \mathbb{1} & M & N & O & \mathbb{1} & \mathbb{1} & \mathbb{1} \\ \mathbb{1} & \mathbb{1} & P & Q & R & \mathbb{1} & \mathbb{1} & \mathbb{1} \\ \mathbb{1} & \mathbb{1} & \mathbb{1} & \mathbb{1} & \mathbb{1} & \mathbb{1} & \mathbb{1} & \mathbb{1} \end{array}$$

2.A.3 Other examples

Below are several more example of Hamiltonian constructed by the above method.

Toric code (Wen Plaquette)

$$I = \{\cdot, 1, \rightarrow\} \quad \rightarrow \quad \begin{array}{c} \cdot \\ \square \quad 1 = 1 \quad \square \quad \cdot = X \\ 1 \quad \quad \cdot \end{array} \quad \begin{array}{c} \cdot \\ 1 \quad \square \quad \cdot = \cdot \quad \square \quad 1 = Y \\ 1 \quad \quad \cdot \end{array}$$

Quantum Compass model/Bacon-Shor code

$$I = \{\cdot, 1, \rightarrow\} \quad \rightarrow \quad \begin{array}{c} \cdot \\ \square \quad 1 = 1 \quad \square \quad \cdot = X \\ \cdot \quad \quad \cdot \end{array} \quad \rightarrow \quad \begin{array}{c} \cdot \\ \square \quad \cdot = \cdot \quad \square \quad \cdot = Y \\ 1 \quad \quad \cdot \end{array}$$

2D Transverse Ising

$$I = \{\cdot, 1, \rightarrow\} \quad \rightarrow \quad \begin{array}{c} \cdot \\ \square \quad \cdot = hZ \\ \cdot \end{array} \quad \rightarrow \quad \begin{array}{c} \cdot \\ \square \quad 1 = \rightarrow \\ \cdot \end{array} \quad \rightarrow \quad \begin{array}{c} \cdot \\ \square \quad \cdot = JX \\ 1 \end{array} \quad \begin{array}{c} \cdot \\ 1 \quad \square \quad \cdot = \cdot \quad \square \quad \cdot = -X \\ \cdot \quad \quad \cdot \end{array}$$

2D Cluster state

$$I = \{\cdot, 1, 2, \rightarrow\} \quad \rightarrow \quad \begin{array}{c} \cdot \\ \square \quad 2 = 1 \quad \square \quad \cdot = \cdot \quad \square \quad \cdot = \cdot \quad \square \quad \cdot = Z \\ \cdot \quad \quad \cdot \quad \quad \cdot \quad \quad 1 \end{array} \quad \begin{array}{c} \cdot \\ 2 \quad \square \quad 1 = X \\ 1 \end{array}$$

Bibliography

- 2.A.1 U. Schollwöck, “The density-matrix renormalization group in the age of matrix product states,” *Annals of Physics* **326**, 96–192, [arXiv:1008.3477](https://arxiv.org/abs/1008.3477), (2011).

2.B Solutions: Introduction to Tensor Networks

Solutions 1

Solutions to problems in section 2.1.5

1. Consider the following tensors, in which all indices are three-dimensional, indexed from 0:

$$\begin{array}{c} \textcircled{A} \\ | \\ j \end{array} \begin{array}{c} i \\ \text{---} \end{array} = i^2 - 2j, \quad \begin{array}{c} i \\ \diagup \\ \textcircled{B} \\ \diagdown \\ k \end{array} = -3^i j + k, \quad (2.B.1)$$

$$\begin{array}{c} j \\ \diagup \\ \textcircled{C} \\ \diagdown \\ i \end{array} = j, \quad \begin{array}{c} i \text{---} \\ \diagdown \\ \textcircled{D} \\ \diagup \\ j \end{array} \begin{array}{c} k \\ \text{---} \end{array} = ijk. \quad (2.B.2)$$

Calculate the value of the following tensor network:

$$\begin{array}{cc} \textcircled{A} & \textcircled{D} \\ & \diagdown \quad \diagup \\ & \textcircled{B} & \textcircled{C} \end{array} \quad (2.B.3)$$

First we begin by picking a global designation of the indices which is consistent with the contractions required:

$$\begin{array}{c} \textcircled{A} \\ | \\ \alpha \end{array} \begin{array}{c} \beta \\ \text{---} \end{array} = \beta^2 - 2\alpha, \quad \begin{array}{c} \alpha \\ \diagup \\ \textcircled{B} \\ \diagdown \\ \delta \end{array} \begin{array}{c} \gamma \\ \text{---} \end{array} = -3^\alpha \gamma + \delta, \quad (2.B.4)$$

$$\begin{array}{c} \epsilon \\ \diagup \\ \textcircled{C} \\ \diagdown \\ \delta \end{array} = \epsilon, \quad \begin{array}{c} \beta \text{---} \\ \diagdown \\ \textcircled{D} \\ \diagup \\ \gamma \end{array} \begin{array}{c} \epsilon \\ \text{---} \end{array} = \beta\gamma\epsilon. \quad (2.B.5)$$

Now that our indices have been matched up, the overall value of the tensor network T is given by the product of the above values, summed over all index labelling

$$T = \sum_{\alpha, \beta, \gamma, \delta, \epsilon=0}^2 A_{\alpha, \beta} B_{\alpha, \gamma, \delta} C_{\delta, \epsilon} D_{\beta, \gamma, \epsilon} \quad (2.B.6)$$

$$= \sum_{\alpha, \beta, \gamma, \delta, \epsilon=0}^2 (\beta^2 - 2\alpha)(-3^\alpha \gamma + \delta)\beta\gamma\epsilon^2 \quad (2.B.7)$$

$$= 1080. \quad (2.B.8)$$

2. In this question we are going to consider expanding out a contraction sequence, in a manner which would be needed when coding up contractions. Given a network, and an associated bubbling, we wish to write out a table keeping track of the indices of the current object, the tensor currently being contracted in, the indices involved in that contraction, and new indices left uncontracted. For example for the network



where the bubbling is performed in alphabetical order, then the table in question looks like

Current	Tensor	Contract	New
–	A	–	α, β
α, β	B	α	γ
β, γ	C	β, γ	δ

For the tensor network



construct a corresponding table, where contraction is once again done in alphabetical order.

Current	Tensor	Contract	New
–	A	–	α, β
α, β	B	α	γ
β, γ	C	γ	δ, ϵ
β, δ, ϵ	D	β, δ	
ϵ	E	ϵ	–

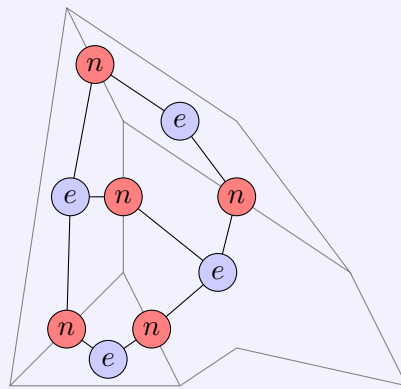
3. (a) Calculate the contraction of the tensor network in Eq. (2.1.19) for bond dimension 3, i.e. calculate the number of three-colourings of the corresponding graph.

Numerically contracting the tensor network given in the notes gives a total number of vertex 3-colourings of 30.

- (b) Using the e and n tensors from Sec. 2.1.5, come up with a construction for a tensor network which gives the number of *edge* colourings. For a planar graphs, construct an analogous network to count *face* colourings.

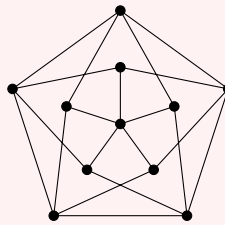
First we note that index values already correspond to edges, thus by simply placing an n tensor at every vertex of a graph, the tensor network given counts edge colourings.

As for a face colouring, we can simple apply the vertex colouring construction to the dual graph. As such we place e tensors on each face, and n on each edge, as below.



(2.B.11)

- (c) Using tensor networks, determine the minimum number of colours required to vertex and edge colour the below graph (known as the chromatic number and index respectively).



(2.B.12)

This is the Grötzsch Graph, it has chromatic number and index 4 and 5 respectively.

4. Much like the singular value decomposition, given a bisection of the indices we can consider norms of tensors.

- (a) Does the operator norm depend on the bisection, i.e. are the operator norms across any two bisections of the same tensor necessarily equal?

Yes it does depend on the bisection. A simple example is given by a generic matrix M . Treating it as a matrix, it has operator norm $\|M\|_\infty$. If however we vectorise M , treating it as a vector, then the operator norm of this vector corresponds to the Frobenius norm of the matrix $\|M\|_F$. In general these two norms differ, and thus the operator norm is bisection-dependent.

- (b) What about the Frobenius norm? If they can differ, give an example, if not draw a tensor network diagram that shows it to be manifestly independent of bisection.

For a matrix M , the square of the Frobenius norm is $\text{Tr}(MM')$. Taking a rank-3 tensor this looks like



$$\text{---} \quad (2.B.13)$$

By simply wrapping the external leg around however we can see that this simply equals



$$\text{---} \quad (2.B.14)$$

which is the squared Frobenius norm of the vectorisation. By a similar argument the Frobenius norm in any grouping can be shown to be equal to that of the vectorisation. Thus the Frobenius norm of a tensor is independent of the bisection with respect to which it is calculated.

$$\|A\|_F = \sqrt{\sum_{i_1, \dots, i_r} |A_{i_1, \dots, i_r}|^2}$$

5. Write out the Einstein notation corresponding to the network in Eq. (2.7.1).

The purpose of this exercise is to show that for networks for which the number of indices is too high for Einstein notation, TNN can remain legible.

2.C Solutions: Quantum information examples

Solutions 2

Solutions to problems in section 2.2.4

1. Consider the inverse of teleportation. Alice wishes to send classical bits to Bob, and possesses a quantum channel through which she can send Bob qubits. How many bits of information can be communicated in a single qubit? For simplicity consider the case where Bob can only perform projective measurements.

As we are dealing with a qubit the only non-trivial projective measurements are projectors on to pure states. As a result, after performing such a measurement the state is entirely fixed, i.e. only the first measurement actually yields useful information. As such a maximum of 1 bit can be extracted in this way. This bound is saturated by the trivial (classical) encoding. This is a specific case of a more general bound known as Holevo's Theorem, which states that only n bits may be extracted from n qubits under a slightly more general setting.

2. Suppose Alice and Bob initially shared a Bell pair. Does this pre-shared entanglement resource boost the amount of classical information that can be successfully communicated, and if so by how much? *Hint: Notice that the four possible Bell states differ by a Pauli acting on a single qubit.*

Yes, indeed 2 bits may be transferred by leveraging this pre-shared entanglement. Suppose that Alice has two bits, i and j . She performs on her Bell qubit the Pauli $p := X^i Z^j$, and then transmits her qubit back to Bob. The state which Bob now possesses is $|\psi\rangle$:

$$\begin{array}{c}
 \boxed{\psi} = \\
 \hline
 \hline
 \end{array}
 =
 \begin{array}{c}
 \boxed{\Omega} \\
 \hline
 \hline
 \end{array}
 \begin{array}{c}
 \xrightarrow{\text{Alice}} \\
 \xrightarrow{\text{Bob}}
 \end{array}
 \begin{array}{c}
 \boxed{p} \\
 \hline
 \hline
 \end{array}
 =
 \begin{array}{c}
 \boxed{\Omega(p)} \\
 \hline
 \hline
 \end{array}
 \quad (2.C.1)$$

If Bob now measures in the Bell basis, he will recover the outcome p , from which he can back out i and j . As such Alice has successfully transmitted two bits to Bob. This procedure is known as *superdense coding*.

2.D Solutions: Matrix Product States

Solutions 3

Solutions to problems in section 2.3.5

- Describe the state given by an MPS with tensor

$$A = \begin{matrix} & 0 & 1 \\ 00 & \begin{pmatrix} 1 & 0 \\ 0 & 1 \end{pmatrix} \\ 10 & \\ 01 & \begin{pmatrix} 1/2 & -1/2 \\ 1/2 & -1/2 \end{pmatrix} \\ 11 & \end{matrix} \quad \begin{matrix} 1 & \boxed{A} & 3 \\ & | & \\ & 2 & \end{matrix}, \quad (2.D.1)$$

where index ordering is as shown and indices 1 and 2 are combined. Boundary conditions require inserting a Pauli Z before closing periodic BCs, similar to Eq. (2.3.19).

Consider the self-inverse Hadamard gate. Performing a gauge transformation corresponding to contracting Hadamards onto each virtual bond, we end up with with a new MPS tensor

$$B = \begin{matrix} & 0 & 1 \\ 00 & \begin{pmatrix} 1 & 0 \\ 0 & 1 \end{pmatrix} \\ 10 & \\ 01 & \begin{pmatrix} 0 & 1 \\ 0 & 1 \end{pmatrix} \\ 11 & \begin{pmatrix} 0 & 0 \\ 0 & 0 \end{pmatrix} \end{matrix}. \quad (2.D.2)$$

and a boundary condition now corresponding to closing on an X gate. We can recognise this as the MPS of Eq. (2.3.18), meaning that this described the W-state.

- Describe the state given by the MPS whose only nonzero components are

$$\begin{matrix} 0 & \boxed{A} & 0 \\ & | & \\ & 0 & \end{matrix} = \begin{matrix} 1 & \boxed{A} & 1 \\ & | & \\ & 0 & \end{matrix} = \begin{matrix} 0 & \boxed{A} & 1 \\ & | & \\ & 1 & \end{matrix} = \begin{matrix} 1 & \boxed{A} & 0 \\ & | & \\ & 1 & \end{matrix} = 1, \quad (2.D.3)$$

where the left and right boundary conditions are $|0\rangle$.

Hint: Writing out the matrices corresponding to fixing the physical index might help!

We have that

$$A_0 = \begin{pmatrix} 1 & 0 \\ 0 & 1 \end{pmatrix} = \mathbb{1}, \quad A_1 = \begin{pmatrix} 0 & 1 \\ 1 & 0 \end{pmatrix} = X. \quad (2.D.4)$$

Therefore, if we begin on the left end in the $\langle 0|$ state, we must insert an even number of A_1 before we reach the right $|0\rangle$. Thus, we obtain the state

$$|\psi[A]\rangle = \sum |\text{even number of 1s}\rangle. \quad (2.D.5)$$

3. Describe the qudit state given by the MPS

$$i \text{---} \boxed{A} \text{---} i \oplus j \quad = 1 \quad (2.D.6)$$

\downarrow
 j

where $i, j \in \mathbb{Z}_d$, \oplus denotes addition mod d , the left boundary condition is $|0\rangle$, and the right boundary is $|q\rangle$ for some $q \in \mathbb{Z}_d$.

We have that

$$A_1 = \begin{pmatrix} 0 & 1 & 0 & \cdots & 0 & 0 & 0 \\ 0 & 0 & 1 & \cdots & 0 & 0 & 0 \\ 0 & 0 & 0 & \cdots & 0 & 0 & 0 \\ \vdots & \vdots & \vdots & \ddots & \vdots & \vdots & \vdots \\ 0 & 0 & 0 & \cdots & 0 & 1 & 0 \\ 0 & 0 & 0 & \cdots & 0 & 0 & 1 \\ 1 & 0 & 0 & \cdots & 0 & 0 & 0 \end{pmatrix} \quad (2.D.7)$$

We can recognise A_1 as the (transpose of) the generalised Pauli X matrix and $A_k = A_1^k$. Therefore, if we begin on the left end in the $\langle 0|$ state, we must insert A_k s such that the sum of the string (mod d) is q before we reach the right $|q\rangle$. Thus, we obtain the state

$$|\psi[A]\rangle = \sum |\text{strings summing to } q\rangle. \quad (2.D.8)$$

4. Let \mathcal{G} be some group. Describe the operator given by the MPO with

$$g \text{---} \boxed{M} \text{---} g \cdot h \quad = 1 \quad (2.D.9)$$

$\begin{matrix} h \\ \downarrow \\ \uparrow \\ h \end{matrix}$

where the left boundary condition is 0, the right boundary is some group element q and \cdot denotes group multiplication.

This is a generalisation of problem 3. Rather than a state, we end up with an operator. Rather than summing to q , the operator terms should multiply to q (under the group operation). We end up with the operator which projects onto states which multiply to q .

5. Suppose the local basis is labelled by particle number. What is the action of the following operator (bond dimension linearly increasing left to right)?

$$\begin{array}{c}
 m \\
 | \\
 n - \boxed{M} - n + m \\
 | \\
 m
 \end{array} = 1 \tag{2.D.10}$$

with left vector $L = |0\rangle$ and right vector $R = \sum_{i=0}^N i|i\rangle$.

This is similar to the operator in problem 4, however rather than projecting onto a subspace, the operator multiplies a state summing to j by the number j . Therefore, taking expectations of this operator returns the expected particle number.

6. Write an MPO for the transverse-field-cluster Hamiltonian

$$H = -J \sum_j Z_{j-1} X_j Z_{j+1} - h \sum_j X_j. \tag{2.D.11}$$

Hint: This can be done with bond dimension 4.

We can use the construction in Appendix 2.A, we obtain

$$M = \begin{pmatrix} \mathbb{1} & 0 & 0 & 0 \\ Z & 0 & 0 & 0 \\ 0 & X & 0 & 0 \\ -hX & 0 & -JZ & \mathbb{1} \end{pmatrix}, \tag{2.D.12}$$

with left and right vectors

$$L = (0 \ 0 \ 0 \ 1) \qquad R = (1 \ 0 \ 0 \ 0)^T. \tag{2.D.13}$$

7. Use the ideas of MPSs and MPOs to prove that log depth quantum circuits can be simulated efficiently on a classical computer.

Suppose we have a log depth circuit acting on $|0\rangle^{\otimes N}$. Breaking U down in to circuit elements, the state we wish to know has the form

$$\psi = U = \left. \begin{array}{c} \text{[Diagram of 5 gates in a brickwork pattern]} \\ \log(n) \end{array} \right\} \quad (2.D.14)$$

Next we decompose our gates into single qubit tensors:

$$\text{[Diagram of gate decomposition]} \quad (2.D.15)$$

We now use this factorisation, and vertically group our tensors together. The resulting state is an MPS.

$$\text{[Diagram of MPS construction]} \quad (2.D.16)$$

As our circuit has only logarithmic depth, the bond dimension is at most polynomial, allowing our classical simulation to be efficient.

2.E Solutions: Classifying Gapped Phases in 1D

Solutions 4

Solutions to problems in section 2.4.4

1. The group $\mathbb{Z}_2 \times \mathbb{Z}_2$ has the presentation $\mathbb{Z}_2 \times \mathbb{Z}_2 = \langle x, z | x^2 = z^2 = e, xz = zx \rangle$. Show that the Pauli matrices form a projective representation of $\mathbb{Z}_2 \times \mathbb{Z}_2$.

Hint: let $v_x = X$, $v_z = Z$, $v_{xz=zx} = Y$ and show that $v_g v_h = \omega[g, h] v_{gh}$, where ω is some phase.

Let $v_x = X$, $v_z = Z$ and $v_{xz} = Y$. We can then calculate $\omega[g, h]$, obtaining

$$\begin{array}{c} e \quad x \quad z \quad xz \\ e \quad \left(\begin{array}{cccc} 1 & 1 & 1 & 1 \\ 1 & 1 & -i & i \\ 1 & i & 1 & -i \\ 1 & -i & i & 1 \end{array} \right) \\ x \\ z \\ xz \end{array} \quad (2.E.1)$$

2. Determine the *factor system* $\omega[g, h]$ for the Pauli matrices.

See Problem 1 above.

3. Show that the Pauli projective representation is not equivalent to a linear representation.

Hint: $xz = zx$, can we rephase v_x and v_z to make $v_x v_z - v_z v_x = 0$?

If we had a linear representation, we would have $u_x u_z - u_z u_x = 0$. Consider rephasing the v s

$$v_g \rightarrow e^{i\phi_g} v_g. \quad (2.E.2)$$

The commutator then becomes

$$e^{i(\phi_x + \phi_z)} (v_x v_z - v_z v_x). \quad (2.E.3)$$

Therefore no rephasing can bring this to 0, so the Paulis do *not* form a linear representation.

4. Recall from Section 2.3.2 that the symmetry of the cluster state is $\mathbb{Z}_2 \times \mathbb{Z}_2$, with the action on the MPS tensor being

$$\begin{array}{c} \square \\ | \\ \square \end{array} = \begin{array}{c} \circ Z \\ | \\ \square \\ | \\ \circ Z \end{array}, \quad \begin{array}{c} \square \\ | \\ \square \end{array} = \begin{array}{c} \circ X \\ | \\ \square \\ | \\ \circ X \end{array}. \quad (2.E.4)$$

What can we conclude about the cluster state?

Since the Paulis form a nontrivial projective representation of $\mathbb{Z}_2 \times \mathbb{Z}_2$, we know that the cluster state is in a nontrivial phase. That is, it cannot be transformed into a product state using a constant depth local circuit with $\mathbb{Z}_2 \times \mathbb{Z}_2$ symmetry.

2.F Solutions: Tensor network algorithms

Solutions 5

Solutions to problems in section 2.5.3

1. Consider the critical transverse Ising model

$$H = - \sum_{i=1}^{n-1} X_i X_{i+1} - \sum_{i=1}^n Z_i. \quad (2.F.1)$$

For open boundary conditions, it is known that the ground state energy as a function of n has the form

$$E(n) = 1 - \csc\left(\frac{\pi}{\alpha n + \beta}\right) \quad (2.F.2)$$

for some integers α and β . Using either DMRG or TEBD, estimate the ground state energy for several chain lengths and calculate α and β .

Running this for moderate system sizes, bond dimensions, and time-scales, with either DMRG or TEBD, it is relatively easy to calculate that $\alpha = 4$, $\beta = 2$.

2. It is known that the LOCAL HAMILTONIAN problem is in P for gapped Hamiltonians. DMRG and TEBD are the most common techniques for numerically finding the ground states of such systems. For a gapped and 1D local Hamiltonian, prove that DMRG or TEBD converge.

This was a somewhat of trick question. Despite the complexity of the underlying problem and the practical power of these algorithms both being well understood, a satisfactory theoretical understanding of the effectiveness of DMRG/TEBD is an elusive open problem. Even a concrete statement of the convergence properties that these algorithms possess is still a topic of debate.

2.G Solutions: Projected Entangled Pair States

Solutions 6

Solutions to problems in section 2.6.5

1. What is the PEPS tensor required to build the GHZ state on the honeycomb lattice where spins reside on vertices?

Let the PEPS tensor be the ‘delta-tensor’, the tensor which is 1 if all indices are equal and zero otherwise. Fixing boundary conditions to be $|+\rangle$ on each index give the GHZ state.

2. Which 2 qubit gate is obtained by contracting the following tensors along the horizontal index?

$$\begin{array}{c} j \\ | \\ \boxed{u} - k \\ | \\ i \end{array} = \delta_{i,j} (\delta_{k,0} + (-1)^i \delta_{k,1}), \quad \begin{array}{c} y \\ | \\ \boxed{v} \\ | \\ x \end{array} = \delta_{x,y,z}. \quad (2.G.1)$$

Performing the contraction over the horizontal bond, we obtain

$$\begin{array}{cccc} & 00 & 10 & 01 & 11 \\ \begin{array}{c} 00 \\ 10 \\ 01 \\ 11 \end{array} & \begin{pmatrix} 1 & 0 & 0 & 0 \\ 0 & 1 & 0 & 0 \\ 0 & 0 & 1 & 0 \\ 0 & 0 & 0 & -1 \end{pmatrix} & & & \end{array} \quad (2.G.2)$$

where the row indices are (ix) and the column indices are (jy) . We recognise this as the CZ gate.

3. The cluster state can be prepared from the all $|+\rangle$ state by applying CZ between all adjacent spins. Show that Eq. (2.6.20) indeed gives the cluster state.

Hint: Consider the decomposition of a gate given in the above problem.

We have a decomposition of the CZ operator in 2. It remains to build a PEPS tensor from this. The only tricky part is ensuring that when the bonds link up, each ‘ u ’ tensor connects to a ‘ v ’ tensor. The PEPS tensor is therefore

$$(2.G.3)$$

Contracting this, we obtain the tensor in Eq. (2.6.20).

- Investigate how logical operators on the physical spins of the Toric code can be pulled onto the virtual level of the PEPS. Can you see why \mathcal{G} -injectivity is so important for topologically ordered PEPS?

The logical operators of the Toric code are build from strings of Z s and X s. Consider placing a single Z on a physical bond of the PEPS tensor in Eq. (2.6.17). It is not hard to see that

$$(2.G.4)$$

We can use this to understand how the physical Z string pulls through to the virtual level.

$$(2.G.5)$$

Which has two physical Z s corresponding to the end points of the string, and a virtual string of Z s. This string can be moved around using the rules of Eq. (2.6.19).

We can do the same exercise for the X string and obtain

$$\text{Diagram} = \text{Diagram}, \quad (2.G.6)$$

$$\text{Diagram} \rightarrow \text{Diagram}. \quad (2.G.7)$$

Thus, the X string pulls through to an isolated pair of X s acting on the virtual level at the ends of the string.

The \mathcal{G} -injectivity property is the ability to pull the Z string through the PEPS tensor, which means the presence of a Z string is not locally observable.

5. Convince yourself that evaluating expectation values on the PEPS constructed from a classical partition function indeed reproduces the thermal expectation values.

Play with the network! Pull the expectation up to the virtual level and flatten.

2.H Solutions: Multiscale Entanglement Renormalisation Ansatz

Solutions 7

Solutions to problems in section 2.7.4

1. Can you find a MERA for the W state?

For this we are going to construct a tree ($u = 1$) that takes the W-state n qubits to the W-state on $2n$ qubits.

$$\begin{array}{c} 0 \\ \diagup \quad \diagdown \\ \triangle \\ \diagdown \quad \diagup \\ 0 \quad 0 \end{array} = \begin{array}{c} 1 \\ \diagup \quad \diagdown \\ \triangle \\ \diagdown \quad \diagup \\ 1 \quad 0 \end{array} = \begin{array}{c} 1 \\ \diagup \quad \diagdown \\ \triangle \\ \diagdown \quad \diagup \\ 0 \quad 1 \end{array} = 1 \quad (2.H.1)$$

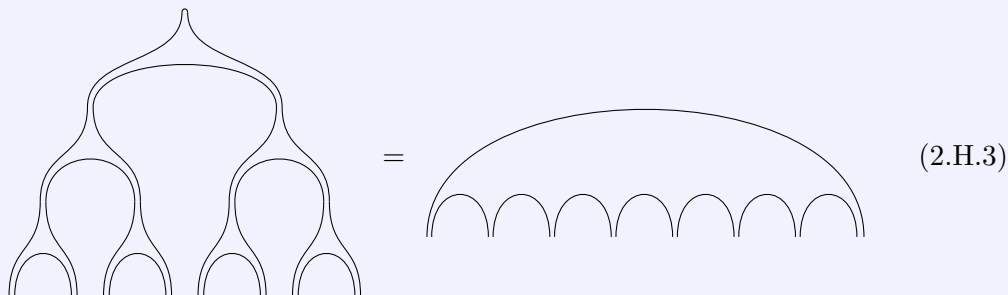
It can be seen that by applying this isometry to a W-state will expand it. Thus if we take a tree with top tensor $T = |1\rangle$, then we recover the full W-state.

2. What state is given by the MERA with

$$\begin{array}{c} \parallel \\ \diagup \quad \diagdown \\ \triangle \\ \diagdown \quad \diagup \\ \parallel \quad \parallel \end{array} = \begin{array}{c} \diagup \quad \diagdown \\ \text{ } \\ \diagdown \quad \diagup \end{array}, \quad (2.H.2)$$

$u = 1$ and top tensor $T = \frac{1}{\sqrt{2}}(|00\rangle + |11\rangle)$?

Firstly note that the top tensor $T \propto |00\rangle + |11\rangle$ is simply the Bell state, i.e. $T = \bigwedge$. Drawing the tree out for 8 sites (16 qubits), we have:



We therefore have the periodic state consisting of Bell states shared between each neighbouring site, i.e. the state on which PEPS is based. As a result we can see that any MPS state can therefore be prepared from a MERA by modifying one single layer.

3. The above state is the ground state of the Hamiltonian

$$H = - \sum_{j=1}^{N/2} (X_{2j}X_{2j+1} + Z_{2j}Z_{2j+1}) \quad (2.H.4)$$

on periodic boundary conditions. Is that clear? Can you find a unitary $U_{2j-1,2j}$ which transforms this Hamiltonian into

$$H = - \sum_{j=1}^{N/2} (Z_{2j-1}X_{2j}Z_{2j+1} + Z_{2j}X_{2j+1}Z_{2j+2})? \quad (2.H.5)$$

Let $U_{2j-1,2j} = (\mathbb{1} \otimes h)CZ$, where h is the Hadamard gate, and let $U = \bigotimes_j U_{2j-1,2j}$, then $U^\dagger H U$ is as desired.

4. Act with the above transformation U on the MERA tensor to obtain another MERA tensor. What is this state?

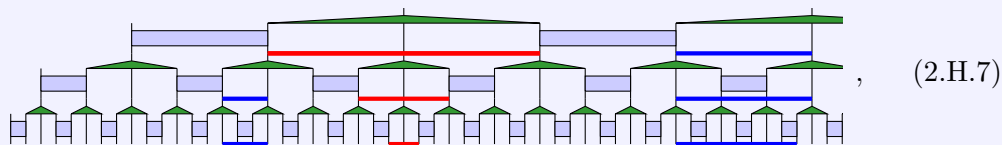
We want this to be a ground state of the transformed Hamiltonian, so we need $U^\dagger|\psi\rangle$. If we transform the lower indices on the second layer of the MERA with U^\dagger (so that each tensor is identical), then we must transform the upper indices of the lower layer (i.e. ensure that above the physical layer, U is acting as a gauge transformation). The tensor we obtain is



so this is the cluster state.

5. What is the maximum range of thermodynamic observables in a ternary MERA scheme?

We can easily see this by examining the causal cones (indicated by a line) of various sized operators in the MERA. We see that there is one special location where 3 site operators are maintained (red line). Elsewhere, each operator eventually shrinks to two sites (blue lines).



6. What does the reduced density matrix on a few sites of the MERA look like? Notice that it corresponds to the top tensor being passed through a CPTP map several times, this is usually called the *descending superoperator*.

Consider taking the MERA in Eq. (2.7.11), and look at the reduced density matrix on the support of the operator.

(2.H.8)

Note that in the above diagram, the five pairs of leg near the centre of the diagram are unconnected, corresponding to the reduced density matrix – all other physical legs are connected corresponding to the partial trace. Firstly we notice that everything outside of the light code (red shaded region) cancels out. Using this, and flipping the diagram inside out, we get that the reduce density matrix has the form:

(2.H.9)

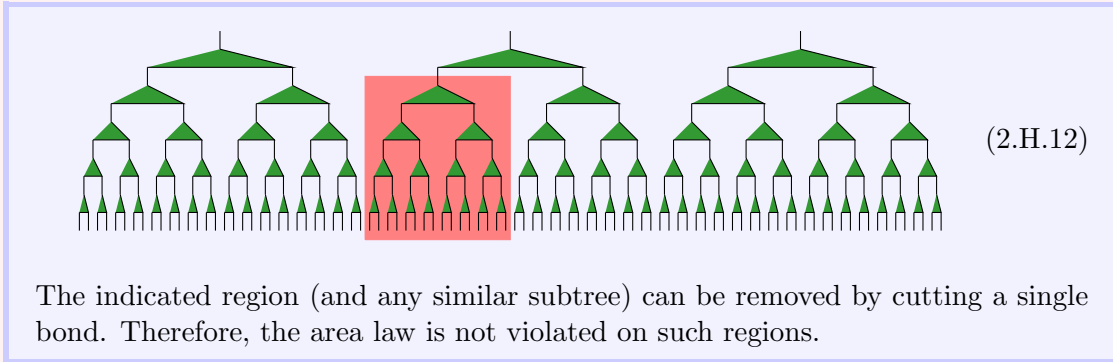
where the blue circle is the top tensor T . We can see that this simply corresponds to applying the map dual to the descending super-channel multiple times

(2.H.10)

Thus we see that reduced density matrices generally take the form

$$\rho = (\mathcal{E}^*)^n (|T\rangle\langle T|). \tag{2.H.11}$$

7. Do tree tensor networks (i.e. MERA for $u = 1$) have any area law violation on contiguous regions?



Chapter 3

Detecting Topological Order with Ribbon Operators

JACOB C. BRIDGEMAN¹, STEVEN T. FLAMMIA¹, AND DAVID POULIN²

¹CENTRE FOR ENGINEERED QUANTUM SYSTEMS, SCHOOL OF PHYSICS, THE UNIVERSITY OF SYDNEY, SYDNEY, AUSTRALIA

²DEPARTMENT OF PHYSICS, UNIVERSITÉ DE SHERBROOKE, SHERBROOKE, QUÉBEC, CANADA

Physical Review B [94, 205123 \(2016\)](#), [arXiv:1603.02275](#)

Abstract

We introduce a numerical method for identifying topological order in two-dimensional models based on one-dimensional bulk operators. The idea is to identify approximate symmetries supported on thin strips through the bulk that behave as string operators associated to an anyon model. We can express these ribbon operators in matrix product form and define a cost function that allows us to efficiently optimize over this ansatz class. We test this method on spin models with abelian topological order by finding ribbon operators for \mathbb{Z}_d quantum double models with local fields and Ising-like terms. In addition, we identify ribbons in the abelian phase of Kitaev's honeycomb model which serve as the logical operators of the encoded qubit for the quantum error-correcting code. We further identify the topologically encoded qubit in the quantum compass model, and show that despite this qubit, the model does not support topological order. Finally, we discuss how the method supports generalizations for detecting nonabelian topological order.

Despite the apparent simplicity of quantum spin models, they can exhibit a wide variety of interesting and potentially useful phenomena. These range from conventional magnetic order to the more novel topological [\[3.1\]](#) and symmetry-protected [\[3.2\]](#) and symmetry-enriched [\[3.3\]](#) topological orders which are of interest in both condensed matter physics [\[3.4\]](#) and quantum information theory. [\[3.5\]](#) These states are disordered in the sense of Landau-Ginzburg-Wilson, however they do exhibit properties distinct from the usual disordered phases. For example, topological phases possess quasiparticle excitations, known as anyons, whose braid relations can be far more exotic than those of fermions or bosons. [\[3.6\]](#) These phases also have ground state degeneracy which depends on the topology of the lattice. [\[3.7\]](#) This protected degeneracy has prompted the investigation of topologically ordered models as quantum memories. [\[3.5, 3.8\]](#) Quantum information stored in the

degenerate subspace can be protected from arbitrary local noise when error correction techniques are employed. [3.9–3.11]

Distinguishing topological phases can be an especially challenging task precisely because of their topological nature: there is no broken symmetry and no local order parameter signalling the phase transition. [3.1] There has been a large amount of previous work which attempts to identify topological order (TO). The existing key techniques, such as the topological entanglement entropy, [3.12–3.17] the entanglement Hamiltonian [3.18], topological degeneracy [3.19] and associated properties, [3.16,3.20] symmetries of particular representations of the ground states, [3.21–3.25] and specific properties of particular TO states, [3.26,3.27] have been highly successful in various domains of applicability. We review these methods below. A common feature of these methods is that they utilize the ground state of the model, which is unfortunately a challenging computational task in general.

Here we propose a numerical method that we call the *ribbon operators* method for identifying TO in the ground state of a given 2D Hamiltonian using only the Hamiltonian, without reference to the ground state. We reduce the search for TO to a 1D problem through the bulk of the material, and we present a variational approach based on standard DMRG [3.28] to identify certain operators – the ribbon operators – supported in the bulk that satisfy the commutation relations relevant for a candidate anyon model. We demonstrate the power of this approach by identifying TO in both integrable and non-integrable models, and contrast this with topologically trivial Hamiltonians. We also demonstrate the ability to identify topologically encoded qubits and logical operators of quantum error-correcting codes, even in a non-integrable model. All of our calculations are focused on the case of abelian TO in spin models, however the ribbon operators method suggests several natural extensions beyond this case, which we leave open for future work.

The following subsection reviews prior approaches, while Section 3.1 reviews anyon models. The expert reader can skip to Section 3.2.

3.0.1 Prior Approaches

One important tool is the *topological entanglement entropy* (TEE) [3.12,3.13] of the ground state wave function. Given the reduced density matrix ρ_R of some many-body ground state on a region R , the von Neumann entropy $S(\rho_R) = -\text{Tr}(\rho_R \log \rho_R)$ typically obeys the area law

$$S(\rho_R) = \alpha|\partial R| - \gamma + \mathcal{O}\left(\frac{1}{|R|}\right), \quad (3.1)$$

where $|R|$ and $|\partial R|$ are the number of spins in the region R and on the boundary of the region R respectively, and $-\gamma$ is the TEE.

In a topologically ordered model, a physical argument suggests that $\gamma = \log\left(\sqrt{\sum_c d_c^2}\right)$, where d_c is the quantum dimension of the anyon with charge c in the associated anyon model. The TEE is clearly nonzero if the ground state is topologically ordered, [3.12] so γ can be used as a signal of such ordering. [3.15–3.17] One can compute γ by obtaining an explicit ground state wavefunction, for example as a PEPS. Additionally, a Rényi entropy variant of γ [3.14] can be computed by sampling the ground state wavefunctions using quantum Monte Carlo. [3.15]

There are two major challenges associated with this approach. Firstly, there exist examples of topologically trivial states for which computing γ leads to nonzero values. [3.29] Secondly, any two topological phases whose associated anyon models have the same total quantum dimension $\mathcal{D} = \sum_c d_c^2$ will have the same TEE, and so it cannot be used to distinguish them. This second problem has already led to difficulty in fully identifying the phase of physically interesting models

including the Heisenberg antiferromagnet on the Kagome lattice, a model thought to describe the low-energy physics of several naturally occurring and synthetic minerals. [3.17]

A less coarse approach is to investigate the full entanglement spectrum, that is, the spectrum of the effective Hamiltonian defined by $\rho_R = e^{-H_{\text{eff}}}$. [3.18] It has been suggested that the universal properties of H_{eff} are intimately linked to the structure of the physical edge state of the model, however H_{eff} can undergo phase transitions without the physical model doing so, [3.30] and at least for models in the same phase as a string-net model [3.31] the spectrum is expected to contain the same universal information as the TEE. [3.14]

One of the characteristic features of topologically ordered models is the topology-dependent ground state degeneracy. [3.7] After obtaining a full set of ground states, one can observe transitions out of topological phases via loss of topological degeneracy, [3.19] and, in the topological phase, compute the \mathcal{S} and \mathcal{U} matrices defining the braiding relations in the associated anyon theory. [3.16, 3.20] Unfortunately, demonstrating topology-dependent ground state degeneracy is not sufficient to ensure robust topological order. [3.32, 3.33]

Given a projected entangled pair state (PEPS) description of the ground state, one can identify the topological order by understanding the symmetry properties of the parent Hamiltonian [3.22] or the environment tensor. [3.25] One can also use the PEPS formalism to identify matrix product operators (MPOs) that ‘pull through’ the PEPS tensors on the virtual level. [3.23, 3.24] These MPOs are in close analogy to the physical operators that act to create and transport anyons. As we will describe, these physical operators are central to our approach.

Finally, given access to a ground state, specific structure such as certain correlation functions or distribution of bond energies can provide evidence for topological ordering. [3.26, 3.27]

As a prerequisite for each of these methods, one must obtain an efficient description of the ground space (e.g. via tensor networks) or obtain expectations with respect to ground states (e.g. via Monte Carlo sampling). Tensor network (TN) methods have proven very useful for this purpose, [3.17, 3.25–3.27, 3.34] however in many cases the result does not conclusively determine the topological order. [3.27] The TN states obtained suffer from several drawbacks. In particular, they are usually computed on infinite cylinders of small circumference. They can also be biased towards low-entanglement states. [3.26] Additionally, properties of a ground state alone are not sufficient to identify a gapped topological phase. For example, one can obtain a gapless Hamiltonian sharing the toric code ground space. [3.35]

Of these methods, the ones closest in spirit to our current approach are the tensor network-based methods, [3.22–3.24] however our approach differs substantially in that we do not require a PEPS description of the ground state wavefunction. We instead variationally create tensor network representations of certain ribbon operators that are supported on 1D strips through the truly two-dimensional bulk; this dimensional reduction is what makes our method numerically tractable. In contrast to state-based variational approaches, where a similar reduction is often included for numerical convenience, we will argue that in our operator-based approach this reduction is an expected feature of the operators. Additionally, if one wishes to use the topologically protected ground space as a quantum memory, knowledge of these ribbon operators is required for information manipulation and extraction. Thus, this method could be used to augment a state-based approach to obtain this additional data.

This paper is organized as follows. In Section 3.1, we review some of the features of anyon models which describe the low energy excitations of topologically ordered spin models. In Section 3.2, we define a ribbon operator, and use the properties of the anyons to define a cost function which quantifies how well a candidate ribbon realizes their behavior. We then describe how the cost function can be minimized numerically in Section 3.4. Using this algorithm, in Section 3.5 we obtain ribbon operators in a number of topologically ordered and topologically trivial models. These

numerics demonstrate that the cost function we define allows identification of abelian topological order in nonintegrable spin models. In Section 3.6, we prove that, under certain assumptions, ribbon operators can be used as approximate logical operators in quantum error correcting codes. We conclude in Section 3.7 with a discussion of extensions of the method to nonabelian topological order and more complex spin models.

3.1 Properties of Anyons

In this section, we review the physical properties of anyon models that characterize a topological phase. Of course, not all topological phases have an associated anyon model, for example the cubic code, [3.36] however we will tailor our method to those phases with anyonic excitations. This discussion of anyon models will motivate our definition in the subsequent section of a *ribbon operator* for a spin model defined by some local Hamiltonian $H = \sum_j h_j$ on a lattice in two dimensions. We will argue that this definition captures the essential features outlined below of a topologically ordered model by thinking about anyons as quasiparticle excitations of the spin model. The simplest realization of this is Kitaev's toric code, [3.5, 3.37] and we will refer to that model to clarify key features.

Creating a pair of anyons, and moving them to the boundary of the lattice leaves no excitations, and so maps the vacuum to the vacuum. In the toric code, anyons are created and transported using string operators, as shown in Fig. 3.1. These operators commute with the Hamiltonian in the bulk, but have excitations localized to the ends. In this way, if the anyons are moved off the edge of the lattice or are fused together, the system remains in its ground state.

More generally, we expect anyonic excitations to be particle like, but to have nontrivial braiding relations. On sufficiently large length scales, it is expected that these braid statistics are governed solely by an anyon model. [3.37] For this reason, the creation operators in this limit should be one dimensional with the particles localized around the end points. Away from a renormalization-group fixed point, we expect these operators to be dressed, and supported on slightly fattened regions, though still effectively one-dimensional. More precisely, the width of these ribbons should be set by the microscopic details of the model, and should not scale with system size.

The family of local commuting projector codes (LCPC) generalizes the toric code and provides a concrete instantiation of these ideas. The LCPCs are families of Hamiltonians where the terms are pairwise commuting projectors onto an unfrustrated ground state. In these models the string operators described above always exist. [3.39] This class of models includes exactly solvable points of most known topological phases [3.40] including the Levin-Wen string nets. [3.31] Away from these exactly solvable points, we can dress the string operators using quasiadiabatic continuation. [3.41] Given a point in a phase for which an initial string operator exists, such as an LCPC, we can dress this operator to any other point in the phase. Generically this operator will have extensive support, however the error made in truncating the width is exponentially small in w/ξ , where w is the width and ξ is the correlation length. Thus string-like operators with width proportional to the correlation length can be found anywhere within the phase.

Since the string operators act as creation operators for pairs of anyons, we argue that they should be only slightly entangling operators. [3.39] These are operators whose Schmidt rank is independent of the system size on any bipartition that cuts the string into two contiguous pieces. In the LCPC case, the string operators are known to be slightly entangling. [3.39] Since the quasiparticles are simply dressed by moving away from these fixed points, we expect this property to remain throughout the phase; although the required Schmidt rank can increase substantially, it will still be independent of the system size. When we remove the dressed quasiparticles from the lattice (by

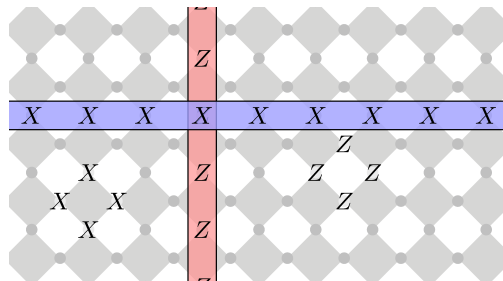


Figure 3.1: The prototypical ribbon operators are the string operators shown above for the toric code. The toric code is defined by X -type and Z -type four-body interactions on alternate plaquettes of a square lattice, and the (exact) ribbon operators are the string-like products of X and Z shown above. These ribbon operators commute with the Hamiltonian terms but anticommute with each other, thus identifying a phase with \mathbb{Z}_2 topological order.

annihilating them or bringing them out to infinity), the system returns to its ground space, which is expected to obey the area law of Eqn. (3.1). This also supports the slightly entangling nature of such operators.

Some of the defining features of an anyon model are the relations that are encoded in the topological \mathcal{S} matrix and the \mathcal{R} matrices. Let $\{a, b, c, \dots\}$ label the anyonic particles in the anyon model describing the low energy excitations of the Hamiltonian H . The \mathcal{R} matrices are defined by

$$\begin{array}{c} b \quad a \\ \diagdown \quad / \\ \circlearrowleft \\ / \quad \diagdown \\ c \end{array} = \mathcal{R}_c^{ab} \begin{array}{c} b \quad a \\ \diagdown \quad / \\ \diagdown \quad / \\ / \quad \diagdown \\ c \end{array}, \quad (3.2)$$

and the \mathcal{S} matrix is

$$\mathcal{S}_{ab} = \frac{1}{\mathcal{D}} \begin{array}{c} \circlearrowleft \quad \circlearrowright \\ a \quad b \end{array}, \quad (3.3)$$

where the lines trace out the worldlines of the particles.

Another approach is to consider the related $\tilde{\mathcal{S}}$ matrix that can be obtained via the twist product. [3.42] If the \mathcal{S} matrix is an object that captures dynamical information from braiding anyons in 2+1 dimensions, then the $\tilde{\mathcal{S}}$ matrix is a static object that captures correlations of ground states in 2+0 dimensions. If π_a is an operator supported on an annulus that projects onto a state with total charge a inside, then

$$\tilde{\mathcal{S}}_{ab} = \langle \psi | \pi_a \infty \pi_b | \psi \rangle = \frac{d_a d_b}{\mathcal{D}} \mathcal{S}_{ab}, \quad (3.4)$$

where $|\psi\rangle$ is any ground state of the spin model. For bipartite operators $X = \sum_{i,j} X_i^A \otimes X_j^B$ and $Y = \sum_{k,l} Y_k^A \otimes Y_l^B$, the twist product with respect to the partition $A|B$ is defined as

$$X \infty Y = \sum_{i,j,k,l} X_i^A Y_k^A \otimes Y_l^B X_j^B, \quad (3.5)$$

where the order is reversed on the B region relative to the A partition. This is clearly closely related to Eqn. (3.3), where the worldline loops are replaced by the corresponding closed loop operators on the lattice. For abelian models where $d_a = 1$ for all particle types a , the \mathcal{S} and $\tilde{\mathcal{S}}$ matrices coincide up to a multiple of \mathcal{D} .

Finally, anyonic quasiparticles should be able to move around the lattice, and the state should not depend upon any smooth deformations of the path they take. In particular, when they are fused back together or moved off the lattice, the system should return to a vacuum state. This is realized in the toric code since the string operators can be deformed by dressing with local operators that are symmetries of the Hamiltonian. This preserves commutativity with H and the \tilde{S} matrix and clearly creates the same particle at the ends.

3.2 Definition of Ribbon Operators

Let us summarize the physical intuition that we've gained in the previous section into a few simple properties that the string-like operators seem to possess in general. These properties hold for known exactly solvable models with TO.

Given a two-dimensional quantum system with TO, we expect that there are operators R supported on one-dimensional strips through the bulk where the following four properties hold, at least approximately:

1. R commutes with the bulk Hamiltonian in the low energy sector.
2. R is supported on a strip of spins with bounded width w .
3. Distinct ribbons R and L should respect the data (e.g. the \mathcal{R} or \mathcal{S} matrix) for an underlying anyon model in the low energy sector.
4. R is smoothly deformable, that is, the ability to satisfy 1-3 should not depend on the chosen strip of spins defining the support of R , given sufficient width.

Since finding a low energy projector appears to be a challenging task, we make the following assumption. Rather than asking for 1-4 to hold only in the low energy sector, we ask for them to hold on the whole spectrum. At first glance, this seems to be too strong for characterizing TO away from an exactly solvable RG fixed point. Nonetheless, by making this assumption, we can arrive at an effective numerical procedure for detecting TO in 2D models. Moreover, in Section 3.3, we provide a heuristic physical justification of this assumption, and some natural avenues for relaxing it in Section 3.7.

3.2.1 The Method of Ribbon Operators

Here we introduce what we call the ribbon operator method for detecting TO. The strategy is simple: we will write a cost function that tries to satisfy the above requirements simultaneously. Since the support of a string-like operator is on a 1D strip, and is expected to be only slightly entangling, we will use the ansatz class of MPOs [3.43] to describe candidate operators. We will then use the highly successful methods of 1D systems such as DMRG [3.28] for optimizing over this ansatz class to find the lowest cost MPO.

We can then *define* a ribbon operator as any MPO supported on any one-dimensional strip of some fixed width. By drawing on the lattice Hamiltonian and an underlying anyon model, we can define a cost function quantifying the fitness of candidate ribbons given the above criteria. A *good* ribbon operator then corresponds to a local minimum of the cost function.

There is clearly considerable scope within this method for how to use it. The art will be to choose a cost function that is tractable to optimize and gives clear signals of TO when appropriate, such that the distinction between which local minima are “good” and “bad” is obvious. We do not claim to have a unique or best choice of cost function or optimization routine. The remainder of this

section details one particular choice of cost function, and as we show in Section 3.5 this particular choice performs quite well for a variety of simple models.

3.2.2 Our Cost Function

We now define our proposed cost function that quantifies how well a candidate ribbon satisfies the above criteria. Let $H = \sum_j h_j$ be some local Hamiltonian and R some candidate ribbon with $\|R\| = 1$ (the Schatten 2-norm, or Frobenius norm $\|R\|^2 = \text{Tr}(R^\dagger R)$) and width w , which ideally should be chosen to be comparable to the correlation length. We will also use the symbol R to denote the region of support of the ribbon R since no confusion should result.

The first condition is that the ribbon should commute with the Hamiltonian of the model. This gives us two terms in the cost function. We can quantify the violation of this condition using $\|[R, H]\|^2$. This can be decomposed into two distinct contributions by writing the Hamiltonian as

$$\begin{aligned} H &= H_R + H_{R^c} + H_{\partial R} \\ &= \sum_{j \in R} h_j + \sum_{j \in R^c} h_j + \sum_{j \in \partial R} h_j, \end{aligned} \quad (3.6)$$

where the first term contains Hamiltonian terms whose support is completely within the support of R , the second contains those whose support has no overlap with R and are hence supported entirely in the complementary region R^c . The final sum contains all those terms in the Hamiltonian with support on both R and R^c . Clearly the second term trivially commutes with R as a consequence of our second condition.

Commutation with the first term cannot be simplified further. However, the term on the boundary ∂R can be simplified as follows. Let h_j be some term on the boundary of the ribbon. Then using the operator Schmidt decomposition, we can split the operator h_j into a sum over interior and exterior components

$$h_j = \sum_k h_{j,k}^{\text{in}} \otimes h_{j,k}^{\text{out}}, \quad (3.7)$$

where $\text{Tr}(h_{j,k}^{\text{out}\dagger} h_{j,k'}^{\text{out}}) = \delta_{k,k'}$.

Using the orthonormality of the $h_{j,k}^{\text{out}}$ terms and the definition of the Frobenius norm, we find that

$$\begin{aligned} \|[R, h_j]\|^2 &= \left\| \sum_k [R, h_{j,k}^{\text{in}}] \otimes h_{j,k}^{\text{out}} \right\|^2 \\ &= \sum_k \|[R, h_{j,k}^{\text{in}}] \otimes h_{j,k}^{\text{out}}\|^2 \\ &= \sum_k \|[R, h_{j,k}^{\text{in}}]\|^2, \end{aligned} \quad (3.8)$$

By appropriate grouping of boundary terms, we can ensure that $\text{Tr}(h_{j,k}^{\text{out}\dagger} h_{j',k'}^{\text{out}}) = \delta_{k,k'} \delta_{j,j'}$. (This is equivalent to applying the Schmidt decomposition to $H_{\partial R}$ instead of just one term.) Thus, we can express the boundary contribution as

$$\sum_{j \in \partial R} \sum_k \|[R, h_{j,k}^{\text{in}}]\|^2. \quad (3.9)$$

We find that the commutation condition together with the bounded width condition gives us a term in the cost function proportional to

$$\|[R, H]\|^2 = \|[R, H_R]\|^2 + \sum_{j,k \in \partial R} \|[R, h_{j,k}^{\text{in}}]\|^2. \quad (3.10)$$

Because commutation with the Hamiltonian can always be achieved by choosing the ribbon to be the identity operator, we require a competing term to enforce the topological properties such as having a nontrivial \mathcal{S} or \mathcal{R} matrix. For the moment, suppose that we already have a given nontrivial ribbon operator L that crosses R as in Fig. 3.1. (We will discuss how to relax this prior-knowledge assumption below.) We can incorporate anyon data with the following term in the cost function,

$$\|[R, L]_\eta\|^2 = \|RL - \eta LR\|^2, \quad (3.11)$$

where η is a complex number different from 1.

This choice of topological term in the cost function intuitively reminds us of the \mathcal{R} matrix relations of Eqn. (3.2). We can see that such a term is in fact sufficient to give a nontrivial \mathcal{R} matrix as follows. Here we specialize to an abelian model, but the discussion could be generalized. Using the \mathcal{R} matrix relation for an abelian model with a fixed total anyon charge $c = a \times b$, we have the relation

$$\begin{array}{c} b \quad a \\ \diagdown \quad / \\ \text{---} \\ / \quad \diagdown \\ c \end{array} = \mathcal{R}_c^{ab} \begin{array}{c} b \quad a \\ / \quad \diagdown \\ \text{---} \\ \diagdown \quad / \\ c \end{array} = \mathcal{R}_c^{ab} \mathcal{R}_c^{ba} \begin{array}{c} b \quad a \\ \diagdown \quad / \\ \text{---} \\ / \quad \diagdown \\ c \end{array} = \eta \begin{array}{c} b \quad a \\ \diagdown \quad / \\ \text{---} \\ / \quad \diagdown \\ c \end{array}. \quad (3.12)$$

Thus if $\eta \neq 1$ then \mathcal{R}_c^{ab} and \mathcal{R}_c^{ba} cannot both be 1. Note that in the abelian case, $\mathcal{S}_{a\bar{b}}$ can be written as [3.37] $\mathcal{R}^{ab}\mathcal{R}^{ba}/\mathcal{D}$, so η is related to the \mathcal{S} matrix and is therefore gauge invariant (invariant under a change of basis of the fusion space).

Since the anyon charge c is fixed already by the labels a and b in an abelian model, this switching relation should hold even when considering this as just a different operator product order, analogous to the case of a twist product for the $\hat{\mathcal{S}}$ matrix:

$$\begin{array}{c} L \quad R \\ \diagdown \quad / \\ \text{---} \\ / \quad \diagdown \end{array} = \eta \begin{array}{c} L \quad R \\ / \quad \diagdown \\ \text{---} \\ \diagdown \quad / \end{array}. \quad (3.13)$$

Since there are many equivalent strips on which L and R can be supported, the cost should be computed for all possible intersection regions. This is achieved by summing $\|[R, L]_\eta\|^2$ over all translates of L , labelled $\mathcal{T}(L)$, that lead to an inequivalent intersection with R . This translation invariance gives us an additional motivation for our choice of topological term: we can use translation-invariant MPOs in our optimization routines. By comparison, an *a priori* equally attractive term would be to encode the \mathcal{S} matrix relations, but then finite-size effects from the periodic boundary conditions might add additional complications to the numerics.

Now, we define the η -cost of a ribbon R given some fixed secondary ribbon L as

$$C(R; \eta) = \frac{1}{|R|} \left(\|[R, H_R]\|^2 + \sum_{j,k \in \partial R} \|[R, h_{j,k}^{\text{in}}]\|^2 + \sum_{\mathcal{T}(L)} \|[R, L]_\eta\|^2 \right), \quad (3.14)$$

where $|R|$ is the number of spins on which R is supported. Note that due to the nonsymmetric nature of $[\cdot, \cdot]_\eta$, it is convenient to define the η -cost of L as

$$C(L; \eta) = \frac{1}{|L|} \left(\|[L, H_L]\|^2 + \sum_{j,k \in \partial L} \|[L, h_{j,k}^{\text{in}}]\|^2 + \sum_{\mathcal{T}(R)} \|[R, L]_\eta\|^2 \right), \quad (3.15)$$

where the appropriate Hamiltonian terms are taken. Here the normalization term is chosen so that the cost of a ribbon is approximately independent of the volume.

One could consider summing these two terms to build a total cost function for the pair of ribbons, however we linearize the problem for a fixed L (or fixed R) and instead do an alternating minimization algorithm.

In the case of the exact toric code, the form of the cost function is relatively simple and gives a concrete instantiation of the translation operation \mathcal{T} . It is easy to check that the standard logical operators of this code have zero η -cost when $\eta = -1$, as expected. We present the explicit cost function derivation in Appendix 3.A for illustration.

Although this cost function only involves a pair of ribbons, it is possible to incorporate braid relations with other particle types by adding terms of the form of Eqn. (3.11) with additional ribbon operators. In this way, it is possible to completely reconstruct the \mathcal{S} matrix of the anyon model up to a column permutation. This ambiguity is due to the difficulty of identifying equivalence of operators on incomparable supports (i.e. those with vertical and horizontal supports in Fig. 3.1). We discuss possible avenues to removing this freedom in Section 3.7.

3.3 Heuristic Justification for the Norm

As discussed in Section 3.2, a key assumption which enables our method to be numerically efficient is that the commutation relations, which are expected to hold only on a topologically ordered ground space, hold on the entire spectrum. While this appears to be a very strong assumption, we believe that our method should continue to work even when this assumption breaks. In this section, we will provide a physically motivated, heuristic justification for this assumption.

At high energies, we expect a gas of short-range interacting anyons. When ribbon operators are used to create additional anyons, braid them, and fuse them in a specific way, the resulting process will in general be affected by the presence of the background anyon gas. Specifically, the expectation value of the braid can be affected by 1) dynamical phases acquired from short range interactions with the background anyons, and 2) topological terms caused by the background anyons enclosed in the braid. To eliminate these effects, we need to make sure that 1) there are no background anyons near the support of the ribbon operator, and 2) the topological charge enclosed in the braid is trivial.

It happens that both of these conditions can be enforced with small width operators. Indeed, 1) requires projecting on the local ground state (LGS), i.e. the subspace with no charges. Similarly, it is possible to fix the topological charge of a region using an operator which acts only on the boundary of this region and is described by a finite bond dimension MPO. [3.42] Let Π_C denote the corresponding projector.

Suppose that R is an MPO ribbon operator which obeys the right commutation relations on the ground space, but not on the entire spectrum. Then, $R' = \Pi_C R \Pi_C$ should be a slightly wider and larger-bond-dimension MPO ribbon operator which obeys the commutation on the entire spectrum. Thus, while our approach cannot find R , it should be able to find R' without any assumptions.

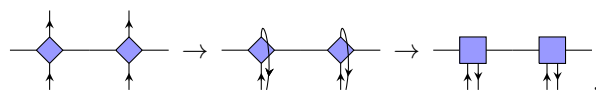
We stress that the above argument is not key to our method, and no ground state projectors are incorporated directly in our algorithm or in the numerical results presented in Section 3.5. One could alter the method to explicitly make use of information about the low energy space. We discuss this further in Section 3.7.

3.4 Finding Ribbon Operators

In many exactly solvable models, an analytic form for the ribbon operators can be found. In more general models, for example ones with a noncommuting Hamiltonian, the ribbons must be found numerically. In this section, we describe how to find ribbon operators using DMRG. [3.28]

We parameterize a width w ribbon by a block-translationally invariant infinite MPO. This MPO is “snaked” along the support of the ribbon to cover the two-dimensional region. That is, the coordinates of the ribbon are treated in a linearized lexicographic order moving along the ribbon lengthwise. This MPO can be vectorized, i.e. interpreted as a vector instead of a matrix. An MPO is also built for the cost function, with the same snaking pattern, and standard DMRG can then be applied to find the ribbon that minimizes the constraints.

This vectorization procedure corresponds to the following transformation, written in tensor network diagram notation:



Given any operator O in MPO form, we can explicitly write the form of the constraint term $\|[R, O]\|^2$ for one site of the MPO as

$$\begin{array}{c}
 R \\
 O \\
 O^\dagger \\
 R^\dagger
 \end{array}
 \begin{array}{c}
 \begin{array}{c} \square \\ \uparrow \downarrow \\ \square \end{array} \\
 - \\
 \begin{array}{c} \square \\ \uparrow \downarrow \\ \square \end{array} \\
 - \\
 \begin{array}{c} \square \\ \uparrow \downarrow \\ \square \end{array} \\
 + \\
 \begin{array}{c} \square \\ \uparrow \downarrow \\ \square \end{array}
 \end{array}
 \quad (3.16)$$

By concatenating this expression and closing the boundaries appropriately, we see that this is equivalent to the expectation of some MPO for some matrix product “state” given by the vectorization of R .

The total cost function can be obtained by summing up the MPOs defining each cost term, corresponding to direct sum on the MPO matrices. The cost function MPO will not generally correspond to a local Hamiltonian, which is the regime where DMRG is usually applied. Indeed, due to the squaring required on the internal commutator, we will have terms like $h_j h_k$ for every pair j, k . Despite this potential challenge, we will demonstrate that DMRG is an effective algorithm for this minimization.

3.4.1 Optimizing

We attempt to optimize $C(R; \eta)$ for various choices of η . In particular, we restrict ourselves to the unit disk as this is sufficient for the models below, although extending to other η does not change any of the results obtained.

When attempting to optimize a pair, we used alternating minimization. First $C(R_1; \eta)$ was minimized in the presence of a random R_2 . Then $C(R_2; \eta)$ was optimized given the R_1 obtained from the previous optimization. The R_2 obtained was then used to seed the next iteration. This process was repeated until convergence.

For each choice of η , several (usually 5 or 10) ribbons or pairs of ribbons were optimized from random initial pairs and the lowest cost pair was retained. This proved necessary to avoid premature convergence to a local minimum, particularly in the alternating minimization, leading to a pair that was orthogonal to the optimal solution. In most cases a total of 5-10 restarts appeared sufficient to ensure that an optimal pair was obtained. For each value of η , an independent random start was generated, rather than using a warm start from the previous nearby values of η .

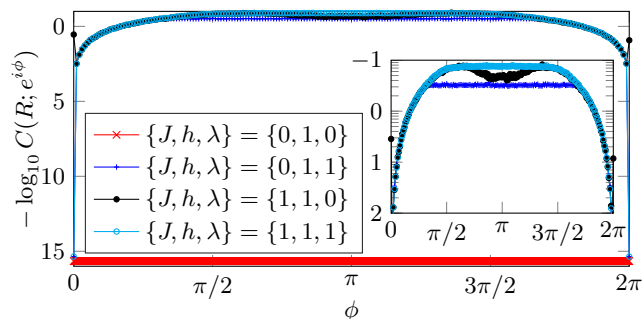


Figure 3.2: Cost for ribbons in topologically trivial phases the QDI₂ model with $\eta = e^{i\phi}$. A pair of ribbons were optimized on two $w = 1$ strips with bond dimension 1 for the paramagnet and 2 in the other cases. We observe two distinct failures to observe topological order. In the case of the paramagnet, a zero-cost ribbon can be found for all ϕ . In fact, this can be extended to all η . In the other cases (closeup in inset plot), there is no η for which a nontrivial low-cost ribbon can be obtained. It is possible that this could be due to insufficient width, although we have not observed this to be the case. Note that averaging over many trials (20) to give a typical picture of the algorithms performance. In the case where the variational minimum is used instead, still no signal of topological order is observed.

3.5 Numerical Results

In this section we use ribbon operators to study several standard models that exhibit both topologically ordered and trivial phases. We demonstrate the efficacy of ribbon operators in identifying TO both at exactly solvable points and away from such points.

3.5.1 \mathbb{Z}_d Quantum Double-Ising model

We define the \mathbb{Z}_d Quantum Double-Ising (QDI _{d}) model as follows. [3.5, 3.9] Let Λ be the bicolored lattice shown in Fig. 3.1. Place a qudit (d level quantum system) at each vertex and define the generalized unitary Pauli operators X and Z such that $ZX = \omega XZ$, $X^d = Z^d = \mathbb{1}$, and $\omega = e^{2\pi i/d}$. We define plaquette operators a and b as

$$a = X^\dagger \begin{array}{c} X^\dagger \\ \blacklozenge \\ X \end{array} X \quad b = Z^\dagger \begin{array}{c} Z \\ \white diamond \\ Z^\dagger \end{array} Z, \quad (3.17)$$

on the dark and light plaquettes respectively. The Hamiltonian is given by

$$H_{\mathbb{Z}_d} = -J \sum_{p \in \{\blacklozenge\}} P_p - J \sum_{p \in \{\white diamond\}} Q_p \quad (3.18a)$$

$$- \frac{h}{2} \sum_j (X_j + X_j^\dagger) \quad (3.18b)$$

$$- \frac{\lambda}{4} \sum_{\langle j,k \rangle} (Z_j + Z_j^\dagger)(Z_k + Z_k^\dagger), \quad (3.18c)$$

where at each plaquette p we have the operators

$$P = \sum_{k=1}^{d-1} a^k, \quad Q = \sum_{k=1}^{d-1} b^k. \quad (3.19)$$

The Hamiltonian contains the topological terms in Eqn. (3.18a) with strength J , a transverse onsite X field in Eqn. (3.18b) with strength h , and a ferromagnetic Ising-type term in Eqn. (3.18c) with strength λ .

When $h = \lambda = 0$, this is a topologically ordered commuting model which reduces to the toric code when $d = 2$. This model also captures a number of other models, including the paramagnet ($\{J, h, \lambda\} = \{0, 1, 0\}$) and a ferromagnet ($\{J, h, \lambda\} = \{0, 0, 1\}$). These latter correspond to distinct topologically trivial phases. At the fixed point of each of these phases, the model is exactly solvable. In the $d = 2$ case, the generic model with $J = 0$ is given by the Hamiltonian

$$H = -h \sum_j X_j - \lambda \sum_{\langle j,k \rangle} Z_j Z_k. \quad (3.20)$$

At the RG fixed points of these phases (corresponding to either $h = 0$ or $\lambda = 0$), we can set $R_1 = \prod |\uparrow\rangle\langle\uparrow|$ and $R_2 = \prod |\downarrow\rangle\langle\downarrow|$, where $|\uparrow\rangle/|\downarrow\rangle$ correspond to the $+1/-1$ eigenstates of the relevant operator (i.e. the eigenstates of X when $\lambda = 0$ and of Z when $h = 0$). These ribbons commute with the Hamiltonian. Since $R_1 R_2 = R_2 R_1 = 0$, their η -commutation relation is not unique, so they do not correspond to good ribbon operators. We therefore expect to be able to find zero-cost ribbons for all η at these points. We note that constraining the ribbons to be unitary would be a natural way to eliminate these spurious solutions in the trivial phases, but this is computationally expensive; we discuss this point further in Section 3.7.

Costs for ribbons at various non-topological points in the QDI_d model are shown in Fig. 3.2. We observe two distinct ways in which trivial order can be signalled. As we have already discussed, one of these corresponds to mutually annihilating operators as in the para- and ferromagnetic phases. In the other case we simply fail to observe any low cost ribbons which form a nontrivial algebra. There are two explanations for this. Either there are no ribbon operators to be found or the chosen width w is too narrow.

The phase which includes the point $\{J, h, \lambda\} = \{1, 0, 0\}$ is topologically ordered, and we expect it to show a signal of \mathbb{Z}_d -topological order. We therefore expect to observe low cost ribbons only when $\eta = e^{i\phi}$ is a d th root of 1. This property is expected to persist away from the exactly solvable point. In Fig. 3.3 we show the data obtained at the fixed points of the \mathbb{Z}_5 and \mathbb{Z}_2 models and when an X field is turned on in the latter. As expected, at the fixed point a very strong signal is observed. Using a large density of points we see that the cost drops dramatically over a very narrow region around the d th root of unity. When we turn on the field term, the signal decreases in magnitude but is still unmistakable, with more than two orders of magnitude in total contrast. Despite the clear signal, we observe that the value of the cost function at the minimum is comparable to the (square of) the perturbation strength. This may lead one to suspect that the method is simply returning the analytically obtainable fixed point ribbon. To refute this hypothesis, in Fig. 3.3c, we compare the cost of numerically obtained ribbons to those of the fixed point strings. Encouragingly, we see that the cost is smaller for the optimized ribbon, indicating that the method is finding a nontrivial result.

In Fig. 3.4, we present cost data for the fixed point of the QDI_3 model over the entire unit disk. As expected, low cost ribbons can only be found around the third root of unity, with no minima occurring inside the disk. This property persists even when an X field is turned on as shown in Fig. 3.5. This figure shows the cost of ribbons in the QDI_2 model with $\{J, h, \lambda\} = \{1, 0.05, 0\}$. Even at this nonintegrable point, no low cost ribbons can be found anywhere away from the d th roots of unity.

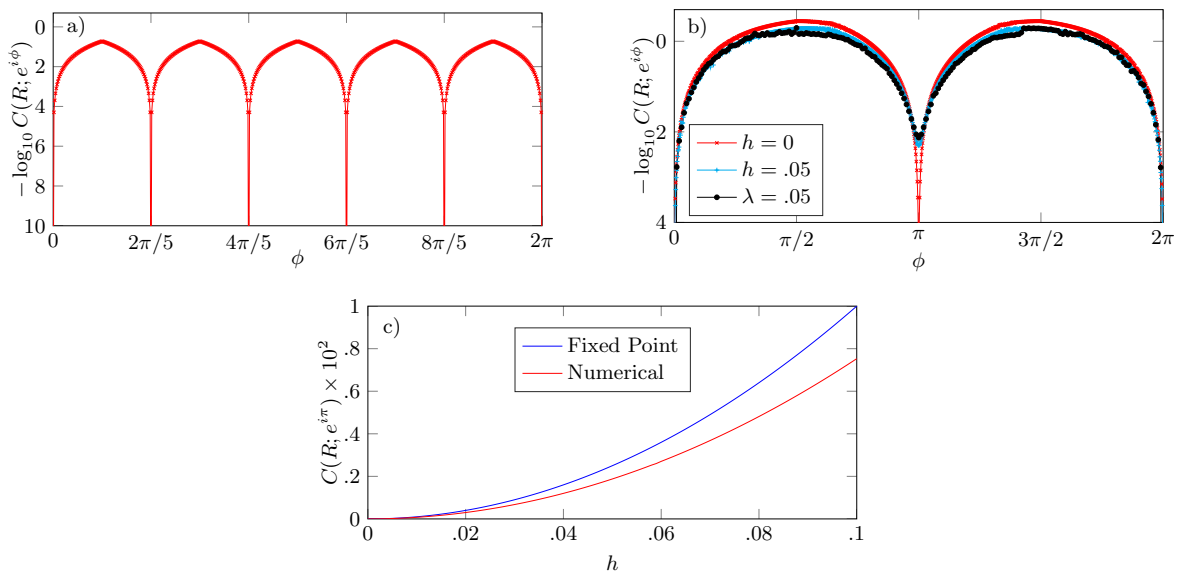


Figure 3.3: a) Cost for a width 1 ribbon found in the QDI₅ model of Eqn. (3.18) with $\{J, h, \lambda\} = \{1, 0, 0\}$ using bond dimension 5 and plotted with $\eta = e^{i\phi}$. The other ribbon was kept as a string of Z s as shown in Fig. 3.1.

b) Cost for ribbons found using alternating minimization on the QDI₂ model with $J = 1$. In the $h = 0$ case a pair of $w = 1$, bond dimension 1 ribbons were sought, in the other cases, the pair consisted of a $w = 1$ and a $w = 2$ ribbon with bond dimensions 1 and 5 respectively. At the exactly solvable points ($h = 0$), we see a dramatic cost decrease at d th roots of unity, signalling both the presence of and type of topological order present in these models. This feature remains even with the addition of an X field or Ising type term which destroys the solvability of the model.

c) Cost of a width 4 ribbon of bond dimension 2 in the QDI₂ model. The cost obtained from our numerical optimization is smaller than that of the fixed point string for all (nonzero) values of h . This demonstrates the nontrivial nature of the ribbon operators we obtain, even in this perturbative regime.

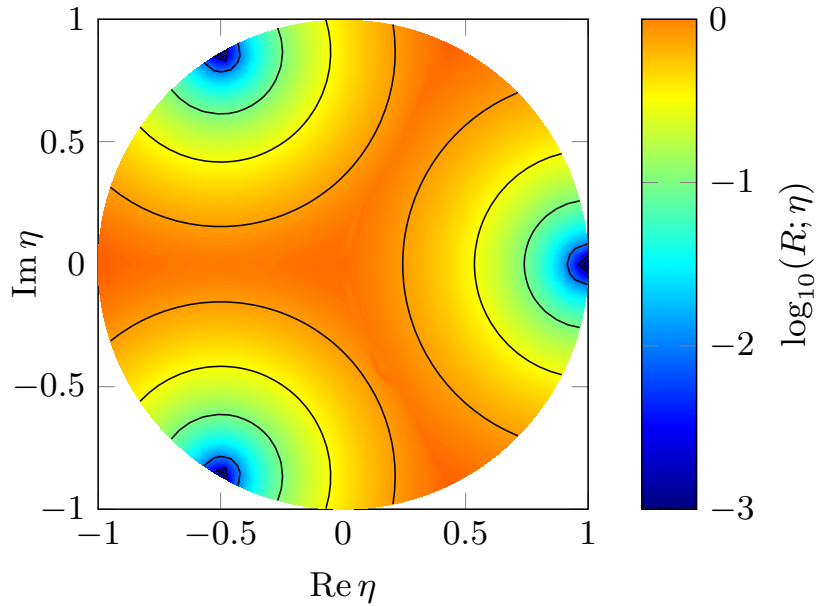


Figure 3.4: Cost for ribbons found using alternating minimization on the QDI₃ model with $\{J, h, \lambda\} = \{1, 0, 0\}$. A pair of $w = 1$ ribbons with bond dimension 1 were optimized. We observe a signal of topological order only at $\eta = e^{2\pi i k/3}$.

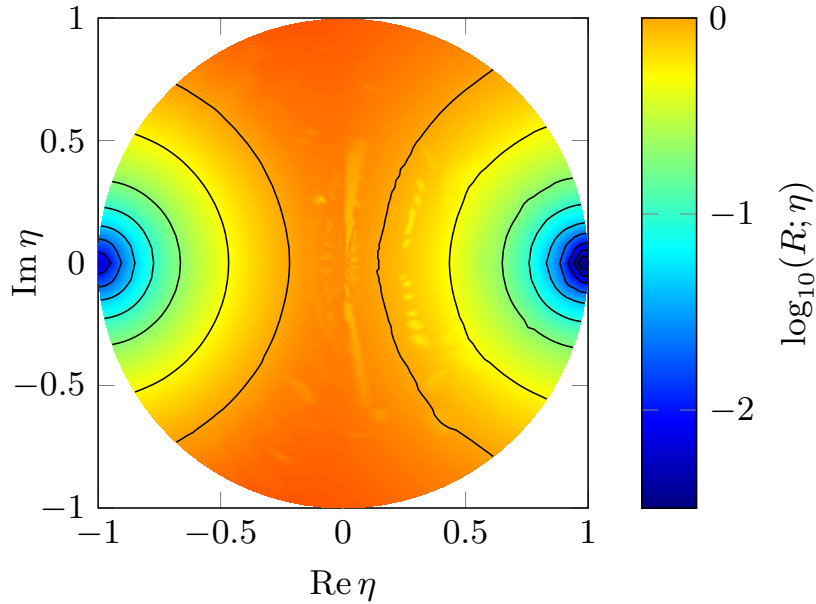


Figure 3.5: Cost for ribbons found using alternating minimization on the QDI₂ model with $\{J, h, \lambda\} = \{1, 0.05, 0\}$ where η runs over points in the complex unit disk. A pair of ribbons with $w = 1$ and $w = 2$ and bond dimensions 1 and 5 respectively were optimized and the total cost is shown. We observe a signal of topological order at $\eta = -1$. Note that Fig. 3.3b corresponds to the edge of this disk. The raw data is displayed, but some contours were subjected to gaussian smoothing for clarity in the nearly flat region where the noise in the data and the gradient of the function are comparable in magnitude.

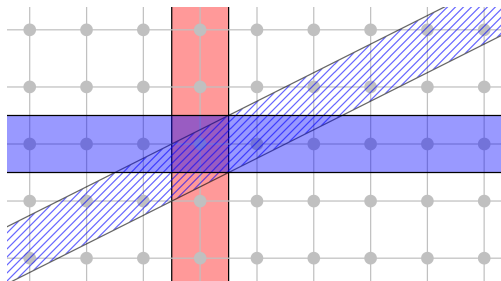


Figure 3.6: Topologically ordered models should support low-cost ribbons on both the horizontal and the rotated blue regions (or some widening of them). This corresponds to insensitivity of the anyon braid relations to the specific worldlines they trace out. Models with specific lattice symmetries such as the quantum compass model might provide false signatures of topological order if ribbon operators are sought only on non-generic strips of the lattice.

3.5.2 The Quantum Compass Model

It is interesting to consider the 2D quantum compass (QC) or Bacon-Shor model [3.44, 3.45] in the context of ribbon operators. This model is defined on a square lattice Λ with Hamiltonian

$$H_{\text{QC}} = -J \sum_{i,j \in \Lambda} (X_{i,j} X_{i,j+1} + Z_{i,j} Z_{i+1,j}). \quad (3.21)$$

This model fails to exhibit many of the features expected of a topologically ordered model. For example, the ground state degeneracy does not depend on the underlying lattice topology. Moreover, this appears to be a gapless model with exponential ground state degeneracy. [3.44] Thus, this Hamiltonian is usually described as not having topological order. However, this model can be used to encode a qubit which is protected against arbitrary local errors, having a code distance extensive in the (linear) lattice size, [3.45] a property which is clearly required of a topological code. This qubit can be defined by the pair of logical operators $\tilde{Z}_i = \prod_j Z_{i,j}$ and $\tilde{X}_j = \prod_i X_{i,j}$. These operators commute with each Hamiltonian term, and intersect at a single point, hence they anticommute, $[\tilde{Z}_i, \tilde{X}_j]_{-1} = 0$, and therefore almost fulfill the conditions we give to be good ribbon operators. We will see below that they are rigid objects that exist due to special lattice symmetries, and they are not deformable.

The Hamiltonian Eqn. (3.21) also commutes with all elements of the *stabilizer group*

$$\mathcal{G} = \left\langle \prod_j Z_{i,j} Z_{i+1,j}, \prod_j X_{j,k} X_{j,k+1} \right\rangle. \quad (3.22)$$

It is therefore clear that $\tilde{Z}_j(\tilde{X}_j)$ is related to $\tilde{Z}_k(\tilde{X}_k)$ by application of a stabilizer element, and so defines the same encoded qubit in the ground space. Hence, the logical operators can be moved along to parallel strips.

To investigate topological order in the QC model, we seek to find logical operators supported on rotated regions as shown in Fig. 3.6 or widened versions thereof. We compare this to the \mathbb{Z}_2 quantum double model where topological order is well understood.

In Fig. 3.7 we show the cost for ribbons obtained in these two models where the vertical ribbons are fixed to be $\prod Z_j$ and a bond dimension ≤ 5 ribbon is optimized with both horizontal and rotated support. As discussed above, zero cost ribbons can be obtained for both models in the unrotated case when $\eta = -1$. Thus we see that each model supports a topologically encoded qubit. Once we rotate the ribbons, we find that in both cases the ribbon disappears when we restrict to $w = 1$. In

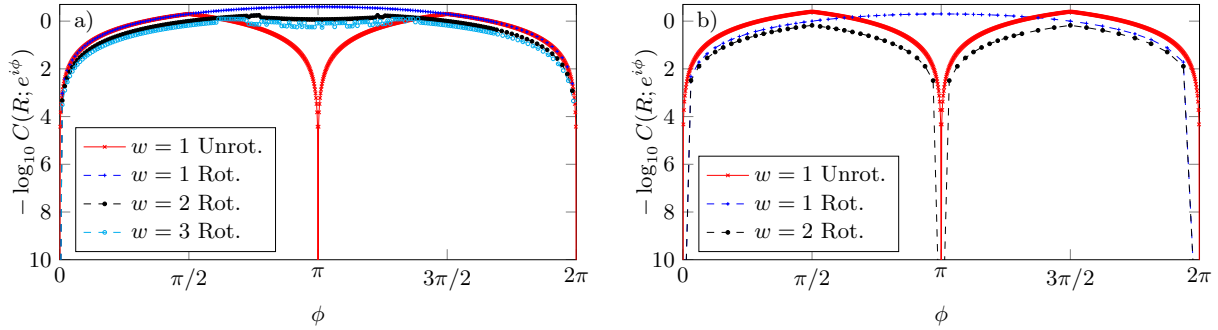


Figure 3.7: Subfigures a) and b) show the cost of ribbons with supports oriented as shown in Fig. 3.6 for two models: a) the quantum compass model and b) the QDI₂ model. The cost is parameterized with $\eta = e^{i\phi}$, and all ribbons were found using bond dimension 5.

a) Cost of ribbons in the quantum compass model of Eqn. (3.21). Because ribbons in this model are sensitive to their support, we conclude that they do not represent genuine topological order.

b) Cost of ribbons in the QDI₂ model of Eqn. (3.18) using $\{J, h, \lambda\} = \{1, 0, 0\}$. Note that the unit cell in the rotated case is $4w - 2$ rather than $2w$ for convenience. Low cost ribbons can be found on both unrotated and rotated supports indicating genuine topological order.

the QDI₂, the ribbon is recovered once we allow the support to grow to $w = 2$, however in the QC model there is no indication of a good ribbon existing even when we allow ribbons of width 3. This indicates that the low cost ribbons in the QC model are anomalies associated to lattice symmetries instead of genuine signatures of topological order.

3.5.3 Kitaev's Honeycomb Model

The honeycomb model [3.37] is a frustrated spin model on the honeycomb lattice with Hamiltonian

$$H = -J_X \sum_{i,j \in X \text{ links}} X_i X_j - J_Y \sum_{i,j \in Y \text{ links}} Y_i Y_j - J_Z \sum_{i,j \in Z \text{ links}} Z_i Z_j, \quad (3.23)$$

where the X , Y , and Z links refer to the three orientations of edges on the lattice. For $0 < J_X + J_Y < J_Z$, this model supports a phase with the same order as the \mathbb{Z}_2 quantum double model. [3.37] Writing a pair of anticommuting logical operators for this phase is a nontrivial task however, since they cannot both be symmetries of the Hamiltonian and will hence not have completely localized support. We can instead attempt to describe them with ribbons having some width w .

In Fig. 3.8, we investigate ribbon operators for the honeycomb model. As before, we observe the characteristic dip at $\eta = -1$ signalling a topologically ordered phase (Fig. 3.8a). We also observe the effect of increasing the allowed ribbon width in Fig. 3.8a. As expected the cost goes down as the width increases, although this is not a smooth decrease. We suggest that this is due to the nature of the widening. Each time the width is increased by three, an additional plaquette lies completely within the support of R . These plaquettes commute with the Hamiltonian, and so correspond to conserved quantities. In the perturbative regime, these plaquettes become those in the toric code model, which are associated with the location of anyonic charge. We note that the correlation length for $J_X = J_Y = J_Z/10$ is approximately .21, [3.38] so all of the widths correspond to several correlation lengths.

We also investigate how restricting the bond dimensions affects the cost. In Fig. 3.8b, we use a fixed width (3) and a fixed strength of $J_X = J_Y = J_Z/10$. At this point, we see that the cost rapidly saturates to a minimum for a small bond dimension of 4-5. This justifies the relatively small bond dimensions used in this work.

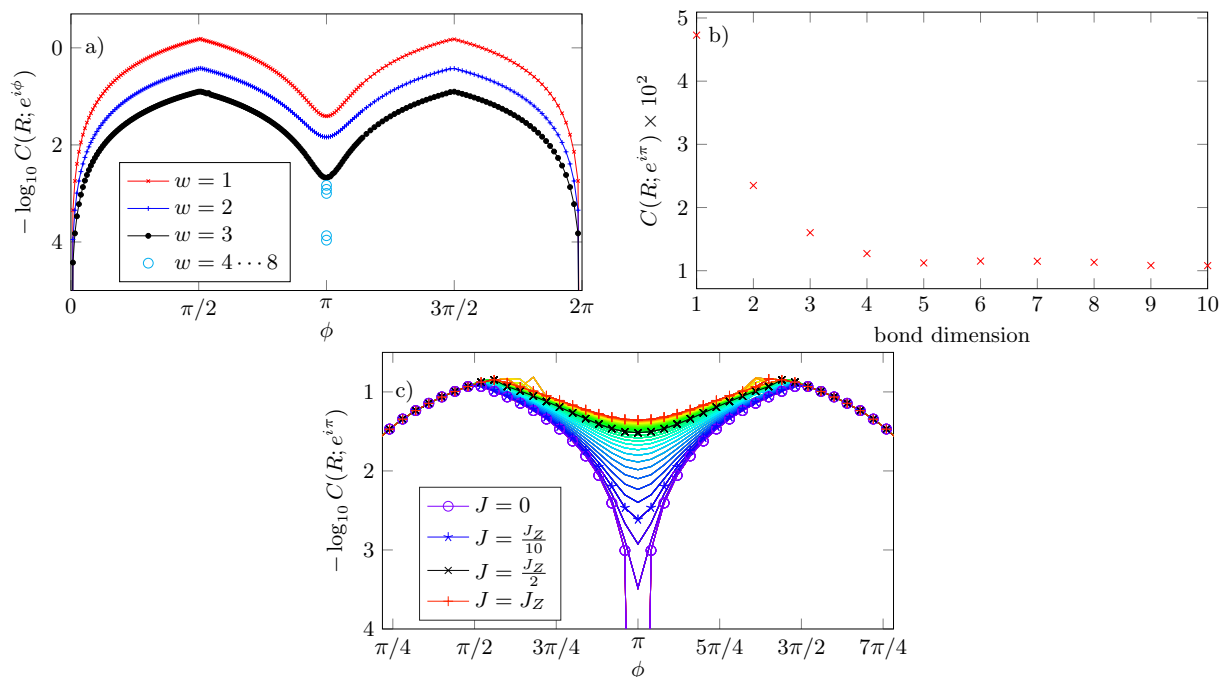


Figure 3.8: Cost of ribbons in the Honeycomb model. Strong indications of the \mathbb{Z}_2 topological order known to be present in this phase are visible. As expected, the cost decreases as the allowed width or bond dimension is increased, however the cost rapidly saturates with increasing bond dimension.

a) Cost for a bond dimension 5 ribbon on the honeycomb model of Eqn. (3.23) with $J_X = J_Y = J_Z/10$ using $\eta = e^{i\phi}$. A second ribbon can be obtained analytically, and was fixed as a product of Z s along the X and Y links of the lattice. The dip at $\phi = \pi$ is characteristic of \mathbb{Z}_2 order, and indicates the topological nature of this phase.

b) Cost for a width 2 ribbon at $\eta = -1$ on the Honeycomb model with $J_X = J_Y = J_Z/10$ as a function of bond dimension. The cost rapidly saturates to a minimum, justifying our assumption that only small bond dimension is required.

c) As we increase the strength of $J = J_X = J_Y$, we eventually cross a phase transition to a gapless phase at $J = J_Z/2$ (indicated by \times). Approaching this point, the signal of \mathbb{Z}_2 topological order essentially vanishes. Here the strength of J is increased in steps of $1/30$ from $J = 0$ (\circ) to $J = 1$ ($+$). Note that the line marked by \star corresponds to plots *a*, *b* and a bond dimension of 4 is used for a width 3 ribbon.

Finally, we examine the effect of increasing the strength of $J = J_X = J_Y$ in Fig. 3.8c. When $J_X = J_Y = J_Z/2$, the model undergoes a transition from a phase supporting \mathbb{Z}_2 topological order to a gapless phase. The latter supports Ising anyons if a time reversal symmetry breaking term is added. [3.37] Although we do not see a strong signal, such as a discontinuity, at this point, we see that the dip associated with $\eta = -1$ becomes very shallow. We expect the width of the required ribbons to be comparable to the correlation length, which we expect to increase as we move out of the perturbative regime. Thus the width 3 ribbon used here is expected to be inadequate for large J_X even within the phase. It remains to be seen whether ribbon operators can be used to identify phase transitions, possibly using a scaling analysis of ribbon width and bond dimension.

3.6 Ribbons As Logical Operators

One of the motivations for the ribbon operator methods is an application to quantum error correcting codes. In this section we show how nontrivial ribbon operators with sufficiently low cost can be used to certify the existence of an approximate topological quantum error correcting code in the ground space of the model. The ribbon operators function as approximate logical operators for these approximate codes. For gapped phases, this will also provide a natural justification for the method, although to apply this justification to the numerical results of Section 3.5 would require similar proofs with weaker assumptions than we are currently able to make here.

Let H be a Hamiltonian with gap Δ and suppose that for some $\epsilon > 0$, $\delta > 0$ and η , there exist ribbon operators L and R such that $\|[H, R]\|_{\text{op}} \leq \epsilon$, $\|[H, L]\|_{\text{op}} \leq \epsilon$, and $\|[R, L]_\eta\|_{\text{op}} \leq \delta$. Here $\|R\|_{\text{op}} = \|L\|_{\text{op}} = 1$, we restrict to hermitian ribbons, and we let $\|\cdot\|_{\text{op}}$ denote the operator norm. Let $|g\rangle$ be some ground state of H with energy E_0 . Then the expected energy of $|h\rangle = R|g\rangle$ is

$$\begin{aligned} \langle g|R^\dagger H R|g\rangle &= \langle g|R^\dagger R H|g\rangle + \langle g|R^\dagger [H, R]|g\rangle \\ &\leq E_0 + \epsilon. \end{aligned} \quad (3.24)$$

Thus, $|h\rangle$ is a low energy state, and we can interpret R as a generator for a unitary approximate logical operator.

It is important to check that R is not mapping out of the ground space, so we need to ensure that there is a large overlap. Let Π denote the ground space projector for H . By assumption the model has a spectral gap Δ , so we find that

$$\begin{aligned} E_0 + \epsilon &\geq \langle h|H|h\rangle \\ &\geq E_0 \langle h|\Pi|h\rangle + (E_0 + \Delta) \langle h|\mathbf{1} - \Pi|h\rangle. \end{aligned} \quad (3.25)$$

Rearranging this, and noting that E_0 can always be set to 0, we obtain

$$\frac{\langle h|\Pi|h\rangle}{\langle h|h\rangle} \geq 1 - \frac{\epsilon}{\langle h|h\rangle \Delta}. \quad (3.26)$$

Thus, the action of the ribbon operators approximately preserves the ground space as long as they approximately preserve the norm of the individual ground states ($\langle h|h\rangle \approx 1$). If this condition does not hold, R is annihilating the ground space.

Given an almost commuting pair of hermitian operators R and H , we can perturb to an exactly commuting hermitian pair \tilde{R} and \tilde{H} such that the following holds: [3.46, 3.47] $\|R - \tilde{R}\|_{\text{op}} \leq \gamma(\epsilon)$ and $\|H - \tilde{H}\|_{\text{op}} \leq \gamma(\epsilon)$, where $\gamma(\epsilon)$ can be taken to be at most $\epsilon^{1/30}$. It is convenient to work with \tilde{H} and \tilde{R} since they can be simultaneously exactly diagonalized. We need to check that the assumed

twisted commutation relation between R and L is approximately maintained when we consider \tilde{R} and L .

$$\begin{aligned}
 \delta &\geq \|RL - \eta LR\|_{\text{op}} \\
 &= \|(R - \tilde{R} + \tilde{R})L - \eta L(R - \tilde{R} + \tilde{R})\|_{\text{op}} \\
 &\geq \|\tilde{R}L - \eta L\tilde{R}\|_{\text{op}} - \|(R - \tilde{R})L - \eta L(R - \tilde{R})\|_{\text{op}}.
 \end{aligned} \tag{3.27}$$

Rearranging and using standard inequalities, we find

$$\|\tilde{R}L - \eta L\tilde{R}\|_{\text{op}} \leq \delta + (1 + |\eta|)\gamma, \tag{3.28}$$

and so the twisted commutator is approximately preserved. The same argument shows that L approximately commutes with \tilde{H} and thus approximately preserves its ground space.

We now check that the action of L on eigenstates of \tilde{R} maps to a nearly orthogonal state and can therefore be used to manipulate information in the code space. Since \tilde{H} and \tilde{R} exactly commute, we can find a joint eigenstate $|\tilde{g}\rangle$ such that $\tilde{R}|\tilde{g}\rangle = \tilde{g}|\tilde{g}\rangle$ and $\tilde{H}|\tilde{g}\rangle = E_0|\tilde{g}\rangle$, then

$$\delta \geq |\langle \tilde{g} | RL - \eta LR | \tilde{g} \rangle|, \tag{3.29}$$

and therefore

$$|\langle \tilde{g} | L | \tilde{g} \rangle| \leq \frac{\delta}{|\tilde{g}| |1 - \eta|}. \tag{3.30}$$

We have already assumed that R maps a ground state to an approximately normalized state, so $|\tilde{g}| \approx 1$. Therefore, the action of L maps $|\tilde{g}\rangle$ to an approximately orthogonal state.

Thus, even approximate ribbon operators preserve the ground space (or annihilate it). Together, these results provide a certificate of topological order, at least when the strong assumptions of the derivation are met. In addition to providing such a certificate, this also shows that the method of ribbon operators can be used to obtain approximate logical operators even if the topological phase is already known. The ribbons can be used to enact logical operations on encoded qudits even when the underlying model is not an exact topological quantum code, such as in the case of the honeycomb model.

Recent work has investigated the possibility of certifying degeneracy in the ground space of a Hamiltonian using ‘‘approximate symmetries’’. [3.48] In the case of unitary ribbons and $\eta = \exp(i\theta)$, the authors showed that if $\|[H, R]\|$, $\|[H, L]\|$, and $\|[R, L]_\eta\|$ are sufficiently small, then the degeneracy of the ground space can indeed be certified as larger than some integer specified by θ . In the nontrivial case (i.e. ground space degeneracy larger than 1), the operators act as approximate logical operators when restricted to the ground space. One could utilize this result, along with the numerical procedures outlined in this work, to *prove* topological degeneracy by investigating the behavior of the cost function on different manifolds.

3.7 Summary and Outlook

We have introduced the method of ribbon operators for detecting topological order. By identifying features expected in topologically ordered spin models, we have defined a cost function which quantifies the extent to which operators on the lattice realize these features.

Using a variational minimization algorithm on this cost function over the space of matrix product operators, we have demonstrated that this method can distinguish nontrivial topological order from

non-topological phases in various models, both integrable and nonintegrable. We have also shown how, with additional assumptions, ribbon operators can be used as approximate logical operators in topological quantum error correcting codes, which provides a specific sense in which they can certify the presence of topological order.

The most obvious open question is to extend these methods to other models, including those with nonabelian topological order. These nonabelian models are particularly interesting from a quantum information perspective as they can be utilized for universal quantum computation. [3.5,3.6] Another open question is whether this method can be extended to detect symmetry-protected or symmetry-enriched topological order, but this would seem to require new ideas.

Even without generalizing the method to deal with nonabelian models, there are several natural ways in which our approach can be improved and extended. One could proceed by either changing the cost function, the variational class, or the optimization method. We begin by discussing a natural restriction on the allowed MPOs.

As shown in Section 3.5.1, some topologically trivial models support zero-cost ribbon operators when the variational class is all MPOs of a given bond dimension. These operators corresponded to products of projectors onto local ground states. Although such operators have low cost, they are not good signals of topological order, since the η for which $[R, L]_\eta = 0$ is not unique because R and L mutually annihilate. This behavior could be removed by insisting that the ribbon operators be unitary. In addition to removing these false signals, a unitary constraint would ensure that ribbon operators properly preserve the norm of states on which they act. As discussed in Section 3.6, this property is important if the ribbons are to be interpreted as approximate logical operators for a quantum error correcting code.

A potential failure mode for this method is ‘high-temperature topological order’. Suppose there is some gapped state high up in the spectrum of the Hamiltonian, for example, at the top of the spectrum. It is conceivable that such a state could possess a ‘topological order’ distinct from the low-energy space. In this case, the method may find signals of TO which are originating from the high-energy portion of the spectrum. Such a failure mode could be combated by incorporating a low-temperature thermal state into the cost function. This would bias the norm towards the low-energy space, without the need for computing the ground state itself. Note that low temperature thermal states have efficient PEPS descriptions, [3.49, 3.50] so the computational benefits of this method may remain.

One may also consider applying the method to seek out such high-energy topologically ordered subspaces in models with trivial ground spaces. This may provide an avenue towards interesting thermal physics with a topological flavor.

There are various alterations which can be made to the cost function defined in Section 3.2.2. Recall that our cost function used the η -commutator to incorporate the topological data. This is associated with the \mathcal{R} matrix of the anyon model. A natural replacement for, or addition to, this term would be a term involving the $\tilde{\mathcal{S}}$ matrix. It is an open question if the current method or any of these suggested generalizations can be used to obtain the complete \mathcal{S} and \mathcal{R} matrices of a model. Recall from Section 3.2 that in the abelian case, there is a column permutation of \mathcal{S} which cannot be fixed. This could be addressed by ensuring all ribbons lie on comparable supports, for example circles or L shaped regions.

As discussed in Section 3.2, insisting that a ribbon R commute with the Hamiltonian on all eigenspaces (e.g. using the Frobenius norm $\|[R, H]\|$) is probably too strong to identify the topological order present in all models. One usually discusses topological order only with respect to the low-energy sector of the model. We propose that rather than taking the norm of the commutator, a variational low-energy state, for example in PEPS [3.22] or MERA [3.51] form, could be used to supplement the algorithm. Alternatively, one could use a low-energy thermal state as discussed

above. Rather than evaluating norms, one could evaluate expectation values on these low energy states. This bypasses problems associated with finding ground states of 2D Hamiltonians, since the state need only be low energy and supported on a strip only just wider than the ribbon itself. Access to a state may be required for the extension to nonabelian models, where the excited spectrum is expected to be more exotic than in the abelian case and reflect the structure of the fusion space of the underlying anyons.

It would be interesting to apply the method to models where the topological order is still debated, for example the Heisenberg model on the Kagome lattice. When our cost function is encoded into an MPO for minimization using DMRG, it has a large bond dimensions since it is quadratic in the Hamiltonian of the model. This makes it computationally expensive to minimize. To approach these more complex models, it may be necessary to make use of properties of this MPO, such as sparsity, to reduce this cost. Alternatively, one could modify the cost function to reduce the bond dimension, or use another method to minimize it.

The assumptions used in Section 3.6 are stronger than the constraints imposed in our numerical work. Understanding how to weaken these assumptions would provide additional justification for this method, and may provide insight into possible additional constraints which a ribbon operator should obey to ensure it is truly certifying topological order. It would also be interesting to blend our algorithm with the results of [3.48] with a view to certifying topological degeneracy.

Acknowledgments

We thank Matthias Bal, Parsa Bonderson, Christopher Chubb, Andrew Doherty, Christopher Granade, Jeongwan Haah, Jutho Haegeman, Robert Pfeifer, Sam Roberts, Norbert Schuch, Tom Stace, Frank Verstraete and Dominic Williamson for useful and enlightening discussions. We also thank the anonymous referee who pointed out the potential failure mode that may result from a model with high-energy topologically ordered subspaces. We acknowledge support from the Australian Research Council via the Centre of Excellence in Engineered Quantum Systems (EQuS), project number CE110001013. STF also acknowledges support from an Australian Research Council Future Fellowship FT130101744. This work was initiated while DP was on sabbatical leave at The University of Sydney, he acknowledges their hospitality and their International Research Collaboration Award for partial support.

Bibliography

- 3.1 Xiao-Gang Wen, Topological Order: From Long-Range Entangled Quantum Matter to a Unified Origin of Light and Electrons, *ISRN Condensed Matter Physics* **2013**, 198710 (2013), [arXiv:1210.1281](#) .
- 3.2 Xie Chen, Zheng-Cheng Gu, Zheng-Xin Liu, and Xiao-Gang Wen, Symmetry protected topological orders and the group cohomology of their symmetry group, *Physical Review B* **87**, 155114 (2013), [arXiv:1106.4772](#) .
- 3.3 Maissam Barkeshli, Parsa Bonderson, Meng Cheng, and Zhenghan Wang, Symmetry, Defects, and Gauging of Topological Phases, [arXiv:1410.4540](#) (2014).
- 3.4 Phillip W. Anderson, The Resonating Valence Bond State in La_2CuO_4 and Superconductivity, *Science* **235**, 1196–1198 (1987).

- 3.5 A. Yu Kitaev, Fault-tolerant quantum computation by anyons, *Annals of Physics* **303**, 2–30 (2003), [arXiv:quant-ph/9707021](#) .
- 3.6 Chetan Nayak, Steven H. Simon, Ady Stern, Michael Freedman, and Sankar Das Sarma, Non-abelian anyons and topological quantum computation, *Reviews of Modern Physics* **80**, 1083 (2008), [arXiv:0707.1889](#) .
- 3.7 X. G. Wen and Q. Niu, Ground-state degeneracy of the fractional quantum Hall states in the presence of a random potential and on high-genus Riemann surfaces, *Physical Review B* **41**, 9377–9396 (1990).
- 3.8 Eric Dennis, Alexei Kitaev, Andrew Landahl, and John Preskill, Topological quantum memory, *Journal of Mathematical Physics* **43**, 4452 (2002), [arXiv:0110143](#) .
- 3.9 B. J. Brown, D. Loss, J. K. Pachos, C. N. Self, and J. R. Wootton, Quantum memories at finite temperature, *Reviews of Modern Physics* **88**, 045005, [arXiv:1411.6643](#) (2016).
- 3.10 Barbara M. Terhal, Quantum error correction for quantum memories, *Reviews of Modern Physics* **87**, 307 (2015), [arXiv:1302.3428](#) .
- 3.11 Courtney G. Brell, Simon Burton, Guillaume Dauphinais, Steven T. Flammia, and David Poulin, Thermalization, Error Correction, and Memory Lifetime for Ising Anyon Systems, *Physical Review X* **4**, 031058 (2014), [arXiv:1311.0019](#) .
- 3.12 Michael Levin and Xiao-Gang Wen, Detecting Topological Order in a Ground State Wave Function, *Physical Review Letters* **96**, 110405 (2006), [arXiv:cond-mat/0510613](#) .
- 3.13 Alexei Kitaev and John Preskill, Topological Entanglement Entropy, *Physical Review Letters* **96**, 110404 (2006), [arXiv:hep-th/0510092](#) [hep-th] .
- 3.14 Steven T. Flammia, Alioscia Hamma, Taylor L. Hughes, and Xiao-Gang Wen, Topological entanglement Rényi entropy and reduced density matrix structure, *Physical Review Letters* **103**, 261601 (2009), [arXiv:0909.3305](#) .
- 3.15 Sergei V. Isakov, Matthew B. Hastings, and Roger G. Melko, Topological entanglement entropy of a Bose-Hubbard spin liquid, *Nature Physics* **7**, 772–775 (2011), [arXiv:1102.1721](#) .
- 3.16 Yi Zhang, Tarun Grover, Ari Turner, Masaki Oshikawa, and Ashvin Vishwanath, Quasiparticle statistics and braiding from ground-state entanglement, *Physical Review B* **85**, 235151 (2012), [arXiv:1111.2342](#) .
- 3.17 Hong-Chen Jiang, Zhenghan Wang, and Leon Balents, Identifying topological order by entanglement entropy, *Nature Physics* **8**, 902–905 (2012), [arXiv:1205.4289](#) .
- 3.18 Hui Li and F. D. M. Haldane, Entanglement Spectrum as a Generalization of Entanglement Entropy: Identification of Topological Order in Non-Abelian Fractional Quantum Hall Effect States, *Physical Review Letters* **101**, 010504 (2008), [arXiv:0805.0332](#) .
- 3.19 Simon Trebst, Philipp Werner, Matthias Troyer, Kirill Shtengel, and Chetan Nayak, Breakdown of a Topological Phase: Quantum Phase Transition in a Loop Gas Model with Tension, *Physical Review Letters* **98**, 070602 (2007), [arXiv:cond-mat/0609048](#) .
- 3.20 L. Cincio and G. Vidal, Characterizing topological order by studying the ground states on an infinite cylinder, *Physical Review Letters* **110**, 067208 (2013), [arXiv:1208.2623](#) .

- 3.21 Oliver Buerschaper, Twisted Injectivity in PEPS and the Classification of Quantum Phases, *Annals of Physics* **351**, 447476 (2014), [arXiv:1307.7763](#) .
- 3.22 Norbert Schuch, Ignacio Cirac, and David Pérez-García, PEPS as ground states: Degeneracy and topology, *Annals of Physics* **325**, 2153–2192 (2010), [arXiv:1001.3807](#) .
- 3.23 Mehmet Burak Şahinoğlu, Dominic Williamson, Nick Bultinck, Michael Mariën, Jutho Haegeman, Norbert Schuch, and Frank Verstraete, Characterizing Topological Order with Matrix Product Operators, [arXiv:1409.2150](#) (2014).
- 3.24 Nick Bultinck, Michael Mariën, Dominic Williamson, Mehmet Burak Şahinoğlu, Jutho Haegeman, and Frank Verstraete, Anyons and matrix product operator algebras, *Annals of Physics* **378**, 183-233 (2017), [arXiv:1511.08090](#) .
- 3.25 Fangzhou Liu and Xiao-Gang Wen, Environment tensor as order parameter for symmetry breaking and (symmetry-protected) topological orders, [arXiv:1504.08365](#) (2015) .
- 3.26 G. Evenbly and G. Vidal, Frustrated antiferromagnets with entanglement renormalization: Ground state of the spin-1/2 heisenberg model on a kagome lattice, *Physical Review Letters* **104**, 187203 (2010), [arXiv:0904.3383](#) .
- 3.27 S. Yan, D. A. Huse, and S. R. White, Spin-Liquid Ground State of the $S = 1/2$ Kagome Heisenberg Antiferromagnet, *Science* **332**, 1173–1176 (2011), [arXiv:1011.6114](#) .
- 3.28 Ulrich Schollwöck, The density-matrix renormalization group in the age of matrix product states, *Annals of Physics* **326**, 96–192 (2011), [arXiv:1008.3477](#) .
- 3.29 Liujun Zou and Jeongwan Haah Spurious long-range entanglement and replica correlation length, *Physical Review B* **94**, 075151 (2016), [arXiv:1604.06101](#) .
- 3.30 Anushya Chandran, Vedika Khemani, and S.L. Sondhi, How Universal Is the Entanglement Spectrum? *Physical Review Letters* **113**, 060501 (2014), [arXiv:1311.2946](#) .
- 3.31 Michael Levin and Xiao-Gang Wen, String-net condensation:A physical mechanism for topological phases, *Physical Review B* **71**, 045110 (2005), [arXiv:cond-mat/0404617](#) .
- 3.32 Zohar Nussinov and Gerardo Ortiz, Symmetry and Topological Order, *Proceedings of the National Academy of Sciences* **106**, 16944 (2009), [arXiv:cond-mat/0605316](#) .
- 3.33 Zohar Nussinov and Gerardo Ortiz, A symmetry principle for Topological Quantum Order, *Annals of Physics* **324**, 977 (2009), [arXiv:cond-mat/0702377](#) .
- 3.34 J. Ignacio Cirac, Didier Poilblanc, Norbert Schuch, and Frank Verstraete, Entanglement spectrum and boundary theories with projected entangled-pair states, *Physical Review B* **83**, 245134 (2011), [arXiv:1103.3427](#) .
- 3.35 Michael Freedman, Chetan Nayak, and Kirill Shtengel, Lieb-Schultz-Mattis theorem for quasi-topological systems, *Physical Review B* **78**, 174411 (2008), [arXiv:cond-mat/0608508](#) .
- 3.36 Jeongwan Haah, Local stabilizer codes in three dimensions without string logical operators, *Physical Review A* **83**, 042330 (2011), [arXiv:1101.1962](#) .
- 3.37 Alexei Kitaev, Anyons in an exactly solved model and beyond, *Annals of Physics* **321**, 2–111 (2006), [arXiv:cond-mat/0506438](#) .

- 3.38 Shuo Yang, Shi-Jian Gu, Chang-Pu Sun, and Hai-Qing Lin, Fidelity susceptibility and long-range correlation in the Kitaev honeycomb model, *Physical Review A* **78**, 012304 (2008), [arXiv:0803.1292](#) .
- 3.39 Jeongwan Haah and John Preskill, Logical-operator tradeoff for local quantum codes, *Physical Review A* **86**, 032308 (2012), [arXiv:1011.3529](#) .
- 3.40 Olivier Landon-Cardinal and David Poulin, Local Topological Order Inhibits Thermal Stability in 2D, *Physical Review Letters* **110**, 090502 (2013), [arXiv:1209.5750](#) .
- 3.41 M. B. Hastings and Xiao-Gang Wen, Quasiadiabatic continuation of quantum states: The stability of topological ground-state degeneracy and emergent gauge invariance, *Physical Review B* **72**, 045141 (2005), [arXiv:cond-mat/0503554](#) .
- 3.42 Jeongwan Haah, An invariant of topologically ordered states under local unitary transformations, *Communications in Mathematical Physics* **342**, 771–801 (2016), [arXiv:1407.2926](#) .
- 3.43 B. Pirvu, V. Murg, J. I. Cirac, and F. Verstraete, Matrix product operator representations, *New Journal of Physics* **12**, 025012 (2010), [arXiv:0804.3976](#) .
- 3.44 Julien Dorier, Federico Becca, and Frédéric Mila, Quantum compass model on the square lattice, *Physical Review B* **72**, 024448 (2005), [arXiv:cond-mat/0501708](#) .
- 3.45 Dave Bacon, Operator quantum error-correcting subsystems for self-correcting quantum memories, *Physical Review A* **73**, 012340 (2006), [arXiv:quant-ph/0506023](#) .
- 3.46 Huaxin Lin, Almost commuting selfadjoint matrices and applications, in *Operator algebras and their applications*, Fields Institute Communications, Vol. 13 (American Mathematical Society, 1997) pp. 193–233.
- 3.47 M. B. Hastings, Making Almost Commuting Matrices Commute, *Communications in Mathematical Physics* **291**, 321–345 (2009), [arXiv:0808.2474](#) .
- 3.48 Christopher T. Chubb and Steven T. Flammia, Approximate symmetries of Hamiltonians, *Journal of Mathematical Physics* **58**, 082202 (2017), [arXiv:1608.02600](#) .
- 3.49 M. B. Hastings, Solving Gapped Hamiltonians Locally, *Physical Review B* **73**, 085115 (2006), [arXiv:cond-mat/0508554](#) .
- 3.50 András Molnár, Norbert Schuch, Frank Verstraete, and Ignacio Cirac, Approximating Gibbs states of local Hamiltonians efficiently with PEPS, *Physical Review B* **91**, 045138 (2015), [arXiv:1406.2973](#) .
- 3.51 G. Vidal, Class of Quantum Many-Body States That Can Be Efficiently Simulated, *Physical Review Letters* **101**, 110501 (2008), [arXiv:quant-ph/0610099](#) .

Appendices

3.A \mathbb{Z}_2 Quantum Double

The cost function for a pair of width 1 ribbon operators in the \mathbb{Z}_2 quantum double model defined in Eq. 3.18 (with $(J, h, \lambda) = (1, 0, 0)$) can easily be written. Define the lattice as in Fig. 3.1, and let the strings R and L have supports on the horizontal and vertical strips respectively. Beginning with ribbon R , we see that there are no Hamiltonian terms contained completely within the support. Thus the first term in the cost vanishes. The same happens for ribbon L .

The next term concerns those Hamiltonian terms which cross the boundary. There are two classes, those with support on a single spin inside R and those supported on a pair of spins in R . Each dark plaquette (\blacklozenge) contributes to a term in the first class, with each spin j in R being touched by a pair of such plaquettes. Therefore at this stage we have an initial cost function C_0 for the commutator part given by

$$C_0(R) = \left(2 \sum_{j=1}^N \|[R, X_j]\|^2 \right), \quad (3.31)$$

where N is the number of spins on which R is supported. Each light plaquette (\lozenge) contributes a two-spin term, so the costs become

$$C_0(R) = \left(2 \sum_{j=1}^N \|[R, X_j]\|^2 + \sum_{j=1}^N \|[R, Z_j Z_{j+1}]\|^2 \right). \quad (3.32)$$

For convenience, assume two-site translationally invariant product operators for both $R = \dots abab \dots$ and $L = \dots cdcd \dots$. This cost function becomes

$$C_0(R) = 2 \frac{N}{2} \|[a, X]\|^2 + 2 \frac{N}{2} \|[b, X]\|^2 + \frac{N}{2} \|[ab, ZZ]\|^2 + \frac{N}{2} \|[ba, ZZ]\|^2, \quad (3.33)$$

since $N/2$ of the sites of R support operator a and $N/2$ sites support operator b .

There are no more terms contributed by the commutator with the Hamiltonian. It remains to include the twisted commutator terms. The ribbon L can intersect R with either a c site or a d site. Recall that we require that all translations of L are considered, so we obtain

$$C_1(R; \eta) = \sum_j \|[r_j, c]_\eta\|^2 + \sum_j \|[r_j, d]_\eta\|^2, \quad (3.34)$$

where r_j is the operator at site j of ribbon R . Notice that each r_j is required to η -commute with both c and d . In this way, the insensitivity of this term to the particular support of L is ensured. This term gives

$$C_1(R; \eta) = \frac{N}{2} \|[a, c]_\eta\|^2 + \frac{N}{2} \|[b, c]_\eta\|^2 + \frac{N}{2} \|[a, d]_\eta\|^2 + \frac{N}{2} \|[b, d]_\eta\|^2. \quad (3.35)$$

Combining these two costs, we obtain the total cost function for ribbon R

$$C(R; \eta) = \frac{1}{N} (C_0(R) + C_1(R; \eta)) \quad (3.36)$$

$$\begin{aligned} &= \|[a, Z]\|^2 + \|[b, Z]\|^2 + \frac{1}{2} \|[ab, XX]\|^2 + \frac{1}{2} \|[ba, XX]\|^2 \\ &\quad + \frac{1}{2} \|[a, c]_\eta\|^2 + \frac{1}{2} \|[b, c]_\eta\|^2 + \frac{1}{2} \|[a, d]_\eta\|^2 + \frac{1}{2} \|[b, d]_\eta\|^2. \end{aligned} \quad (3.37)$$

The cost for ribbon L can be obtained analogously, giving

$$\begin{aligned} C(L; \eta) &= \|[c, Z]\|^2 + \|[d, Z]\|^2 + \frac{1}{2} \|[cd, XX]\|^2 + \frac{1}{2} \|[dc, XX]\|^2 \\ &\quad + \frac{1}{2} \|[a, c]_\eta\|^2 + \frac{1}{2} \|[b, c]_\eta\|^2 + \frac{1}{2} \|[a, d]_\eta\|^2 + \frac{1}{2} \|[b, d]_\eta\|^2. \end{aligned} \quad (3.38)$$

Notice that $C_1(R; \eta) = C_1(L; \eta)$. Care should be taken with this term since $[\cdot, \cdot]_\eta$ is not symmetric in its arguments.

It is easy to check that, as expected, these cost functions are both zero when we set $a = b = X$, $c = d = Z$ and $\eta = -1$, corresponding to the known string operators for this model.

Chapter 4

Anomalies and entanglement renormalization

JACOB C. BRIDGEMAN¹ AND DOMINIC J. WILLIAMSON²

¹CENTRE FOR ENGINEERED QUANTUM SYSTEMS, SCHOOL OF PHYSICS, THE UNIVERSITY OF SYDNEY, SYDNEY, AUSTRALIA

²VIENNA CENTER FOR QUANTUM TECHNOLOGY, UNIVERSITY OF VIENNA, BOLTZMANNGASSE 5, 1090 VIENNA, AUSTRIA

Physical Review B [96, 125104 \(2017\)](#), arXiv:[1703.07782](#)

Abstract

We study 't Hooft anomalies of discrete groups in the framework of (1+1)-dimensional multiscale entanglement renormalization ansatz states on the lattice. Using matrix product operators, general topological restrictions on conformal data are derived. An ansatz class allowing for optimization of MERA with an anomalous symmetry is introduced. We utilize this class to numerically study a family of Hamiltonians with a symmetric critical line. Conformal data is obtained for all irreducible projective representations of each anomalous symmetry twist, corresponding to definite topological sectors. It is numerically demonstrated that this line is a protected gapless phase. Finally, we implement a duality transformation between a pair of critical lines using our subclass of MERA.

Quantum many-body models of strongly interacting spins display surprisingly complex emergent physics. Understanding general classes of collective behaviors corresponds to understanding which phases of matter can be realized through local interactions. The universal behavior of phases, and their transitions, is determined by the fixed points under renormalization group (RG) flows [\[4.1, 4.2\]](#).

Symmetries play a fundamental role in the understanding of phases, due to constraints they impose on RG. Indeed, the conventional classification of phases describes how a symmetry can be broken [\[4.3\]](#). Distinct quantum phases emerge even without a broken symmetry [\[4.4–4.8\]](#). In the absence of intrinsic topological order, these phases are known as *symmetry protected topological* (SPT) phases [\[4.9–4.12\]](#). Despite having no topological order and no local order parameter, SPT phases are resources for quantum computation [\[4.13–4.17\]](#).

On the lattice, symmetries are usually assumed to act independently on each site. More exotic symmetries, which cannot be made on-site, have recently been studied in chains of anyons [\[4.18–4.22\]](#) and at the boundary of SPT phases [\[4.23–4.32\]](#). In fact, a classification of SPTs can be obtained

by considering possible boundary actions of the symmetry. Equivalence classes of such symmetries are labeled by the 't Hooft anomalies [4.33] of a discrete group. Such anomaly labels are preserved by symmetric RG transformations, so restrict the possible fixed points [4.34].

Tensor network methods [4.35–4.37] allow anomalous symmetries to be realized directly on the lattice. In $(1 + 1)$ dimensions, *matrix product operators* (MPOs) capture all 't Hooft anomalies of discrete groups [4.23–4.26]. Within the framework of tensor networks, phases are classified at the level of states. For example, *matrix product states* (MPS) have proven particularly successful for the study of gapped spin chains [4.38–4.47]. Despite substantial complications arising for tensor networks in higher dimensions; significant progress has been made, particularly in the study of topological states [4.48–4.57].

Imposing on-site symmetries on tensor network representations of quantum states is well understood [4.58–4.60]. Far less effort has been made to study the effect of anomalous group actions on these states. Such group actions naturally arise as the effective edge symmetries of $(d + 1)$ D SPTs [4.28–4.30]. In $(2 + 1)$ D, the edge theory must either spontaneously break this symmetry or be gapless. Since all MPS break the symmetry [4.23], to study gapless, symmetric edge theories we turn to another class of tensor networks known as *multiscale entanglement renormalization ansatz* (MERA) [4.61]. These networks draw on ideas from RG to represent the low energy states of gapless Hamiltonians [4.61–4.63].

In this work we define a variational subclass of MERA which can be used to simulate SPT edge physics in a manifestly symmetric way. This subclass allows us to investigate the interplay between RG and anomalies in the framework of tensor networks. We use tensor network methods to derive general consequences of an anomalous symmetry on the conformal field theory (CFT) data of an RG fixed point. For a family of Hamiltonians, corresponding to a line of fixed points, we numerically optimize within our variational class to find the lowest energy states and extract conformal data [4.64,4.65]. We observe the effects of the anomaly in these results. Furthermore, we demonstrate that as a consequence of the anomaly these Hamiltonians admit no relevant, symmetric perturbations. The Hamiltonians therefore support a gapless phase which is protected by an anomalous symmetry.

More generally, RG fixed points may transform non-trivially under an anomalous group action. Our variational class accommodates this possibility, and hence permits the study of gapless models which are not symmetric. We utilize this in a numerical simulation of two critical lines that are related by a duality transformation, which we implement at the level of a single tensor.

This paper is organized as follows: In Section 4.1, we introduce background material on anomalies, symmetries and tensor networks. In particular, we introduce the 't Hooft anomaly of a discrete symmetry. We then briefly review the MERA and what it means for it to be symmetric under an on-site group action. The difficulties in enforcing anomalous MPO symmetries locally are then discussed. In Section 4.2, we derive general consequences of an anomalous symmetry on a MERA, which are later utilized in the numerical simulations. We study anomalous symmetry twists and the projective representations under which they transform. From these ingredients, projectors onto definite topological sectors are constructed. Consequences for fields within a sector are discussed. In Section 4.3, we define a variational subclass of MERA which is later used for manifestly symmetric simulations. We present a disentangling unitary capable of decoupling a local piece of an anomalous \mathbb{Z}_N^3 group action. This allows the unconstrained variational parameters of any symmetric MERA scheme to be isolated, and therefore optimized over. In Section 4.4, we bring together tools developed in the preceding sections to simulate a family of Hamiltonians with three critical lines. One of these lines possesses an anomalous symmetry, whilst the other two are dual under the anomalous group action. We present conformal data for these critical lines obtained from a numerically optimized MERA, including two nontrivial topological sectors for the symmetric line. Additionally, we demonstrate that the symmetric line is in fact a protected gapless phase. In Section 4.5 we

summarize the results and suggest several possible extensions of this work.

We have included several appendices for completeness. In Appendix 4.A we provide conformal data obtained from a symmetric MERA in all topological sectors for the symmetric line of our example model. Additionally, we present fusion rules for these topological sectors computed using a symmetric MERA. In Appendix 4.B we review the notion of third cohomology for an MPO representation of a finite group. In Appendix 4.C we provide details of our ansatz for MPO symmetric MERA including example tensors for two MERA schemes. In Appendix 4.D we describe a generalization of the CZX model [4.23] to arbitrary finite groups \mathcal{G} , such that the bulk symmetry acts as an MPO duality of \mathcal{G} -SPT phases on the boundary.

4.1 Symmetries and anomalies in MERA

This section introduces the main tools and concepts utilized in the remainder of this manuscript. We begin by discussing 't Hooft anomalies of group actions, including some historical context. Lattice realizations of these anomalies, and their influence on tensor network states, are our primary objects of study. Readers unfamiliar with this terminology may skip to Section 4.1.1 for the definition of anomaly used throughout this work. We then review the MERA, the tensor network designed for critical behavior, and define what it means for it to be symmetric under a unitary group action. We briefly explain how one enforces an on-site symmetry via a local constraint before moving on to discuss the difficulties in enforcing an anomalous symmetry in a similar fashion.

Recently anomalies have played an important role in the classification and study of topological phases of matter [4.27, 4.66, 4.67]. Particularly relevant are 't Hooft anomalies, which describe obstructions to gauging a global symmetry [4.33]. SPT phases, and their higher symmetry generalizations [4.68–4.70], can be classified by the possible 't Hooft anomalies on their boundaries [4.28–4.31]. Conversely one can think of the possible 't Hooft anomalies as being classified by what is known as anomaly inflow from one dimension higher [4.27–4.29, 4.31, 4.32].

A global symmetry with an 't Hooft anomaly has an interesting interplay with the renormalization group (RG). For a connected Lie group symmetry, an 't Hooft anomaly restricts the possible RG fixed points, even if the symmetry is spontaneously broken [4.71, 4.72]. In the case of a broken discrete symmetry, this is no longer true. For a symmetry respecting RG flow, however, the 't Hooft anomaly can not change and hence constrains the possible fixed points [4.28].

Symmetry actions which can be realized independently on each site have trivial 't Hooft anomaly because they can be gauged directly on the lattice [4.26, 4.73, 4.74]. Conversely, this gauging procedure cannot be applied directly to symmetries which cannot be made on site. Therefore, we treat the 't Hooft anomaly as an obstruction to making a symmetry action on-site [4.25, 4.27, 4.32].

For a discrete symmetry group \mathcal{G} in $(1+1)D$, all 't Hooft anomalies of bosonic unitary representations occur on the boundaries of $(2+1)D$ SPT phases, in other words they arise from anomaly inflow. The anomalies can therefore be classified by $\mathcal{H}^3(\mathcal{G}, U(1))$, the same set of labels as the SPT phases [4.23, 4.29, 4.30]. In the next section, we describe how *matrix product operators* can be utilized to represent these anomalous actions.

4.1.1 Symmetries on the lattice

In this work, we consider unitary representations of finite groups on the lattice. We say a state $|\psi\rangle$ is *symmetric* under a group \mathcal{G} if $U_g|\psi\rangle = |\psi\rangle$ for all $g \in \mathcal{G}$, where U_g is some unitary representation of the group.

The symmetry is *on-site* if the representation can be decomposed as $U_g = \otimes_{j=1}^N (u_g)_j$, where each $(u_g)_j$ is a (local) unitary representation.

Although group actions are usually considered to be on-site, this is not the most general way a symmetry can be represented. A more general class of group actions can be represented by matrix product operators (MPOs). Using the conventional tensor network notation [4.35–4.37], these are denoted

$$U_g = \begin{array}{c} \text{---} \text{---} \text{---} \text{---} \text{---} \text{---} \text{---} \text{---} \\ | \quad | \quad | \quad | \quad | \quad | \quad | \\ \text{---} \text{---} \text{---} \text{---} \text{---} \text{---} \text{---} \end{array} g, \quad (4.1)$$

where g next to the MPO indicates which group element it represents. We refer to the dimension of the horizontal indices as the *bond dimension* of the MPO. The on-site case corresponds to bond dimension 1, whilst arbitrary bond dimension allows representation of any unitary. We consider the case of a constant bond dimension in the length of the MPO.

To form a representation, the MPOs must obey

$$\begin{array}{c} \text{---} \text{---} \text{---} \text{---} \text{---} \text{---} \\ | \quad | \quad | \quad | \quad | \\ \text{---} \text{---} \text{---} \text{---} \text{---} \end{array} h \quad \begin{array}{c} \text{---} \text{---} \text{---} \text{---} \text{---} \text{---} \\ | \quad | \quad | \quad | \quad | \\ \text{---} \text{---} \text{---} \text{---} \text{---} \end{array} g = \begin{array}{c} \text{---} \text{---} \text{---} \text{---} \text{---} \text{---} \\ | \quad | \quad | \quad | \quad | \\ \text{---} \text{---} \text{---} \text{---} \text{---} \end{array} gh, \quad (4.2)$$

for all lengths. In contrast to on-site representations, for bond dimensions larger than one this does not hold at the level of the local tensors. Rather there is a tensor $X(g, h)$, referred to as the *reduction tensor* [4.23, 4.42, 4.44] (Appendix 4.B) such that

$$\begin{array}{c} \text{---} \text{---} \\ | \quad | \\ \text{---} \text{---} \end{array} h \quad \begin{array}{c} \text{---} \text{---} \\ | \quad | \\ \text{---} \text{---} \end{array} g = \begin{array}{c} \text{---} \text{---} \\ | \quad | \\ \text{---} \text{---} \end{array} gh. \quad (4.3)$$

The reduction procedure need not be associative. When reducing three tensors, there are two distinct orders of reduction which may differ by a phase ϕ

$$\begin{array}{c} \text{---} \text{---} \\ | \quad | \\ \text{---} \text{---} \end{array} h \quad \begin{array}{c} \text{---} \text{---} \\ | \quad | \\ \text{---} \text{---} \end{array} g \quad \begin{array}{c} \text{---} \text{---} \\ | \quad | \\ \text{---} \text{---} \end{array} f = \phi(f, g, h) \begin{array}{c} \text{---} \text{---} \\ | \quad | \\ \text{---} \text{---} \end{array} fg \quad \begin{array}{c} \text{---} \text{---} \\ | \quad | \\ \text{---} \text{---} \end{array} h. \quad (4.4)$$

As discussed in Appendix 4.B, ϕ is a 3-cocycle with $[\phi] \in \mathcal{H}^3(\mathcal{G}, \text{U}(1))$. Since on-site representations are locally associative they have a trivial cocycle. Hence a nontrivial $[\phi]$ indicates an obstruction to making the symmetry action on-site. We can therefore regard a nontrivial $[\phi]$ as a nontrivial 't Hooft anomaly for \mathcal{G} in (1 + 1)D. We remark that each class of 't Hooft anomaly can be realized using MPOs in this way [4.26, 4.53].

4.1.2 MERA and symmetry

In its most general form [4.61, 4.62], the MERA can be thought of as a series of locality preserving isometric maps

$$\mathcal{L}_{(i)} : \left(\mathbb{C}^{d_{i+1}} \right)^{\otimes N_{i+1}} \rightarrow \left(\mathbb{C}^{d_i} \right)^{\otimes N_i}, \quad (4.5)$$

where $d_{i+1}^{N_{i+1}} \leq d_i^{N_i}$. Since the size of the lattice decreases at each step, these maps can be thought of as enacting a renormalization group on the real-space lattice. At the base (layer 0), the high energy, short-wavelength, lattice scale Hamiltonian $H^{(0)}$ is defined, with subsequent layers defining increasingly low-energy, long-wavelength effective theories

$$H^{(i+1)} := \mathcal{L}_{(i)}^\dagger H^{(i)} \mathcal{L}_{(i)}. \quad (4.6)$$

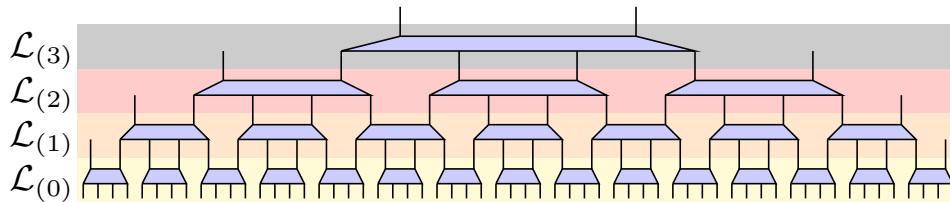


Figure 4.1: The MERA represents a quantum state using layers of isometric tensors. Together, these tensors define a quantum circuit of logarithmic depth which can be used to prepare an entangled state from a product state. If the tensors are chosen appropriately, the network is thought to be able to accurately represent the ground state of gapless one-dimensional Hamiltonians. Throughout the paper we use a convention such that tensor network diagrams read bottom-to-top correspond to matrix multiplication read left-to-right.

To correctly describe the physical RG fixed points, the MERA layers must be chosen to preserve the low-energy physics of $H^{(0)}$.

For concreteness, in this discussion we specialize to the MERA depicted in Fig. 4.1, which we refer to as the 4:2 MERA. This MERA is built from a single kind of tensor, an isometry from 4 sites to 2 sites. In general, these tensors may all contain distinct coefficients, although space-time symmetries such as scale invariance can be imposed by, for example, forcing the tensors on each layer to be identical. We remark that our results are not specific to this choice, rather they work for all MERA schemes. In particular, in Appendix 4.C, we describe how the results apply to the commonly used ternary MERA [4.62, 4.63].

In the MERA the fundamental constraint that a symmetry is preserved under renormalization is that each coarse-graining circuit acts as an intertwiner of \mathcal{G} representations. That is, the renormalized symmetry

$$U_g^{(i+1)} := \mathcal{L}_{(i)}^\dagger U_g^{(i)} \mathcal{L}_{(i)}, \quad (4.7)$$

is again a representation of \mathcal{G} . When this condition is satisfied the third cohomology anomaly label of the symmetry does not change along the renormalization group flow [4.28, 4.31]. Hence the presence of an anomaly does not introduce any additional constraints on the renormalization process (which is to be expected for a discrete group).

For both practical and physically motivated reasons it is common to require further restrictions on the form of a symmetry throughout renormalization. For example, at a scale invariant renormalization group fixed point, the symmetry is also required to be scale invariant [4.63]. Furthermore, along an RG flow one may require that the bond dimension of an MPO symmetry remain constant, or grow subexponentially with the renormalization step. An extreme case is that of an on-site symmetry where the bond dimension is always required to be one, such that the symmetry remains strictly on-site.

4.1.3 On-site symmetry

In the case of a trivial 't Hooft anomaly, a physical symmetry can be realized by an on-site representation. For a MERA satisfying Eqn. 4.7, the 't Hooft anomaly is preserved and hence it should remain possible to realize the symmetry in an on-site fashion at each RG step. This additional constraint is imposed by insisting that $U_g^{(i+1)}$ remains an on-site representation. Therefore the symmetry constraint becomes completely local [4.59].

The symmetry can then be enforced on a MERA state by ensuring that the local tensors are

in Eqn. 4.9. We demonstrate such an action in Section 4.4.3. One can also use the MPO to create a domain wall between the two critical theories by applying the MPO to a half-infinite chain. In the case where the dual theories coincide (i.e. the MPO acts as a symmetry) this corresponds to a symmetry twist (topological defect) or twisted boundary condition. This will be the subject of Section 4.2.

4.1.5 Physical data from MERA

Once a MERA has been obtained, a variety of physical data can be extracted. The most straightforward of these is the energy of the MERA, which simply requires evaluation of $\langle \psi | H | \psi \rangle$.

For a MERA representing the ground state of a gapless Hamiltonian, one can also extract a variety of data about the associated conformal field theory (CFT) [4.64, 4.65]. One can compute the central charge as discussed in Refs. 4.63, 4.75 using the scaling of entanglement entropy in the state. One can also obtain the scaling dimensions of the associated CFT [4.63, 4.75] by seeking eigenoperators of the scaling superoperator

$$\mathcal{S}_1(\text{MPO}) = \text{Diagram} = \lambda \text{MPO} . \quad (4.10)$$

The scaling dimensions describe the decay of correlations in the theory. We will refer to $\Delta = -\log_2(\lambda)$ as the *scaling dimension* corresponding to a particular *scaling field*.

The scaling fields obtained from the scaling superoperator correspond to local fields in the CFT. Given a symmetric MERA, one can also obtain nonlocal scaling fields by constructing the ‘symmetry twisted’ scaling superoperators

$$\mathcal{S}_g(\text{MPO} \circledast) = \text{Diagram} = \lambda \text{MPO} \circledast , \quad (4.11)$$

where \circledast is the symmetry MPO for the group element g . These fields correspond to a half infinite symmetry twist, as in Fig. 4.2, terminated by a local tensor. Previously, nonlocal scaling operators with a tensor product structure have been obtained in the same way [4.76], but this more general class involving an anomalous symmetry was not investigated.

4.2 Symmetry twists and topological sectors

Once a symmetric MERA is optimized to represent the ground state of a critical model, conformal data can be obtained as discussed in Section 4.1.5. In this section, we investigate the impact that an anomalous symmetry has on such conformal data. In particular, we use the properties of MPO group representations to obtain possible topological corrections to the conformal spins when a symmetry twist is applied. We observe these corrections in our example model, as shown in Table 4.1. Additionally, we construct the projective representations under which the nonlocal scaling fields (as defined in Eqn. 4.11) transform. These allow us to construct projectors onto irreducible topological sectors, extending the usual decomposition into symmetry sectors. We discuss the constraints that this decomposition imposes on the operator product expansion of the CFT. For our example model, we observe these constraints in Table 4.2.

Throughout this section, for simplicity of presentation, we treat the case of scale invariant MERA with scale invariant MPO symmetry. Furthermore, we assume the technical condition that

the MPO representation satisfies the *zipper condition* [4.26]

$$\begin{array}{c} \text{---} \\ | \\ \text{---} \end{array} X_{(g,h)} \begin{array}{c} \text{---} \\ | \\ \text{---} \end{array} X_{(g,h)}^\dagger = \begin{array}{c} \text{---} \\ | \\ \text{---} \end{array} \begin{array}{c} h \\ | \\ g \end{array} \begin{array}{c} \text{---} \\ | \\ \text{---} \end{array}. \quad (4.12)$$

These assumptions imply that the MPOs can be deformed freely through a symmetric MERA network. We remark that representative MPOs satisfying the zipper condition have been given for all anomalous discrete symmetries in $(1+1)\text{D}$ [4.26]. Additionally, we have suppressed possible orientation dependencies of the MPOs, although this effect is accounted for in our results. For a full treatment of the intricacies that arise due to orientation dependence see Ref. 4.26. We note that similar reasoning applies to MPOs not satisfying these simplifying assumptions.

4.2.1 Symmetry twist and topological correction to conformal spin

For a model described by symmetric Hamiltonian H , a symmetry twist can be created by acting with an element of the group on a half-infinite chain. Hamiltonian terms far away from the end of the twist are left invariant and the only remnant is a single twisted Hamiltonian term crossing the end. This is captured by the MERA in Fig. 4.2 with uniform tensors.

The twisted Hamiltonian term can be used to close a chain into a ring of length L . In the case of a trivial (identity) twist this yields periodic boundary conditions. For a nontrivial group element this corresponds to a flux insertion through the ring as there is now a nontrivial monodromy around the ring given by the group element.

The introduction of an MPO twist by group element g leads to a twisted translation operator

$$\tau_g = \cdots \text{---} \text{---} \text{---} \begin{array}{c} | \\ g \end{array} \text{---} \text{---} \text{---} \cdots, \quad (4.13)$$

which translates the system by one site without moving the end of the twist (previously noted in Refs. 4.77, 4.78). We will see that this leads to corrections to the conformal spin.

The untwisted translation operator for periodic boundary conditions satisfies $\tau_1^L = \mathbb{1}$ which implies that local fields have integer conformal spin [4.79]. The twisted translation operator satisfies $\tau_g^L = T_g$ where

$$T_g = \cdots \begin{array}{c} | \\ g \end{array} \begin{array}{c} | \\ g \end{array} \begin{array}{c} | \\ g \end{array} \text{---} \begin{array}{c} | \\ g \end{array} \begin{array}{c} | \\ g \end{array} \begin{array}{c} | \\ g \end{array} \cdots \quad (4.14)$$

is the Dehn twist operator. For a faithful on-site representation of g the order of T_g is simply the order of g , denoted n_g . Hence the conformal spins of g -twisted fields may have a topological correction leading them to take values [4.79] in $\frac{1}{n_g}\mathbb{Z}$.

We now consider anomalous representations and show that the order of T_g is $2n_g$ in some cases, reflecting a further correction due to the anomaly. We observe this additional correction in our numerical example, as shown in Table 4.1.

First we define

$$M_h^{(g)} = \begin{array}{c} \text{---} \\ | \\ \text{---} \end{array} \begin{array}{c} X(h,g) \\ | \\ X(g,h)^\dagger \end{array} \begin{array}{c} \text{---} \\ | \\ \text{---} \end{array}, \quad (4.15)$$

which corresponds to the action of h on the g twisted MERA shown in Fig. 4.2. It was shown in Ref. 4.26 that

$$T_g M_h^{(g)} = \phi(g, h, g) M_{gh}^{(g)}, \quad (4.16)$$

where ϕ is the 3-cocycle of the MPO representation. Applying the Dehn twist n_g times results in a phase

$$T_g^{n_g} M_1^{(g)} = \prod_{i=1}^{n_g-1} \phi(g, g^i, g) M_1^{(g)}, \quad (4.17)$$

where again n_g denotes the order of g . Since g generates a subgroup $\mathbb{Z}_{n_g} \leq \mathcal{G}$ and

$$\phi_g(i, j, k) := \phi(g^i, g^j, g^k) \quad (4.18)$$

defines a 3-cocycle of \mathbb{Z}_{n_g} . Denote the relevant cohomology class by $[\phi_g] \in \mathcal{H}^3(\mathbb{Z}_{n_g}, \mathbf{U}(1)) \cong \mathbb{Z}_{n_g}$. For simplicity, assume it has been brought into the normal form [4.80]

$$\phi_g(i, j, k) = \omega^{[\phi_g]i(j+k-j \oplus k)/n_g}, \quad (4.19)$$

where ω is a primitive n_g^{th} root of unity and \oplus denotes addition modulo n_g . Hence

$$\prod_{i=1}^{n_g-1} \phi(g, g^i, g) = \omega^{[\phi_g]} \quad (4.20)$$

and

$$T_g^{n_g} = \omega^{[\phi_g]} \mathbb{1}. \quad (4.21)$$

Consequently an anomaly $[\phi]$ for g -twisted fields may induce a further topological correction to their conformal spins. In particular, the correction to the conformal spins take values in

$$\frac{1}{n_g} \mathbb{Z}_{n_g} + \frac{[\phi_g]}{n_g^2}. \quad (4.22)$$

To make this argument we fixed a particular representative of ϕ , however the topological correction to conformal spin is a gauge invariant quantity and should not depend on this choice.

For the case of $\mathcal{G} = \mathbb{Z}_2^3$, we observe this anomalous correction in our numerical example, where we see quarter- and three-quarter- integer conformal spins (displayed in Table 4.1).

4.2.2 Projective representations and topological sectors

We proceed to construct topological sectors that have a definite topological correction to the conformal spin. These topological sectors are an extension of the usual symmetry sectors used to block diagonalize a Hamiltonian.

Topological sectors are labeled by a conjugacy class $\mathcal{C} \subset \mathcal{G}$, indicating twist symmetry twist, and a (projective) irreducible representation (irrep.) χ_g^μ of the centralizer of a representative element $g \in \mathcal{C}$. The topological sectors are mathematically described by $D^\phi(\mathcal{G})$, the quantum double of the symmetry group \mathcal{G} twisted by the 3-cocycle anomaly ϕ . This category determines all topological properties of the sectors.

Since the MPO symmetry commutes with the MERA tensors, one can simultaneously diagonalize the twisted scaling superoperator $\mathcal{S}_g(\cdot)$ and the action of the symmetry. The vector space spanned by g -twisted scaling fields (see Eqn. 4.11) transforms under a projective representation $V_h^{(g)}$ of the centralizer \mathcal{Z}_g . This projective representation has 2-cocycle $\phi^{(g)}$ defined by

$$\phi^{(g)}(h, k) = \frac{\phi(g, h, k)\phi(h, k, g)}{\phi(h, g, k)}, \quad (4.23)$$

which is the slant product of ϕ . The action is explicitly given by [4.26]

$$V_h^{(g)} = \begin{array}{c} X(h, h^{-1}gh) \\ \downarrow \\ \text{---} \circ \text{---} \\ \uparrow \\ X(g, h)^\dagger \end{array} \quad , \quad (4.24)$$

where $h^{-1}gh = g$ for $h \in \mathcal{Z}_g$.

The g -twisted scaling superoperator commutes with the projective representation

$$\mathcal{S}_g(V_h^{(g)}(\cdot)) = V_h^{(g)}(\mathcal{S}_g(\cdot)), \quad (4.25)$$

and hence can be block diagonalized into projective irreps.

Topological sectors that contribute a definite correction to the conformal spin can be constructed following the approach of Ref. 4.55. The first step is to form projectors $|g, \mu\rangle\langle g, \mu|$ onto the projective irreps of \mathcal{Z}_g . For a twist g and projective irrep μ with 2-cocycle $\phi^{(g)}$

$$|g, \mu\rangle\langle g, \mu| := \frac{d_\mu}{|\mathcal{Z}_g|} \sum_{h \in \mathcal{Z}_g} \bar{\chi}_g^\mu(h) V_h^{(g)}, \quad (4.26)$$

where d_μ its dimension, χ_g^μ its character and $\bar{\cdot}$ denotes complex conjugation.

The full scaling superoperator, taking into account all sectors, is given by

$$\mathcal{S}_{\mathcal{G}}(\cdot) := \bigoplus_g \mathcal{S}_g(\cdot). \quad (4.27)$$

This commutes with the full $|\mathcal{G}|^2$ dimensional algebra spanned by $V_h^{(g)}$ (note $V_l^{(k)} V_h^{(g)} = 0$ unless $k = h^{-1}gh$). This is a C^* algebra [4.55] and can be diagonalized into blocks. The simple central idempotents that project onto each irreducible block are given by

$$|\mathcal{C}_g, \mu\rangle\langle \mathcal{C}_g, \mu| := \sum_{k \in \mathcal{C}_g} |k, \mu\rangle\langle k, \mu|, \quad (4.28)$$

where \mathcal{C}_g is the conjugacy class of g in \mathcal{G} . These projectors block diagonalize $\mathcal{S}_{\mathcal{G}}(\cdot)$ into irreducible topological sectors. For the numerical example in Appendix 4.A, all conformal data is decomposed into these sectors.

The topological sectors thus constructed have definite topological spin [4.55] (correction to conformal spin), which we observe in our example in Table 4.1. Additionally, these sectors obey a set of fusion rules, and support a notion of braiding monodromy and exchange statistics. The full set of topological data can be extracted from the idempotents constructed in Eqn. 4.28 via the procedure outlined in Ref. 4.55.

In the MERA, with an MPO symmetry, the operator product expansion (OPE) [4.64, 4.65] for scaling fields a and b in topological sectors labeled (\mathcal{C}_0, μ_0) and (\mathcal{C}_1, μ_1) can be computed using [4.63, 4.76]

$$a \times b = \sum_{\substack{g \in \mathcal{C}_0 \\ h \in \mathcal{C}_1}} X(g, h)^\dagger \begin{array}{c} \text{---} \text{---} \\ \text{---} \text{---} \\ \text{---} \text{---} \\ \text{---} \text{---} \\ \text{---} \text{---} \end{array} = \sum_c C_{ab}^c, \quad (4.29)$$

where the sum is over scaling fields c . Eqn. 4.29 is a tensor network realization of a pair of pants topology with a and b at the feet and c at the waist. The fusion rules imply topological restrictions on the OPE of scaling fields, generalizing symmetry constraints on the local fields. In particular, $C_{ab}^c = 0$ unless the sector labeling c appears in the fusion product

$$(\mathcal{C}_0, \mu_0) \times (\mathcal{C}_1, \mu_1) = \sum_{(\mathcal{C}_2, \mu_2)} N_{(\mathcal{C}_0, \mu_0)(\mathcal{C}_1, \mu_1)}^{(\mathcal{C}_2, \mu_2)} (\mathcal{C}_2, \mu_2). \quad (4.30)$$

We observe the constraints directly in the numerical MERA in Table 4.2.

Technically the symmetry twists and their fusion structure are described by the unitary fusion category (UFC) $\text{Vec}_{\mathcal{G}}^{\phi}$ while the topological sectors are given by its Drinfeld center $Z(\text{Vec}_{\mathcal{G}}^{\phi})$ — equivalently the twisted quantum double $D^{\phi}(\mathcal{G})$ — which is a modular tensor category (MTC) [4.81–4.86]. The mathematical structure of this MTC determines all topological properties of the fields in each sector, including the topological correction to their conformal spin (equivalently the exchange statistics), topological restriction on the OPE and monodromies (braiding) [4.87–4.91].

Interestingly the fusion rules for the topological sectors can be nonabelian, even when the symmetry group is abelian. This requires a nontrivial anomaly ϕ . This occurs in our numerical example as discussed in Section 4.4 and Table 4.2.

4.3 A class of MPO symmetric MERA

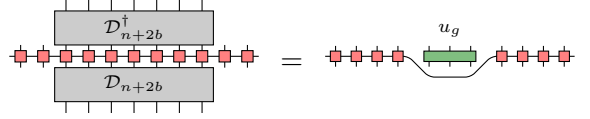
To enforce a constraint on a MERA state requires an identification of the remaining variational parameters in such a way that it is possible to optimize over them. In this section we describe an approach that relies on a property of the MPO symmetry: the existence of a local unitary capable of disentangling a contiguous region of each MPO into an inner part that forms a local representation of the symmetry and is decoupled from the original MPO on the outer section. Given such a local representation, conventional techniques can be used to ensure the MERA is symmetric. We construct a large class of MPOs with this property and find the resulting constraints on the form of symmetric MERA tensors.

4.3.1 Disentangling an MPO

For scale invariant MERA, where the MPO symmetry is required to be identical at all layers, the goal is to identify a family of MERA circuits which locally coarse grains each MPO to itself. If the MPOs form an on-site symmetry, standard techniques of representation theory allow this to be achieved. For MPOs with bond dimension greater than one it is unclear how to apply these techniques. Our approach involves disentangling a local piece out of each MPO. We can then use representation theory to coarse grain this piece, allowing us to identify the desired family of MERA circuits.

This approach may seem counter-intuitive since no local constant depth circuit is capable of disentangling an MPO representation with a nontrivial third cohomology label into an on-site representation. This does not rule out the possibility of disentangling a contiguous region without decoupling the tensors in its complement. More precisely, there may exist constants $b, k \in \mathbb{N}$ such that for all $n \in k\mathbb{N}$ (where k accounts for possible blocking of sites), and MPOs of arbitrary length N , sufficiently larger than n , there exists some unitary \mathcal{D}_{n+2b} acting on $n + 2b$ sites (where b is a

buffer depending on the correlation length of the MPO) such that



$$(4.31)$$

for a local representation $u_g^{(n)}$ acting on n sites.

This leads to a special form for a MERA tensor that coarse grains i sites into j sites, given by



$$(4.32)$$

In this form the MPO symmetry condition in Eqn. 4.9 becomes



$$(4.33)$$

which can be handled using standard techniques from representation theory.

4.3.2 A class of anomalous \mathbb{Z}_N^3 MPO symmetries

We now define a class of anomalous symmetries for the groups \mathbb{Z}_N^3 . These symmetries exemplify the role played by an anomalous symmetry both at the boundary of a two dimensional SPT phase and as a duality of distinct one dimensional SPT phases [4.92–4.95]. They occur as the boundary symmetry actions of \mathbb{Z}_N^3 SPTs labeled by a type-III anomaly in two spatial dimensions [4.80]. In addition, they can be seen to act transitively on the set of one dimensional SPT phases with \mathbb{Z}_N^2 symmetry. This particular example is an instance of a more general relation between a two dimensional $\mathcal{G} \times \mathcal{H}^2(\mathcal{G}, \text{U}(1))$ SPT and the set of dualities of one dimensional \mathcal{G} SPTs. Further details about the specifics of the \mathbb{Z}_N^3 models, including a fixed point bulk model, bulk to boundary mapping and boundary Hamiltonian, as well as the more general case are contained in Appendix 4.D.

We consider a spin chain with a pair of N -dimensional spins at each site. For this discussion, we label the first spin in red and the second in blue. Let $\omega = \exp(2i\pi/N)$ and define the generalized Pauli operators via $ZX = \omega XZ$. Below we work in the basis where Z is the diagonal clock matrix and X is the shift matrix. We define the generalized controlled X and Z operators as

$$\leftarrow \oplus = \left(\leftarrow \oplus \right)^\dagger = \frac{1}{N} \sum_{i,j=0}^{N-1} \omega^{ij} Z^i X^j \quad (4.34a)$$

$$\leftarrow \rightarrow = \left(\leftarrow \rightarrow \right)^\dagger = \frac{1}{N} \sum_{i,j=0}^{N-1} \omega^{ij} Z^i Z^j \quad (4.34b)$$

respectively.

Using the notation $(\alpha_1, \alpha_2, \alpha_3)$ for an element of \mathbb{Z}_N^3 , the group action is defined by the generators

$$(1, 0, 0) \rightarrow \bigotimes_j X_j^{(1)} \quad (4.35a)$$

$$(0, 1, 0) \rightarrow \bigotimes_j X_j^{(2)} \quad (4.35b)$$

$$(0, 0, 1) \rightarrow \mathcal{C}, \quad (4.35c)$$

where \mathcal{C} is defined by the (periodic) circuit

$$\mathcal{C} = \begin{array}{c} \begin{array}{cccc} \uparrow \downarrow & \uparrow \downarrow & \uparrow \downarrow & \uparrow \downarrow \\ \downarrow \uparrow & \downarrow \uparrow & \downarrow \uparrow & \downarrow \uparrow \\ \hline \text{site} \end{array} \end{array}. \quad (4.36)$$

The symmetry operators can be realized using a translationally invariant MPO with on-site tensor defined by

$$\begin{array}{c} i + \alpha_1 \quad j + \alpha_2 \\ \begin{array}{|c|} \hline (\alpha_1, \alpha_2, \alpha_3) \\ \hline \end{array} \\ i \quad j \end{array} = \sum_{k=0}^{N-1} \omega^{j\alpha_3(k-i)} |i\rangle\langle k|, \quad (4.37)$$

with all other elements being zero. The reduction tensor (defined in Appendix 4.B) associated to these MPOs is given by

$$\begin{array}{|c|} \hline X(\alpha, \beta) \\ \hline \end{array} = \sum_{x=0}^{N-1} \omega^{-x\alpha_2\beta_3} \begin{array}{|c|} \hline x + \alpha_1 \\ \hline x \end{array} \langle x|. \quad (4.38)$$

From this, one can verify that this MPO representation has cocycle $\phi(\alpha, \beta, \gamma) = \omega^{\alpha_1\beta_2\gamma_3}$ which is a representative of the root ‘type-III’ anomaly [4.80].

4.3.3 Symmetric MERA tensors

The disentangling circuit, as defined in Eqn. 4.31, for this representation is given by

$$\mathcal{D}_{2K} = \prod_{j=1}^{K-1} CX_{1,2j+1} CX_{2K,2j}, \quad (4.39)$$

and the residual local symmetry is given by

$$u_{(\alpha_1, \alpha_2, \alpha_3)}^{(2K-2)} = \left(\prod_{j=1}^{K-1} CZ_{2j,2j+1} \prod_{j=2}^{K-1} CZ_{2j-1,2j}^\dagger \right)^{\alpha_3}. \quad (4.40)$$

For further details see Appendix 4.C. This leads to the ansatz for MERA tensors

$$\begin{array}{c} \text{blue trapezoid} \\ \uparrow \uparrow \uparrow \uparrow \end{array} = \begin{array}{c} \text{red triangle} \\ \uparrow \uparrow \uparrow \uparrow \\ \downarrow \downarrow \downarrow \downarrow \end{array}, \quad (4.41)$$

which allows the symmetry to be enforced by a local condition on each tensor.

The symmetry can then be enforced by ensuring the residual tensors obey the local conditions

$$\begin{array}{c} \text{red triangle} \\ \uparrow \uparrow \end{array} = \begin{array}{c} \text{red triangle} \\ \uparrow \uparrow \end{array}, \quad (4.42)$$

which can be achieved using standard techniques of representation theory. We remark that the on-site \mathbb{Z}_N^2 symmetry is automatically enforced, without any further constraints.

Since the action can be applied locally, this ansatz class can also be used to investigate how the group acts on numerically optimized states which have not been constrained to be invariant. This allows investigation of theories which are dual under anomalous group actions.

The constraint in Eqn. 4.41 was used in an exact renormalization scheme introduced in Ref. 4.96 for the case of a $\mathbb{Z}_2 \times \mathbb{Z}_2$ symmetry [4.97]. The form of the information transmitted to the next scale of renormalization is extremely restricted in this case. By considering more spins per site we find a less restrictive ansatz, described in Appendix 4.C, capable of attaining accurate results as demonstrated in Section 4.4. The scheme described in Ref. 4.96 does not see similar improvement at larger blocking on a model which is unitarily equivalent to the one considered here [4.97]. After blocking at least two spins per site, our ansatz cannot be captured by the approach of Ref. 4.96.

Analogous circuits exist for all MERA such that the number of ingoing/outgoing N -dimensional indices is even. This leads to a family of symmetric MERA with increasing bond dimension and a larger number of variational parameters. Eqn. 4.41 can also be generalized to other MERA schemes, such as the ternary MERA as discussed in Appendix 4.C.

4.4 Example: A \mathbb{Z}_2^3 symmetric model

In this section we focus on the $N = 2$ case of the ansatz described in the previous section. We consider a particular Hamiltonian which transforms under the type-III anomalous \mathbb{Z}_2^3 group action. This Hamiltonian has three critical lines, one is symmetric and the other two are dual under the group action. We numerically optimize over the ansatz class presented in the previous section along these three lines. We present resulting conformal data for the local fields along each line, and for two nontrivial topological sectors along the symmetric line. Furthermore, we numerically implement the duality on the remaining pair of lines. Finally, we demonstrate that the symmetric line is a gapless phase protected by the anomalous symmetry and translation.

For a MERA with bond dimension 8 corresponding to three qubits per site, the ansatz for the tensors is

$$(4.43)$$

with symmetry constraint

$$(4.44)$$

This tensor contains all degrees of freedom which are not fixed by the symmetry, so can be optimized over.

4.4.1 Family of Hamiltonians

The Hamiltonian we study is

$$H = -a \sum (X_j^{(1)} + X_j^{(2)}) - b \sum (Z_j^{(1)} Z_{j+1}^{(1)} + Z_j^{(2)} Z_{j+1}^{(2)}) - c \sum (Z_j^{(1)} X_j^{(2)} Z_{j+1}^{(1)} + Z_j^{(2)} X_j^{(1)} Z_{j+1}^{(2)}), \quad (4.45)$$

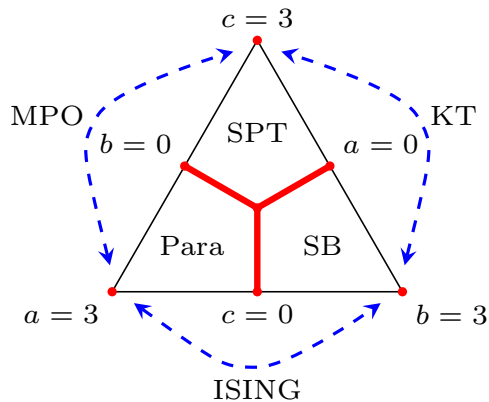


Figure 4.3: Phase diagram of the abc model where $a + b + c = 3$. SB=Symmetry breaking, ferromagnetic phase. SPT= $\mathbb{Z}_2 \times \mathbb{Z}_2$ symmetry protected topological phase. Para=Paramagnetic/disordered phase. RG fixed points are indicated in red, and the dashed blue lines indicate the unitary mappings between the phases. ISING=Ising duality map, KT=(Generalized) Kennedy-Tasaki transformation [4.98, 4.99], MPO=action of $(1,1,1)$ defined in Eqn. 4.35.

for positive values of (a, b, c) . Here $X_j^{(1)}(Z_j^{(1)})$ and $X_j^{(2)}(Z_j^{(2)})$ are the qubit Pauli operators action on the first and second qubit on site j . This model, which we refer to as the *abc model*, has a rich phase diagram as depicted in Fig. 4.3, possessing fully symmetric disordered and SPT phases, in addition to a fully symmetry breaking phase. For all values of (a, b, c) , this Hamiltonian has an on-site $\mathbb{Z}_2 \times \mathbb{Z}_2$ symmetry corresponding to Eqn. 4.35a and Eqn. 4.35b, whilst the anomalous action exchanges the terms with strength a and c , so is only a symmetry when $a = c$. The SPT phase is protected by the on-site symmetry.

We note that unitarily equivalent models have previously been studied [4.100–4.105]. The critical lines in this model can all be exchanged by (nonlocal) unitary transformations, so all are known to be described by a conformal field theory (CFT) with central charge 1. Additionally, the ground state energy along each of these lines is known [4.103–4.105].

In Fig. 4.4, we study the model with $a = c$ (referred to as the b line) using a MERA with full anomalous symmetry enforced. For convenience, we allow a single transitional layer followed by a scale invariant portion. This leaves a pair of tensors which completely specify the state. After optimizing these residual degrees of freedom (2×16376 real parameters) within this symmetric manifold, we obtain a good approximation to the ground state for all values of b , as evidenced by the ground state energy in Fig. 4.4a (relative error $\mathcal{O}(10^{-4})$). When the symmetry operator is applied to the state, we see that the state is unchanged (a property which was explicitly enforced). The central charge remains within 4.2% of the analytic value for all values of b , comparable to that found in Ref. 4.105.

4.4.2 Scaling dimensions and topological sectors

From our optimized MERA tensors, we have obtained the scaling dimensions of the associated CFT in each symmetry sector using Eqn. 4.10. The data is shown in Fig. 4.4b. As expected, the scaling dimensions vary continuously with the parameter b .

The local fields are those of the compactified boson CFT at a radius

$$R^2 = \frac{\pi}{2 \cos^{-1}\left(\frac{2b}{b-3}\right)}. \quad (4.46)$$

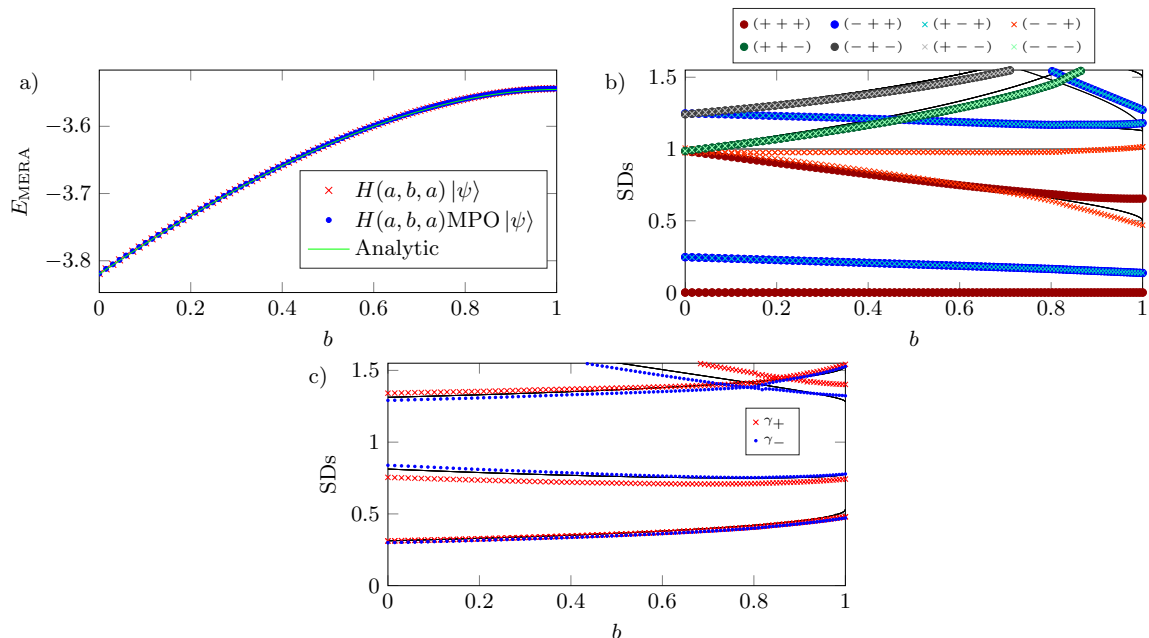


Figure 4.4: MERA data for the abc model along the ‘ b line’. This line is symmetric under the full \mathbb{Z}_2^3 . CFT data, including averaging process, is discussed in more detail in Appendix 4.A.

a) The energy of the optimized MERA state. The state remains a ground state when the anomalous symmetry operator is applied.

b) Scaling dimensions of the associated CFT. These vary continuously with the parameter b . Points are averaged MERA data, whilst black lines correspond to Eqn. 4.47a for integer e and m . Distinct colors/markers indicate under which irrep. the fields transform.

c) Scaling dimensions of nonlocal operators corresponding to applying an anomalous symmetry (for group element $(1, 1, 1)$ defined in Eqn. 4.35) twist to half of the chain. Points are averaged MERA data, whilst black lines correspond to Eqn. 4.47a for $e, m \in \mathbb{Z} + 1/2$. Distinct colors/markers indicate under which projective irrep. the fields transform.

The fields can be labeled by a pair of integers, and have scaling dimension Δ and conformal spin s given by [4.64, 4.65]

$$\Delta_{e,m} = \frac{e^2}{R^2} + \frac{m^2 R^2}{4}, \quad (4.47a)$$

$$s_{e,m} = em, \quad (4.47b)$$

$$e, m \in \mathbb{Z}.$$

Finally, we investigate the effect of $(1, 1, 1)$ symmetry twist in Fig. 4.4c. By applying the symmetry to half of the infinite chain we create the twist, and a set of nonlocal (with respect to the original theory) twisted fields can be obtained [4.76]. These operators correspond to eigenoperators of the ‘symmetry twisted’ scaling superoperator (Eqn. 4.11). Since the symmetry acts projectively on the twisted fields, they can be decomposed into projective irreps corresponding to definite topological sectors. We can then diagonalize $\mathcal{S}_g(\cdot)$ within each sector, allowing us to label the twisted fields by the projective irrep under which they transform.

Again we can compare the numerically calculated twisted scaling dimensions to the analytic results to identify conformal spins of the twisted fields. As displayed in Table 4.1, within each topological sector, all conformal spins receive the same correction.

From the MERA data, we can identify the fields with a $(1, 1, 1)$ twist as carrying scaling dimension and conformal spin given by Eqn. 4.47a and Eqn. 4.47b respectively, but with $e, m \in \mathbb{Z} + \frac{1}{2}$,

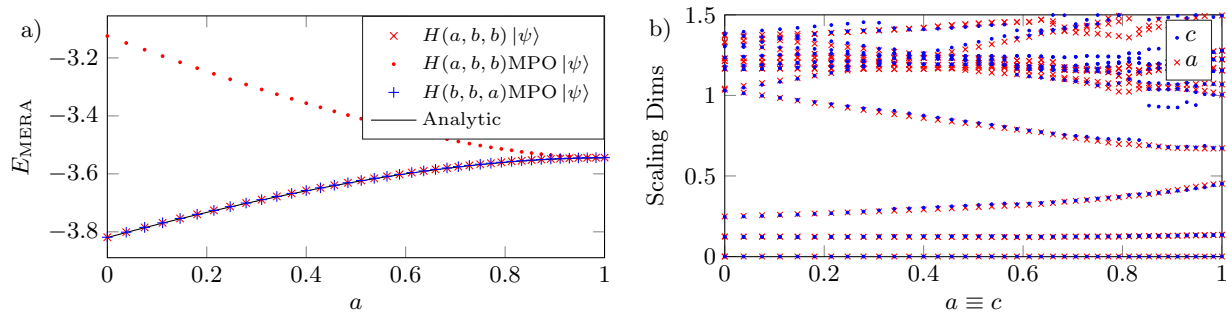


Figure 4.5: MERA data for the abc model along the ‘ a ’ and ‘ c ’ lines. These are exchanged by the symmetry action.

a) Ground state energy of the optimized MERA. By applying the symmetry operator to a state optimized for the Hamiltonian with (a, b, b) , we obtain a state which is the ground state of the Hamiltonian with parameters (b, b, a) . This demonstrates that the states are transforming properly.

b) The local fields in the CFTs describing these two lines are identical, but distinct from those on the ‘ b ’ line.

leading to quarter- and three-quarter- integer spins in this sector.

To examine the effect of the anomalous symmetry on the OPE, we computed fusion rules for the topological sectors using Eqn. 4.29 for a symmetric MERA tensor. Despite the fact that the symmetry group is abelian, we observe nonabelian fusion for all sectors with nontrivial twist. For example, fusion of sectors with twist $(1, 1, 1)$ results in only half of the trivial twist sectors. The full set of fusion rules is given in Table 4.2 (Appendix 4.A).

In this example, the modular tensor category describing the topological sectors is $D^\phi(\mathbb{Z}_2^3)$. This category is known to be equivalent to $D(D_4)$, where D_4 is the symmetry group of a square. The fusion table obtained from MERA matches that of $D^\phi(\mathbb{Z}_2^3) \cong D(D_4)$ [4.80, 4.106–4.109].

The data for all topological sectors is displayed in full in Appendix 4.A.

4.4.3 Duality and domain walls

We have also studied the ‘ a ’ and ‘ c ’ lines which are not symmetric under the anomalous \mathbb{Z}_2 , but are exchanged by its action. We optimize over tensors of the form Eqn. 4.43, but do not enforce the symmetry constraint on the residual degrees of freedom.

The ground state energy obtained after optimization along the $b = c$ line is shown in Fig. 4.5a. If the symmetry MPO corresponding to group element $(1, 1, 1)$ is applied to the optimized state (via local application of Eqn. 4.44), the result is an excited state. If the energy of this state is measured using the Hamiltonian with parameters a and c switched, we see that it is a ground state. This confirms that the state is transforming as expected under the anomalous action, that is, the MPO is acting as a duality transformation of the ‘ a ’ and ‘ c ’ critical lines.

We also show the scaling dimensions of the CFTs corresponding to the two dual lines (Fig. 4.5b). We observe that the local field content is identical, indicating that the same CFT describes these two lines. This CFT is distinct (in its local content) from that describing the ‘ b ’ line, although it still has central charge 1.

4.4.4 An anomaly protected gapless phase

In Ref. 4.23 it was shown that a phase with anomalous MPO symmetry can either be gapped and spontaneously break the symmetry, or be gapless. Furthermore it is known from Refs. 4.18–4.20, 4.110, 4.111 that a topological symmetry, together with translation, can protect a gapless phase.

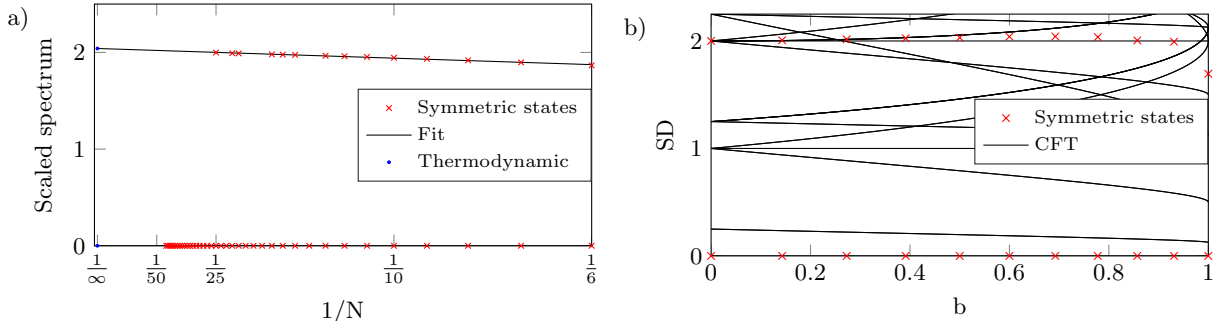


Figure 4.6: Finite size scaling data for the fully symmetric sector of the model.

a) After rescaling the spectrum so that the lowest excitation is consistent with the lowest nontrivial primary of the CFT, the fully symmetric states can be extracted. Fitting the data and extrapolating to the thermodynamic limit gives the scaling dimension.

b) For almost the whole ‘ b ’ line, we observe that there are no fully symmetric states with scaling dimension less than 2 (RG relevant). This implies that no local, symmetric, translationally invariant terms can be added to the Hamiltonian to gap it out, thus the gapless phase is protected.

An anomalous MPO symmetry is in fact an example of a topological symmetry. Hence one may suspect that there exist gapless phases protected by such a symmetry.

Here we demonstrate that under an anomalous \mathbb{Z}_2^3 symmetry, along with translations, the gaplessness of the Hamiltonian along the ‘ b ’ line is protected. That is, there are no translation invariant terms which are both symmetric under the full anomalous symmetry and are relevant in the renormalization group sense, and would therefore gap the Hamiltonian.

Since the effect of translations cannot be tested in the MERA framework, we performed a finite size scaling analysis [4.79] to test this. Using the ALPS MPS library [4.112, 4.113], the lowest 40 eigenstates of the Hamiltonian (Eqn. 4.45) along the ‘ b ’ line were obtained. Bond dimensions were capped at 100 and lengths of between 6 and 55 sites (12-110 qubits) were considered. Scaling dimensions are obtained by first normalizing the Hamiltonian such that the ground state has energy 0 and the first excited state has energy corresponding to the smallest nonzero scaling dimension of the CFT [4.114]. The energy levels are then fitted as a function of $1/N$ and extrapolated to $N = \infty$. This is shown in Fig. 4.6a for $b = .6$.

The Hamiltonian and symmetry operators were then simultaneously diagonalized within this subspace. In the fully symmetric sector (all symmetries acting as $+1$), the translation operator was diagonalized, allowing the momentum to be extracted.

Under the combined action of the anomalous symmetry group and translations by a single spin, there are no fully symmetric states with scaling dimension less than 2 (Fig. 4.6b). This implies there are no local symmetric terms which can gap the Hamiltonian, thus the gapless phase is protected. We remark that under the operator which translates by a full site; an RG relevant, fully symmetric state with momentum zero does exist and therefore the Hamiltonian can be gapped by a staggered term. A similar effect was observed in Ref. 4.18.

4.5 Conclusions

We have studied anomalous MPO symmetries in the framework of MERA. Following Ref. 4.28, the third cohomology class of an MPO representation of a finite group was identified with an ‘t Hooft anomaly.

The properties of a fully MPO symmetric MERA were derived, including anomalous symmetry twists and the projective representations they carry. These were used to construct all topological sectors. This construction allows the complete set of topological data to be extracted, including a definite topological correction to the conformal spins of the fields in each sector and topological restrictions on the OPE.

A local condition to enforce the symmetry in the MERA was formulated, which allows for optimization of states with an anomalous symmetry. This ansatz works by locally disentangling the symmetry action, decoupling degrees of freedom on which the action can be expressed locally.

By way of an example, MERA states were optimized for a Hamiltonian with an anomalous \mathbb{Z}_2^3 symmetry. We have obtained accurate energy and conformal data for states optimized over our ansatz class, and demonstrated that the states transform as expected. All topological sectors were constructed and the resultant topological data was extracted. The conformal data was computed within each topological sector, and the projective action of the symmetry on the scaling fields was found. Furthermore, a correction to the conformal spin was identified, and shown to match the topological spin.

We applied the ansatz to study a duality of two critical lines. By extracting conformal data from optimized MERA the local content of the dual CFTs was shown to match. It was demonstrated that the action of the MPO mapped MERA ground-states optimized for Hamiltonians along one line to ground-states of the dual Hamiltonians. This required the ability to apply the MPO in a local fashion, which our ansatz permits.

We performed a finite size scaling analysis of the anomalous \mathbb{Z}_2^3 symmetric line for large system sizes. It was numerically demonstrated that the anomalous MPO symmetry, together with translation, protects a gapless phase.

There are several extensions of this work which suggest themselves. Our restricted MERA ansatz was only constructed for a particular class of anomalous group actions. It would be interesting to extend this to other MPOs, such as: nonabelian group representations with different cocycle anomalies, the Ising duality map or the translation operator.

The most general extension conceivable is to a set of MPOs described by a unitary fusion category [4.55, 4.115, 4.116]. While the construction of topological sectors is known in this general case [4.55, 4.83, 4.84, 4.115–4.119], an ansatz which allows the symmetry to be enforced locally in the MERA remains to be found.

It would be interesting to determine which of these general symmetries protects a gapless phase such as the one observed in this work and those in Refs. 4.18–4.20, 4.110, 4.111.

One could adapt these results to the recent tensor network renormalization (TNR) [4.120–4.123] scheme, constraining the RG flow to remain MPO symmetric. We remark that the Ising duality has previously been studied both numerically, using TNR but without manifestly enforcing the symmetry, in Ref. 4.77 and theoretically in Ref. 4.78.

It would also be interesting to consider the influence of an MPO symmetry on the entanglement entropy. We remark that by considering MPO symmetries of topologically ordered tensor network states in $(2 + 1)$ D one recovers the topological entanglement entropy [4.54, 4.55, 4.124–4.126].

A particularly interesting future direction is to generalize our MPO symmetric MERA ansatz to a $(2 + 1)$ D MERA describing a topologically ordered state that is symmetric under an anomalous PEPO symmetry.

Acknowledgments

The authors thank Dave Aasen, Matthias Bal, Stephen Bartlett, Nick Bultinck, Christopher Chubb, Andrew Doherty, Steve Flammia, Michaël Mariën, Sam Roberts, Thomas Smith, Ryan Thorngren, Frank Verstraete, Guifre Vidal and Juven Wang for useful discussions. DW especially thanks Dave Aasen for pointing out the connection between the tube algebra and topological defects in conformal field theories. JB acknowledges support from the Australian Research Council via the Center of Excellence in Engineered Quantum Systems (EQuS), project number CE110001013. The authors acknowledge the University of Sydney HPC service at The University of Sydney for providing HPC resources. DW acknowledges The University of Sydney quantum theory group for their hospitality, and the Perimeter Institute Visiting Graduate Fellowship program.

Optimal contraction sequences of the networks used in this work were computed using the netcon package of Ref. [4.127](#).

Bibliography

- 4.1 L. P. Kadanoff, Scaling laws for Ising models near T_c , [Physics](#) **2**, 263 (1966).
- 4.2 K. G. Wilson, The renormalization group: Critical phenomena and the Kondo problem, [Reviews of Modern Physics](#) **47**, 773 (1975).
- 4.3 L. D. Landau and E. M. Lifshitz, *Course of theoretical physics* (Pergamon Press, 1965).
- 4.4 F. J. Wegner, Duality in generalized Ising models and phase transitions without local order parameters, [Journal of Mathematical Physics](#) **12**, 2259 (1971).
- 4.5 J. M. Kosterlitz and D. J. Thouless, Ordering, metastability and phase transitions in two-dimensional systems, [Journal of Physics C: Solid State Physics](#) **6**, 1181 (1973).
- 4.6 X.-G. Wen, Vacuum degeneracy of chiral spin states in compactified space, [Physical Review B](#) **40**, 7387 (1989).
- 4.7 T. Einarsson, Fractional statistics on a torus, [Physical Review Letters](#) **64**, 1995 (1990).
- 4.8 X.-G. Wen, Topological Orders in Rigid States, [International Journal of Modern Physics B](#) **04**, 239 (1990).
- 4.9 F. D. M. Haldane, Nonlinear Field Theory of Large-Spin Heisenberg Antiferromagnets: Semiclassically Quantized Solitons of the One-Dimensional Easy-Axis Néel State, [Physical Review Letters](#) **50**, 1153 (1983).
- 4.10 Z.-C. Gu and X.-G. Wen, Tensor-entanglement-filtering renormalization approach and symmetry-protected topological order, [Physical Review B](#) **80**, 155131, [arXiv:0903.1069](#) (2009).
- 4.11 F. Pollmann, A. M. Turner, E. Berg, and M. Oshikawa, Entanglement spectrum of a topological phase in one dimension, [Physical Review B](#) **81**, 064439, [arXiv:0910.1811](#) (2010).
- 4.12 X. Chen, Z.-C. Gu, Z.-X. Liu, and X.-G. Wen, Symmetry protected topological orders and the group cohomology of their symmetry group, [Physical Review B](#) **87**, 155114, [arXiv:1106.4772](#) (2013).

- 4.13 A. Miyake, Quantum Computation on the Edge of a Symmetry-Protected Topological Order, *Physical Review Letters* **105**, 040501, [arXiv:1003.4662](#) (2010).
- 4.14 J. M. Renes, A. Miyake, G. K. Brennen, and S. D. Bartlett, Holonomic quantum computing in symmetry-protected ground states of spin chains, *New Journal of Physics* **15**, 025020, [arXiv:1103.5076](#) (2013).
- 4.15 D. V. Else, I. Schwarz, S. D. Bartlett, and A. C. Doherty, Symmetry-protected phases for measurement-based quantum computation, *Physical Review Letters* **108**, 240505, [arXiv:1201.4877](#) (2012).
- 4.16 D. V. Else, S. D. Bartlett, and A. C. Doherty, Symmetry protection of measurement-based quantum computation in ground states, *New Journal of Physics* **14**, 113016, [arXiv:1207.4805](#) (2012).
- 4.17 D. J. Williamson and S. D. Bartlett, Symmetry-protected adiabatic quantum transistors, *New Journal of Physics* **17**, 053019, [arXiv:1408.3415](#) (2015).
- 4.18 A. Feiguin, S. Trebst, A. W. W. Ludwig, M. Troyer, A. Kitaev, Z. Wang, and M. H. Freedman, Interacting anyons in topological quantum liquids: The golden chain, *Physical Review Letters* **95**, 160409, [arXiv:cond-mat/0612341](#) (2007).
- 4.19 R. N. C. Pfeifer, O. Buerschaper, S. Trebst, A. W. W. Ludwig, M. Troyer, and G. Vidal, Translation invariance, topology, and protection of criticality in chains of interacting anyons, *Physical Review B* **86**, 155111, [arXiv:1005.5486](#) (2012).
- 4.20 C. Gils, E. Ardonne, S. Trebst, D. A. Huse, A. W. W. Ludwig, M. Troyer, and Z. Wang, Anyonic quantum spin chains: Spin-1 generalizations and topological stability, *Physical Review B* **87**, 235120, [arXiv:1303.4290](#) (2013).
- 4.21 R. N. C. Pfeifer, P. Corboz, O. Buerschaper, M. Aguado, M. Troyer, and G. Vidal, Simulation of anyons with tensor network algorithms, *Physical Review B* **82**, 115126, [arXiv:1006.3532](#) (2010).
- 4.22 R. König and E. Bilgin, Anyonic entanglement renormalization, *Physical Review B* **82**, 125118, [arXiv:1006.2478](#) (2010).
- 4.23 X. Chen, Z.-X. Liu, and X.-G. Wen, Two-dimensional symmetry-protected topological orders and their protected gapless edge excitations, *Physical Review B* **84**, 235141, [arXiv:1106.4752](#) (2011).
- 4.24 L. H. Santos and J. Wang, Symmetry-protected many-body Aharonov-Bohm effect, *Physical Review B* **89**, 195122, [arXiv:1310.8291](#) (2014).
- 4.25 J. C. Wang, L. H. Santos, and X.-G. Wen, Bosonic anomalies, induced fractional quantum numbers, and degenerate zero modes: The anomalous edge physics of symmetry-protected topological states, *Physical Review B* **91**, 195134, [arXiv:1403.5256](#) (2015).
- 4.26 D. J. Williamson, N. Bultinck, M. Mariën, M. B. Şahinoğlu, J. Haegeman, and F. Verstraete, Matrix product operators for symmetry-protected topological phases: Gauging and edge theories, *Physical Review B* **94**, 205150, [arXiv:1412.5604](#) (2016).

- 4.27 X.-G. Wen, Classifying gauge anomalies through symmetry-protected trivial orders and classifying gravitational anomalies through topological orders, [Physical Review D](#) **88**, 045013, [arXiv:1303.1803](#) (2013).
- 4.28 A. Kapustin and R. Thorngren, Anomalous Discrete Symmetries in Three Dimensions and Group Cohomology, [Physical Review Letters](#) **112**, 231602, [arXiv:1403.0617](#) (2014).
- 4.29 A. Kapustin, Symmetry protected topological phases, anomalies, and cobordisms: beyond group cohomology, [arXiv:1403.1467](#) (2014).
- 4.30 D. V. Else and C. Nayak, Classifying symmetry-protected topological phases through the anomalous action of the symmetry on the edge, [Physical Review B](#) **90**, 235137, [arXiv:1409.5436](#) (2014).
- 4.31 A. Kapustin and R. Thorngren, Anomalies of discrete symmetries in various dimensions and group cohomology, [arXiv:1404.3230](#) (2014).
- 4.32 J. Wang and X.-G. Wen, A Lattice Non-Perturbative Hamiltonian Construction of 1+ 1D Anomaly-Free Chiral Fermions and Bosons-on the equivalence of the anomaly matching conditions and the boundary fully gapping rules, [arXiv:1307.7480](#) (2013).
- 4.33 G. 't Hooft, Naturalness, chiral symmetry, and spontaneous chiral symmetry breaking, [Recent Developments in Gauge Theories](#) , 135 (1980).
- 4.34 S. C. Furuya and M. Oshikawa, Symmetry Protection of Critical Phases and a Global Anomaly in 1 + 1 Dimensions, [Physical Review Letters](#) **118**, 021601, [arXiv:1503.07292](#) (2017).
- 4.35 F. Verstraete, J. I. Cirac, and V. Murg, Matrix Product States, Projected Entangled Pair States, and variational renormalization group methods for quantum spin systems, [Advances in Physics](#) **57**, 143, [arXiv:0907.2796](#) (2009).
- 4.36 R. Orús, A practical introduction to tensor networks: Matrix product states and projected entangled pair states, [Annals of Physics](#) **349**, 117, [arXiv:1306.2164](#) (2014).
- 4.37 J. C. Bridgeman and C. T. Chubb, Hand-waving and Interpretive Dance: An Introductory Course on Tensor Networks, [Journal of Physics A: Mathematical and Theoretical](#) **50**, 223001, [arXiv:1603.03039](#) (2017).
- 4.38 S. R. White, Density matrix formulation for quantum renormalization groups, [Physical Review Letters](#) **69**, 2863 (1992).
- 4.39 S. Östlund and S. Rommer, Thermodynamic Limit of Density Matrix Renormalization, [Physical Review Letters](#) **75**, 3537, [arXiv:cond-mat/9503107](#) (1995).
- 4.40 J. Dukelsky, M. A. Martín-Delgado, T. Nishino, and G. Sierra, Equivalence of the variational matrix product method and the density matrix renormalization group applied to spin chains, [Europhysics Letters](#) **43**, 457, [arXiv:cond-mat/9710310](#) (1998).
- 4.41 I. Affleck, T. Kennedy, E. H. Lieb, and H. Tasaki, Rigorous results on valence-bond ground states in antiferromagnets, [Physical Review Letters](#) **59**, 799 (1987).
- 4.42 M. Fannes, B. Nachtergaele, and R. F. Werner, Finitely correlated states on quantum spin chains, [Communications in Mathematical Physics](#) **144**, 443 (1992).

- 4.43 A. Klumper, A. Schadschneider, and J. Zittartz, Matrix Product Ground States for One-Dimensional Spin-1 Quantum Antiferromagnets, *Europhysics Letters* **24**, 293, [arXiv:cond-mat/9307028](#) (1993).
- 4.44 D. Pérez-García, F. Verstraete, M. M. Wolf, and J. I. Cirac, Matrix Product State Representations, *Quantum Information & Computation* **7**, 401, [arXiv:quant-ph/0608197](#) (2007).
- 4.45 X. Chen, Z.-C. Gu, and X.-G. Wen, Classification of gapped symmetric phases in one-dimensional spin systems, *Physical Review B* **83**, 035107, [arXiv:1008.3745](#) (2011).
- 4.46 N. Schuch, D. Pérez-García, and I. Cirac, Classifying quantum phases using matrix product states and projected entangled pair states, *Physical Review B* **84**, 165139, [arXiv:1010.3732](#) (2011).
- 4.47 J. Cirac, D. Pérez-García, N. Schuch, and F. Verstraete, Matrix product density operators: Renormalization fixed points and boundary theories, *Annals of Physics* **378**, 100, [arXiv:1606.00608](#) (2017).
- 4.48 T. Nishino, Y. Hieida, K. Okunishi, N. Maeshima, Y. Akutsu, and A. Gendiar, Two-Dimensional Tensor Product Variational Formulation, *Progress of Theoretical Physics* **105**, 409, [arXiv:cond-mat/0011103](#) (2001).
- 4.49 F. Verstraete and J. I. Cirac, Renormalization algorithms for Quantum-Many Body Systems in two and higher dimensions, [arXiv:cond-mat/0407066](#) (2004).
- 4.50 N. Schuch, I. Cirac, and D. Perez-Garcia, PEPS as ground states: Degeneracy and topology, *Annals of Physics* **325**, 2153, [arXiv:1001.3807](#) (2010).
- 4.51 J. Dubail and N. Read, Tensor network trial states for chiral topological phases in two dimensions and a no-go theorem in any dimension, *Physical Review B* **92**, 205307, [arXiv:1307.7726](#) (2015).
- 4.52 T. B. Wahl, H.-H. Tu, N. Schuch, and J. I. Cirac, Projected Entangled-Pair States Can Describe Chiral Topological States, *Physical Review Letters* **111**, 236805, [arXiv:1308.0316](#) (2013).
- 4.53 O. Buerschaper, Twisted injectivity in projected entangled pair states and the classification of quantum phases, *Annals of Physics* **351**, 447, [arXiv:1307.7763](#) (2014).
- 4.54 M. B. Şahinoğlu, D. Williamson, N. Bultinck, M. Mariën, J. Haegeman, N. Schuch, and F. Verstraete, Characterizing topological order with matrix product operators, [arXiv:1409.2150](#) (2014).
- 4.55 N. Bultinck, M. Marin, D. Williamson, M. B. Şahinoğlu, J. Haegeman, and F. Verstraete, Anyons and matrix product operator algebras, *Annals of Physics* **378**, 183, [arXiv:1511.08090](#) (2017).
- 4.56 J. Bridgeman, S. T. Flammia, and D. Poulin, Detecting Topological Order with Ribbon Operators, *Physical Review B* **94**, 205123, [arXiv:1603.02275](#) (2016).
- 4.57 D. J. Williamson, N. Bultinck, J. Haegeman, and F. Verstraete, Fermionic Matrix Product Operators and Topological Phases of Matter, [arXiv:1609.02897](#) (2016).

- 4.58 D. Pérez-García, M. M. Wolf, M. Sanz, F. Verstraete, and J. I. Cirac, String Order and Symmetries in Quantum Spin Lattices, [Physical Review Letters](#) **100**, 167202, [arXiv:0802.0447](#) (2008).
- 4.59 S. Singh, R. Pfeifer, and G. Vidal, Tensor network decompositions in the presence of a global symmetry, [Physical Review A](#) **82**, 050301, [arXiv:0907.2994](#) (2010).
- 4.60 D. Pérez-García, M. Sanz, C. E. González-Guillén, M. M. Wolf, and J. I. Cirac, Characterizing symmetries in a projected entangled pair state, [New Journal of Physics](#) **12**, 025010, [arXiv:0908.1674](#) (2010).
- 4.61 G. Vidal, Entanglement Renormalization, [Physical Review Letters](#) **99**, 220405, [arXiv:cond-mat/0512165](#) (2007).
- 4.62 G. Evenbly and G. Vidal, Algorithms for entanglement renormalization, [Physical Review B](#) **79**, 144108, [arXiv:0707.1454](#) (2009).
- 4.63 R. Pfeifer, G. Evenbly, and G. Vidal, Entanglement renormalization, scale invariance, and quantum criticality, [Physical Review A](#) **79**, 040301, [arXiv:0810.0580](#) (2009).
- 4.64 P. Ginsparg, in *Fields, Strings and Critical Phenomena*, Les Houches 1988, Session XLIX, edited by E. Brézin and J. Z. Justin (North-Holland, Amsterdam, 1990) , [arXiv:hep-th/9108028](#) .
- 4.65 P. Di Francesco, *Conformal field theory* (Springer, New York, 1997).
- 4.66 S. Ryu, J. E. Moore, and A. W. W. Ludwig, Electromagnetic and gravitational responses and anomalies in topological insulators and superconductors, [Physical Review B](#) **85**, 045104, [arXiv:1010.0936](#) (2012).
- 4.67 J. C. Wang, Z.-C. Gu, and X.-G. Wen, Field-Theory Representation of Gauge-Gravity Symmetry-Protected Topological Invariants, Group Cohomology, and Beyond, [Physical Review Letters](#) **114**, 031601, [arXiv:1405.7689](#) (2015).
- 4.68 A. Kapustin and R. Thorngren, Higher symmetry and gapped phases of gauge theories, [arXiv:1309.4721](#) (2013).
- 4.69 D. Gaiotto, A. Kapustin, N. Seiberg, and B. Willett, Generalized global symmetries, [Journal of High Energy Physics](#) **2015**, 172, [arXiv:1412.5148](#) (2015).
- 4.70 R. Thorngren and C. von Keyserlingk, Higher SPT's and a generalization of anomaly in-flow, [arXiv:1511.02929](#) (2015).
- 4.71 J. Wess and B. Zumino, Consequences of anomalous ward identities, [Physics Letters B](#) **37**, 95 (1971).
- 4.72 S. Weinberg, *The quantum theory of fields. Vol. 2: Modern applications* (Cambridge University Press, 2013).
- 4.73 M. Levin and Z.-C. Gu, Braiding statistics approach to symmetry-protected topological phases, [Physical Review B](#) **86**, 115109, [arXiv:1202.3120](#) (2012).

- 4.74 J. Haegeman, K. Van Acoleyen, N. Schuch, J. I. Cirac, and F. Verstraete, Gauging quantum states: from global to local symmetries in many-body systems, [Physical Review X](#) **5**, 011024, [arXiv:1407.1025](#) (2015).
- 4.75 G. Evenbly and G. Vidal, in *Strongly Correlated Systems-Numerical Methods*, Springer Series in Solid-State Sciences, Vol. 176, edited by A. Avella and F. Mancini (Springer, Berlin New York, 2013) pp. 99–130, [arXiv:1109.5334](#) .
- 4.76 G. Evenbly, P. Corboz, and G. Vidal, Nonlocal scaling operators with entanglement renormalization, [Physical Review B](#) **82**, 132411, [arXiv:0912.2166](#) (2010).
- 4.77 M. Hauru, G. Evenbly, W. W. Ho, D. Gaiotto, and G. Vidal, Topological conformal defects with tensor networks, [Physical Review B](#) **94**, 115125, [arXiv:1512.03846](#) (2016).
- 4.78 D. Aasen, R. S. K. Mong, and P. Fendley, Topological Defects on the Lattice I: The Ising model, [Journal of Physics A: Mathematical and Theoretical](#) **49**, 354001, [arXiv:1601.07185](#) (2016).
- 4.79 P. Christe and M. Henkel, *Introduction to Conformal Invariance and Its Applications to Critical Phenomena* (Springer-Verlag, Berlin, 1993), [arXiv:cond-mat/9304035](#) .
- 4.80 M. de Wild Propitius, *Topological interactions in broken gauge theories*, Ph.D. thesis, University of Amsterdam, [arXiv:hep-th/9511195](#) (1995).
- 4.81 V. Drinfeld, Quantum groups, [Proceedings of the International Congress of Mathematicians](#) **1**, 798 (1986).
- 4.82 G. Moore and N. Seiberg, Classical and quantum conformal field theory, [Communications in Mathematical Physics](#) **123**, 177 (1989).
- 4.83 D. Evans and Y. Kawahigashi, On Ocneanu’s theory of asymptotic inclusions for subfactors, topological quantum field theories and quantum doubles, [International Journal of Mathematics](#) **6**, 205 (1995).
- 4.84 M. Muger, From subfactors to categories and topology II: The quantum double of tensor categories and subfactors, [Journal of Pure and Applied Algebra](#) **180**, 159 , [arXiv:math/0111205](#) (2003).
- 4.85 B. Bakalov and A. A. Kirillov, *Lectures on tensor categories and modular functors*, Vol. 21 (American Mathematical Soc., 2001).
- 4.86 P. Etingof, D. Nikshych, and V. Ostrik, On fusion categories, [Annals of Mathematics](#) **162**, 581, [arXiv:math/0203060](#) (2005).
- 4.87 J. Fuchs, I. Runkel, and C. Schweigert, Conformal correlation functions, frobenius algebras and triangulations, [Nuclear Physics B](#) **624**, 452 , [arXiv:hep-th/0110133](#) (2002).
- 4.88 J. Fuchs, I. Runkel, and C. Schweigert, TFT construction of RCFT correlators I: partition functions, [Nuclear Physics B](#) **646**, 353 , [arXiv:hep-th/0204148](#) (2002).
- 4.89 J. Fröhlich, J. Fuchs, I. Runkel, and C. Schweigert, Kramers-wannier duality from conformal defects, [Physical Review Letters](#) **93**, 070601, [arXiv:cond-mat/0404051](#) (2004).

- 4.90 J. Fröhlich, J. Fuchs, I. Runkel, and C. Schweigert, Duality and defects in rational conformal field theory, *Nuclear Physics B* **763**, 354 , [arXiv:hep-th/0607247](#) (2007).
- 4.91 J. Fröhlich, J. Fuchs, I. Runkel, and C. Schweigert, Defect lines, dualities, and generalised orbifolds, [arXiv:0909.5013](#) (2009).
- 4.92 X. Chen, F. Wang, Y.-M. Lu, and D.-H. Lee, Critical theories of phase transition between symmetry protected topological states and their relation to the gapless boundary theories, *Nuclear Physics B* **873**, 248 , [arXiv:1302.3121](#) (2013).
- 4.93 L. Tsui, H.-C. Jiang, Y.-M. Lu, and D.-H. Lee, Quantum phase transitions between a class of symmetry protected topological states, *Nuclear Physics B* **896**, 330 , [arXiv:1503.06794](#) (2015).
- 4.94 L. Tsui, F. Wang, and D.-H. Lee, Topological versus landau-like phase transitions, [arXiv:1511.07460](#) (2015).
- 4.95 L. Tsui, Y.-T. Huang, H.-C. Jiang, and D.-H. Lee, The phase transitions between $Z_n Z_n$ bosonic topological phases in 1+1 D, and a constraint on the central charge for the critical points between bosonic symmetry protected topological phases, *Nuclear Physics B* **919**, 470 , [arXiv:1701.00834](#) (2017).
- 4.96 A. Kubica and B. Yoshida, Precise estimation of critical exponents from real-space renormalization group analysis, [arXiv:1402.0619](#) (2014).
- 4.97 A. O'Brien, S. D. Bartlett, A. C. Doherty, and S. T. Flammia, Symmetry-respecting real-space renormalization for the quantum Ashkin-Teller model, *Physical Review E* **92**, 042163, [arXiv:1507.00038](#) (2015).
- 4.98 T. Kennedy and H. Tasaki, Hidden $\mathbb{Z}_2 \times \mathbb{Z}_2$ symmetry breaking in Haldane-gap antiferromagnets, *Physical Review B* **45**, 304 (1992).
- 4.99 D. V. Else, S. D. Bartlett, and A. C. Doherty, The hidden symmetry-breaking picture of symmetry-protected topological order, *Physical Review B* **88**, 085114, [arXiv:1304.0783](#) (2013).
- 4.100 S.-K. Yang, Modular invariant partition function of the Ashkin-Teller model on the critical line and $N=2$ superconformal invariance, *Nuclear Physics B* **285**, 183 (1987).
- 4.101 M. Baake, G. von Gehlen, and V. Rittenberg, Operator content of the Ashkin-Teller quantum chain-superconformal and Zamolodchikov-Fateev invariance: II. Boundary conditions compatible with the torus, *Journal of Physics A: Mathematical and General* **20**, 6635 (1987).
- 4.102 F. C. Alcaraz, M. Baake, U. Grimm, and V. Rittenberg, Operator content of the XXZ chain, *Journal of Physics A: Mathematical and General* **21**, L117 (1988).
- 4.103 F. C. Alcaraz, M. N. Barber, and M. T. Batchelor, Conformal invariance, the XXZ chain and the operator content of two-dimensional critical systems, *Annals of Physics* **182**, 280 (1988).
- 4.104 J. C. Bridgeman, *Effective Edge States of Symmetry Protected Topological Systems*, [Master's thesis](#), Perimeter Institute (2014).

- 4.105 J. C. Bridgeman, A. O'Brien, S. D. Bartlett, and A. C. Doherty, Multiscale entanglement renormalization ansatz for spin chains with continuously varying criticality, [Physical Review B](#) **91**, 165129, [arXiv:1501.02817](#) (2015).
- 4.106 M. de Wild Propitius, (Spontaneously broken) Abelian Chern-Simons theories, [Nuclear Physics B](#) **489**, 297, [arXiv:hep-th/9606029](#) (1997).
- 4.107 C. Goff, G. Mason, and S.-H. Ng, On the Gauge Equivalence of Twisted Quantum Doubles of Elementary Abelian and Extra-Special 2-Groups, [Journal of Algebra](#) **312**, 849, [arXiv:math/0603191](#) (2007).
- 4.108 J. Wang and X.-G. Wen, Non-Abelian String and Particle Braiding in Topological Order: Modular $SL(3, \mathbb{Z})$ Representation and 3 + 1D Twisted Gauge Theory, [Physical Review B](#) **91**, 035134, [arXiv:1404.7854](#) (2015).
- 4.109 H. He, Y. Zheng, and C. von Keyserlingk, Field theories for gauged symmetry-protected topological phases: Non-Abelian anyons with Abelian gauge group $\mathbb{Z}_2^{\otimes 3}$, [Physical Review B](#) **95**, 035131, [arXiv:1608.05393](#) (2017).
- 4.110 S. Trebst, E. Ardonne, A. Feiguin, D. A. Huse, A. W. W. Ludwig, and M. Troyer, Collective States of Interacting Fibonacci Anyons, [Physical Review Letters](#) **101**, 050401, [arXiv:0801.4602](#) (2008).
- 4.111 C. Gils, S. Trebst, A. Kitaev, A. W. Ludwig, M. Troyer, and Z. Wang, Topology-driven quantum phase transitions in time-reversal-invariant anyonic quantum liquids, [Nature Physics](#) **5**, 834, [arXiv:0906.1579](#) (2009).
- 4.112 B. Bauer, L. D. Carr, H. Evertz, A. Feiguin, J. Freire, S. Fuchs, L. Gamper, J. Gukelberger, E. Gull, S. Guertler, A. Hehn, R. Igarashi, S. Isakov, D. Koop, P. Ma, P. Mates, H. Matsuo, O. Parcollet, G. Pawłowski, J. Picon, L. Pollet, E. Santos, V. Scarola, U. Schollwck, C. Silva, B. Surer, S. Todo, S. Trebst, M. Troyer, M. Wall, P. Werner, and S. Wessel, The ALPS project release 2.0: Open source software for strongly correlated systems, [Journal of Statistical Mechanics: Theory and Experiment](#) **2011**, P05001, [arXiv:1101.2646](#) (2011).
- 4.113 M. Dolfi, B. Bauer, S. Keller, A. Kosenkov, T. Ewart, A. Kantian, T. Giamarchi, and M. Troyer, Matrix Product State applications for the ALPS project, [Computer Physics Communications](#) **185**, 3430, [arXiv:1407.0872](#) (2014).
- 4.114 G. von Gehlen and V. Rittenberg, The Ashkin-Teller quantum chain and conformal invariance, [Journal of Physics A: Mathematical and General](#) **20**, 227 (1987).
- 4.115 D. Aasen *et al.*, in preparation .
- 4.116 M. Buican and A. Gromov, Anyonic Chains, Topological Defects, and Conformal Field Theory, [arXiv:1701.02800](#) (2017).
- 4.117 T. Lan and X.-G. Wen, Topological quasiparticles and the holographic bulk-edge relation in (2+1)-dimensional string-net models, [Physical Review B](#) **90**, 115119, [arXiv:1311.1784](#) (2014).
- 4.118 J. Haah, An invariant of topologically ordered states under local unitary transformations, [Communications in Mathematical Physics](#) **342**, 771, [arXiv:quant-ph/1407.2926](#) (2016).

- 4.119 Y. Hu, N. Geer, and Y.-S. Wu, Full Dyon Excitation Spectrum in Generalized Levin-Wen Models, [arXiv:1502.03433](#) (2015).
- 4.120 G. Evenbly and G. Vidal, Tensor Network Renormalization, *Physical Review Letters* **115**, 180405, [arXiv:1412.0732](#) (2015).
- 4.121 G. Evenbly, Algorithms for tensor network renormalization, *Physical Review B* **95**, 045117, [arXiv:1509.07484](#) (2017).
- 4.122 S. Yang, Z.-C. Gu, and X.-G. Wen, Loop optimization for tensor network renormalization, *Phys. Rev. Lett* **118**, 110504, [arXiv:1512.04938](#) (2017).
- 4.123 M. Bal, M. Mariën, J. Haegeman, and F. Verstraete, Renormalization group flows of Hamiltonians using tensor networks, [arXiv:1703.00365](#) (2017).
- 4.124 S. Flammia, A. Hamma, T. Hughes, and X.-G. Wen, Topological entanglement Renyi entropy and reduced density matrix structure, *Physical Review Letters* **103**, 261601, [arXiv:0909.3305](#) (2009).
- 4.125 A. Kitaev and J. Preskill, Topological Entanglement Entropy, *Physical Review Letters* **96**, 110404, [arXiv:hep-th/0510092](#) (2006).
- 4.126 M. Levin and X.-G. Wen, Detecting Topological Order in a Ground State Wave Function, *Physical Review Letters* **96**, 110405, [arXiv:cond-mat/0510613](#) (2006).
- 4.127 R. N. C. Pfeifer, J. Haegeman, and F. Verstraete, Faster identification of optimal contraction sequences for tensor networks, *Physical Review E* **90**, 033315, [arXiv:1304.6112](#) (2014).

Appendices

4.A Conformal data in all topological sectors

In this appendix, we present the full set of scaling dimensions extracted from the bond dimension 8 MERA with full anomalous symmetry enforced. The data is shown in Fig. 4.7 for the trivial twist, and Fig. 4.8 and Fig. 4.9 for the nontrivial twists. Each subplot in these figures corresponds to a distinct topological sector.

When examining the gray points, one notices a broken degeneracy. This was previously noted in Ref. 4.105. We conjecture that this occurs via coupling of states which, in the field theoretic limit, would be forbidden from coupling due to the full conformal symmetry. As such, we conjecture that the scaling dimensions corresponding to degenerate fields obtained from the MERA experience a splitting $\Delta_{\text{MERA}} = \Delta_{\text{CFT}} \pm \epsilon$, where the size of the splitting ϵ decreases with increased bond dimension as the full conformal symmetry is effectively recovered.

To combat this splitting, we average the MERA scaling dimensions in an attempt to recover the CFT values. When choosing which lines should be averaged together, we have taken all lines of similar gradient and position on the plot. The result of this procedure is indicated in red, and closely matches the CFT values.

The scaling dimensions and conformal spins in each topological sector are given in Table 4.1. Table 4.2 shows the fusion rules for the sectors, computed using the symmetric MERA.

The irreps are given explicitly in Eqn. 4.48. Those below the line are nontrivial projective representations.

$$\chi_{\pm}^1(100) = +1 \quad \chi_{\pm}^1(010) = +1 \quad \chi_{\pm}^1(001) = \pm 1 \quad (4.48a)$$

$$\chi_{\pm}^2(100) = -1 \quad \chi_{\pm}^2(010) = +1 \quad \chi_{\pm}^2(001) = \pm 1 \quad (4.48b)$$

$$\chi_{\pm}^3(100) = +1 \quad \chi_{\pm}^3(010) = -1 \quad \chi_{\pm}^3(001) = \pm 1 \quad (4.48c)$$

$$\chi_{\pm}^4(100) = -1 \quad \chi_{\pm}^4(010) = -1 \quad \chi_{\pm}^4(001) = \pm 1 \quad (4.48d)$$

$$\alpha_{\pm}^1(100) = \pm \mathbb{1} \quad \alpha_{\pm}^1(010) = X \quad \alpha_{\pm}^1(001) = Z \quad (4.48e)$$

$$\alpha_{\pm}^2(100) = Z \quad \alpha_{\pm}^2(010) = \pm \mathbb{1} \quad \alpha_{\pm}^2(001) = X \quad (4.48f)$$

$$\alpha_{\pm}^3(100) = X \quad \alpha_{\pm}^3(010) = Z \quad \alpha_{\pm}^3(001) = \pm \mathbb{1} \quad (4.48g)$$

$$\beta_{\pm}^1(100) = Z \quad \beta_{\pm}^1(010) = X \quad \beta_{\pm}^1(001) = \pm X \quad (4.48h)$$

$$\beta_{\pm}^2(100) = \pm X \quad \beta_{\pm}^2(010) = Z \quad \beta_{\pm}^2(001) = X \quad (4.48i)$$

$$\beta_{\pm}^3(100) = X \quad \beta_{\pm}^3(010) = \pm X \quad \beta_{\pm}^3(001) = Z \quad (4.48j)$$

$$\gamma_{\pm}(100) = \pm X \quad \gamma_{\pm}(010) = \pm Y \quad \gamma_{\pm}(001) = \pm Z \quad (4.48k)$$

Topological Sector		Topological spin	Scaling Dimension	Conformal spin	Parameters		
Twist	Proj. Irrep.						
(000)	χ_+^1	0	$\frac{e^2}{R^2} + \frac{m^2 R^2}{4}$	em	$e, m \in 2\mathbb{Z}$		
	χ_+^4	0	$\{\frac{e^2}{R^2} + \frac{m^2 R^2}{4}, 1\}$	em	$e, m \in 2\mathbb{Z}, em \neq 0$		
	χ_+^2	0	$\frac{e^2}{R^2} + \frac{m^2 R^2}{4}$	em	$e \in 2\mathbb{Z}, m \in 2\mathbb{Z} + 1$		
	χ_+^3	0			$e \in 2\mathbb{Z}, m \in 2\mathbb{Z} + 1$		
	χ_-^1	0			$e \in 2\mathbb{Z} + 1, m \in 2\mathbb{Z}$		
	χ_-^2	0			$e \in 2\mathbb{Z} + 1, m \in 2\mathbb{Z} + 1$		
	χ_-^3	0			$e \in 2\mathbb{Z} + 1, m \in 2\mathbb{Z} + 1$		
	χ_-^4	0			$e \in 2\mathbb{Z} + 1, m \in 2\mathbb{Z}$		
(100)	α_+^1	0			$h + \bar{h}$	$h - \bar{h}$	$h, \bar{h} \in \{\frac{1}{16}, \frac{9}{16}\}$ $h - \bar{h} \in \mathbb{Z}$
	α_-^1	$\frac{1}{2}$					$h - \bar{h} \in \mathbb{Z} + \frac{1}{2}$
(010)	α_+^2	0	$h + \bar{h}$	$h - \bar{h}$	$h, \bar{h} \in \{\frac{1}{16}, \frac{9}{16}\}$ $h - \bar{h} \in \mathbb{Z}$		
	α_-^2	$\frac{1}{2}$			$h - \bar{h} \in \mathbb{Z} + \frac{1}{2}$		
(110)	β_+^3	0	$\frac{e^2}{R^2} + \frac{m^2 R^2}{4}$	em	$e \in \mathbb{Z} + \frac{1}{2}, m \in \mathbb{Z}$ $em \in \mathbb{Z}$		
	β_-^3	$\frac{1}{2}$			$em \in \mathbb{Z} + \frac{1}{2}$		
(001)	α_+^3	0	$\frac{e^2}{R^2} + \frac{m^2 R^2}{4}$	em	$e \in \mathbb{Z}, m \in \mathbb{Z} + \frac{1}{2}$ $em \in \mathbb{Z}$		
	α_-^3	$\frac{1}{2}$			$em \in \mathbb{Z} + \frac{1}{2}$		
(101)	β_+^2	0	$h + \bar{h}$	$h - \bar{h}$	$h, \bar{h} \in \{\frac{1}{16}, \frac{9}{16}\}$ $h - \bar{h} \in \mathbb{Z}$		
	β_-^2	$\frac{1}{2}$			$h - \bar{h} \in \mathbb{Z} + \frac{1}{2}$		
(011)	β_+^1	0	$h + \bar{h}$	$h - \bar{h}$	$h, \bar{h} \in \{\frac{1}{16}, \frac{9}{16}\}$ $h - \bar{h} \in \mathbb{Z}$		
	β_-^1	$\frac{1}{2}$			$h - \bar{h} \in \mathbb{Z} + \frac{1}{2}$		
(111)	γ_+	$\frac{3}{4}$	$\frac{e^2}{R^2} + \frac{m^2 R^2}{4}$	em	$e, m \in \mathbb{Z} + \frac{1}{2}$ $em \in \mathbb{Z} + \frac{3}{4}$		
	γ_-	$\frac{1}{4}$			$em \in \mathbb{Z} + \frac{1}{4}$		

Table 4.1: Primary fields in each topological sector labeled by a twist (an element of $\mathcal{G} = \mathbb{Z}_2^3$) and an irreducible (projective) representation. These sectors are the simple objects of $D^\phi(\mathbb{Z}_2^3) \cong D(\mathbb{D}_4)$.

Note that the choices of e and m allowed for each representation under the trivial twist corresponds to $(-1)^e = \chi(001)$ and $(-1)^m = \chi(110)$, where χ is the representation being considered.

Projective representations in each topological sector are indicated in Eqn. 4.48, reproduced from Ref. 4.80.

The fusion table, computed using the symmetric MERA, for these sectors is explicitly presented in Table 4.2.

All sectors with a nontrivial twist have quantum dimension 2, and so are nonabelian.

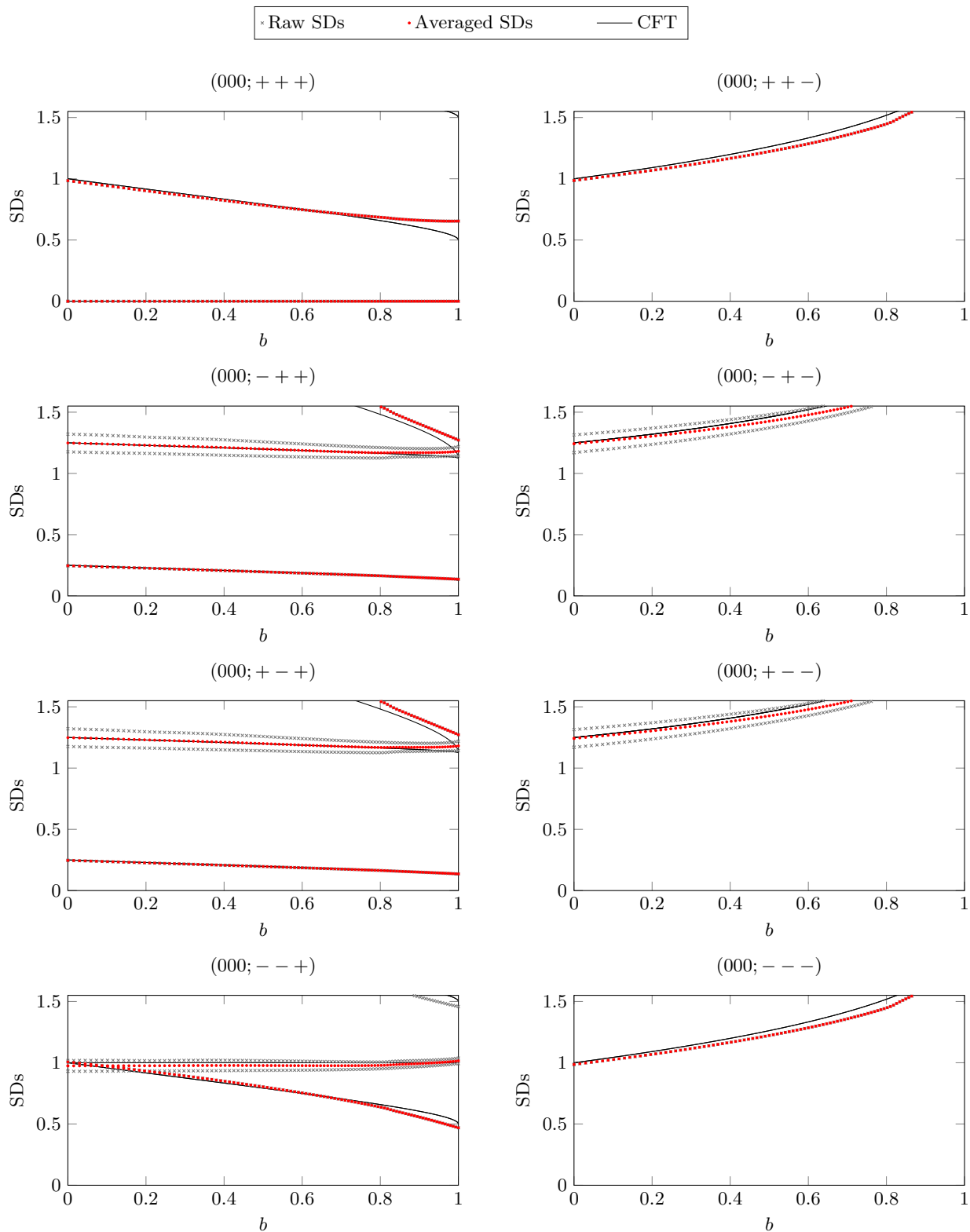


Figure 4.7: MERA scaling dimensions for the trivial twist of the abc model along the ‘b’ line. This line is symmetric under the anomalous action of \mathbb{Z}_2^3 .

Figure titles label: (twist label; irreducible representation label).

Grey points are the raw data extracted from the MERA. Red points correspond to averaged data as discussed in Appendix 4.A. Black lines correspond to local fields of the compactified free boson CFT.

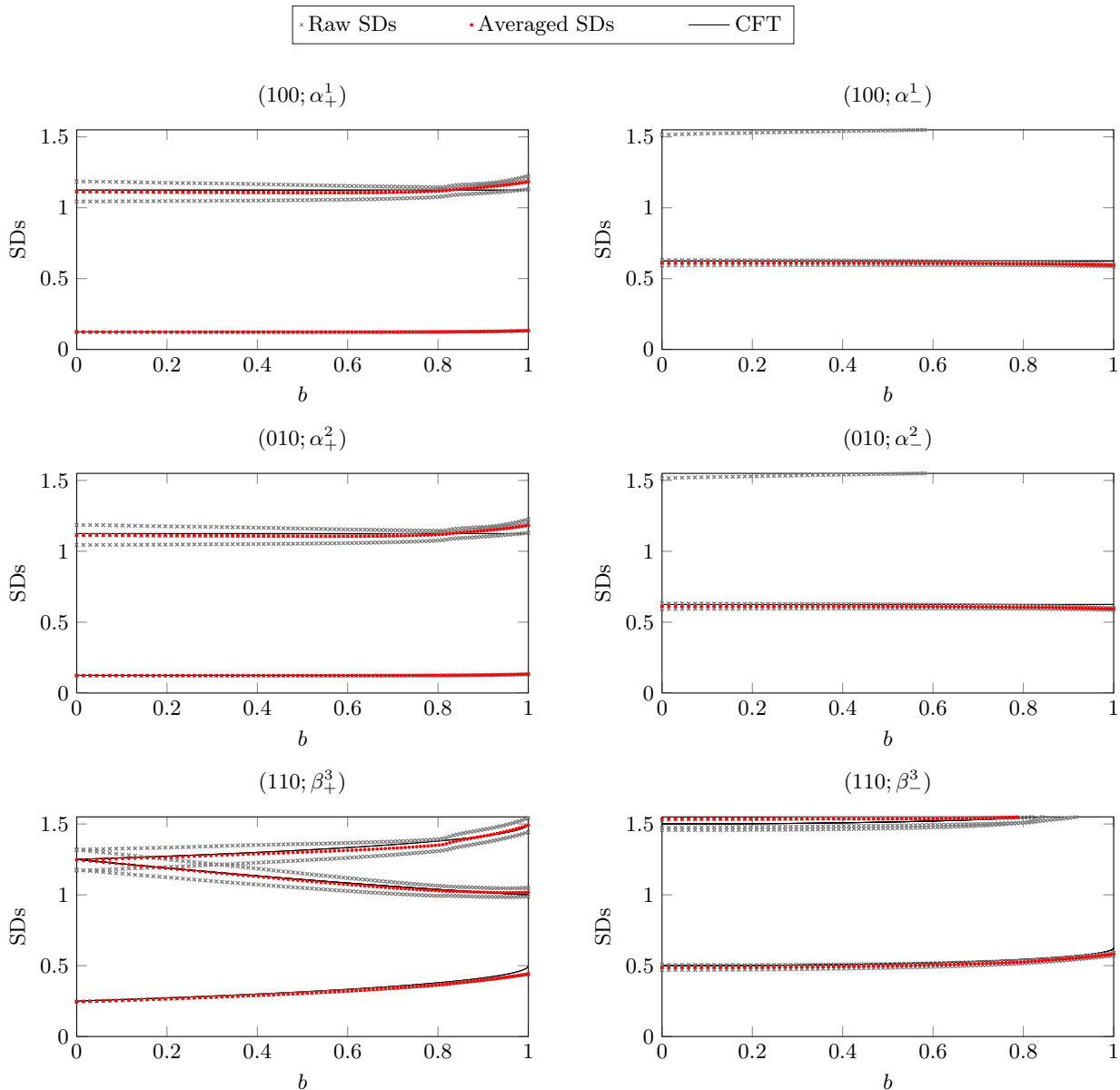


Figure 4.8: Scaling dimensions for topological sectors with twists of the form $(x, y, 0)$.

Figure titles label: (twist label; irreducible projective representation label).

Grey points are the raw data extracted from the MERA. Red points correspond to averaged data as discussed in Appendix 4.A. Black lines correspond to equations in Table 4.1.

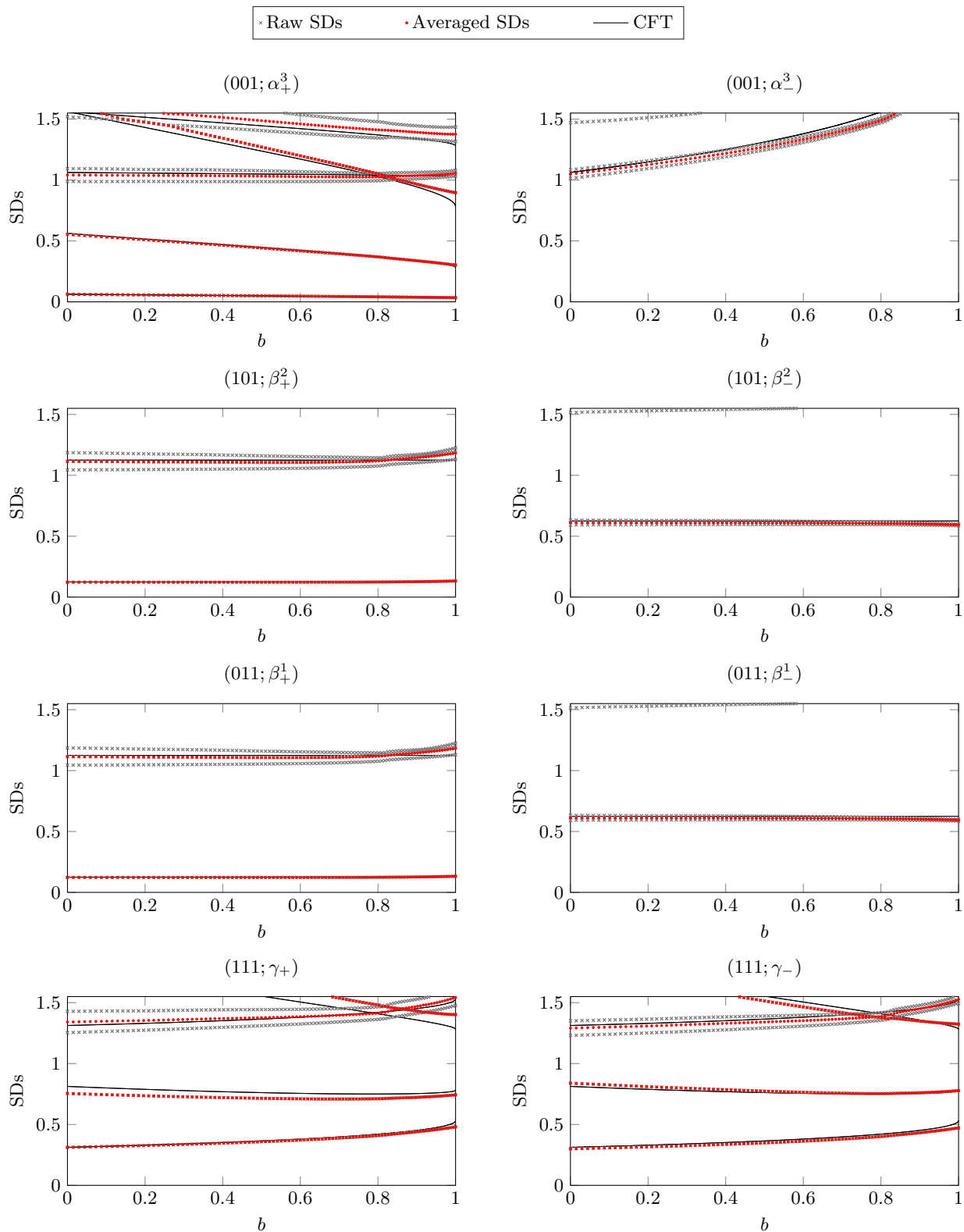


Figure 4.9: Scaling dimensions for topological sectors with twists of the form $(x, y, 1)$.

Figure titles label: (twist label; irreducible projective representation label).

Grey points are the raw data extracted from the MERA. Red points correspond to averaged data as discussed in Appendix 4.A. Black lines correspond to equations in Table 4.1.

$a \times b$	χ_+^1	χ_+^2	χ_+^3	χ_+^4	χ_-^1	χ_-^2	χ_-^3	χ_-^4	α_+^1	α_-^1	α_+^2	α_-^2	β_+^3	β_-^3	α_+^3	α_-^3	β_+^2	β_-^2	β_+^1	β_-^1	γ_+	γ_-
χ_+^1	χ_+^1	χ_+^2	χ_+^3	χ_+^4	χ_-^1	χ_-^2	χ_-^3	χ_-^4	α_+^1	α_-^1	α_+^2	α_-^2	β_+^3	β_-^3	α_+^3	α_-^3	β_+^2	β_-^2	β_+^1	β_-^1	γ_+	γ_-
χ_+^2	χ_+^1	χ_+^4	χ_+^3	χ_+^2	χ_-^1	χ_-^4	χ_-^3	χ_-^2	α_+^1	α_-^1	α_+^2	α_-^2	β_+^3	β_-^3	α_+^3	α_-^3	β_+^2	β_-^2	β_+^1	β_-^1	γ_+	γ_-
χ_+^3	χ_+^1	χ_+^4	χ_+^2	χ_+^3	χ_-^1	χ_-^4	χ_-^2	χ_-^3	α_+^1	α_-^1	α_+^2	α_-^2	β_+^3	β_-^3	α_+^3	α_-^3	β_+^2	β_-^2	β_+^1	β_-^1	γ_+	γ_-
χ_+^4	χ_+^1	χ_+^3	χ_+^2	χ_+^4	χ_-^1	χ_-^3	χ_-^2	χ_-^4	α_+^1	α_-^1	α_+^2	α_-^2	β_+^3	β_-^3	α_+^3	α_-^3	β_+^2	β_-^2	β_+^1	β_-^1	γ_+	γ_-
χ_-^1	χ_-^1	χ_-^2	χ_-^3	χ_-^4	χ_+^1	χ_+^2	χ_+^3	χ_+^4	α_+^1	α_-^1	α_+^2	α_-^2	β_+^3	β_-^3	α_+^3	α_-^3	β_+^2	β_-^2	β_+^1	β_-^1	γ_+	γ_-
χ_-^2	χ_-^1	χ_-^4	χ_-^3	χ_-^2	χ_+^1	χ_+^4	χ_+^3	χ_+^2	α_+^1	α_-^1	α_+^2	α_-^2	β_+^3	β_-^3	α_+^3	α_-^3	β_+^2	β_-^2	β_+^1	β_-^1	γ_+	γ_-
χ_-^3	χ_-^1	χ_-^4	χ_-^2	χ_-^3	χ_+^1	χ_+^4	χ_+^2	χ_+^3	α_+^1	α_-^1	α_+^2	α_-^2	β_+^3	β_-^3	α_+^3	α_-^3	β_+^2	β_-^2	β_+^1	β_-^1	γ_+	γ_-
χ_-^4	χ_-^1	χ_-^3	χ_-^2	χ_-^4	χ_+^1	χ_+^3	χ_+^2	χ_+^4	α_+^1	α_-^1	α_+^2	α_-^2	β_+^3	β_-^3	α_+^3	α_-^3	β_+^2	β_-^2	β_+^1	β_-^1	γ_+	γ_-
α_+^1	α_+^1	α_+^1	α_+^1	α_+^1	α_+^1	α_+^1	α_+^1	α_+^1	α_+^1	α_-^1	α_+^2	α_-^2	β_+^3	β_-^3	α_+^3	α_-^3	β_+^2	β_-^2	β_+^1	β_-^1	γ_+	γ_-
α_-^1	α_+^1	α_+^1	α_+^1	α_+^1	α_+^1	α_+^1	α_+^1	α_+^1	α_-^1	α_-^1	α_+^2	α_-^2	β_+^3	β_-^3	α_+^3	α_-^3	β_+^2	β_-^2	β_+^1	β_-^1	γ_+	γ_-
α_+^2	α_+^2	α_+^2	α_+^2	α_+^2	α_+^2	α_+^2	α_+^2	α_+^2	α_+^2	α_-^2	α_+^3	α_-^3	β_+^2	β_-^2	α_+^1	α_-^1	β_+^3	β_-^3	α_+^4	α_-^4	β_+^1	β_-^1
α_-^2	α_+^2	α_+^2	α_+^2	α_+^2	α_+^2	α_+^2	α_+^2	α_+^2	α_-^2	α_-^2	α_+^3	α_-^3	β_+^2	β_-^2	α_+^1	α_-^1	β_+^3	β_-^3	α_+^4	α_-^4	β_+^1	β_-^1
β_+^3	β_+^3	β_+^3	β_+^3	β_+^3	β_+^3	β_+^3	β_+^3	β_+^3	β_+^3	β_-^3	β_+^2	β_-^2	α_+^1	α_-^1	β_+^3	β_-^3	α_+^4	α_-^4	β_+^1	β_-^1	γ_+	γ_-
β_-^3	β_+^3	β_+^3	β_+^3	β_+^3	β_+^3	β_+^3	β_+^3	β_+^3	β_-^3	β_-^3	β_+^2	β_-^2	α_+^1	α_-^1	β_+^3	β_-^3	α_+^4	α_-^4	β_+^1	β_-^1	γ_+	γ_-
α_+^3	α_+^3	α_+^3	α_+^3	α_+^3	α_+^3	α_+^3	α_+^3	α_+^3	α_+^3	α_-^3	α_+^2	α_-^2	β_+^1	β_-^1	α_+^3	α_-^3	β_+^4	β_-^4	α_+^5	α_-^5	β_+^3	β_-^3
α_-^3	α_+^3	α_+^3	α_+^3	α_+^3	α_+^3	α_+^3	α_+^3	α_+^3	α_-^3	α_-^3	α_+^2	α_-^2	β_+^1	β_-^1	α_+^3	α_-^3	β_+^4	β_-^4	α_+^5	α_-^5	β_+^3	β_-^3
β_+^2	β_+^2	β_+^2	β_+^2	β_+^2	β_+^2	β_+^2	β_+^2	β_+^2	β_+^2	β_-^2	β_+^1	β_-^1	α_+^3	α_-^3	β_+^2	β_-^2	α_+^4	α_-^4	β_+^3	β_-^3	γ_+	γ_-
β_-^2	β_+^2	β_+^2	β_+^2	β_+^2	β_+^2	β_+^2	β_+^2	β_+^2	β_-^2	β_-^2	β_+^1	β_-^1	α_+^3	α_-^3	β_+^2	β_-^2	α_+^4	α_-^4	β_+^3	β_-^3	γ_+	γ_-
β_+^1	β_+^1	β_+^1	β_+^1	β_+^1	β_+^1	β_+^1	β_+^1	β_+^1	β_+^1	β_-^1	β_+^3	β_-^3	α_+^2	α_-^2	β_+^1	β_-^1	α_+^5	α_-^5	β_+^4	β_-^4	γ_+	γ_-
β_-^1	β_+^1	β_+^1	β_+^1	β_+^1	β_+^1	β_+^1	β_+^1	β_+^1	β_-^1	β_-^1	β_+^3	β_-^3	α_+^2	α_-^2	β_+^1	β_-^1	α_+^5	α_-^5	β_+^4	β_-^4	γ_+	γ_-
γ_+	γ_+	γ_-	γ_-	γ_+	γ_-	γ_+	γ_-	γ_+	β_+^1	β_-^1	β_+^2	β_-^2	α_+^3	α_-^3	β_+^1	β_-^1	α_+^5	α_-^5	β_+^4	β_-^4	γ_+	γ_-
γ_-	γ_+	γ_-	γ_+	γ_-	γ_+	γ_-	γ_+	γ_-	β_+^1	β_-^1	β_+^2	β_-^2	α_+^3	α_-^3	β_+^1	β_-^1	α_+^5	α_-^5	β_+^4	β_-^4	γ_+	γ_-

Table 4.2: Fusion rules for $D^\phi(\mathbb{Z}_3^3)$ sectors computed from symmetric MERA. Cell entries denote the allowed fusion outcome sectors for $a \times b$. The OPE coefficients defined in Eqn. 4.29 are zero if the resultant field c does not lie in an allowed sector.

4.B MPO group representations and third cohomology

In this appendix we recount the definition of the third cohomology class of an injective MPO representation of a finite group \mathcal{G} , as first introduced in Ref. 4.23. MPO representations appear in the study of $(2 + 1)$ D SPT tensor network states and it was shown in Ref. 4.26 that they are always injective. The presence of such an MPO symmetry has an important physical consequence; all short range entangled states must break the symmetry, either explicitly or spontaneously. For details about group cohomology theory in the context of SPT order we refer the reader to Ref. 4.12.

In an MPO representation of \mathcal{G} , multiplying a pair of MPOs labeled by the group elements g_0 and g_1 is equal to the MPO labeled by g_0g_1 for every length. For injective MPOs there exists a gauge transformation on the virtual indices that brings both representations into the same canonical form [4.42, 4.44, 4.47]. This implies that there exists an operator (the reduction tensor) $X(g_0, g_1) : (\mathbb{C}^x)^{\otimes 2} \rightarrow \mathbb{C}^x$ such that

$$\begin{array}{c}
 \text{---} \\
 | \\
 X^\dagger(g_0, g_1) \left[\begin{array}{c} \text{---} \\ | \\ \text{---} \end{array} \right] \begin{array}{c} \text{---} \\ | \\ \text{---} \end{array} \\
 | \\
 \text{---} \\
 \text{---} \\
 | \\
 \text{---} \\
 | \\
 X(g_0, g_1) \left[\begin{array}{c} \text{---} \\ | \\ \text{---} \end{array} \right] \\
 | \\
 \text{---}
 \end{array}
 = \begin{array}{c}
 \text{---} \\
 | \\
 \text{---} \\
 | \\
 \text{---} \\
 | \\
 \text{---} \\
 | \\
 \text{---} \\
 | \\
 \text{---} \\
 | \\
 \text{---}
 \end{array}, \quad (4.49)$$

where $X(g_0, g_1)$ is only defined up to multiplication by a complex phase $\beta(g_0, g_1)$.

If we now multiply three MPOs labeled by g_0, g_1 and g_2 there are two ways to reduce the multiplied MPOs to the MPO labeled by $g_0g_1g_2$. When only acting on the right virtual indices these two reductions are equivalent up to a complex phase

$$\begin{array}{c}
 \text{---} \\
 | \\
 X(g_1, g_2) \left[\begin{array}{c} \text{---} \\ | \\ \text{---} \end{array} \right] \\
 | \\
 X(g_0, g_1g_2) \left[\begin{array}{c} \text{---} \\ | \\ \text{---} \end{array} \right] \\
 | \\
 \text{---} \\
 \text{---} \\
 | \\
 \text{---} \\
 | \\
 \text{---}
 \end{array}
 = \phi(g_0, g_1, g_2) \begin{array}{c}
 \text{---} \\
 | \\
 X(g_0g_1, g_2) \left[\begin{array}{c} \text{---} \\ | \\ \text{---} \end{array} \right] \\
 | \\
 X(g_0, g_1) \left[\begin{array}{c} \text{---} \\ | \\ \text{---} \end{array} \right] \\
 | \\
 \text{---} \\
 \text{---} \\
 | \\
 \text{---} \\
 | \\
 \text{---}
 \end{array}. \quad (4.50)$$

When multiplying four MPOs, one observes that ϕ has to obey certain consistency conditions. By performing a series of moves (changing order of reduction), one can achieve the same reduction

$$\begin{array}{c}
 \text{---} \\
 | \\
 X(g_2, g_3) \left[\begin{array}{c} \text{---} \\ | \\ \text{---} \end{array} \right] \\
 | \\
 X(g_1, g_2g_3) \left[\begin{array}{c} \text{---} \\ | \\ \text{---} \end{array} \right] \\
 | \\
 X(g_0, g_1g_2g_3) \left[\begin{array}{c} \text{---} \\ | \\ \text{---} \end{array} \right] \\
 | \\
 \text{---} \\
 \text{---} \\
 | \\
 \text{---} \\
 | \\
 \text{---}
 \end{array}
 = \phi(g_1, g_2, g_3) \begin{array}{c}
 \text{---} \\
 | \\
 X(g_2, g_3) \left[\begin{array}{c} \text{---} \\ | \\ \text{---} \end{array} \right] \\
 | \\
 X(g_1, g_2) \left[\begin{array}{c} \text{---} \\ | \\ \text{---} \end{array} \right] \\
 | \\
 X(g_0, g_1g_2) \left[\begin{array}{c} \text{---} \\ | \\ \text{---} \end{array} \right] \\
 | \\
 \text{---} \\
 \text{---} \\
 | \\
 \text{---} \\
 | \\
 \text{---}
 \end{array}
 = \phi(g_1, g_2, g_3) \phi(g_0, g_1g_2, g_3) \begin{array}{c}
 \text{---} \\
 | \\
 X(g_2, g_3) \left[\begin{array}{c} \text{---} \\ | \\ \text{---} \end{array} \right] \\
 | \\
 X(g_1, g_2) \left[\begin{array}{c} \text{---} \\ | \\ \text{---} \end{array} \right] \\
 | \\
 X(g_0, g_1) \left[\begin{array}{c} \text{---} \\ | \\ \text{---} \end{array} \right] \\
 | \\
 \text{---} \\
 \text{---} \\
 | \\
 \text{---} \\
 | \\
 \text{---}
 \end{array} \\
 = \phi(g_1, g_2, g_3) \phi(g_0, g_1g_2, g_3) \phi(g_0, g_1, g_2) \begin{array}{c}
 \text{---} \\
 | \\
 X(g_2, g_3) \left[\begin{array}{c} \text{---} \\ | \\ \text{---} \end{array} \right] \\
 | \\
 X(g_1, g_2) \left[\begin{array}{c} \text{---} \\ | \\ \text{---} \end{array} \right] \\
 | \\
 X(g_0, g_1) \left[\begin{array}{c} \text{---} \\ | \\ \text{---} \end{array} \right] \\
 | \\
 \text{---} \\
 \text{---} \\
 | \\
 \text{---} \\
 | \\
 \text{---}
 \end{array}$$

$$\begin{aligned}
 &= \frac{\phi(g_1, g_2, g_3)\phi(g_0, g_1g_2, g_3)\phi(g_0, g_1, g_2)}{\phi(g_0g_1, g_2, g_3)} \\
 &= \frac{\phi(g_1, g_2, g_3)\phi(g_0, g_1g_2, g_3)\phi(g_0, g_1, g_2)}{\phi(g_0g_1, g_2, g_3)\phi(g_0, g_1, g_2g_3)}, \tag{4.51}
 \end{aligned}$$

implying that

$$\frac{\phi(g_0, g_1, g_2)\phi(g_0, g_1g_2, g_3)\phi(g_1, g_2, g_3)}{\phi(g_0g_1, g_2, g_3)\phi(g_0, g_1, g_2g_3)} = 1. \tag{4.52}$$

This condition is known as the 3-cocycle condition and identifies ϕ as a 3-cocycle. As mentioned above $X(g_0, g_1)$ is only defined up to a complex phase $\beta(g_0, g_1)$. This freedom can change the ϕ , giving the equivalence relation

$$\phi'(g_0, g_1, g_2) = \phi(g_0, g_1, g_2) \frac{\beta(g_1, g_2)\beta(g_0, g_1g_2)}{\beta(g_0, g_1)\beta(g_0g_1, g_2)}, \tag{4.53}$$

so ϕ is only defined up to a 3-coboundary. For this reason the single block MPO group representation is endowed with the label $[\phi]$ from the third cohomology group $\mathcal{H}^3(\mathcal{G}, \mathbb{U}(1))$. One can check that multiplying any larger number of MPOs does not give additional conditions/equivalences on ϕ .

One can use a similar argument to demonstrate that no injective MPS can possess an anomalous symmetry. Assuming an injective MPS with tensor A is symmetric under an MPO symmetry for all lengths, similar reasoning that lead to Eqn. 4.49 implies the existence of another reduction tensor $Y(g)$ satisfying

$$\begin{array}{c} Y^\dagger(g) \\ \text{---} \diamond \text{---} \end{array} \begin{array}{c} A \\ \text{---} \\ g \\ \text{---} \end{array} \begin{array}{c} Y(g) \\ \text{---} \diamond \text{---} \end{array} = \begin{array}{c} A \\ \text{---} \end{array}. \tag{4.54}$$

Similar to Eqn. 4.50 we find that acting with multiple group elements leads to a complex phase $\beta(g_0, g_1)$

$$\begin{array}{c} A \\ \text{---} \\ g_1 \\ \text{---} \\ g_0 \\ \text{---} \end{array} \begin{array}{c} Y(g_1) \\ \text{---} \diamond \text{---} \\ Y(g_0) \\ \text{---} \diamond \text{---} \end{array} = \beta(g_0, g_1) \begin{array}{c} A \\ \text{---} \\ g_1 \\ \text{---} \\ g_0 \\ \text{---} \end{array} \begin{array}{c} Y(g_0g_1) \\ \text{---} \diamond \text{---} \\ X(g_0, g_1) \\ \text{---} \circ \text{---} \end{array}. \tag{4.55}$$

We now consider the application of three group elements

$$\begin{array}{c} A \\ \text{---} \\ g_2 \\ \text{---} \\ g_1 \\ \text{---} \\ g_0 \\ \text{---} \end{array} \begin{array}{c} \text{---} \diamond \text{---} \\ \text{---} \diamond \text{---} \\ \text{---} \diamond \text{---} \end{array} = \beta(g_1, g_2) \begin{array}{c} A \\ \text{---} \\ g_2 \\ \text{---} \\ g_1 \\ \text{---} \\ g_0 \\ \text{---} \end{array} \begin{array}{c} \text{---} \diamond \text{---} \\ \text{---} \circ \text{---} \\ \text{---} \diamond \text{---} \end{array} = \beta(g_1, g_2)\beta(g_0, g_1g_2) \begin{array}{c} A \\ \text{---} \\ g_2 \\ \text{---} \\ g_1 \\ \text{---} \\ g_0 \\ \text{---} \end{array} \begin{array}{c} \text{---} \diamond \text{---} \\ \text{---} \circ \text{---} \\ \text{---} \circ \text{---} \\ \text{---} \diamond \text{---} \end{array}$$

$$\begin{aligned}
 &= \beta(g_1, g_2)\beta(g_0, g_1g_2)\phi(g_0, g_1, g_2) \quad \begin{array}{c} \text{A} \\ | \\ g_2 \\ | \\ g_1 \\ | \\ g_0 \end{array} \\
 &= \frac{\beta(g_1, g_2)\beta(g_0, g_1g_2)\phi(g_0, g_1, g_2)}{\beta(g_0g_1, g_2)} \quad \begin{array}{c} \text{A} \\ | \\ g_2 \\ | \\ g_1 \\ | \\ g_0 \end{array} \\
 &= \frac{\beta(g_1, g_2)\beta(g_0, g_1g_2)\phi(g_0, g_1, g_2)}{\beta(g_0g_1, g_2)\beta(g_0, g_1)}, \quad \begin{array}{c} \text{A} \\ | \\ g_2 \\ | \\ g_1 \\ | \\ g_0 \end{array} , \tag{4.56}
 \end{aligned}$$

which leads to a consistency equation

$$\phi(g_0, g_1, g_2) = \frac{\beta(g_0g_1, g_2)\beta(g_0, g_1)}{\beta(g_1, g_2)\beta(g_0, g_1g_2)}, \tag{4.57}$$

implying ϕ is a coboundary. Therefore $\phi \sim 1$, is in the trivial cohomology class. Hence no injective MPS can be symmetric under an anomalous MPO symmetry. This leaves open the possibility of a non-injective MPS, describing a state which spontaneously breaks the symmetry. Alternatively a symmetric state may be gapless and hence have no MPS description (with a fixed bond dimension).

4.C Ansatz for MERA tensors with type-III \mathbb{Z}_N^3 symmetry

In this appendix, we describe an ansatz for the tensors in a MERA with type-III \mathbb{Z}_N^3 symmetry. Let $\mathcal{G} = \mathbb{Z}_N^3$, with action as defined in Eqn. 4.35. Let T be an isometric tensor with $2A$ upper indices and $2B$ ($B \geq A$) lower indices

$$T : (\mathbb{C}^N)^{\otimes 2A} \rightarrow (\mathbb{C}^N)^{\otimes 2B}, \quad (4.58)$$

$$T^\dagger T = \mathbb{1}_N^{\otimes 2A}. \quad (4.59)$$

Define the decoupling circuit on $2K$ indices as

$$\mathcal{D}_{2K} = \prod_{j=1}^{K-1} CX_{1,2j+1} CX_{2K,2j}. \quad (4.60)$$

Allowed MERA tensors are those given by

$$T = \mathcal{D}_{2B}^\dagger (\mathbb{1}_N \otimes t \otimes \mathbb{1}_N) \mathcal{D}_{2A}, \quad (4.61)$$

where

$$t : (\mathbb{C}^N)^{\otimes 2(A-1)} \rightarrow (\mathbb{C}^N)^{\otimes 2(B-1)}, \quad (4.62)$$

$$t^\dagger t = \mathbb{1}_N^{\otimes 2(A-1)}. \quad (4.63)$$

The X portion of the symmetry is automatically enforced by this circuit. To enforce the CZ part, one must ensure that

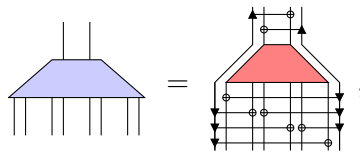
$$\left(\prod_{j=1}^{B-1} CZ_{2j-1,2j}^\dagger \right) \left(\prod_{j=1}^{B-2} CZ_{2j,2j+1} \right) t = t \left(\prod_{j=1}^{A-1} CZ_{2j-1,2j}^\dagger \right) \left(\prod_{j=1}^{A-2} CZ_{2j,2j+1} \right). \quad (4.64)$$

4.C.1 4:2 MERA

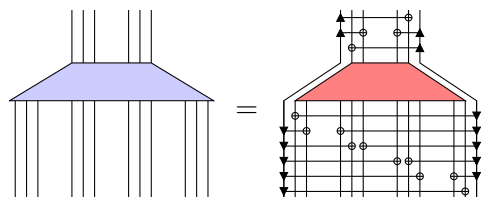
For clarity, we now include the form of the constraint on the 4:2 MERA (introduced in Fig. 4.1) with bond dimension N , N^2 and N^3 :



$$(4.65a)$$



$$(4.65b)$$



$$(4.65c)$$

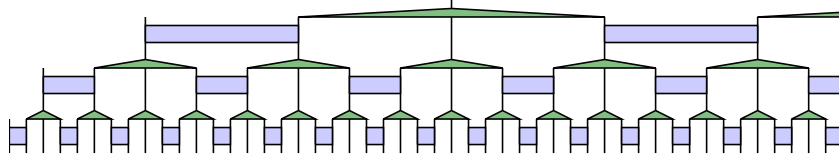


Figure 4.10: The ternary MERA represents a quantum state using two types of tensors; unitary ‘disentangles’ (rectangles) and isometric tensors (triangles).

4.C.2 Ternary MERA

For completeness, we show how our ansatz is applied to the ternary MERA shown in Fig. 4.10. The ternary ansatz is commonly seen in the literature due to its relatively low optimization cost. A ternary MERA is built from two kinds of tensors; unitary ‘disentangles’ v (rectangles in Fig. 4.10) and isometric tensors w (triangles in Fig. 4.10). In the general case, these tensors may all contain distinct coefficients, although symmetries such as scale invariance can be imposed by, for example, forcing the tensors on each layer to be identical.

For bond dimension N^2 and N^4 , the constraint on the tensors is

$$\begin{array}{ccc}
 \begin{array}{c} \text{rectangle} \\ \text{with 3 legs} \end{array} = \begin{array}{c} \text{grid of } \phi \\ \text{with } \phi \text{ on legs} \end{array}, & \begin{array}{c} \text{triangle} \\ \text{with 3 legs} \end{array} = \begin{array}{c} \text{grid of } \phi \\ \text{with } \phi \text{ on legs} \end{array}, & (4.66a)
 \end{array}$$

$$\begin{array}{ccc}
 \begin{array}{c} \text{rectangle} \\ \text{with 4 legs} \end{array} = \begin{array}{c} \text{grid of } \phi \\ \text{with } \phi \text{ on legs} \end{array}, & \begin{array}{c} \text{triangle} \\ \text{with 4 legs} \end{array} = \begin{array}{c} \text{grid of } \phi \\ \text{with } \phi \text{ on legs} \end{array}, & (4.66b)
 \end{array}$$

with the obvious generalization to other bond dimensions.

We remark that although our examples drawn here map χ dimensional sites to χ dimensional sites, this can be relaxed. This allows the effective dimension of the sites to be increased as desired.

4.D Generalized \mathbb{Z}_N CZX model and its gapless boundary theory

The CZX model was introduced in Ref. 4.23 as a simple exactly solvable representative of the nontrivial \mathbb{Z}_2 SPT phase in two spatial dimensions. In this paper we have considered the larger symmetry group \mathbb{Z}_2^3 of the model for which it is a representative of the \mathbb{Z}_2^3 type-III SPT phase. In this appendix we describe a simple generalization of the CZX model to a Hamiltonian with \mathbb{Z}_N^3 symmetry that is a representative of the root type-III \mathbb{Z}_N^3 SPT. We then outline how this fits into the more general setting of $(1+1)$ D \mathcal{G} -SPT dualities at the edge of a particular $\mathcal{G} \times \mathcal{H}^2(\mathcal{G}, \text{U}(1))$ -SPT bulk in $(2+1)$ D.

4.D.1 Definitions

The model is defined on a two dimensional square lattice with four \mathbb{Z}_N spins per site. For concreteness we label them counterclockwise as follows



$$(4.67)$$

Before stating the Hamiltonian, ground-state, and symmetries of the model we establish some definitions:

$$P_2 = \sum_{i=0}^{N-1} |i\rangle^{\otimes 2} \langle i|^{\otimes 2} \quad (4.68)$$

$$X_4 = \sum_{i=0}^{N-1} |i+1\rangle^{\otimes 4} \langle i|^{\otimes 4} \quad (4.69)$$

$$|\text{GHZ}_4\rangle = \frac{1}{\sqrt{N}} \sum_{i=0}^{N-1} |i\rangle^{\otimes 4} \quad (4.70)$$

$$u_X^- = X_1 \otimes X_3 \quad (4.71)$$

$$u_X^+ = X_2 \otimes X_4 \quad (4.72)$$

$$u_{CZ} = CZ_{12} CZ_{23}^\dagger CZ_{34} CZ_{41}^\dagger, \quad (4.73)$$

where X, CZ are defined in Section 4.3.

4.D.2 Hamiltonian and ground state

The Hamiltonian is a sum of local terms acting on each plaquette of a square lattice $H = \sum_p h_p$. The terms are given by

$$h_p = - \sum_{i=0}^{N-1} X_4^i \otimes P_2 \otimes P_2 \otimes P_2 \otimes P_2, \quad (4.74)$$

which act on the lattice as



$$(4.75)$$

The ground state is unique for closed boundary conditions and is given by a tensor product of the state $|\text{GHZ}_4\rangle$ on the four spins around each plaquette

$$|\Psi_{\text{GS}}\rangle = \bigotimes_p |\text{GHZ}_4\rangle. \quad (4.76)$$

Note that this ground state is not a product state with respect to the locality structure we have chosen by our grouping of spins into sites (if sites were instead defined to group the spins around each plaquette it would be a product state).

4.D.3 Symmetry

To describe the \mathbb{Z}_N^3 symmetry of the Hamiltonian in Eqn. 4.74 we first bipartition the lattice into black (b) and white (w) sites, as indicated in Fig. 4.11. The generators are then given by

$$U_{X^{(1)}} = \bigotimes_b u_X^- \bigotimes_w u_X^+ \quad (4.77)$$

$$U_{X^{(2)}} = \bigotimes_b u_X^+ \bigotimes_w u_X^- \quad (4.78)$$

$$U_{CZ} = \bigotimes_b u_{CZ}^\dagger \bigotimes_w u_{CZ}. \quad (4.79)$$

One can verify that each of these operators is of order N and that they mutually commute. Furthermore each local Hamiltonian term commutes with all symmetries and they leave the ground state invariant. Note the U_{CZ} symmetry is an on-site symmetry for our definition of site but would not be if sites were instead defined by grouping the spins around each plaquette.

4.D.4 Boundary theory

In the presence of an open boundary the bulk Hamiltonian is extensively degenerate as it only projects pairs of spins along the edge into the support subspace of P_2 . We identify effective \mathbb{Z}_N edge spins with the N states in this subspace via the projector $\sum_i |i\rangle\langle ii|$. This identification is indicated by \rightsquigarrow in Fig. 4.11. An edge site is formed by a pair of these spins, as shown in Fig. 4.11. This identification provides an exact mapping from bulk operators to the boundary. The symmetry acts on the edge as follows

$$U_{X^{(1)}} \mapsto \bigotimes_j X_j^{(1)} \quad (4.80)$$

$$U_{X^{(2)}} \mapsto \bigotimes_j X_j^{(2)} \quad (4.81)$$

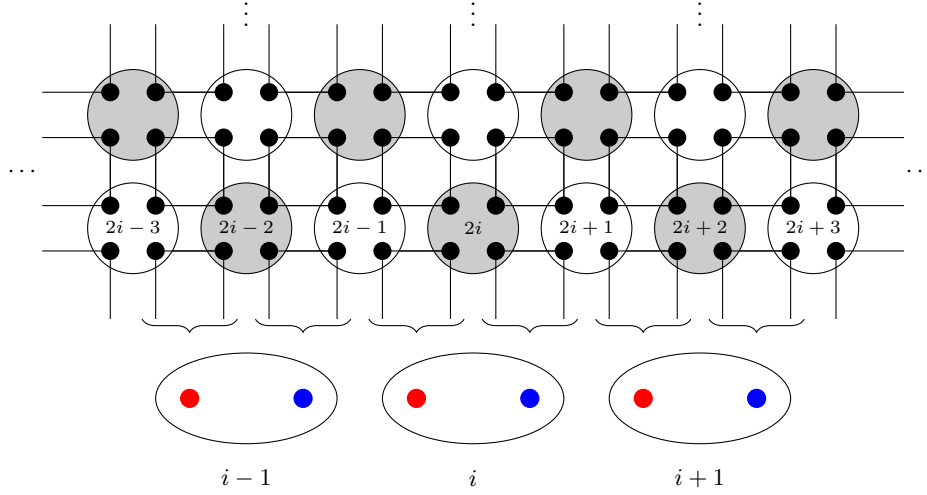


Figure 4.11: Identification of the edge degrees of freedom.

$$U_{CZ} \mapsto \mathcal{C} = \begin{array}{c} \uparrow \downarrow \uparrow \downarrow \uparrow \downarrow \uparrow \downarrow \\ \text{---} \text{---} \text{---} \text{---} \text{---} \text{---} \text{---} \text{---} \\ \downarrow \uparrow \downarrow \uparrow \downarrow \uparrow \downarrow \uparrow \\ \text{site} \end{array} . \quad (4.82)$$

Due to the grouping of edge spins into sites only the subgroup generated by $U_{X^{(1)}}$ and $U_{X^{(2)}}$ acts on-site.

The bulk to boundary mapping can be used to find the edge action of certain operators that leave no residual effect on the bulk of the ground state. In particular

$$(Z_1)_{2i}^b \mapsto Z_i^{(1)} \quad (4.83)$$

$$(Z_2)_{2i-1}^w \mapsto Z_i^{(1)} \quad (4.84)$$

$$(Z_1)_{2i+1}^w \mapsto Z_i^{(2)} \quad (4.85)$$

$$(Z_2)_{2i}^b \mapsto Z_i^{(2)} \quad (4.86)$$

$$(X_2)_{2i-1}^w (X_1)_{2i}^b \mapsto X_i^{(1)} \quad (4.87)$$

$$(X_2)_{2i}^b (X_1)_{2i+1}^w \mapsto X_i^{(2)}, \quad (4.88)$$

where the numbering is indicated in Fig. 4.11. We find an effective edge Hamiltonian by considering symmetric perturbations in the bulk with minimal support.

$$(Z_1^\dagger Z_3)_{2i}^b (Z_2 Z_4)_{2i+1}^w \mapsto Z_i^\dagger Z_{i+1}^{(1)} \quad (4.89)$$

$$(Z_1 Z_3)_{2i+1}^w (Z_2^\dagger Z_4)_{2i+2}^b \mapsto Z_i^{(2)} \tilde{Z}_{i+1}^\dagger \quad (4.90)$$

$$(X_2)_{2i-1}^w (X_1)_{2i}^b + (Z_1 X_2 Z_3)_{2i-1}^w (X_1 Z_2^\dagger Z_4)_{2i}^b \mapsto X_i^{(1)} + Z_{i-1}^{(2)} X_i^{(1)} \tilde{Z}_i^\dagger \quad (4.91)$$

$$(X_2)_{2i}^b (X_1)_{2i+1}^w + (Z_1^\dagger X_2 Z_3)_{2i}^b (X_1 Z_2 Z_4)_{2i+1}^w \mapsto X_i^{(2)} + Z_i^\dagger X_i^{(2)} Z_{i+1}^{(1)}. \quad (4.92)$$

The edge Hamiltonian is given by

$$\begin{aligned}
 H_{\text{Edge}} = & - \sum_i \sum_{k=0}^{N-1} c_k \sum_{j=0}^{N-1} (Z_i^{\dagger j k} X_i^{(2)j} Z_{i+1}^{(1)jk} + Z_{i-1}^{(2)jk} X_i^{(1)j} \tilde{Z}_i^{\dagger j k}) \\
 & - \sum_i \sum_{k=0}^{N-1} b_k (Z_i^{\dagger k} Z_{i+1}^{(1)k} + Z_i^{(2)k} \tilde{Z}_{i+1}^{\dagger k}).
 \end{aligned} \tag{4.93}$$

where $b_k = b_{N-k}$. The Hamiltonian is fully symmetric under $U_{X^{(1)}}$ and $U_{X^{(2)}}$ while the parameters transform as follows under \mathcal{C}

$$c_k \mapsto c_{k-1}, \tag{4.94}$$

$$b_k \mapsto b_k. \tag{4.95}$$

When c_k is the only nonzero parameter the Hamiltonian is in the $[k] \in \mathcal{H}^2(\mathcal{G}, \mathbf{U}(1))$ SPT phase, while for $b_k = b_{N-k}$ the only nonzero parameters it describes a symmetry broken phase. Hence the \mathcal{C} operator cycles the SPT phases $[k] \mapsto [k+1]$ and the Hamiltonian is fully symmetric when all $c_k = c_0$. This may correspond to an SPT critical point or a symmetry breaking point depending upon the relative strength of the b_k parameters.

4.D.5 General (1 + 1)D \mathcal{G} SPT duality at the edge of a (2 + 1)D $\mathcal{G} \times \mathcal{H}^2(\mathcal{G}, \mathbf{U}(1))$ SPT

The above construction for \mathbb{Z}_N^3 is a specific instance of a general connection between duality of (1 + 1)D edge \mathcal{G} SPT phases and a (2 + 1)D bulk $\mathcal{G} \times \mathcal{H}^2(\mathcal{G}, \mathbf{U}(1))$ SPT phase. This connection may be of independent interest. The action of the bulk $\mathcal{H}^2(\mathcal{G}, \mathbf{U}(1))$ symmetry can be thought of as pumping \mathcal{G} SPTs onto the edge.

Similarly to the case above, the Hilbert space of each spin is given by $\mathbb{C}[\mathcal{G}]$ and 4 spins are grouped per site of a square lattice. R_g denotes the right regular representation, we fix a choice of representative for a set of generators of $\mathcal{H}^2(\mathcal{G}, \mathbf{U}(1)) \cong \prod_k \mathbb{Z}_{N_k}$ (their products fix all other representatives) and

$$R_g^{\otimes 4} P_4 := \sum_{g \in \mathcal{G}} |hg^{-1}\rangle^{\otimes 4} \langle h|^{\otimes 4} \tag{4.96}$$

$$C\omega_{12} := \sum_{g_0, g_1} \omega(g_0 g_1^{-1}, g_1) |g_0, g_1\rangle \langle g_0, g_1| \tag{4.97}$$

$$u_\omega := C\omega_{12} C\omega_{23} C\omega_{34} C\omega_{41} \tag{4.98}$$

for $[\omega] \in \mathcal{H}^2(\mathcal{G}, \mathbf{U}(1))$.

The local Hamiltonian terms are given by

$$h_p = - \sum_{g \in \mathcal{G}} R_g^{\otimes 4} P_4 \otimes P_2 \otimes P_2 \otimes P_2 \otimes P_2 \tag{4.99}$$

acting on the square lattice similarly to the term in Eqn. 4.75. The ground state is again given by

$$|\Psi_{\text{GS}}\rangle = \bigotimes_p |GHZ_4\rangle. \tag{4.100}$$

The global on-site symmetry is generated by

$$U_g = \bigotimes R_g^{\otimes 4} \quad (4.101)$$

$$U_\omega = \bigotimes_b u_\omega^\dagger \bigotimes_w u_\omega \quad (4.102)$$

which can be seen to mutually commute and also commute with h_p . These symmetries also leave the ground state invariant.

As above, the effective edge spins are identified with the ground state subspace of plaquettes crossing the boundary, via the projector $\sum_g |g\rangle\langle gg|$. The action of the symmetry on the edge is given by

$$U_g \mapsto \bigotimes_i R_g \quad (4.103)$$

$$U_\omega \mapsto \prod_i C\omega_{2i,2i+1} C\omega_{2i-1,2i}^\dagger. \quad (4.104)$$

This forms a matrix product operator representation of $\mathcal{G} \times \mathcal{H}^2(\mathcal{G}, \text{U}(1))$ with 3-cocycle

$$\alpha((g_0, \omega_0), (g_1, \omega_1), (g_2, \omega_2)) = \omega_2(g_0, g_1). \quad (4.105)$$

The edge action of U_ω maps a \mathcal{G} SPT phase $[\beta]$ to $[\beta + \omega]$. This can be seen by examining the effect of U_ω on a fixed point local Hamiltonian such as the \mathcal{G} -paramagnet

$$H = - \sum_v \sum_g (R_g)_v. \quad (4.106)$$

Alternatively, note the edge action of U_ω restricted to an open chain is an MPO with two dangling virtual indices associated to its boundaries. Denote this MPO M_ω . M_ω obeys the following commutation rules $R_g^{\otimes L} M_\omega R_g^{\dagger \otimes L} = V_g M_\omega V_g^\dagger$. Here V_g is a projective representation of \mathcal{G} , with cocycle ω , given by

$$V_g = \sum_h \omega(h, g) |hg\rangle\langle h|, \quad (4.107)$$

which acts on one dangling virtual bond of the MPO. Hence applying M_ω to a unique symmetric ground state, such as $|+\rangle^{\otimes N}$, maps it to a state in the SPT phase $[\omega]$.

Chapter 5

Tensor Networks with a Twist: Anyon-permuting domain walls and defects in PEPS

JACOB C. BRIDGEMAN, STEPHEN D. BARTLETT AND ANDREW C. DOHERTY
CENTRE FOR ENGINEERED QUANTUM SYSTEMS, SCHOOL OF PHYSICS, THE UNIVERSITY OF SYDNEY, SYDNEY, AUSTRALIA

arXiv:[1708.08930](https://arxiv.org/abs/1708.08930)

Abstract

We study the realization of anyon-permuting symmetries of topological phases on the lattice using tensor networks. Working on the virtual level of a projected entangled pair state, we find matrix product operators (MPOs) that realize all unitary topological symmetries for the toric and color codes. These operators act as domain walls that enact the symmetry transformation on anyons as they cross. By considering open boundary conditions for these domain wall MPOs, we show how to introduce symmetry twists and defect lines into the state.

The low energy states of strongly interacting spin models can exhibit complex and exotic physics. A particularly interesting class of models are those that are topologically ordered [5.1–5.3]. The ground spaces of these models are promising candidates for robust storage of quantum information [5.4–5.8].

If quantum information is encoded in the degenerate ground space of topologically ordered systems, the action of anyon-permuting symmetries (APS) can be used to apply logical transformations [5.4]. These symmetries map among quasi-particle excitations without changing the topological phase. Large classes of symmetry actions give the potential for fault-tolerant logic manipulation, a prerequisite for effective quantum computation. Additionally, the introduction of symmetry defects can increase the functionality of the code for quantum computation [5.9]. It is therefore important to understand the interplay of symmetry and topological order in such spin models [5.10–5.16].

Recently, a connection has been made between fault-tolerant logical gates, locality-preserving symmetries and anyon-permuting domain walls. In particular, an equivalence was established between such logical gates and domain walls for topological stabilizer codes [5.17–5.20].

In this paper, we take this connection as our starting point and investigate realizations of such domain walls in two-dimensional topologically ordered models using projected entangled pair

states (PEPS) and matrix product operators (MPOs) [5.21–5.24]. These tools allow the efficient representation of ground states of topologically ordered models [5.25–5.29], and provide a useful framework for the construction of domain walls.

By working with two important examples, the toric and color codes, we show how to construct the domain walls corresponding to all APS and investigate their properties. In particular, we do this without modifying the underlying PEPS description of the state. We are further able to construct states containing APS defects [5.12–5.14, 5.30–5.34]. These defects enrich the properties of the underlying topological model. In particular, they may allow more exotic fusion and braiding than the original anyons [5.12, 5.13, 5.30], which can lead to increased computational power within a model of topological quantum computing. The defects can also be used to introduce additional encoded qubits, increasing the storage capacity of a code [5.9].

Although our discussion centers around two exactly solvable spin systems, the framework we are advocating should be far more general. PEPS make it straightforward to move away from simple fixed point models (models with zero correlation length). On the physical lattice, one expects the string operators associated to the anyons to ‘spread out’ into wider ribbons [5.35, 5.36], which makes the local action of the APS operators much more complicated, whilst on the virtual level of the PEPS these anyon string operators remain fully localized [5.29].

This paper is organized as follows: In Section 5.1 we review some ideas important to this work, and introduce some notation for the remainder of the paper. In Section 5.2 we introduce the toric code, including the anyon-permuting symmetries. We then introduce a PEPS for the ground states of this model and discuss the realization of an anyon-permuting domain wall on this PEPS. Finally, we show how to introduce APS defects carrying a definite generalized charge, and discuss fusion and parent Hamiltonians of such defects. In Section 5.3 we discuss the color code, a topological model with far richer symmetries than the toric code. We construct all domain walls of this topological phase, and the corresponding defects. In Section 5.4 we summarize the results and discuss possible extensions. For completeness, we include stabilizers for topological states with symmetry twists in Appendix 5.A, and construct the domain wall MPOs for the \mathbb{Z}_N generalizations of the toric code in Appendix 5.B.

5.1 Review: Topological order and PEPS

In this section, we review some key concepts, notation and conventions required for the remainder of the paper.

We begin with a discussion of topologically ordered phases, the kind of symmetries they support and the connections to fault-tolerant quantum computation. This motivates the discussion of locality preserving APS actions, domain walls, and defects. These topics form the primary objects of study in this paper.

We introduce PEPS, the main tool used in this work, and a streamlined notation we use throughout the paper. Following this, we discuss how local symmetries can be realized in PEPS for systems without topological order. This motivates our realization of APS domain walls using matrix product operators. We then describe topologically ordered PEPS, which form the basis of the remainder of the paper.

5.1.1 Topological order and anyon-permuting symmetries

For our purposes, an intrinsic topological phase is defined by a set of anyon labels $\{a_i\}$ and their braiding and fusion rules. These quasi-particles are a generalization of bosons and fermions, and

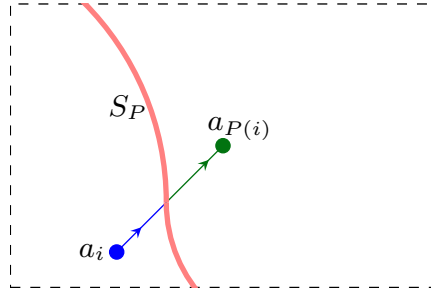


Figure 5.1: Domain walls S_P induce a permutation P on the set of anyons $\{a_i\}$ when they cross. To ensure the topological phase is the same on both sides of the wall, only permutations that preserve the matrices \mathcal{S} and \mathcal{T} of Eqn. 5.1 are allowed.

can exhibit more complex braid relations. These relations are captured by the \mathcal{T} and \mathcal{S} matrices of the theory

$$\mathcal{T}_a = \frac{1}{d_a} \text{loop}_a, \quad \mathcal{S}_{a,b} = \frac{1}{D} \text{cross}_{a,b}, \quad (5.1)$$

where d_a is the quantum dimension of anyon a and $D = \sqrt{\sum_a d_a^2}$ is the total quantum dimension. These matrices define the self- and mutual- braid relations of the particles respectively [5.11], and implicitly define the fusion rules.

We consider symmetries of the topological phase corresponding to a permutation of the anyon labels that preserves these braiding relations [5.12, 5.14–5.16, 5.18, 5.30–5.34]. We call this an anyon-permuting symmetry (APS). As a consequence, the fusion rules are also preserved. In particular, this means the vacuum must be invariant under any APS.

An anyon model can arise as the low energy spectrum of a gapped many-body spin model. On the microscopic spin model, the APS may be realized via some complicated operator. The essential features, however, are captured by the action on the emergent quasi-particles ¹.

In general, the action of an APS has no locality constraints, however it is natural to assume they will respect the underlying locality of the model. This means that the action of the symmetry should map local operators to local operators. The most simple example is a transversal (on-site) action, but more generally the APS may be realized as finite depth quantum circuits and spatial transformations such as translations.

Domain walls

When a locality preserving APS acts on some region \mathcal{R} of the lattice, it must act trivially far away from the boundary of \mathcal{R} . This is because, from the point of view of any operator within \mathcal{R} with support far from the boundary, the symmetry has been applied to the entire system. If the state to which the symmetry was applied was a ground state, far from the boundary the state still looks locally like a ground state. Conversely, if there was an anyon of type a_i within the region \mathcal{R} , it is transformed to an anyon of type $a_{P(i)}$, where P is some permutation. The symmetry operator can then be identified with a transparent domain wall in the vicinity of the boundary [5.18] of \mathcal{R} . Anyons are transformed when they cross such a domain wall as shown in Fig. 5.1.

¹A given spin model may break the APS, leading to a richer theory of symmetry enriched topological phases [5.12–5.16, 5.34]. We will focus on models that do not break the symmetry.

Topological order and fault-tolerant quantum computation

Topologically ordered models are of great interest in quantum information theory. Logical information can be encoded in the degenerate ground space of the model [5.4–5.8], and is protected from local noise processes by the topological properties of the model. A logical gate is any transformation that maps among the allowed logical states. In the case of a topological code this is any transformation that preserves the ground space. Since any APS preserves the ground space of a topologically ordered spin model, the action of such symmetries can be used to enact logical operations. Locality preserving APS are particularly interesting from a quantum information perspective. This kind of locality preservation means that the action does not spread errors in the code to the point where encoded information is corrupted, and is referred to as a fault-tolerant logical gate [5.6, 5.7]. A key question in quantum information is how to identify sets of fault-tolerant logic gates for a given quantum error correcting code [5.37–5.40]. The identification of anyon-permuting domain walls attempts to address this question for topological codes [5.18, 5.19].

5.1.2 Projected entangled pair states

In this section we review some of the key properties of PEPS representations of symmetric states, and some aspects of topologically ordered PEPS. For simplicity, we will assume translation invariance, although this is not crucial.

A PEPS representation of a state is described using a set of tensors A , which we represent as

$$A_{\alpha,\beta,\gamma,\delta}^i = \alpha \begin{array}{c} \beta \\ \square \\ \delta \\ i \end{array} \gamma, \quad (5.2)$$

where the greek indices are referred to as virtual, and the roman index is ‘physical’. A PEPS corresponds to a network of these tensors

$$|\psi[A]\rangle = \begin{array}{c} \square \square \square \square \\ \square \square \square \square \\ \square \square \square \square \\ \square \square \square \square \end{array}, \quad (5.3)$$

where a line joined to a pair of tensors indicates contraction of indices, and some choice of boundary conditions should be chosen. For a review of tensor network notation and PEPS, we refer the reader to Ref. 5.24. A tensor may have more than one physical index attached to it, and we will usually neglect drawing these to simplify the diagrams. Frequently, we will also suppress drawing the tensors themselves. They will be implied at the intersection of indices. The notation for the above state will therefore be

$$|\psi[A]\rangle = \begin{array}{c} | \\ | \\ | \\ | \\ | \\ | \\ | \\ | \\ | \\ | \end{array} \begin{array}{c} | \\ | \\ | \\ | \\ | \\ | \\ | \\ | \\ | \\ | \end{array}. \quad (5.4)$$

We now review the inclusion of local, physical symmetries in PEPS without intrinsic topological order, and the inclusion of topological order via a virtual symmetry. In Section 5.2, we show how these two properties can be combined.

Local symmetries in PEPS

Consider, for the moment, the class of PEPS describing ground states of systems with no topological order, and no spontaneous breaking of the symmetry. Within this class of PEPS, the action of a transversal symmetry on a region \mathcal{R} can be realized by an MPO domain wall acting on the virtual bonds around the edge [5.41] of \mathcal{R}

$$(5.5)$$

where the MPO tensors occur at the intersection of a red and black line. The four-index MPO tensors have two (black) indices acting on the virtual bonds of the PEPS, and two (red) ‘virtual’ indices. These virtual indices are contracted to give the operator. The MPOs are labelled by a group element g , and the collection of MPOs forms a representation of the symmetry group, so

$$(5.6)$$

The MPO can be pulled through the PEPS, leaving behind the physical symmetry action

$$(5.7)$$

thereby allowing the symmetry transformed domain to be enlarged. In this way, we can propagate the domain wall across the lattice, at the expense of a physical action. This ‘pulling through’ condition ensures the domain wall/symmetry correspondence holds on all regions.

This framework of virtual MPO representations allows for all symmetry protected topological phases with on-site symmetry action to be realized in PEPS [5.41]. As discussed in Section 5.1.2, a similar framework allows for the construction of PEPS with intrinsic topological order but no symmetry. The aim of this paper is to combine these two properties in familiar PEPS states, without altering the underlying topologically ordered state.

Topologically ordered PEPS

In this section, we briefly review a class of PEPS supporting intrinsic topological order. We restrict our discussion to \mathcal{G} -injective PEPS, which describe the ground states of quantum double models [5.25].

Unlike the PEPS discussed in Section 5.1.2, a \mathcal{G} -injective PEPS does not necessarily have any physical symmetry, but does support a virtual symmetry

$$(5.8)$$

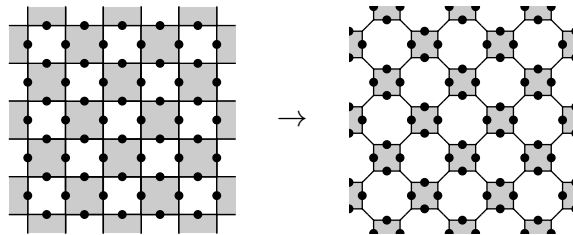


Figure 5.2: The toric code is defined on a square lattice, with spins on edges. It is convenient to write a PEPS tensor for each shaded plaquette. By inserting a bond at the vertex connecting adjacent gray plaquettes, a 4.8.8 lattice is obtained.

when sufficiently many PEPS tensors have been blocked together. This is not a gauge transformation as it holds at the single tensor level rather than u and u^\dagger being applied to adjacent tensors. This condition is encoding a version of Gauss' law for the anyons.

The PEPS is said to be injective if the tensor realizes an injective map from the virtual to physical indices. A PEPS with a virtual symmetry cannot be injective (if the representation u_g is not the trivial representation), but can be \mathcal{G} -injective, meaning the map is injective on the \mathcal{G} -invariant subspace.

Anyons can be represented on the virtual level of the PEPS [5.25, 5.42, 5.43]. Magnetic particles, labelled by a conjugacy class containing g , can be inserted into the PEPS by inserting open strings of u_g on the virtual level. The bulk of these strings can be deformed using Eqn. 5.8, but the end points are pinned in place and can therefore be measured. Electric (e) charges, labelled by an irreducible representation χ , can also be included. For simplicity, assume that \mathcal{G} is abelian. An e particle can then be inserted using an operator X_χ on the virtual level such that $X_\chi u_g = \chi(g) u_g X_\chi$, which ensures the correct braiding relations. We remark that the insertion of an electric particle is not associated to a string. One can therefore define a state with a single e , but there is no physical operator that can construct such a state. We will describe this for the special case $\mathcal{G} = \mathbb{Z}_2$ in Section 5.2.

5.2 Anyon-permuting symmetries of the toric code

In this section, we find an MPO that realizes the \mathbb{Z}_2 APS of the simplest topological phase, the toric code [5.5]. This model describes a phase with a topological order known as the \mathbb{Z}_2 quantum double. We will first introduce the model and a PEPS realizing this topological order.

The topological phase is defined by four anyons, conventionally labelled $\{1, e, m, em\}$. The fusion rules are $a \times a = 1$ for all anyons and $e \times m = em$. The only nontrivial element of the \mathcal{T} matrix is $\mathcal{T}_{em} = -1$, whilst all nontrivial \mathcal{S} matrix elements are obtained from $\mathcal{S}_{e,m} = -1/2$. The only APS is a \mathbb{Z}_2 symmetry defined by the action $\mathcal{D}(e) = m$ and $\mathcal{D}(m) = e$. Note that this APS is distinct from the \mathbb{Z}_2 symmetry defining the phase, which preserves the charge mod 2.

5.2.1 Topological PEPS

To construct the minimal square lattice PEPS realizing the \mathbb{Z}_2 quantum double topological order, we consider Eqn. 5.8 with $u_g = Z$, the qubit Pauli Z operator. To construct a \mathbb{Z}_2 -injective PEPS with this symmetry, we must ensure the dimension of the PEPS tensor in Eqn. 5.8 is at least $2^4/2$, since there are four virtual bonds each with dimension 2 and half of the virtual space is symmetric (the even-parity subspace). It is therefore convenient to construct a PEPS tensor for each shaded plaquette in Fig. 5.2, so that there are four physical qubits per tensor.

Due to the topological order, the tensor must have a local, virtual \mathbb{Z}_2 symmetry

$$\begin{array}{|c|} \hline Z \\ \hline \square \\ \hline Z \\ \hline \end{array} = \begin{array}{|c|} \hline \square \\ \hline \end{array}, \quad (5.9)$$

and must be an injective map (on the \mathbb{Z}_2 -invariant subspace) from virtual to physical indices [5.25]. It is straightforward to check that a PEPS with nonzero elements

$$\begin{array}{|c|} \hline l+i \quad i+j \\ \hline l \quad j \\ \hline k+l \quad j+k \\ \hline \end{array} = 1, \quad (5.10)$$

has this symmetry. Here, we place a physical spin on each horizontal/vertical edge, diagonal edges correspond to the virtual indices, and all additions are taken modulo 2.

Anyons can be represented directly on the virtual bonds of the PEPS. As discussed in Section 5.1.2, a state with a pair of m particles is created by

$$\begin{array}{|c|} \hline \square \quad \square \quad \square \\ \hline \diagdown \quad \diagup \quad \diagdown \\ \hline \square \quad \square \quad \square \\ \hline \diagup \quad \diagdown \quad \diagup \\ \hline \square \quad \square \quad \square \\ \hline \end{array}, \quad (5.11)$$

where the path of the string is arbitrary since the virtual symmetry Eqn. 5.9 can be used to move it. A state with two e anyons is created by

$$\begin{array}{|c|} \hline \square \quad \square \quad \square \\ \hline \diagdown \quad \diagup \quad \diagdown \\ \hline \square \quad \square \quad \square \\ \hline \diagup \quad \diagdown \quad \diagup \\ \hline \square \quad \square \quad \square \\ \hline \end{array}, \quad (5.12)$$

where the X operators are only placed at the end points of the string, corresponding to the location of the excitations. Unlike the m type anyons, there is no string associated to the e particles on the virtual level of the PEPS. In this sense, the e anyons are ‘localized’ since the presence of an X operator signals the location of a particle. On the other hand, a Z does not signal the location of an m since strings of Z operators can be fluctuated through the PEPS using Eqn. 5.9. It is therefore possible to define a single e particle, by inserting a single X operator, although there is no operation on the physical bonds that creates such a state. Conversely, no state with a single m excitation can be defined.

5.2.2 Anyon-permuting symmetry

The only APS of this model is the transformation $e \leftrightarrow m$. On the virtual level, this can be implemented by an operator that transforms pairs of X operators to strings of Z s. We recognize this transformation as the Ising duality map $\mathcal{D}^{(o)}$

$$\mathcal{D}^{(o)\dagger} X_j \mathcal{D}^{(o)} = \prod_{k \leq j} Z_k \quad (5.13)$$

$$\mathcal{D}^{(o)\dagger} Z_j \mathcal{D}^{(o)} = X_j X_{j+1} \quad (5.14)$$

performs has the desired action. On a line, this can be implemented by the circuit

$$\mathcal{D}^{(o)} = \begin{array}{c} \boxed{H} \\ \bullet \\ \oplus \end{array} \begin{array}{c} \boxed{H} \\ \bullet \\ \oplus \end{array} \begin{array}{c} \boxed{H} \\ \bullet \\ \oplus \end{array} \begin{array}{c} \boxed{H} \\ \bullet \\ \oplus \end{array} \begin{array}{c} \boxed{H} \\ \bullet \\ \oplus \end{array} \begin{array}{c} \boxed{H} \\ \bullet \\ \oplus \end{array}, \quad (5.15)$$

where H is the Hadamard operator and $\bullet\text{---}\oplus$ is the controlled- X operator.

Since domain walls act around closed paths, corresponding to the boundary of a domain of symmetry action, it is important to define a periodic version of this circuit. This can be done by noting that the circuit \mathcal{D} is realized by the MPO

$$\mathcal{D}^{(o)} = \begin{array}{c} \boxed{\tilde{H}} \\ \boxed{\tilde{H}} \\ \boxed{\tilde{H}} \end{array} \begin{array}{c} \boxed{\tilde{H}} \\ \boxed{\tilde{H}} \\ \boxed{\tilde{H}} \end{array} \begin{array}{c} \boxed{\tilde{H}} \\ \boxed{\tilde{H}} \\ \boxed{\tilde{H}} \end{array} \begin{array}{c} \boxed{\tilde{H}} \\ \boxed{\tilde{H}} \\ \boxed{\tilde{H}} \end{array} \begin{array}{c} \boxed{\tilde{H}} \\ \boxed{\tilde{H}} \\ \boxed{\tilde{H}} \end{array} \begin{array}{c} \boxed{\tilde{H}} \\ \boxed{\tilde{H}} \\ \boxed{\tilde{H}} \end{array}, \quad (5.16)$$

where $\tilde{H} = \sqrt{2}H$, and

$$\begin{array}{c} j \\ \diagdown \\ i \\ \diagup \\ k \end{array} = \begin{cases} 1 & \text{if } i = j = k \\ 0 & \text{otherwise} \end{cases}. \quad (5.17)$$

The virtual indices of this MPO can be connected to produce a periodic operator that will be referred to as \mathcal{D} . The translationally invariant domain wall MPO is defined by

$$\begin{array}{c} \rightarrow \\ \boxed{\mathcal{D}} \\ \rightarrow \end{array} = \begin{array}{c} \boxed{H} \\ \boxed{H} \\ \boxed{H} \end{array}, \quad (5.18)$$

where the arrow indicates that in Eqn. 5.14 we made a choice $Z_j \rightarrow X_j X_{j+1}$ rather than $Z_j \rightarrow X_{j-1} X_j$.

Since this MPO tensor is injective (as a map from virtual to physical indices), the tensor is unique up to gauge transformations [5.44]. One such gauge transformation is the choice to block \tilde{H} on the right, rather than the left, of the tensor in Eqn. 5.16.

On periodic boundaries, this operator ceases to be unitary, but remains an isometry up to a rescaling of $1/\sqrt{2}$. This can be seen by noting that

$$\begin{array}{c} \rightarrow \\ \boxed{\mathcal{D}} \\ \rightarrow \\ \boxed{\mathcal{D}^\dagger} \\ \rightarrow \end{array} = \begin{array}{c} \rightarrow \\ \boxed{u} \\ \rightarrow \\ \boxed{F} \\ \rightarrow \\ \boxed{u^\dagger} \\ \rightarrow \end{array}, \quad (5.19)$$

where

$$\begin{array}{c} \rightarrow \\ \boxed{F} \\ \rightarrow \end{array} = \begin{pmatrix} \mathbb{1} & 0 & 00 \\ 0 & Z & 00 \\ X & 0 & 00 \\ 0 & XZ & 00 \end{pmatrix}, \quad (5.20)$$

and u is a unitary gauge transformation. The notation here identifies left (right) virtual indices to row (column) indices of the matrix and up (down) physical indices (black) correspond to operator indices of matrix entries.

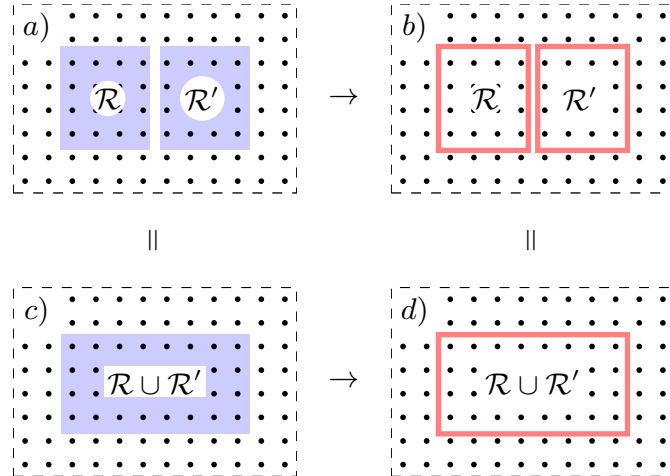


Figure 5.3: Applying a transversal (on-site) symmetry to regions \mathcal{R} and \mathcal{R}' (a) corresponds to domain walls at the boundaries $\partial\mathcal{R}$ and $\partial\mathcal{R}'$ (b). If the symmetry is transversal, is the same as applying the symmetry to $\mathcal{R} \cup \mathcal{R}'$ (c), so the domain walls should merge (d). For a non-transversal symmetry, a nontrivial operator will remain along the merge.

The matrix u is unitary, so on periodic MPOs, these cancel with u^\dagger from the neighboring tensor. The off-diagonal elements of F do not contribute on periodic MPOs since the trace (with respect to the virtual indices) is taken. The MPO on N sites is therefore $\mathbb{1}^{\otimes N} + Z^{\otimes N}$, corresponding to (twice) the projector onto the even parity subspace. On this subspace, which corresponds to the support of the PEPS, \mathcal{D} is unitary. We remark that the wall defined by \mathcal{D}^\dagger permutes the set of anyons in the same way as \mathcal{D} , so corresponds to the same topological symmetry action.

By using the representation of anyons on the PEPS, along with the \mathbb{Z}_2 APS, we have constructed an explicit MPO realizing the APS. For the remainder of this section we describe the properties of this domain wall MPO, including how to terminate open walls to create APS twists with definite generalized topological charge.

Algebra of domain walls

It is important to understand the algebra of the domain walls so that the action of multiple walls can be computed. As an example, we will study the effect of applying the APS operator to disjoint regions of the lattice. The MPOs form a representation the APS group when multiplied along their whole length, as in Eqn. 5.6, but not at the local tensor level. Therefore, the multiplication of domain walls on regions such as that in Fig. 5.3b) cannot be deduced directly from the group multiplication.

Consider applying an APS to adjacent regions \mathcal{R} and \mathcal{R}' as depicted in Fig. 5.3. This corresponds to applying domain walls around the two boundaries $\partial\mathcal{R}$ and $\partial\mathcal{R}'$. For a transversal (on-site) action, the action on the full region $\mathcal{R} \cup \mathcal{R}'$, so the domain walls should merge, leaving a single wall around $\partial(\mathcal{R} \cup \mathcal{R}')$. For a non-transversal action, corresponding to a finite depth circuit, acting on \mathcal{R} and \mathcal{R}' separately is not equivalent to acting on $\mathcal{R} \cup \mathcal{R}'$ (i.e. Fig. 5.3a and Fig. 5.3c are not equal). There are missing gates along the shared boundary.

We study this merging effect using the domain wall constructed in Eqn. 5.18. To determine the difference between Fig. 5.3b and Fig. 5.3d, we proceed by applying the inverse of the larger wall (d), followed by the action on the smaller regions (b). If the APS is realized transversally these actions will cancel out, but if the symmetry is merely locality preserving there will be an action along the

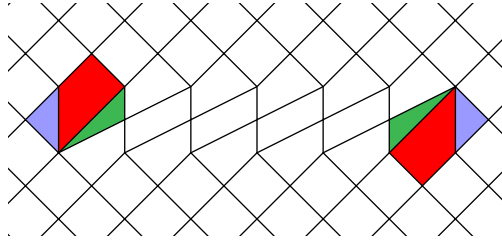


Figure 5.4: When merging two domain walls, the lattice geometry is altered along the wall. This is because the symmetry does not act transversally. Along the interface, a lattice translation is implemented. The colors correspond to those in the tensor network of Eqn. 5.22.

‘join’. Denoting \mathcal{D}^\dagger by a blue line and \mathcal{D} by a red line, the action on the PEPS is

$$\begin{aligned}
 & \text{Diagram with blue and red lines} = \sum_{i,j=0}^1 \text{Diagram with indices } i, j, i', j' \\
 & \hspace{15em} (5.21)
 \end{aligned}$$

$$\begin{aligned}
 & \text{Diagram with colored regions} \\
 & \hspace{15em} (5.22)
 \end{aligned}$$

where

$$\begin{aligned}
 & \text{Diagram with indices } i, j, k \\
 & \hspace{15em} (5.23)
 \end{aligned}$$

Recall that our notation only indicates virtual indices, with a tensor at each vertex. The colors in the PEPS diagram of Eqn. 5.22 are included for comparison with the lattice diagram in Fig. 5.4 as described below. The presence of a nontrivial operation along the line where the MPOs were merged indicates the symmetry is not transversal.

The end points of this line correspond to lattice dislocations as shown in Fig. 5.4a. The state (5.22) is the ground state of the toric code defined on this lattice. By performing unitary gates and adding/removing ancilla qubits along the defect line, the lattice geometry can be restored. We remark that this line has no effect on the anyons, and so corresponds to a topologically trivial symmetry.

In this section, we have identified the behavior of MPO domain walls corresponding to symmetry action on adjacent regions of the toric code. From this we observed that the physical APS action is not transversal (on-site), rather the merging of walls leads to a lattice dislocation.

Symmetry action on excited states

The domain wall constructed in Eqn. 5.18 corresponds to the action of the symmetry on the vacuum. We want to understand how to transform other low energy states, namely those with anyons inserted. This will allow us to propagate the domain wall across the lattice. From a quantum computing perspective, this will allow us to understand the action of fault-tolerant logic gates on states with local errors. Since the APS action permutes the set of anyons, we expect the anyons in the interior of the domain to be transformed appropriately.

Following Ref. 5.30, we define a generalized charge as a twist that is invariant under this process.

For the toric code, Eqn. 5.26, reduces to

$$\begin{array}{c} \rightarrow \\ \mathcal{D} \rightarrow \mathcal{D} \rightarrow XZ \rightarrow \textcircled{v} \end{array} = \lambda \begin{array}{c} \rightarrow \\ \mathcal{D} \rightarrow \mathcal{D} \rightarrow \textcircled{v} \end{array}. \quad (5.27)$$

The ends should therefore be chosen to be eigenstates of XZ . We will refer to the twist with $v = |\pm i\rangle$ as the end vector as σ_{\pm} for consistency with Ref. 5.30. Choosing other end points corresponds to a superposition of σ_+ and σ_- .

We will now explore the topological properties of the twist defects resulting from this construction.

Fusion

We can use the twist MPOs to compute the enriched fusion rules. Fusing a twist with an m excitation

$$\begin{array}{c} \text{Diagram 1} \\ \text{Diagram 2} \\ \text{Diagram 3} \end{array} = \begin{array}{c} \text{Diagram 4} \\ \text{Diagram 5} \\ \text{Diagram 6} \end{array}, \quad (5.28)$$

changes the type of twist at the end point. The same is true when an e is fused with a twist

$$\begin{array}{c} \text{Diagram 1} \\ \text{Diagram 2} \\ \text{Diagram 3} \end{array} = \pm i \begin{array}{c} \text{Diagram 4} \\ \text{Diagram 5} \\ \text{Diagram 6} \end{array}. \quad (5.29)$$

The situation is more complicated when two twists are fused. Following the discussion of domain wall mergers in Section 5.2.2, we consider fusing a twist at the end of a \mathcal{D} line with one that terminates a \mathcal{D}^\dagger wall. If one instead attempted to fuse a pair of \mathcal{D} , there would be some topologically trivial transformation (corresponding to a lattice translation) which may conceal the nontrivial action. The result is

$$\begin{array}{c} \text{Diagram 1} \\ \text{Diagram 2} \\ \text{Diagram 3} \end{array} = \begin{array}{c} \text{Diagram 4} \\ \text{Diagram 5} \\ \text{Diagram 6} \end{array}, \quad (5.30)$$

$$\begin{array}{c} \text{Diagram 1} \\ \text{Diagram 2} \\ \text{Diagram 3} \end{array} = \begin{array}{c} \text{Diagram 4} \\ \text{Diagram 5} \\ \text{Diagram 6} \end{array}, \quad (5.31)$$

where

$$\begin{array}{c} | \\ \hline \hline \end{array} = \begin{pmatrix} 1 & 0 \\ 0 & Z \end{pmatrix} \quad (5.32)$$

$$\begin{array}{c} \text{Diagram 1} \\ \text{Diagram 2} \\ \text{Diagram 3} \end{array} = \begin{pmatrix} 1 & 0 \\ 0 & 1 \\ 0 & 0 \\ 0 & 0 \end{pmatrix} \quad (5.33)$$

$$\begin{array}{c} \textcircled{a_{\pm}} \\ \downarrow \end{array} = \frac{1}{\sqrt{2}} \begin{pmatrix} \mathbb{1} \\ \pm i ZX \end{pmatrix} \quad (5.34)$$

$$\begin{array}{c} \textcircled{b_{\pm}} \\ \downarrow \end{array} = \frac{1}{\sqrt{2}} \begin{pmatrix} X \\ \pm i Z \end{pmatrix}. \quad (5.35)$$

The notation here identifies left (right) virtual indices to row (column) indices of the matrix and up (down) physical indices (black) correspond to operator indices of matrix entries. Therefore, fusing σ_{\pm} with σ_{\pm} leaves a superposition of: a string of $\mathbb{1}$ terminated at the location of the tensor marked a_{\pm} by a $\mathbb{1}$ (i.e. vacuum), and a string of Z terminated by ZX (i.e. an m and e at the same place, so therefore an em particle). The fusion of σ_{\pm} with σ_{\mp} gives a superposition of: a string of $\mathbb{1}$ terminated by an X (an e), and a string of Z terminated by a Z (an m). The full set of fusion rules (neglecting phases) of the defects are therefore

$$\sigma_{\pm} \times e = \sigma_{\mp} \quad \sigma_{\pm} \times m = \sigma_{\mp} \quad (5.36)$$

$$\sigma_{\pm} \times \sigma_{\pm} = 1 + em \quad \sigma_{\pm} \times \sigma_{\mp} = e + m. \quad (5.37)$$

These rules are consistent with the known rules for this enriched model [5.30]. This shows that the MPO construction gives an explicit realization of these defects.

Hamiltonian terms for twists

Using the domain wall/twist MPOs, one can construct Hamiltonians whose ground states correspond to the PEPS with twists inserted. One such set of Hamiltonian terms is

$$S = \left\{ \begin{array}{c} \text{---} X \text{---} \\ \text{---} X \text{---} \\ \text{---} X \text{---} \end{array}, \begin{array}{c} Z \\ \text{---} Z \\ \text{---} Z \end{array}, \begin{array}{c} \text{---} X \text{---} \\ \text{---} X \text{---} \\ \text{---} Z \end{array}, \begin{array}{c} \text{---} Z \text{---} \\ \text{---} X \text{---} \\ \text{---} X \end{array}, \begin{array}{c} \text{---} X \text{---} \\ \text{---} X \text{---} \\ \text{---} Z \end{array}, \begin{array}{c} \text{---} X \text{---} \\ \text{---} X \text{---} \\ \text{---} Z \end{array}, \begin{array}{c} \text{---} X \text{---} \\ \text{---} X \text{---} \\ \text{---} Y \end{array}, \begin{array}{c} \text{---} X \text{---} \\ \text{---} X \text{---} \\ \text{---} Y \end{array} \right\}, \quad (5.38)$$

where the final two terms correspond to the location of a twist of type σ_{\pm} . By contracting these terms against the PEPS tensors, one can check that the PEPS is a +1 eigenstate of each. Since these terms are commuting stabilizers, the PEPS is the ground state of $H = -\sum_{h \in S} h$. We remark that this Hamiltonian was constructed without needing knowledge of the physical action of the APS on the underlying spin model, only the action on the anyon theory. Since the ground states of the toric code with twist defects gives increased functionality for quantum computation compared with the bare model [5.9], it is important to know how to prepare such states. The parent Hamiltonian construction for PEPS [5.25, 5.45] may provide a way to find such Hamiltonians away from fixed point models, where the physical APS action may be complicated.

5.3 Color Code

As a second illustrative example, we now construct the domain wall MPOs for a model with a richer APS group than that of the toric code: the color code or $\mathbb{Z}_2 \times \mathbb{Z}_2$ quantum double. This phase is particularly interesting from a quantum computing viewpoint, since the APS group is sufficiently rich that the full logical Clifford group can be implemented. This is the largest group of gates that can be fault-tolerantly implemented on a 2D qubit stabilizer or subsystem code [5.39, 5.46].

The color code is locally equivalent to two copies of the toric code [5.38, 5.40]. We will make extensive use of this equivalence. The color code phase therefore has 16 abelian anyons, referred to as e_T, e_B, m_T, m_B and their fusion products. The anyons labeled T (top) and those labeled B (bottom) independently generate two copies of the toric code particles. The \mathcal{T} matrix of the theory

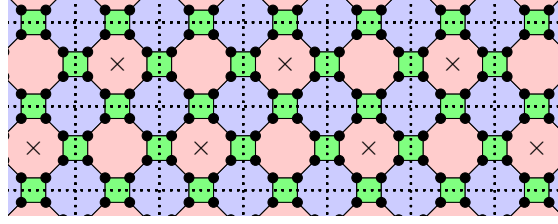


Figure 5.6: The color code is defined on a three-colorable lattice. In this work, we consider the 4.8.8 lattice for simplicity. Qubits are located on the vertices. By applying a unitary transformation to each green square of qubits, the color code can be decoupled into a pair of toric codes (located on the dashed lattice) and a pair of local qubits. The PEPS tensors end up centered on the plaquettes indicated by ‘x’.

is defined by $\mathcal{T}_{e_i m_j} = -\delta_{i,j}$, where $e_i m_j := e_i \times m_j$ and $\delta_{i,j} = 1$ if $i = j$. The \mathcal{S} matrix is defined by $\mathcal{S}_{e_i, m_j} = -\delta_{i,j}/4$. Unlike the toric code, the symmetry group of this theory is nonabelian, and has 72 elements. We will discuss the APS in detail in Section. 5.3.1.

A stabilizer Hamiltonian that realizes the two dimensional color code can be defined on any three-colorable, three-valent lattice. In particular, we specify to the 4.8.8 lattice (Fig. 5.6) for simplicity. The Hamiltonian defining the code is

$$H_{CC} = - \sum_{p \in \text{plaq.}} (\bar{X}_p + \bar{Z}_p), \quad (5.39)$$

where \bar{P}_p indicates the tensor product of P acting on all spins in plaquette p .

On the lattice, the equivalence to two copies of the toric code can be seen by acting with a local unitary circuit. This circuit acts independently on each green (square) plaquette. It is convenient to number the qubits

$$(5.40)$$

where the dotted lines correspond to those in Fig. 5.6. The circuit then acts as

$$(5.41)$$

with the leftmost gate being applied first. In this transformed code, the ‘ L ’ qubits are fully localized, with the ground state being $|0\rangle^{\otimes N}$, so can be discarded. On the remaining spins, the Hamiltonian corresponds to two independent toric codes, one defined on the ‘top’ T qubits and the other on the ‘bottom’ B spins. As mentioned above, the color code is interesting despite this equivalence as the full Clifford group can be implemented transversally.

At all (green) plaquettes, the output qubits are labelled

$$(5.42)$$

Following this transformation, the stabilizers of the color code become

$$\bar{X}_R \mapsto \begin{array}{c} \cdots X_T \cdots \\ \dot{X}_T \quad X_T Z_{L_1} \\ \cdots X_T Z_{L_1} \cdots \end{array} \quad \bar{Z}_R \mapsto \begin{array}{c} \cdots X_B \cdots \\ \dot{X}_B \quad X_B Z_{L_2} \\ \cdots X_B Z_{L_2} \cdots \end{array} \quad (5.43)$$

$$\bar{X}_B \mapsto \begin{array}{c} \cdot \cdot \cdot \\ \cdot Z_B Z_{L_1} \cdot \\ \cdot Z_B \cdot \\ \cdot \cdot \cdot \end{array} \cdot Z_B \cdot \quad \bar{Z}_B \mapsto \begin{array}{c} \cdot \cdot \cdot \\ \cdot Z_T Z_{L_2} \cdot \\ \cdot Z_T \cdot \\ \cdot \cdot \cdot \end{array} \quad (5.44)$$

$$\bar{X}_G \mapsto Z_{L_1}, \quad \bar{Z}_G \mapsto Z_{L_2}, \quad (5.45)$$

where the new code is defined on the dotted lattice in Fig. 5.6 with four spins per edge. The PEPS tensor for this code is simply two copies of that in Eqn. 5.10



$$:= \quad (5.46)$$

To construct the full PEPS tensor for the color code, the discarded L qubits need to be inserted and the (inverse of) the circuit Eqn. 5.41 applied.

5.3.1 Excitations, anyon-permuting symmetries and domain wall operators

We now introduce a generating set of APS transformations for the color code anyons [5.18], and then construct domain wall MPOs implementing the appropriate transformation. The color code supports four anyons and their fusion products. Generating anyons correspond to violating either a Z or X type plaquette of color red or blue. We will refer to these particles using these labels, for example the anyon corresponding to a violation of a red Z type stabilizer will be labelled r_z , whilst b_x will refer to a violation of a blue X type plaquette. The green particles can be seen as a fusion of these, for example $g_z = r_z \times b_z$. We can use the circuit (5.41) to find the toric code anyons corresponding to those in the color code

$$r_x \mapsto e_T \quad b_z \mapsto m_T \quad (5.47)$$

$$r_z \mapsto e_B \quad b_x \mapsto m_B. \quad (5.48)$$

The permuting symmetries of these particles correspond to permutations of Pauli labels and exchanging Pauli labels and colors. Following the notation of Ref. 5.18, we label the symmetry elements as W_i . The APS group is generated by the 3-cycle $z \rightarrow x \rightarrow xz$

	Color code	Toric codes	
$W_1 :$	$r_z \mapsto r_x$	$e_B \mapsto e_T$	(5.49)
	$b_z \mapsto b_x$	$m_T \mapsto m_B$	
	$r_x \mapsto r_x r_z$	$e_T \mapsto e_T e_B$	
	$b_x \mapsto b_x b_z$	$m_B \mapsto m_T m_B$	

the 2-cycle $x \leftrightarrow z$

$W_2 :$	$r_z \mapsto r_x$	$e_B \mapsto e_T$	(5.50)
	$b_z \mapsto b_x$	$m_T \mapsto m_B$	
	$r_x \mapsto r_z$	$e_T \mapsto e_B$	
	$b_x \mapsto b_z$	$m_B \mapsto m_T$	

and the Pauli/color exchanging transformation $r \leftrightarrow x, b \leftrightarrow z$

$W_5 :$	$r_z \mapsto b_x r_x$	$e_B \mapsto m_B$	(5.51)
	$b_z \mapsto b_z$	$m_T \mapsto m_T$	
	$r_x \mapsto r_x$	$e_T \mapsto e_T$	
	$b_x \mapsto r_z$	$m_B \mapsto e_B$	

We have already seen that the toric code supports an $e \leftrightarrow m$ APS. The color code therefore supports this symmetry too. Applying this duality to the bottom toric code corresponds to W_5 . The transformation W_2 corresponds to swapping the two toric codes. The operator W_1 corresponds to a transversal controlled X gate from the top toric code to the bottom, followed by a swap. It will be more convenient to work with the generators $\{\tilde{W}_1 = W_2W_1, W_2, W_5\}$.

Domain wall operators

It is very straightforward to construct domain wall MPOs for the color code PEPS. The wall corresponding to W_5 is simply the one constructed in Eqn. 5.18 on the second toric code, with identity on the first. The wall operator for \tilde{W}_1 is a controlled X operator on each doubled bond, controlled on the top toric code. Finally, the wall for W_2 is a swap gate applied to each doubled bond.

$$\tilde{W}_1 \rightarrow \text{Diagram 1}, \quad (5.52)$$

$$W_2 \rightarrow \text{Diagram 2}. \quad (5.53)$$

5.3.2 Anyon-permuting symmetry twists for the color code

The APS twists for \tilde{W}_1 and W_2 are straightforward to construct as the MPO already has trivial bond dimension and the twists correspond to definite generalized charges. Using the same arguments as in Sec. 5.2.3, one can check that the modified Hamiltonian terms for \tilde{W}_1 are

$$\left\{ \begin{array}{c} Y-Y \\ X-X \\ X-X \\ Y-Y \end{array}, \begin{array}{c} X-X \\ Y-Y \\ X-X \\ Y-Y \end{array}, - \begin{array}{c} Y-Y \\ X-X \\ X-X \\ Y-Y \end{array}, - \begin{array}{c} X-X \\ Y-Y \\ X-X \\ Y-Y \end{array}, \begin{array}{c} Z-Z \\ Z-Z \\ Z-Z \\ Z-Z \end{array} \right\}, \quad (5.54)$$

where the X type term at the location of the twist is removed. For the twists associated with W_2 , the modified terms are

$$\left\{ \begin{array}{c} Z-Z \\ X-X \\ Z-Z \\ X-X \end{array}, \begin{array}{c} X-X \\ Z-Z \\ X-X \\ Z-Z \end{array}, \begin{array}{c} X-X \\ Z-Z \\ X-X \\ Z-Z \end{array}, \begin{array}{c} Z-Z \\ X-X \\ Z-Z \\ X-X \end{array}, \begin{array}{c} X-X \\ Z-Z \\ X-X \\ Z-Z \end{array}, \begin{array}{c} Z-Z \\ X-X \\ Z-Z \\ X-X \end{array}, \begin{array}{c} X-X \\ Z-Z \\ X-X \\ Z-Z \end{array}, \begin{array}{c} Z-Z \\ X-X \\ Z-Z \\ X-X \end{array}, \begin{array}{c} Y-Y \\ Y-Y \\ Y-Y \\ Y-Y \end{array} \right\}, \quad (5.55)$$

where the Y type operator at the twist location is the only term there. For W_5 , the modified terms are

$$\left\{ \begin{array}{c} Z-Z \\ X-X \\ Z-Z \\ X-X \end{array}, \begin{array}{c} X-X \\ Z-Z \\ X-X \\ Z-Z \end{array}, \begin{array}{c} Z-Z \\ X-X \\ Z-Z \\ X-X \end{array}, \begin{array}{c} X-X \\ Z-Z \\ X-X \\ Z-Z \end{array}, \pm \begin{array}{c} Z-Z \\ X-X \\ Z-Z \\ X-X \end{array}, \pm \begin{array}{c} X-X \\ Z-Z \\ X-X \\ Z-Z \end{array} \right\}. \quad (5.56)$$

Although these Hamiltonians were not constructed using the usual parent Hamiltonian approach, we posit that such a construction could be used to find gapped Hamiltonian for more general APS twists. The Hamiltonian terms for these states at the level of the doubled toric code are provided in Appendix 5.A.

5.3.3 Symmetry protected nature of the domain wall

It was noted in Ref. 5.18 that the domain wall \tilde{W}_1 is associated with a one-dimensional Hamiltonian in a nontrivial $\mathbb{Z}_2 \times \mathbb{Z}_2$ symmetry protected topological (SPT) phase. Given the MPOs we have constructed, we can explore this correspondence in the MPO framework. On the physical lattice, this required the definition of an ‘excitation basis’. Using this basis required care as a state corresponding to a single anyon is unphysical. In the framework of PEPS, this observation becomes straightforward.

Since the \tilde{W}_1 domain wall acts on the top toric code with only $\mathbb{1}$ and Z , it can only create 1 and m anyons. On the bottom toric code, only 1 and e particles can be created.

Looking at Eqn. 5.12, we notice that the e particle becomes ‘localized’ on the PEPS. By this we mean that the occurrence of an X operator on the virtual level signals the location of an excitation, with no string attached to it. When looking for the presence on an m particle, it is not enough to look at a single bond since a Z may be part of a string. By modifying the PEPS, we can ‘localize’ all particles to a single bond in this sense. The modified PEPS is

$$(5.57)$$

where the top (red) PEPS tensor is that in Eqn. 5.10 with a Hadamard gate contracted onto each index, both virtual and physical. The bottom (blue) tensor is left unchanged. Red bonds of this new PEPS correspond to plaquettes in the top toric code. On this PEPS, m_T excitations are created by inserting X onto the appropriate red bond, whilst m_B still corresponds to X on the appropriate blue bond. There are no strings for either type of excitation, and in this way the existence of an X directly corresponds to an excitation.

On this PEPS, we can write the \tilde{W}_1 wall as

$$(5.58)$$

where the virtual gate is a controlled phase gate in the X basis. This circuit can be recognized as the one that creates the cluster state [5.47, 5.48] from the vacuum $|0\rangle^{\otimes N}$. The domain wall therefore has nontrivial SPT order with respect to a $\mathbb{Z}_2 \times \mathbb{Z}_2$ symmetry. On this modified PEPS, the virtual symmetry identifying the topological phase is

$$(5.59)$$

which commutes with the circuit Eqn. 5.58. We therefore see that the SPT nature of this domain wall is protected by the virtual symmetry present throughout the phase, rather than being associated with any property of the stabilizer code.

A similar analysis could be performed for other walls, for example $W_2\tilde{W}_1W_2$. In this case, we would also identify the wall as having an SPT property since the MPO is as in Eqn. 5.52, but with the control and target qubits exchanged. We believe that this framework of virtual MPOs provides a promising avenue to understanding the origin and nature of this SPT.

5.4 Conclusions

We have investigated the interplay between topological order and anyon-permuting symmetries in projected entangled pair states. By finding anyon-permuting domain walls, in the form of matrix product operators, we have realized the full APS in two models of interest.

Using these MPOs, we have shown how to introduce APS defect (twists) into the PEPS by finding appropriate boundary conditions for the MPO. This allows the defect fusion rules to be obtained directly on the PEPS. Further, Hamiltonians that realize the PEPS with twist insertions can easily be constructed.

The most obvious extension of this work is to the more general class of MPO-injective PEPS [5.28, 5.29, 5.49]. This class realizes all known topological orders, by using virtual MPO symmetries in place of the virtual group symmetry in Eqn. 5.8. The examples we have discussed generalize straightforwardly to that framework, but a general condition for permuting anyons is unclear. In particular, we do not know how to formulate a local rule for finding an MPO tensor such that the full MPO performs the appropriate permutation of anyon sectors.

This work aimed to construct domain wall operators without otherwise altering the PEPS. In particular, we did not require that the APS acts in a transversal manner. Using a generalization of the string-net PEPS tensors [5.28, 5.29], one can construct states and MPO domain walls for symmetry enriched topological orders with an transversal symmetry action [5.50]. Ref. 5.50 requires that the symmetry action can be made transversal. As a result of our work, we conjecture that the restriction to transversal APS is not required.

It would be interesting to deform the PEPS away from the fixed point and observe the effect on the domain wall operators. In particular, we expect the SPT discussed in Section 5.3.3 to be a property of the topological phase. It would be interesting to investigate the breakdown at the phase transition to a trivial phase.

One of the primary uses of PEPS is as a variational class for numerical optimization. The identification of domain wall MPOs in numerically obtained tensors would provide a way to identify the logical gates in models away from the fixed point.

The Hamiltonians in Eqns. 5.38, 5.54-5.56 and Appendix 5.A did not make use of the parent Hamiltonian [5.25, 5.45] construction. It may be possible to extend the proofs of gapped parents to the case of PEPS with MPO twist insertions, which would allow construction of gapped Hamiltonians for states with twist defects away from fixed point models.

In this paper, we have focused on the simplest topologically ordered models: the toric and color codes. The general approach is not limited to these models, and we see no obstruction to generalizing general quantum double models. In Appendix 5.B, we construct domain walls for some of the symmetries of the cyclic quantum doubles. The extension to all abelian phases follows by stacking layers, in the same way that the color code is built from stacked toric codes. The extension to general groups is extremely interesting.

Acknowledgments

We acknowledge support from the Australian Research Council via the Centre of Excellence in Engineered Quantum Systems (EQUS), project number CE110001013, and via project DP170103073. We thank Rafael Alexander, Daniel Barter, Benjamin Brown, Nick Bultinck, Christopher Chubb, Sam Elman, Steven Flammia, Robin Harper, Markus Kesselring, Sam Roberts, Thomas Smith and especially Dominic Williamson for useful discussions.

Bibliography

- 5.1 X.-G. Wen, Topological orders in rigid states, [International Journal of Modern Physics B](#) **04**, 239 (1990).
- 5.2 C. Nayak, S. H. Simon, A. Stern, M. Freedman, and S. Das Sarma, Non-abelian anyons and topological quantum computation, [Reviews of Modern Physics](#) **80**, 1083, [arXiv:0707.1889](#) (2008).
- 5.3 X.-G. Wen, Topological Order: From Long-Range Entangled Quantum Matter to a Unified Origin of Light and Electrons, [ISRN Condensed Matter Physics](#) **2013**, 198710, [arXiv:1210.1281](#) (2013).
- 5.4 E. Dennis, A. Kitaev, A. Landahl, and J. Preskill, Topological quantum memory, [Journal of Mathematical Physics](#) **43**, 4452, [arXiv:quant-ph/0110143](#) (2002).
- 5.5 A. Y. Kitaev, Fault-tolerant quantum computation by anyons, [Annals of Physics](#) **303**, 2, [arXiv:quant-ph/9707021](#) (2003).
- 5.6 B. J. Brown, D. Loss, J. K. Pachos, C. N. Self, and J. R. Wootton, Quantum memories at finite temperature, [Reviews of Modern Physics](#) **88**, 045005, [arXiv:1411.6643](#) (2016).
- 5.7 B. M. Terhal, Quantum error correction for quantum memories, [Reviews of Modern Physics](#) **87**, 307, [arXiv:1302.3428](#) (2015).
- 5.8 C. G. Brell, S. Burton, G. Dauphinais, S. T. Flammia, and D. Poulin, Thermalization, Error Correction, and Memory Lifetime for Ising Anyon Systems, [Physical Review X](#) **4**, 031058, [arXiv:1311.0019](#) (2014).
- 5.9 B. J. Brown, K. Laubscher, M. S. Kesselring, and J. R. Wootton, Poking Holes and Cutting Corners to Achieve Clifford Gates with the Surface Code, [Physical Review X](#) **7**, 021029, [arXiv:1609.04673](#) (2017).
- 5.10 P. Etingof, D. Nikshych, and V. Ostrik, Fusion categories and homotopy theory, [Quantum Topology](#) **1**, 209, [arXiv:0909.3140](#) (2010).
- 5.11 A. Kitaev, Anyons in an exactly solved model and beyond, [Annals of Physics](#) **321**, 2, [arXiv:cond-mat/0506438](#) (2006).
- 5.12 M. Barkeshli, C.-M. Jian, and X.-L. Qi, Theory of defects in Abelian topological states, [Physical Review B](#) **88**, 235103, [arXiv:1305.7203](#) (2013).
- 5.13 M. Barkeshli, P. Bonderson, M. Cheng, and Z. Wang, Symmetry, Defects, and Gauging of Topological Phases, [arXiv:1410.4540](#) (2014).
- 5.14 N. Tarantino, N. H. Lindner, and L. Fidkowski, Symmetry fractionalization and twist defects, [New Journal of Physics](#) **18**, 035006, [arXiv:1506.06754](#) (2016).
- 5.15 C. Heinrich, F. Burnell, L. Fidkowski, and M. Levin, Symmetry-enriched string nets: Exactly solvable models for SET phases, [Physical Review B](#) **94**, 235136, [arXiv:1606.07816](#) (2016).
- 5.16 M. Cheng, Z.-C. Gu, S. Jiang, and Y. Qi, Exactly Solvable Models for Symmetry-Enriched Topological Phases, [arXiv:1606.08482](#) (2016).

- 5.17 M. E. Beverland, O. Buerschaper, R. Koenig, F. Pastawski, J. Preskill, and S. Sijher, Protected gates for topological quantum field theories, *Journal of Mathematical Physics* **57**, 022201, [arXiv:1409.3898](#) (2016).
- 5.18 B. Yoshida, Topological color code and symmetry-protected topological phases, *Physical Review B* **91**, 245131, [arXiv:1503.07208](#) (2015).
- 5.19 B. Yoshida, Gapped boundaries, group cohomology and fault-tolerant logical gates, *Annals of Physics* **377**, 387, [arXiv:1509.03626](#) (2017).
- 5.20 P. Webster and S. D. Bartlett, Locality-Preserving Logical Operators in Topological Stabiliser Codes, (To appear) .
- 5.21 F. Verstraete, V. Murg, and J. Cirac, Matrix product states, projected entangled pair states, and variational renormalization group methods for quantum spin systems, *Advances in Physics* **57**, 143, [arXiv:0907.2796](#) (2008).
- 5.22 B. Pirvu, V. Murg, J. I. Cirac, and F. Verstraete, Matrix product operator representations, *New Journal of Physics* **12**, 025012, [arXiv:0804.3976](#) (2010).
- 5.23 R. Orús, A practical introduction to tensor networks: Matrix product states and projected entangled pair states, *Annals of Physics* **349**, 117, [arXiv:1306.2164](#) (2014).
- 5.24 J. C. Bridgeman and C. T. Chubb, Hand-waving and interpretive dance: an introductory course on tensor networks, *Journal of Physics A: Mathematical and Theoretical* **50**, 223001, [arXiv:1603.03039](#) (2017).
- 5.25 N. Schuch, I. Cirac, and D. Pérez-García, PEPS as ground states: Degeneracy and topology, *Annals of Physics* **325**, 2153, [arXiv:1001.3807](#) (2010).
- 5.26 N. Schuch, D. Poilblanc, J. I. Cirac, and D. Pérez-García, Topological Order in the Projected Entangled-Pair States Formalism: Transfer Operator and Boundary Hamiltonians, *Physical Review Letters* **111**, 090501, [arXiv:1210.5601](#) (2013).
- 5.27 M. Schwarz, K. Temme, F. Verstraete, D. Perez-Garcia, and T. S. Cubitt, Preparing topological projected entangled pair states on a quantum computer, *Physical Review A* **88**, 032321, [arXiv:1211.4050](#) (2013).
- 5.28 M. B. Şahinoğlu, D. Williamson, N. Bultinck, M. Mariën, J. Haegeman, N. Schuch, and F. Verstraete, Characterizing Topological Order with Matrix Product Operators, [arXiv:1409.2150](#) (2014).
- 5.29 N. Bultinck, M. Mariën, D. Williamson, M. Şahinoğlu, J. Haegeman, and F. Verstraete, Anyons and matrix product operator algebras, *Annals of Physics* **378**, 183, [arXiv:1511.08090](#) (2017).
- 5.30 H. Bombin, Topological order with a twist: Ising anyons from an Abelian model, *Physical Review Letters* **105**, 030403, [arXiv:1004.1838](#) (2010).
- 5.31 A. Kitaev and L. Kong, Models for Gapped Boundaries and Domain Walls, *Communications in Mathematical Physics* **313**, 351, [arXiv:1104.5047](#) (2012).
- 5.32 B. J. Brown, S. D. Bartlett, A. C. Doherty, and S. D. Barrett, Topological Entanglement Entropy with a Twist, *Physical Review Letters* **111**, 220402, [arXiv:1303.4455](#) (2013).

- 5.33 J. C. Teo, T. L. Hughes, and E. Fradkin, Theory of twist liquids: Gauging an anyonic symmetry, *Annals of Physics* **360**, 349, [arXiv:1503.06812](#) (2015).
- 5.34 J. C. Y. Teo, Globally symmetric topological phase: from anyonic symmetry to twist defect, *Journal of Physics: Condensed Matter* **28**, 143001, [arXiv:1511.00912](#) (2016).
- 5.35 M. B. Hastings and X.-G. Wen, Quasiadiabatic continuation of quantum states: The stability of topological ground-state degeneracy and emergent gauge invariance, *Physical Review B* **72**, 045141, [arXiv:cond-mat/0503554](#) (2005).
- 5.36 J. C. Bridgeman, S. T. Flammia, and D. Poulin, Detecting topological order with ribbon operators, *Physical Review B* **94**, 205123, [arXiv:1603.02275](#) (2016).
- 5.37 B. Eastin and E. Knill, Restrictions on Transversal Encoded Quantum Gate Sets, *Physical Review Letters* **102**, 110502, [arXiv:0811.4262](#) (2009).
- 5.38 H. Bombin, G. Duclos-Cianci, and D. Poulin, Universal topological phase of two-dimensional stabilizer codes, *New Journal of Physics* **14**, 073048, [arXiv:1103.4606](#) (2012).
- 5.39 S. Bravyi and R. König, Classification of Topologically Protected Gates for Local Stabilizer Codes, *Physical Review Letters* **110**, 170503, [arXiv:1206.1609](#) (2013).
- 5.40 A. Kubica, B. Yoshida, and F. Pastawski, Unfolding the color code, *New Journal of Physics* **17**, 083026, [arXiv:1503.02065](#) (2015).
- 5.41 D. J. Williamson, N. Bultinck, M. Mariën, M. B. Şahinoğlu, J. Haegeman, and F. Verstraete, Matrix product operators for symmetry-protected topological phases: Gauging and edge theories, *Physical Review B* **94**, 205150, [arXiv:1412.5604](#) (2016).
- 5.42 J. Haegeman, V. Zauner, N. Schuch, and F. Verstraete, Shadows of anyons and the entanglement structure of topological phases, *Nature Communications* **6**, 8284, [arXiv:1410.5443](#) (2015).
- 5.43 K. Duivenvoorden, M. Iqbal, J. Haegeman, F. Verstraete, and N. Schuch, Entanglement phases as holographic duals of anyon condensates, *Physical Review B* **95**, 235119, [arXiv:1702.08469](#) (2017).
- 5.44 J. Haegeman and F. Verstraete, Diagonalizing Transfer Matrices and Matrix Product Operators: A Medley of Exact and Computational Methods, *Annual Review of Condensed Matter Physics* **8**, 355, [arXiv:1611.08519](#) (2017).
- 5.45 D. Perez-Garcia, F. Verstraete, J. I. Cirac, and M. M. Wolf, PEPS as unique ground states of local Hamiltonians, *Quantum Information and Computation* **8**, 650, [arXiv:0707.2260](#) (2008).
- 5.46 F. Pastawski and B. Yoshida, Fault-tolerant logical gates in quantum error-correcting codes, *Physical Review A* **91**, 012305, [arXiv:1408.1720](#) (2015).
- 5.47 H. J. Briegel and R. Raussendorf, Persistent Entanglement in Arrays of Interacting Particles, *Physical Review Letters* **86**, 910, [arXiv:quant-ph/0004051](#) (2001).
- 5.48 R. Raussendorf, D. Browne, and H. Briegel, The one-way quantum computer—a non-network model of quantum computation, *Journal of Modern Optics* **49**, 1299, [arXiv:quant-ph/0108118](#) (2002).

- 5.49 O. Buerschaper, Twisted injectivity in projected entangled pair states and the classification of quantum phases, [Annals of Physics](#) **351**, 447, [arXiv:1307.7763](#) (2014).
- 5.50 D. J. Williamson, N. Bultinck, J. Haegeman, and F. Verstraete, Symmetry-enriched topological order in tensor networks: Gauging and anyon condensation, (To appear) .
- 5.51 A. Coste, T. Gannon, and P. Ruelle, Finite group modular data, [Nuclear Physics B](#) **581**, 679, [arXiv:hep-th/0001158](#) (2000).
- 5.52 R. Coquereaux, Character tables (modular data) for Drinfeld doubles of finite groups, [Proceedings of Science, POS \(ICMP 2012\)](#) 024 , 7, [arXiv:1212.4010](#) (2012).
- 5.53 S. Lentner and J. Priel, A decomposition of the BrauerPicard group of the representation category of a finite group, [Journal of Algebra](#) **489**, 264, [arXiv:1506.07832](#) (2017).
- 5.54 D. Nikshych and B. Riepel, Categorical Lagrangian Grassmannians and BrauerPicard groups of pointed fusion categories, [Journal of Algebra](#) **411**, 191, [arXiv:1309.5026](#) (2014).
- 5.55 V. Ostrik, Module categories over the Drinfeld double of a finite group, [International Mathematics Research Notices](#) **2003**, 1507, [arXiv:math/0202130](#) (2002).

Appendices

5.A Hamiltonians for twists

In this appendix, we provide complete stabilizer Hamiltonians for the color code symmetry twisted states, both on the doubled toric code and color code level.

The symmetry twists for \tilde{W}_1 and W_2 are straightforward to construct as the MPO already has trivial bond dimension and the twists correspond to definite generalized charges. The toric code Hamiltonian for the \tilde{W}_1 twist is given by the stabilizers

$$\left\{ \begin{array}{l} \left[\begin{array}{c} \overline{X_T} \\ X_T \quad X_T \\ \overline{X_T} \end{array} \right], \left[\begin{array}{c} \overline{X_B} \\ X_B \quad X_B \\ \overline{X_B} \end{array} \right], \begin{array}{c} Z_T \\ Z_T + Z_T \\ Z_T \end{array}, \begin{array}{c} Z_B \\ Z_B + Z_B \\ Z_B \end{array}, \begin{array}{c} X_T X_B \\ X_T X_B \\ \overline{X_T} \end{array}, \begin{array}{c} \overline{X_B} \\ X_B \quad X_B \\ \overline{X_B} \end{array}, \begin{array}{c} Z_T \\ Z_T \\ Z_T \end{array}, \begin{array}{c} Z_B \\ Z_B \\ Z_B \end{array}, \begin{array}{c} X_T X_B \\ X_T X_B \\ \overline{X_T} \end{array}, \left[\begin{array}{c} \overline{X_B} \\ X_B \quad X_B \\ \overline{X_B} \end{array} \right], \begin{array}{c} Z_T \\ Z_T \\ Z_T \end{array}, \\ \begin{array}{c} Z_T Z_B \\ Z_T Z_B \\ Z_B \end{array}, \left[\begin{array}{c} \overline{X_B} \\ X_B \quad X_B \\ \overline{X_B} \end{array} \right], \begin{array}{c} Z_T \\ Z_T \\ Z_T \end{array}, \begin{array}{c} Z_B \\ Z_B \\ Z_B \end{array} \end{array} \right\}, \quad (5.60)$$

and on the color code

$$\left\{ \begin{array}{l} \begin{array}{c} X-X \\ X-X \\ X-X \end{array}, \begin{array}{c} Z-Z \\ Z-Z \\ Z-Z \end{array}, \begin{array}{c} X-X \\ X-X \\ X-X \end{array}, \begin{array}{c} Z-Z \\ Z-Z \\ Z-Z \end{array}, \begin{array}{c} X-X \\ X-X \\ X-X \end{array}, \begin{array}{c} Z-Z \\ Z-Z \\ Z-Z \end{array}, \begin{array}{c} Y-Y \\ Y-Y \\ Y-Y \end{array}, \begin{array}{c} Z-Z \\ Z-Z \\ Z-Z \end{array}, \begin{array}{c} X-X \\ X-X \\ X-X \end{array}, \begin{array}{c} Z-Z \\ Z-Z \\ Z-Z \end{array}, - \begin{array}{c} Y-Y \\ Y-Y \\ Y-Y \end{array}, \\ \begin{array}{c} Z-Z \\ Z-Z \\ Z-Z \end{array}, - \begin{array}{c} X-X \\ X-X \\ X-X \end{array}, \begin{array}{c} Z-Z \\ Z-Z \\ Z-Z \end{array}, \begin{array}{c} Z-Z \\ Z-Z \\ Z-Z \end{array} \end{array} \right\}. \quad (5.61)$$

For W_2 , the stabilizers are

$$\left\{ \begin{array}{l} \left[\begin{array}{c} \overline{X_T} \\ X_T \quad X_T \\ \overline{X_T} \end{array} \right], \left[\begin{array}{c} \overline{X_B} \\ X_B \quad X_B \\ \overline{X_B} \end{array} \right], \begin{array}{c} Z_T \\ Z_T + Z_T \\ Z_T \end{array}, \begin{array}{c} Z_B \\ Z_B + Z_B \\ Z_B \end{array}, \begin{array}{c} \overline{X_B} \\ X_B \quad X_T \\ \overline{X_B} \end{array}, \begin{array}{c} \overline{X_T} \\ X_T \quad X_B \\ \overline{X_T} \end{array}, \begin{array}{c} Z_T \\ Z_T \\ Z_T \end{array}, \begin{array}{c} Z_B \\ Z_B \\ Z_B \end{array}, \begin{array}{c} \overline{X_B} \\ X_B \quad X_B \\ \overline{X_B} \end{array}, \begin{array}{c} \overline{X_T} \\ X_T \quad X_T \\ \overline{X_T} \end{array}, \begin{array}{c} Z_T \\ Z_T \\ Z_T \end{array}, \\ \begin{array}{c} Z_B \\ Z_B \\ Z_T \end{array}, \begin{array}{c} X_B X_B \\ X_B X_B \\ \overline{X_B} \end{array}, \begin{array}{c} Z_T \\ Z_T \\ Z_B \end{array}, \begin{array}{c} Z_B \\ Z_B \\ Z_T \end{array} \end{array} \right\} \quad (5.62)$$

on the toric code. On the color code, these become

$$\left\{ \begin{array}{l} \begin{array}{c} X-X \\ X-X \\ X-X \end{array}, \begin{array}{c} Z-Z \\ Z-Z \\ Z-Z \end{array}, \begin{array}{c} X-X \\ X-X \\ X-X \end{array}, \begin{array}{c} Z-Z \\ Z-Z \\ Z-Z \end{array}, \begin{array}{c} X-X \\ X-X \\ X-X \end{array}, \begin{array}{c} Z-Z \\ Z-Z \\ Z-Z \end{array}, \begin{array}{c} Z-Z \\ Z-Z \\ X-X \end{array}, \begin{array}{c} X-X \\ X-X \\ Z-Z \end{array}, \begin{array}{c} X-X \\ X-X \\ Z-Z \end{array}, \begin{array}{c} Z-Z \\ Z-Z \\ X-X \end{array}, \begin{array}{c} X-X \\ X-X \\ Z-Z \end{array}, \\ \begin{array}{c} Z-Z \\ Z-Z \\ X-X \end{array}, \begin{array}{c} X-X \\ X-X \\ Z-Z \end{array}, \begin{array}{c} Z-Z \\ Z-Z \\ X-X \end{array}, \begin{array}{c} Y-Y \\ Y-Y \\ Y-Y \end{array} \end{array} \right\}. \quad (5.63)$$

For W_5 , the toric code terms are

$$\left\{ \begin{array}{l} \left[\begin{array}{c} \overline{X_B} \\ X_B \quad X_B \\ \overline{X_B} \end{array} \right], \begin{array}{c} Z_B \\ Z_B + Z_B \\ Z_B \end{array}, \begin{array}{c} \overline{X_B} \\ X_B \quad X_B \\ \overline{X_B} \end{array}, \begin{array}{c} Z_B \\ Z_B \\ Z_B \end{array}, \begin{array}{c} \overline{X_B} \\ X_B \quad X_B \\ \overline{X_B} \end{array}, \begin{array}{c} Z_B \\ Z_B \\ Z_B \end{array}, \mp \begin{array}{c} \overline{X_B} \\ X_B \quad Y_B \\ \overline{X_B} \end{array}, \mp \begin{array}{c} \overline{Y_B} \\ X_B \quad X_B \\ \overline{X_B} \end{array} \end{array} \right\}, \quad (5.64)$$

along with all of the stabilizers of the top toric code, which remain unchanged. For the color code, we obtain

$$\left\{ \begin{array}{l}
 \begin{array}{cccccccccccc}
 \begin{array}{c} X \\ \square \\ X \end{array}, & \begin{array}{c} Z \\ \square \\ Z \end{array}, & \begin{array}{c} X-X \\ \circ \\ X-X \end{array}, & \begin{array}{c} Z-Z \\ \circ \\ Z-Z \end{array}, & \begin{array}{c} X-X \\ \circ \\ X-X \end{array}, & \begin{array}{c} Z-Z \\ \circ \\ Z-Z \end{array}, & \begin{array}{c} X-X \\ \diagdown \\ X-X \end{array}, & \begin{array}{c} Z-Z \\ \diagdown \\ Z-Z \end{array}, & \begin{array}{c} X-X \\ \diagdown \\ X-X \end{array}, & \begin{array}{c} Z-Z \\ \diagdown \\ Z-Z \end{array}, & \begin{array}{c} X-X \\ \diagdown \\ X-X \end{array}, & \begin{array}{c} Z-Z \\ \diagdown \\ Z-Z \end{array}, \\
 \begin{array}{c} X-X \\ \diagdown \\ X-X \end{array}, & \begin{array}{c} Z-Z \\ \diagdown \\ Z-Z \end{array}, & \begin{array}{c} X-X \\ \diagdown \\ X-X \end{array}, & \begin{array}{c} Z-Z \\ \diagdown \\ Z-Z \end{array}, & \begin{array}{c} X-X \\ \diagdown \\ X-X \end{array}, & \begin{array}{c} Z-Z \\ \diagdown \\ Z-Z \end{array}, & \begin{array}{c} X-X \\ \diagdown \\ X-X \end{array}, & \begin{array}{c} Z-Z \\ \diagdown \\ Z-Z \end{array}, & \begin{array}{c} X-X \\ \diagdown \\ X-X \end{array}, & \begin{array}{c} Z-Z \\ \diagdown \\ Z-Z \end{array}, & \begin{array}{c} X-X \\ \diagdown \\ X-X \end{array}, & \begin{array}{c} Z-Z \\ \diagdown \\ Z-Z \end{array}, \\
 \begin{array}{c} X-X \\ \diagdown \\ X-X \end{array}, & \begin{array}{c} Z-Z \\ \diagdown \\ Z-Z \end{array}, & \begin{array}{c} X-X \\ \diagdown \\ X-X \end{array}, & \begin{array}{c} Z-Z \\ \diagdown \\ Z-Z \end{array}, & \begin{array}{c} X-X \\ \diagdown \\ X-X \end{array}, & \begin{array}{c} Z-Z \\ \diagdown \\ Z-Z \end{array}, & \begin{array}{c} X-X \\ \diagdown \\ X-X \end{array}, & \begin{array}{c} Z-Z \\ \diagdown \\ Z-Z \end{array}, & \begin{array}{c} X-X \\ \diagdown \\ X-X \end{array}, & \begin{array}{c} Z-Z \\ \diagdown \\ Z-Z \end{array}, & \begin{array}{c} X-X \\ \diagdown \\ X-X \end{array}, & \begin{array}{c} Z-Z \\ \diagdown \\ Z-Z \end{array}
 \end{array} \right\}.
 \end{array}
 \tag{5.65}$$

5.B Abelian quantum double models

In this appendix, we generalize the domain walls to the case of the \mathbb{Z}_N toric code [5.5]. There are N^2 anyons in this theory which we label as $e^\alpha m^\beta$. The fusion rules for these particles are

$$e^g m^\alpha \times e^h m^\beta = e^{g+h} m^{\alpha+\beta}, \quad (5.66)$$

where $+$ denotes addition mod N . The \mathcal{T} and \mathcal{S} matrices are given by [5.51, 5.52]

$$\mathcal{T}_{e^g m^\alpha} = \chi^\alpha(g), \quad (5.67)$$

$$= \omega^{\alpha g}, \quad (5.68)$$

$$\mathcal{S}_{e^g m^\alpha, e^h m^\beta} = \frac{1}{N^2} \left(\chi^\alpha(h) \chi^\beta(g) \right)^*, \quad (5.69)$$

where χ^i is the i th irreducible representation of \mathbb{Z}_N , $\omega = \exp(2\pi i/N)$, and \cdot^* denotes complex conjugation.

The symmetry group of these particles is rather complicated [5.13, 5.53–5.55], so we restrict to a $\mathbb{Z}_2 \times \mathbb{Z}_2$ subgroup generated by

$$\mathcal{D} : e^g m^\alpha \mapsto e^\alpha m^g \quad (5.70)$$

$$\mathcal{C} : e^g m^\alpha \mapsto e^{-g} m^{-\alpha}, \quad (5.71)$$

which we will refer to as the duality and charge conjugation symmetry respectively. As we have discussed, this collapses to a \mathbb{Z}_2 when $N = 2$ since \mathcal{C} the particles are self inverse.

5.B.1 Lattice Hamiltonian and PEPS

The Hamiltonian for which Eqn. 5.10 is the ground state can be generalized to the \mathbb{Z}_N topological order by replacing the two dimensional spins with N dimensional ones. Define the generalized Pauli operators so that

$$Z|j\rangle = \omega^j |j\rangle \quad (5.72)$$

$$X|j\rangle = |j-1\rangle, \quad (5.73)$$

where $j \in \mathbb{Z}_N$. The fixed point Hamiltonian we consider is

$$H_{\mathbb{Z}_N} = -\frac{1}{2} \sum \left(\begin{bmatrix} \cdot^x & \\ X & X \\ \cdot^x & \end{bmatrix} + \begin{bmatrix} \cdot^{x^\dagger} & \\ X^\dagger & X^\dagger \\ \cdot^{x^\dagger} & \end{bmatrix} \right) - \frac{1}{2} \sum \left(\begin{bmatrix} \cdot^z & \\ Z^\dagger & Z^\dagger \\ \cdot^z & \end{bmatrix} + \begin{bmatrix} \cdot^{z^\dagger} & \\ Z & Z \\ \cdot^{z^\dagger} & \end{bmatrix} \right). \quad (5.74)$$

Define the generalized Hadamard gate as

$$H = \frac{1}{\sqrt{N}} \sum_{j,k=0}^{N-1} \omega^{jk} |j\rangle \langle k|, \quad (5.75)$$

which acts on the Pauli operators as

$$HXH^\dagger = Z^\dagger \quad (5.76)$$

$$HZH^\dagger = X. \quad (5.77)$$

One can readily verify that

$$\begin{array}{c}
 i-l \quad i \quad j-i \\
 \diagdown \quad \diagup \\
 l \quad \square \quad j \\
 \diagup \quad \diagdown \\
 k-l \quad k \quad j-k
 \end{array} = 1, \tag{5.78}$$

defines a ground state for Eqn. 5.74. This PEPS has a \mathbb{Z}_N virtual symmetry generated by

$$\begin{array}{c}
 Z \quad Z \\
 \text{---} \quad \text{---} \\
 \diagdown \quad \diagup \\
 \square \\
 \diagup \quad \diagdown \\
 Z^\dagger \quad Z^\dagger
 \end{array} = \begin{array}{c}
 \diagdown \quad \diagup \\
 \square \\
 \diagup \quad \diagdown
 \end{array}. \tag{5.79}$$

A state with an m, m^{-1} pair is given by

$$\begin{array}{c}
 \diagdown \quad \diagup \quad \diagdown \quad \diagup \\
 \square \quad \square \quad \square \\
 \diagup \quad \diagdown \quad \diagup \quad \diagdown \\
 Z \quad Z^\dagger \quad Z^\dagger \quad Z
 \end{array}, \tag{5.80}$$

where the path of the string is arbitrary since the virtual symmetry can be used to move it. A state with an e, e^{-1} pair is created by

$$\begin{array}{c}
 \diagdown \quad \diagup \quad \diagdown \quad \diagup \\
 \square \quad \square \quad \square \\
 \diagup \quad \diagdown \quad \diagup \quad \diagdown \\
 X^\dagger \quad X
 \end{array}. \tag{5.81}$$

5.B.2 Domain wall operators

We begin with the MPO for the \mathcal{C} symmetry, which implements charge conjugation on both e and m anyons. On the level of the virtual strings, this can be implemented using

$$\begin{array}{c}
 \diagdown \quad \diagup \\
 H^2 \quad H^2 \\
 \text{---} \quad \text{---} \\
 \diagup \quad \diagdown \\
 H^2 \quad H^2
 \end{array}, \tag{5.82}$$

where

$$H^2 = \sum_{j=0}^{N-1} |j\rangle\langle -j|. \tag{5.83}$$

is the square of the \mathbb{Z}_N Hadamard operator (Eqn. 5.75).

The domain wall constructed for the \mathbb{Z}_2 case in Eqn. 5.18 can be generalized to the \mathbb{Z}_N case. Since the symmetry generator is no longer self-inverse, we need two MPO tensors

$$\begin{array}{c}
 \uparrow \\
 \square \mathcal{D} \\
 \uparrow
 \end{array} \rightarrow = \sqrt{N} \times \begin{array}{c}
 \square H \\
 \square H \\
 \square H^\dagger
 \end{array} \tag{5.84}$$

$$\rightarrow \boxed{\mathcal{D}} \rightarrow = \sqrt{N} \times \begin{array}{c} \boxed{H^\dagger} \\ \boxed{H^\dagger} \\ \boxed{H^\dagger} \end{array} \begin{array}{c} \text{---} \\ \text{---} \\ \text{---} \end{array}, \quad (5.85)$$

where the PEPS tensors are dressed with arrows

$$\begin{array}{c} \diagup \\ \square \\ \diagdown \end{array}, \quad (5.86)$$

indicating which bonds the symmetry in Eqn. 5.79 acts as Z (outgoing) and which it acts as Z^\dagger (ingoing).

Definite symmetry twists can be found by eigenstates of the double braiding process depicted in Eqn. 5.26, which results in eigenvectors of $Z^\dagger X$ being used to close the MPOs. There are N distinct \mathcal{D} twists, differing by the absorption of an e or m particle: $\sigma_j \times e = \sigma_{j+1}$, $\sigma_j \times m = \sigma_{j+1}$.

5.B.3 Prime dimension codes

For the special case of \mathbb{Z}_p toric codes, with p prime, we can characterize the full symmetry group. Consider the transformations

$$\mathcal{D} : e^g m^\alpha \mapsto e^\alpha m^g \quad (5.87)$$

$$\mathcal{Q}_n : e^g m^\alpha \mapsto e^{ng} m^{\alpha i_n}, \quad (5.88)$$

where i_n is the *modular inverse* of n so $i_n \cdot n = 1 \pmod{p}$. These transformations define a group $\mathcal{G} = \mathbb{Z}_p^\times \rtimes \mathbb{Z}_2 \cong \text{Dih}_{p-1}$ of order $2(p-1)$, where \mathbb{Z}_p^\times is the multiplicative group of integers modulo p , $\mathcal{D}\mathcal{Q}_n\mathcal{D} = \mathcal{Q}_{i_n}$ and Dih_n is the dihedral group of order $2n$.

One can check that the \mathcal{S} and \mathcal{T} are preserved by this group. The symmetry \mathcal{C} described above corresponds to \mathcal{Q}_{p-1} .

The domain wall MPO for the transformation \mathcal{Q}_n is described by the matrix

$$\mathcal{Q}_n := \sum_{j=0}^{p-1} |nj\rangle\langle j|, \quad (5.89)$$

where nj is taken modulo p .

Chapter 6

Conclusion

Tensor network methods have proven to be extremely useful for the study of strongly interacting quantum systems. In this thesis, we have used techniques to study models in a variety of quantum phases.

In Chapter 2, we reviewed the notation commonly used for tensor networks. We then discussed some of the key tensor networks used in both quantum information theory and the study of many-body spin models. Finally, we described some of the key results and techniques of the field.

In Chapter 3, we introduced a technique designed to identify the topological order from a given spin Hamiltonian. This method aimed to bypass the hardness of finding ground states by working directly with operators. Motivated by features of anyons, this algorithm attempts to optimise logical operators for a ground-space quantum code. We demonstrated that this technique could efficiently diagnose topological order in the nonperturbative regime.

In Chapter 4, we studied one dimensional spin models with exotic symmetry actions. We considered spin models describing the low energy physics of two dimensional SPT states, where the inherited symmetry exhibits an anomaly or obstruction to being made to act on-site. The models could also be understood as self-dual one dimensional systems. We showed how to write a tensor network with manifest anomalous symmetry using MERA and MPOs. We showed how to variationally optimise over this class of symmetric networks. Given the optimised state, we extracted the conformal and topological data of the spin model.

In Chapter 5, we brought together symmetry and topological order within a PEPS description of the ground state of a spin model. We identified MPOs acting on the virtual level of the PEPS which performed a permutation of anyons corresponding to a topological symmetry. We then showed how to introduce symmetry twists into the tensor network by finding boundary conditions on the MPOs. This allowed us to compute fusion rules for symmetry defects, and parent Hamiltonians for the PEPS states with defects inserted.

Tensor networks have proven to be an incredibly powerful tool for the study of strongly-correlated matter. For gapped Hamiltonians in one-dimension, matrix-product states have proven incredibly powerful. In addition to the heuristic techniques such as DMRG (described in Sec. 2.5), there are provably efficient algorithms for obtaining MPS ground states of 1D Hamiltonians [29–32]. Unfortunately, the overhead associated with these rigorous algorithms currently makes their implementation impractical. It would be extremely useful to find ways to reduce these overheads. The use of heuristic algorithms such as DMRG is extremely prevalent in many-body physics, and look set to become an important tool in other disciplines such as quantum chemistry [33, 34] and machine learning [35–38]. Finding algorithms which certify convergence to a global extremum would be extremely useful in these applications.

The applications of tensor networks have, so far, been mostly limited to one-dimensional systems.

One of the main challenges to their use in higher dimensions is finding the ‘correct’ class of network. In one dimension, MPS and MERA are efficiently contractable, so they can be optimised and physical data extracted. Unfortunately the most natural two-dimensional generalisation, PEPS, seems to be too large. Computationally hard problems can be embedded into these networks, so they cannot be efficiently contractable. The 2D version of the MERA network can be contracted [39, 40], but although the contraction is efficient in a complexity theoretic sense, the scaling makes their application very limited. The primary methods employed to study two dimensional models are ‘snaked’ MPS [41, 42] and approximate contraction of PEPS [43–48]. In Chapter 3, we proposed a physically motivated algorithm which attempts to bypass some of these issues for topologically ordered models.

A great deal of progress has been made in the understanding of quantum phases via tensor networks. Fixed point (zero correlation length) tensor network state have been found for many phases, including topologically ordered [49–53], symmetry-protected [54, 55] and symmetry-enriched states [54, 56]. These fixed point models teach us a great deal about the physics of these phases, but it is important to know how to identify the special structure which characterises these networks in more general tensor networks, such as those obtained by numerical optimisation. In Chapter 5, we show how to identify the symmetry defects of a symmetry enriched phase without building it into the PEPS.

One of the most important strongly-interacting models we know is the standard model of particle physics. Tensor network techniques have allowed us to study condensed matter systems in a nonperturbative way, and people are now turning to the continuum [57–67]. Just as in spin models, progress so far has been largely restricted to one-dimensional models. Although there are many obstacles to the study of the full (3+1) dimensional standard model, tensor networks seem like a promising framework.

Perhaps one of the most surprising applications of tensor networks is the study of the AdS/CFT conjecture. First noted using the MERA network in Ref. 68, the connection has become a major area of research in its own right [69–75]. By providing a concrete playground for study of the conjecture in regimes (low central charge CFTs) that are challenging for more traditional methods, tensor networks promise to shed light on theories of quantum gravity.

Bibliography

- 1 M. Troyer and U.-J. Wiese, Computational Complexity and Fundamental Limitations to Fermionic Quantum Monte Carlo Simulations, [Physical Review Letters](#) **94**, 170201, [arXiv:cond-mat/0408370](#) (2005).
- 2 A. Y. Kitaev, Fault-tolerant quantum computation by anyons, [Annals of Physics](#) **303**, 2, [arXiv:quant-ph/9707021](#) (2003).
- 3 A. Kitaev, Anyons in an exactly solved model and beyond, [Annals of Physics](#) **321**, 2, [arXiv:cond-mat/0506438](#) (2006).
- 4 B. J. Brown, D. Loss, J. K. Pachos, C. N. Self, and J. R. Wootton, Quantum memories at finite temperature, [Reviews of Modern Physics](#) **88**, 045005, [arXiv:1411.6643](#) (2016).
- 5 Y. Zhou, K. Kanoda, and T.-K. Ng, Quantum spin liquid states, [Reviews of Modern Physics](#) **89**, 025003, [arXiv:1607.03228](#) (2017).
- 6 S. Sachdev, *Quantum phase transitions*, 2nd ed. (Cambridge University Press, Cambridge, UK, 2011).
- 7 K. G. Wilson, Confinement of quarks, [Physical Review D](#) **10**, 2445 (1974).
- 8 J. Kogut and L. Susskind, Hamiltonian formulation of Wilson's lattice gauge theories, [Physical Review D](#) **11**, 395 (1975).
- 9 J. B. Kogut, An introduction to lattice gauge theory and spin systems, [Reviews of Modern Physics](#) **51**, 659 (1979).
- 10 M. Levin and X.-G. Wen, String-net condensation: A physical mechanism for topological phases, [Physical Review B](#) **71**, 045110, [arXiv:cond-mat/0404617](#) (2005).
- 11 R. Raussendorf and H. J. Briegel, A One-Way Quantum Computer, [Physical Review Letters](#) **86**, 5188 (2001).
- 12 J. M. Kosterlitz and D. J. Thouless, Ordering, metastability and phase transitions in two-dimensional systems, [Journal of Physics C](#) **6**, 1181 (1973).
- 13 X.-G. Wen, Topological Order: From Long-Range Entangled Quantum Matter to a Unified Origin of Light and Electrons, [ISRN Condensed Matter Physics](#) **2013**, 198710, [arXiv:1210.1281](#) (2013).
- 14 M. B. Hastings and X.-G. Wen, Quasiadiabatic continuation of quantum states: The stability of topological ground-state degeneracy and emergent gauge invariance, [Physical Review B](#) **72**, 045141, [arXiv:cond-mat/0503554](#) (2005).

- 15 M. H. Freedman, A. Kitaev, M. J. Larsen, and Z. Wang, Topological Quantum Computation, [arXiv:quant-ph/0101025](#) (2001).
- 16 V. Lahtinen and J. K. Pachos, A Short Introduction to Topological Quantum Computation, [arXiv:1705.04103](#) (2017).
- 17 B. J. Brown, K. Laubscher, M. S. Kesselring, and J. R. Wootton, Poking Holes and Cutting Corners to Achieve Clifford Gates with the Surface Code, *Physical Review X* **7**, 021029, [arXiv:1609.04673](#) (2017).
- 18 A. Kitaev and L. Kong, Models for Gapped Boundaries and Domain Walls, *Communications in Mathematical Physics* **313**, 351, [arXiv:1104.5047](#) (2012).
- 19 R. Alicki, M. Horodecki, P. Horodecki, and R. Horodecki, On Thermal Stability of Topological Qubit in Kitaev's 4D Model, *Open Systems & Information Dynamics* **17**, 1, [arXiv:0811.0033](#) (2010).
- 20 J. Haah, Local stabilizer codes in three dimensions without string logical operators, *Physical Review A* **83**, 042330, [arXiv:1101.1962](#) (2011).
- 21 H. Bombín, Single-Shot Fault-Tolerant Quantum Error Correction, *Physical Review X* **5**, 031043, [arXiv:1404.5504](#) (2015).
- 22 C. G. Brell, A proposal for self-correcting stabilizer quantum memories in 3 dimensions (or slightly less), *New Journal of Physics* **18**, 013050, [arXiv:1411.7046](#) (2016).
- 23 B. J. Brown, A. Al-Shimary, and J. K. Pachos, Entropic Barriers for Two-Dimensional Quantum Memories, *Physical Review Letters* **112**, 120503, [arXiv:1307.6222](#) (2014).
- 24 D. Bacon, Operator quantum error-correcting subsystems for self-correcting quantum memories, *Physical Review A* **73**, 012340, [arXiv:quant-ph/0506023](#) (2006).
- 25 S. Bravyi and J. Haah, Quantum self-correction in the 3D cubic code model, *Physical Review Letters* **111**, 200501, [arXiv:1112.3252](#) (2013).
- 26 A. Kómár, O. Landon-Cardinal, and K. Temme, Necessity of an energy barrier for self-correction of Abelian quantum doubles, *Physical Review A* **93**, 052337, [arXiv:1601.01324](#) (2016).
- 27 A. Y. Kitaev, A. Shen, and M. N. Vyalyi, *Classical and quantum computation* (American Mathematical Society, 2002).
- 28 J. Kempe, A. Kitaev, and O. Regev, The Complexity of the Local Hamiltonian Problem, *SIAM Journal on Computing* **35**, 1070, [arXiv:quant-ph/0406180](#) (2006).
- 29 Z. Landau, U. Vazirani, and T. Vidick, A polynomial-time algorithm for the ground state of 1D gapped local Hamiltonians, *Nature Physics* **11**, 566, [arXiv:1307.5143](#) (2013).
- 30 C. T. Chubb and S. T. Flammia, Computing the Degenerate Ground Space of Gapped Spin Chains in Polynomial Time, *Chicago Journal of Theoretical Computer Science* **2016**, 9, [arXiv:1502.06967](#) (2016).
- 31 Y. Huang, Computing energy density in one dimension, [arXiv:1505.00772](#) (2015).

- 32 I. Arad, Z. Landau, U. Vazirani, and T. Vidick, Rigorous RG Algorithms and Area Laws for Low Energy Eigenstates in 1D, *Communications in Mathematical Physics* **2017**, 1, [arXiv:1602.08828](#) (2017).
- 33 S. Wouters, *Accurate variational electronic structure calculations with the density matrix renormalization group*, *Ph.D. thesis*, Ghent University, [arXiv:1405.1225](#) (2014).
- 34 S. Wouters and D. Van Neck, The density matrix renormalization group for ab initio quantum chemistry, *The European Physical Journal D* **68**, 272, [arXiv:1407.2040](#) (2014).
- 35 Z. Chen, K. Batselier, J. A. K. Suykens, and N. Wong, Parallelized Tensor Train Learning of Polynomial Classifiers, [arXiv:1612.06505](#) (2016).
- 36 A. Cichocki, N. Lee, I. Oseledets, A.-H. Phan, Q. Zhao, and D. P. Mandic, Tensor Networks for Dimensionality Reduction and Large-scale Optimization: Part 1 Low-Rank Tensor Decompositions, *Foundations and Trends® in Machine Learning* **9**, 249, [arXiv:1609.00893](#) (2016).
- 37 E. M. Stoudenmire and D. J. Schwab, Supervised Learning with Quantum-Inspired Tensor Networks, *Advances in Neural Information Processing Systems* **29**, 6211, [arXiv:1605.05775](#) (2016).
- 38 A. Novikov, M. Trofimov, and I. Oseledets, Exponential Machines, [arXiv:1605.03795](#) (2016).
- 39 G. Evenbly and G. Vidal, Entanglement Renormalization in Two Spatial Dimensions, *Physical Review Letters* **102**, 180406, [arXiv:0811.0879](#) (2009).
- 40 G. Evenbly and G. Vidal, Frustrated Antiferromagnets with Entanglement Renormalization: Ground State of the Spin-1/2 Heisenberg Model on a Kagome Lattice, *Physical Review Letters* **104**, 187203, [arXiv:0904.3383](#) (2010).
- 41 S. Yan, D. A. Huse, and S. R. White, Spin-Liquid Ground State of the $S = 1/2$ Kagome Heisenberg Antiferromagnet, *Science* **332**, 1173, [arXiv:1011.6114](#) (2011).
- 42 S. Depenbrock, I. P. McCulloch, and U. Schollwöck, Nature of the Spin-Liquid Ground State of the $S=1/2$ Heisenberg Model on the Kagome Lattice, *Physical Review Letters* **109**, 067201, [arXiv:1205.4858](#) (2012).
- 43 J. Jordan, R. Orús, G. Vidal, F. Verstraete, and J. I. Cirac, Classical Simulation of Infinite-Size Quantum Lattice Systems in Two Spatial Dimensions, *Physical Review Letters* **101**, 250602, [arXiv:cond-mat/0703788](#) (2008).
- 44 B. Bauer, G. Vidal, and M. Troyer, Assessing the accuracy of projected entangled-pair states on infinite lattices, *Journal of Statistical Mechanics: Theory and Experiment* **2009**, P09006, [arXiv:0905.4880](#) (2009).
- 45 J. Jordan, *Studies of Infinite Two-Dimensional Quantum Lattice Systems with Projected Entangled Pair States*, *Ph.D. thesis*, The University of Queensland (2011).
- 46 M. Lubasch, J. I. Cirac, and M.-C. Bañuls, Algorithms for finite projected entangled pair states, *Physical Review B* **90**, 064425, [arXiv:1405.3259](#) (2014).
- 47 H. N. Phien, J. A. Bengua, H. D. Tuan, P. Corboz, and R. Orús, Infinite projected entangled pair states algorithm improved: Fast full update and gauge fixing, *Physical Review B* **92**, 035142, [arXiv:1503.05345](#) (2015).

- 48 J. O. Iregui, M. Troyer, and P. Corboz, Infinite Matrix Product States vs Infinite Projected Entangled-Pair States on the Cylinder: a comparative study, [arXiv:1705.03222](#) (2017).
- 49 N. Schuch, I. Cirac, and D. Pérez-García, PEPS as ground states: Degeneracy and topology, *Annals of Physics* **325**, 2153, [arXiv:1001.3807](#) (2010).
- 50 O. Buerschaper, Twisted injectivity in projected entangled pair states and the classification of quantum phases, *Annals of Physics* **351**, 447, [arXiv:1307.7763](#) (2014).
- 51 N. Schuch, D. Poilblanc, J. I. Cirac, and D. Pérez-García, Topological Order in the Projected Entangled-Pair States Formalism: Transfer Operator and Boundary Hamiltonians, *Physical Review Letters* **111**, 090501, [arXiv:1210.5601](#) (2013).
- 52 M. B. Şahinoğlu, D. Williamson, N. Bultinck, M. Mariën, J. Haegeman, N. Schuch, and F. Verstraete, Characterizing Topological Order with Matrix Product Operators, [arXiv:1409.2150](#) (2014).
- 53 N. Bultinck, M. Mariën, D. Williamson, M. Şahinoğlu, J. Haegeman, and F. Verstraete, Anyons and matrix product operator algebras, *Annals of Physics* **378**, 183, [arXiv:1511.08090](#) (2017).
- 54 D. J. Williamson, N. Bultinck, M. Mariën, M. B. Şahinoğlu, J. Haegeman, and F. Verstraete, Matrix product operators for symmetry-protected topological phases: Gauging and edge theories, *Physical Review B* **94**, 205150, [arXiv:1412.5604](#) (2016).
- 55 K. Shiozaki and S. Ryu, Matrix product states and equivariant topological field theories for bosonic symmetry-protected topological phases in (1+1) dimensions, *Journal of High Energy Physics* **2017**, 100, [arXiv:1607.06504](#) (2017).
- 56 D. J. Williamson, N. Bultinck, J. Haegeman, and F. Verstraete, Symmetry-enriched topological order in tensor networks: Gauging and anyon condensation, (To appear) .
- 57 F. Verstraete and J. I. Cirac, Continuous Matrix Product States for Quantum Fields, *Physical Review Letters* **104**, 190405, [arXiv:1002.1824](#) (2010).
- 58 C. Brockt, J. Haegeman, D. Jennings, T. J. Osborne, and F. Verstraete, The continuum limit of a tensor network: a path integral representation, [arXiv:1210.5401](#) (2012).
- 59 J. Haegeman, T. J. Osborne, H. Verschelde, and F. Verstraete, Entanglement Renormalization for Quantum Fields in Real Space, *Physical Review Letters* **110**, 100402, [arXiv:1102.5524](#) (2013).
- 60 J. Haegeman, J. I. Cirac, T. J. Osborne, and F. Verstraete, Calculus of continuous matrix product states, *Physical Review B* **88**, 085118, [arXiv:1211.3935](#) (2013).
- 61 F. Quijandría, J. J. García-Ripoll, and D. Zueco, Continuous matrix product states for coupled fields: Application to Luttinger liquids and quantum simulators, *Physical Review B* **90**, 235142, [arXiv:1409.4709](#) (2014).
- 62 D. Jennings, C. Brockt, J. Haegeman, T. J. Osborne, and F. Verstraete, Continuum tensor network field states, path integral representations and spatial symmetries, *New Journal of Physics* **17**, 063039, [arXiv:1212.3833](#) (2015).
- 63 J. Rincón, M. Ganahl, and G. Vidal, Lieb-Liniger model with exponentially decaying interactions: A continuous matrix product state study, *Physical Review B* **92**, 115107, [arXiv:1508.04779](#) (2015).

- 64 G. D. las Cuevas, N. Schuch, D. Perez-Garcia, and J. I. Cirac, Continuum limits of Matrix Product States, [arXiv:1708.00880](#) (2017).
- 65 A. Franco-Rubio and G. Vidal, Entanglement and correlations in the continuous multi-scale renormalization ansatz, [arXiv:1706.02841](#) (2017).
- 66 Q. Hu and G. Vidal, Spacetime Symmetries and Conformal Data in the Continuous Multiscale Entanglement Renormalization Ansatz, *Physical Review Letters* **119**, 010603, [arXiv:1703.04798](#) (2017).
- 67 M. Ganahl, J. Rincón, and G. Vidal, Continuous Matrix Product States for Quantum Fields: An Energy Minimization Algorithm, *Physical Review Letters* **118**, 220402, [arXiv:1611.03779](#) (2017).
- 68 B. Swingle, Entanglement renormalization and holography, *Physical Review D* **86**, 065007, [arXiv:0905.1317](#) (2012).
- 69 G. Evenbly and G. Vidal, Tensor Network States and Geometry, *Journal of Statistical Physics* **145**, 891, [arXiv:1106.1082](#) (2011).
- 70 B. Swingle, Constructing holographic spacetimes using entanglement renormalization, [arXiv:1209.3304](#) (2012).
- 71 M. Nozaki, S. Ryu, and T. Takayanagi, Holographic geometry of entanglement renormalization in quantum field theories, *Journal of High Energy Physics* **2012**, 193, [arXiv:1208.3469](#) (2012).
- 72 C. Bény, Causal structure of the entanglement renormalization ansatz, *New Journal of Physics* **15**, 023020, [arXiv:1110.4872](#) (2013).
- 73 F. Pastawski, B. Yoshida, D. Harlow, and J. Preskill, Holographic quantum error-correcting codes: toy models for the bulk/boundary correspondence, *Journal of High Energy Physics* **2015**, 149, [arXiv:1503.06237](#) (2015).
- 74 N. Bao, C. Cao, S. M. Carroll, A. Chatwin-Davies, N. Hunter-Jones, J. Pollack, and G. N. Remmen, Consistency conditions for an AdS multiscale entanglement renormalization ansatz correspondence, *Physical Review D* **91**, 125036, [arXiv:1504.06632](#) (2015).
- 75 M. Miyaji, T. Takayanagi, and K. Watanabe, From path integrals to tensor networks for the AdS/CFT correspondence, *Physical Review D* **95**, 066004, [arXiv:1609.04645](#) (2017).